INNOVATIVE NANOCATALYSTS FOR SUSTAINABLE NON-OXIDATIVE DEHYDROGENATION OF PROPANE

Laia Gil Jiménez

UNIVERSITAT ROVIRA i VIRGILI

Innovative nanocatalysts for sustainable non-oxidative dehydrogenation of propane

Laia Gil Jiménez

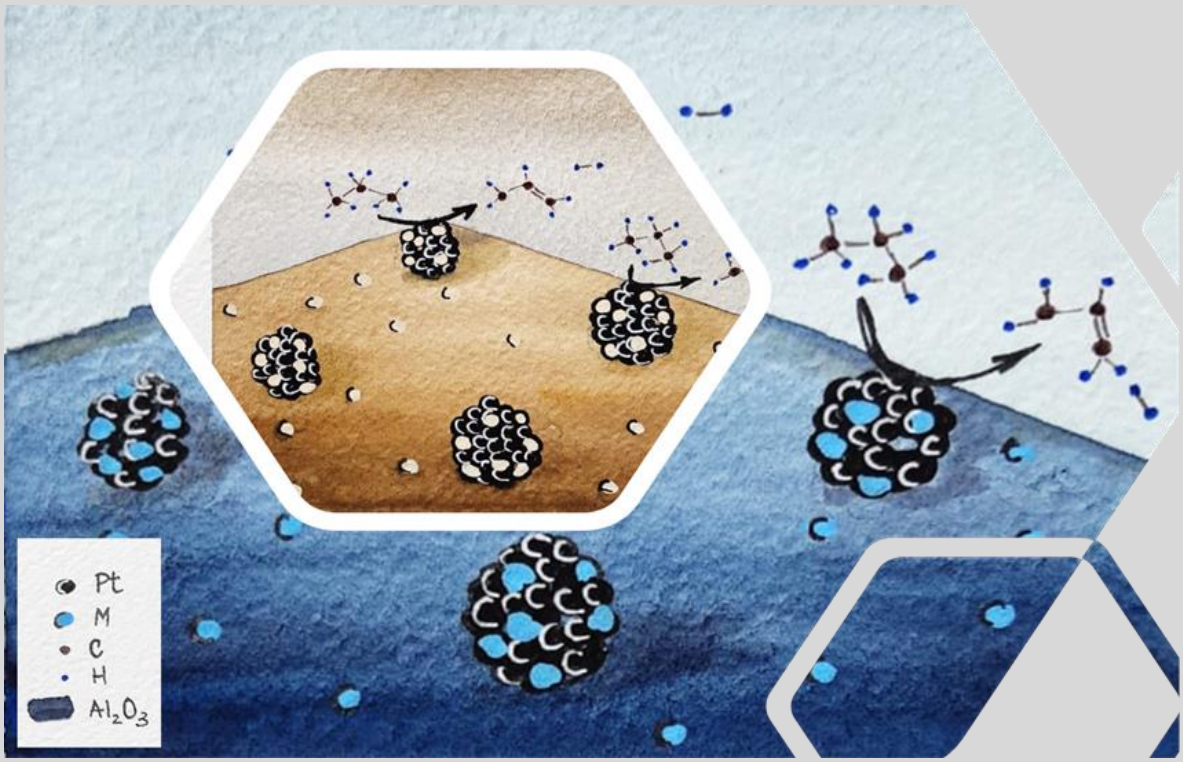

DOCTORAL THESIS
2022

Laia Gil Jiménez

Innovative nanocatalysts for sustainable non-oxidative dehydrogenation of propane

DOCTORAL THESIS

Supervised by

Dr. Aitor Gual, Dr. Isabel Vicente and Dr. Cyril Godard.

Department of Physical and Inorganic Chemistry

Fundació EURECAT – Unitat de Tecnologies Químiques

TARRAGONA

2022

UNIVERSITAT ROVIRA i VIRGILI

Departament de Química Física i Inorgànica
c/ Marcel·lí Domingo s/n, Edifici N4
Campus Sescelades, 43007 Tarragona
Tel. 977 55 80 46

Els sotasignants Dr. Cyril Godard, professor agregat del Departament de Química Física i Inorgànica de la Universitat Rovira i Virgili, el Dr. Aitor Gual Gozalbo, Cap de Línia de Desenvolupament de Processos i Planta Pilot de la Unitat de Tecnologies Químiques de la Fundació EURECAT i la Dra. Isabel Vicente Valverde, investigadora avançada de la Unitat de Tecnologies Químiques de la Fundació EURECAT,

FEM CONSTAR que aquest treball, titulat "Innovative nanocatalysts for sustainable non-oxidative dehydrogenation of propane", que presenta Laia Gil Jiménez per al'obtenció del títol de Doctor i que acompleix els requeriments per a poder optar a Menció Internacional, ha estat realitzat sota la nostra direcció al Departament de Química Física i Inorgànica de la Universitat Rovira i Virgili.

Tarragona, Juny 2022

Els directors de la tesi doctoral

Dr. Cyril Godard Dr. Aitor Gual Dra. Isabel Vicente

The presented Doctoral Thesis has been developed with financial supports by HORIZON 2020 of EUROPEAN COMISSION (Bifunctional zeolite-based catalyst and innovative process for sustainable hydrocarbon transformation (BIZEOLCAT), project ID 814671), the Ministerio de Economia y Competividad and the Fondo Europeo de Desarrollo Regional FEDER (PID2019-104427RB-I00) are gratefully acknowledged.

BiZeolCat

GOBIERNO DE ESPAÑA
MINISTERIO DE ECONOMÍA Y COMPETITIVIDAD

UNIÓN EUROPEA
Fondo Europeo de Desarrollo Regional
"Una manera de hacer Europa"

UNIVERSITAT ROVIRA i VIRGILI

eurecat
Centre Tecnològic de Catalunya

Agraïments

A vegades encara penso que jo no hauria de ser aquí. Hauria d'haver acabat la tesi que vaig començar a Anglaterra. Després, la vida em va portar altre cop a la UAB, on també m'havia de quedar a allà a fer la tesi amb el grup del Xavi Sala. Però tampoc. I de cop i volta, em trobo començant una tesi aquí a Tarragona, sense conèixer a ningú i també sense idea del tema del qual tractava. Meravellós desastre. El meu primer agraïment va pel Xavi Sala, de no ser per ell, no m'hauria assabentat d'aquesta oportunitat i no estaria aquí ara escrivint això. Gràcies, per tot i no poder-me quedar al teu grup, animar-me a seguir amb la ciència i haver-me recomanat un lloc on tu sabies que em sentiria com a casa i aprendria com mai, i així ha estat.

Vull començar pels meus supervisors, per acceptar-me com a doctoranda sense conèixer-me. Aitor, eres de los mejores químicos que he conocido hasta el momento. Siempre tienes una explicación para todo, y si algo he aprendido es que nunca voy a terminar de aprender. Cuando hay curvas en el camino siempre hay que decir, "*i avant*" y seguir adelante o, mejor dicho, ¡catálisis a catálisis! Cyril, muchas gracias por estar siempre disponible a discutir de todo, de química y a veces, de la vida. Siempre consigues aportar otro punto de vista en el cual no había pensado, ampliando la perspectiva y también la *Table of Contents* jeje. Gracias por tu sinceridad en todo momento y todo el soporte recibido. Isabel, muchas gracias por siempre tener las puertas abiertas y también el teams, que soy muy preguntona. Te agradezco mucho tu paciencia y sensibilidad que has tenido conmigo desde el inicio. También nunca hay que subestimar que si la cosa se pone fea poner una velita en la Catedral de Santiago nunca hace daño a nadie.

Mis niños. Mi flor favorita de todo el jardín, mi Emmita, no miento cuando digo que no me imaginaría esta etapa sin ti caminando a mi lado. Eres de las mejores personas que he conocido, y las dos sabemos que nuestra conexión supera la telepatía. Gracias por todo el apoyo, cariño y soporte que me transmites, mi carbono. Roger, compi de PhD! Que això ja ho tenim noi, recorda que el compi de PhD es "pa" toda la vida hijo. Gràcies per aguantar totes les xapes que t'he fotut amb una orxateta a la ma i treure'm un somriure quan més ho necessitava ensenyant-me a relativitzar a la teva manera, acompanyant-me a "no" fer-me un *piercing* o rajant de tot a muerte i dient, *la vida*!

Anna, quina pau em dones i que maca ets. Gràcies per tot el teu suport, i per tota la paciència invertida en mi quan em venia a baix. M'encanta el nostre moment de *chill*, ja saps sense tele, compartint temps a la nostra manera (envoltades d'encara poques plantes jaja). A tota la gent de la UTQ d'Eurecat, quin equipàs esteu fets. M'he sentit còmode des del primer moment, quina sort que m'acollíssiu així de bé. Montse, gràcies per sempre estar allà, sempre m'he sentit molt cuidada especialment per tu, serà perquè ets ajudadora i compartim eneatip, m'encanta la nostra connexió, ets estupenda en tots els sentits. Miriam, mai et podré agrair el suficient que m'hagis descobert així el ioga. Amb tu he après que s'ha d'anar "tocho a tocho", res de construir la muralla Xina en un dia i que la tesi també és conèixer-se a un mateix i anar creixent a poc a poquet, sense voler córrer. David Domi, el meu compi prefe de cafés, tot i que em xutis la capsa dels peus pq ets patilargo, gràcies per haver-me aguantat aquest temps, ets un solete. David Raya, quina alegria dones amb aquestes camises tant estiuenques, divino com tu no hi ha ningú a Eurecat. Iuliana, siempre recordaré el menú de navidad con mucho cariño, gracias por cuidarme y enseñarnos como tendré que bailar una vez tenga el doctorado, espero estar a la altura. Alberto, gracias por endulzarnos los días. Òscar, tus "Buenos días" a veces me asustan, pero transmiten mucha energía, si te aburres de la ciencia monta un bar tío. Andreu i Caramelito, merci per les tardes d'escalada. També vull agrair als altres integrants de la UTQ: Bartek (y el "chiringuito"), David (per les classes compartides d'anglès, algun dia et faré un matcha latte), Ada, Magda, Meritxell, Pere, Alexey, Josep Maria, Ricard, per estar allà! Quiero agradecer también a Carmen Claver por todo su apoyo, eres todo un ejemplo a seguir. Ojalá todo el mundo transmitiese tanta vitalidad como tú.

Gracias a Lola, porque, aunque vayas también a tope con el doctorado nos entendemos genial y siempre te interesas por todo. Raquel, merci per tota l'ajuda donada i també pel teu constant bon humor i disponibilitat, molta sort en aquesta bonica etapa.

Voldria agrair també als tècnics del Servei, sense vosaltres aquesta tesi no hagués estat possible. Vull fer especial menció a la Rita, quins riures sempre amb tu. M'encanta poder xerrar de tot i res a la vegada, encara que intentem parlar en francès, trobar animals al TEM o veure dibuixos amagats a les fotos, sempre m'alegres els dies quan vinc al Servei, ets la chica 10. También gracias a Mariana, por el tiempo compartido.

Francesc, super tècnic de XRD, gràcies per tanta paciència de veritat, em sap greu totes les preguntes que t'he arribat a fer, és un plaer discutir amb tu rodejada de pothus.

També me'n recordo dels que ja no estan a Tarragona. Benedetta, María, Txordi i el grup de "la playa VIP". Nico, Ander y Albert, os echo mucho de menos y aun se me hace raro no veros por los pasillos. Gracias por todo lo vivido, las risas compartidas, los catanes, los risks, los ratos abrazando a Nico, el día de la liada de subir el sofá en casa de Albert entre muchas otras más. Merci a les meves ex-compis de pis, Arantxa, Mireia i Clàudia, el pisito de Pin i Soler per ser la meva primera casa a Tarragona.

Also, I would like to thank all the people I met in Lyon during my internship at CPE. First, thank you Mostafa Taoufik to have accepted me there to do my internship and welcomed me so well in your lab. It is incredible how much I learnt in such a short period of time. Since the day one I was feeling like another member of your group, thank you very much. Also, I would like to thank Kai Szeto for his patience with the author because I asked him many questions, but he always replied nicely and responded to everything incredibly well. Thank you Aimery, for helping me as well. Jessy, without you the lab and the Bizeolcat project would have not been the same. You are such a hard-working person, you will obtain everything you propose, I learnt a lot about your constancy and your kindness. Grazie Paolo, for sharing not only grids for TEM, but nice coffees and some bouldering sessions. Thanks to Isah and CC, for sharing your energy. Nicolas, I really appreciate your patience with me showing me how to do everything at the begging in the lab, merci beaucoup. Felipe, mi profesor brasileño de francés, what a polyglot! Gracias por compartir tu carisma conmigo. A mi tapatía favorita, mi Mariana. Que suerte haberte encontrado, eres de las mejores personas que me llevo de esta etapa, el camino une amiga, y sin tí, a esta tesis le faltaría algo. Baptiste, mi francés-andaluz favorito, realmente ha sido gracias a ti que he podido aprender otra lengua tan complicada como el francés, pq os inventáis las palabras macho! Gracias por la paciencia conmigo, tu música y las buenas charlas. Dimitry, thank you very much for your sensitivity, your energy is incredible, a sincere thank you for the time shared. I would like to mention my favorite Indian, Martin and my favorite Sudanese, Abram, without you two, Lyon would have not been the same.

Gràcies al grup de Ioga Holos i a l'Enoc, on els dijous aconseguia ressetejar-me, simplement respirant i sortint d'allà molt més tranquil·la del que havia entrat.

Gràcies al Jordi, per cuidar-me, aguantar-me quan jo dubtava de tot. Sempre has confiat més en mi més del que jo mateixa faig. Ets de les persones més bones que he conegut mai, la bondat personificada. M'alegro que ens hàgim retrobat.

Gràcies a les "Tres Mosqueteres", per aquest bon rotllo constant i harmonia que despreneu.

No m'oblido dels altres amics de Barcelona. Centralita, tot i la distància sempre ens donem suport, ets un tio 10. A les meves Andreas: Andrea Elias i Androide, gràcies per escoltar-me i trobar un ratet per a mi. Crispeta, la parte buena de terminar esto es que ya no te daré la chapa con el doctorado, que será ahora? Plantas?

Les "Metro y medio", suport des de ja fa molts anys. Carla i Nu, gràcies per estar allà i compartir tan intensament totes les històries de vida, drames i peripècies. Espero continuar caminant al vostre costat molts anys més.

A la tita Mer i a la Marinuski, quina sort tenir-vos i conservar-vos. Tot i la distància, sempre us penso i us tinc presents. Gràcies per tot i els km, saber estar donant-nos suport d'aquesta manera tan maca i tan nostra, quin gust estar solvatada així.

Als meus avis, la iaia Menxi, l'avi Vicenç i la yaya Emi, gràcies per fer-me costat i animar-me a continuar estudiant, posant hores i sent constant, he vist que al final tot té recompensa. Als titos i al cigronet més bonic del món, l'Alex. Amb vosaltres, la diversió sempre està assegurada, gràcies per tot el suport i el afecte que em doneu. Sou casa.

A la meva Ta. Qui sempre ha cregut en mi, i m'ha ensenyat i empentat a ser millor persona. Ets molt més que una àvia per a mi. Si he pogut amb aquesta tesi és perquè tu m'has ensenyat a ser valenta. Tant de bo algun dia ser la meitat de valenta que tu.

Mama, gràcies per aquesta portada en aquarel·la, no hauria pogut trobar-ne una millor i m'encanta que estiguis present en la tesi des de l'inici. Gràcies als meus pares, per estar sempre, recolzant-me, creient en mi i animant-me a seguir. Per ser el meu suport principal i incondicional. Sense vosaltres, res de tot això haguera estat possible. Gràcies a la vostra educació m'heu ensenyat que al final, la constància fa que la formigueta arribi on ella vol, per molt alta que sembli la muntanya.

Tot el que soc avui és gràcies a vosaltres, aquesta tesi és vostra també.

Believe you can and you are halfway there.

Theodore Roosevelt.

Table of Contents

Summary

Currently, the production of polymer building blocks, i.e., propene, is carried out by cracking process of fossil naphtha, producing large CO_2 emissions due to its high-energy demanding nature (i.e., reaction temperatures 800-1200^o C). Recently, the dehydrogenation of light alkanes emerged as a more efficient and sustainable alternative to produce such building blocks. To date, the non-oxidative dehydrogenation (nODH) is applied at industrial scale with limited success due to the inefficient catalyst stability as well as thermodynamic limitations. The present PhD thesis aims at the sustainable propane dehydrogenation (PDH) using innovative nanocatalysts to attain competitive performance at lower temperatures.

In this context, efficient PDH nanocatalysts based on nanoparticles (NPs) of different compositions and supported onto alumina-based materials were prepared and tested in the PDH reaction.

Chapter 1 describes a general introduction on the importance of propylene as a feedstock and its increasing demand. However, it is mainly produced using cracking of naphtha and light diesel. Propane Dehydrogenation is an alternative that targets specifically propylene production. The commercial technologies available and the state-of-the-art concerning the supported nanoparticles are described.

Chapter 2 sets out the general objectives of this thesis.

Chapter 3 describes the synthesis of Pt and PtSn supported catalysts using the surface organometallic chemistry (SOMC) approach. An optimization regarding Pt loading, Pt/Sn ratio, Li loading in the alumina is assessed. Moreover, an exhaustive study of the operation conditions of Propane Dehydrogenation (PDH) is assessed concerning the effect of H_2, temperature, pressure, contact time, oxygen poisoning and long-time studies for stability. Additionally, the

optimized catalyst prepared by SOMC is compared with a benchmark catalyst for comparison purposes.

Chapter 4 is focused on the preparation of PtSn supported catalysts via the one-pot organometallic approach (OPOA). First, the optimization of synthesis conditions is assessed, including metal precursor and its concentration, organic stabilizing agent, temperature, and time to produce small (i.e., 1-2 nm) and well-dispersed colloidal and supported NPs. The effect of PPh_3 and NHC as stabilizing ligands, of the nature of Sn precursor and of various alumina-based supports are detailed. Moreover, exhaustive characterization of the catalysts is described and, when necessary, the colloidal analogues were also synthesized to obtain further information. Finally, the performance of these catalysts in PDH is assessed.

Chapter 5 focuses on the preparation and testing of alternative catalysts such as PtGa and NiSn in the PDH reaction. A novel approach combining OPOA and SOMC is described for the synthesis PtGa and PtSn nanocatalysts. OPOA provides excellent control on the Pt-NPs formation and SOMC, an outstanding control for the selective grafting of Sn or Ga by reaction of the precursors with the Pt-H groups present at the surface of the NPs. The as-prepared catalysts were characterized by combination of microscopic and spectroscopic techniques providing insights into the NP dimensions, catalysts compositions, crystalline phase, and oxidation state of the surface elements. The efficiency of these catalysts in the PDH reaction was evaluated. Then, selected catalysts were also evaluated in the butadiene production from butane and 1-butene dehydrogenation to amplify the scope of alkenes.

UNIVERSITAT ROVIRA I VIRGILI
INNOVATIVE NANOCATALYSTS FOR SUSTAINABLE NON-OXIDATIVE DEHYDROGENATION OF PROPANE
Laia Gil Jiménez

1

General Introduction

1. General Introduction

1.1 Context and motivations

Olefins, also commonly named alkenes, can be described as hydrocarbons containing one or more carbon-carbon double bond.[1] Light olefins (i.e., ethylene (C2), propylene (C3) or butene (C4)), are strategic chemical building blocks to produce a broad range of interesting high-value-added products such as polymers, or other interesting chemical intermediates. The demand for light olefins has been regularly increasing since 1930, and its continuous growing is forecasted. Propylene (C_3H_6), is a particularly interesting raw material due to its high versatility for the production of materials such as polypropylene (PP), acetone, acrylonitrile, acrolein, acrylic acid and acrylates and propylene oxide (**Figure 1.1**).[2,3] In our never-ending growing society, the demand for propylene (C_3H_6) is expected to grow at an average annual rate (2-3% between 2016-2035) that will exceed the current production capacity.[2,4] Thus, there is a propylene gap that needs to be fulfilled (**Figure 1.2**).

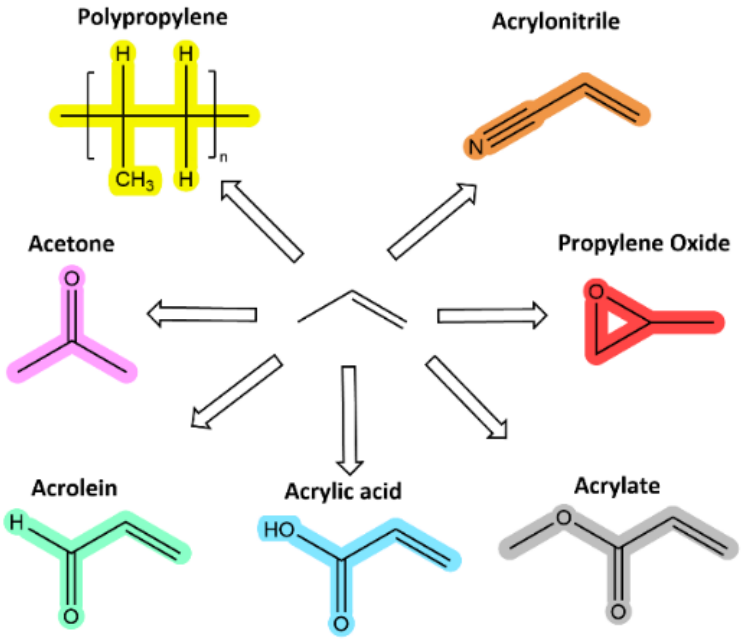

Figure 1.1. Propylene and its main derivatives.

Figure 1.2. Global Propylene Market trends and forecast from 2018 to 2028 in metric tons. Source: BlueWeave Consulting, 2022.

75% of propylene production is accomplished as a by-product from the fluid catalytic cracking (FCC) and the steam cracking of naphtha and light diesel, thus with a large dependency on fossil energy.[5] These technologies are not expected to fulfil the increasing demands in terms of CO_2 emissions because its high-energy demanding nature (i.e., reaction temperatures 800-1200 ^{o}C).[6,7] Furthermore, the CO_2 from light alkane gas flaring represents *ca.* 0.6% of anthropogenic greenhouse gas worldwide emissions.[8] One of the current challenges in the chemical industry is the production of building blocks by using "on-purpose" technologies to target them specifically.[9] Over the last few years, various propylene production methodologies have been widely developed, such as the methanol-to-olefins (MTO),[10,11] the Fischer-Tropsch-to-olefins process[12,13] and the propane dehydrogenation (PDH).[14–16]

1.2 Propane Dehydrogenation (PDH)

Among the proposed alternatives, the propane dehydrogenation (PDH) (**Scheme 1.1**) to propylene and hydrogen has been proposed as one of the most promising approaches, because it leads only to the target molecule propylene and not a hybrid mixture of products.[3,17] Moreover, this technology is particularly interesting due to the availability of a relatively economic feedstock (propane).

Scheme 1.1. Propane dehydrogenation (PDH) reaction.

1.2.1 Thermodynamics of PDH

High reaction temperatures (i.e., 550-750 ^{o}C) and/or low partial pressures (i.e., 0.1 MPa) are necessary to achieve high conversions in the PDH process due to its highly endothermic nature (ΔH_1^o = 124.3 kJ mol^{-1}) (**Figure 1.3**, (1)) and the increase of the number of gas molecules during the dehydrogenation process.[18] Additionally, the competitive C–C cleavage side reactions, can lead to ethylene and methane (**Figure 1.3**, (2)). To enhance the selectivity towards propylene, the reaction conditions and kinetics should be adjusted.

In this context, the nature and the physical-chemical properties of the heterogeneous catalysts, generally consisting of nanoparticles (NPs) supported onto a solid support, appeared as a key tool to achieve PDH performance with optimal utilization of energy and chemicals.[19]

For instance, the effect of the NPs size is reported.[20] Larger particles are keen to favor side reactions such as hydrogenolysis, hydrogenation or even coke formation (**Figure 1.3**, (3), (4) and (5), respectively).

(1) $C_3H_8 \leftrightarrow C_3H_6 + H_2$ $\quad \Delta H_1^o{}_{298} = 124.3$ KJ·mol^{-1}

(2) $C_3H_8 \leftrightarrow CH_4 + C_2H_4$ $\quad \Delta H_2^o{}_{298} = 98.9$ KJ·mol^{-1}

(3) $C_3H_8 + H_2 \leftrightarrow C_2H_6 + CH_4$ $\quad \Delta H_3^o{}_{298} = -37.7$ KJ·mol^{-1}

(4) $C_2H_4 + H_2 \leftrightarrow C_2H_6$ $\quad \Delta H_4^o{}_{298} = -136.6$ KJ·mol^{-1}

(5) $C_3H_8 \leftrightarrow 3C + 4H_2$ $\quad \Delta H_5^o{}_{298} = 119.5$ KJ·mol^{-1}

Figure 1.3. Propane dehydrogenation (PDH, 1) and side reactions (2-5).

It is of crucial importance to describe the thermodynamics in terms of heat reaction as well as the highest achievable conversion to define the limits of the system.[21] According to Rothenberg *et al.*[22], knowing the specific enthalpy (ΔH, [KJ·mol^{-1}]) within 723 and 823 K (**Figure 1.4,** (1)), the specific Gibbs free energy (ΔG, [KJ·mol^{-}

[1]) (**Figure 1.4,** (2)), and the equilibrium constant (Kp, [atm]) (**Figure 1.4,** (3)); the equilibrium conversion of the PDH reaction can be expressed as function of P and Kp (**Figure 1.4,** (4)). **Figure 1.5,** displays the plot of the propane equilibrium conversion as a function of the temperature (considering 0.1 MPa as the pressure) and a selection of state-of-the-art nanostructured catalysts.

(1) $\Delta H = (6.97 \cdot 10^{-9})T^3 + (-2.69 \cdot 10^{-5})T^2 + (3.25 \cdot 10^{-2})T + 116.78$

(2) $\Delta G = (-0.137)T + 128.102$

(3) $K_p = (1.48 \cdot 10^{7}) \cdot e^{(-15403/T)}$

(4) $\text{Equilibrium conversion} = \sqrt{\frac{1}{\frac{1+P}{K_p}}}$

Figure 1.4. Thermodynamic expressions of PDH (1) specific enthalpy, (2) specific Gibbs free energy, (3) equilibrium constant and (4) equilibrium conversion.

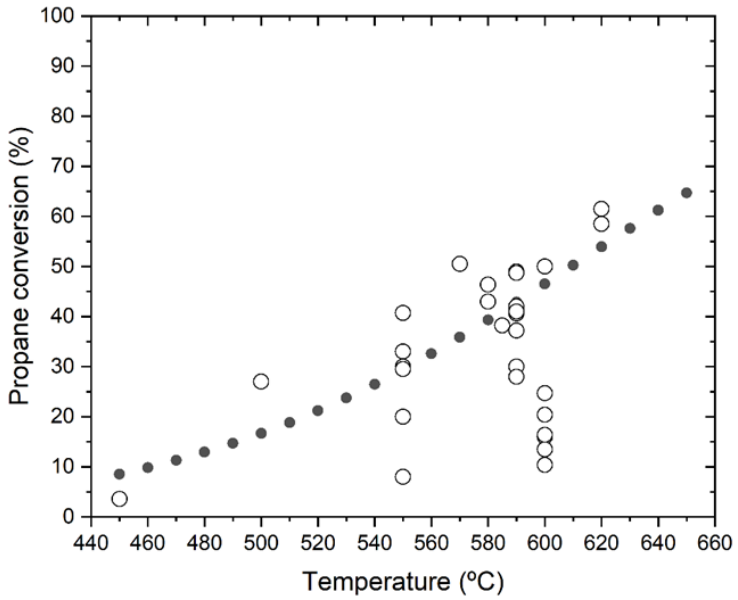

Figure 1.5. Propane dehydrogenation conversion as a function of the temperature: (●) equilibrium conversion calculated (at 0.1 MPa) using literature models,[22] and (○) selection of the most relevant results reported in the literature using Pt-based catalyst (**Table 1.1**).[3]

Table 1.1. Pt based catalysts for PDH.

Entry	Catalyst	Pt (wt. %)	T (^{o}C)	Initial Propane Conversion (%)	Reference
1	PtZn@SiO_2	2.9	550	30.2	[23]
2	PtMn@SiO_2	2	550	8.0	[24]
3	PtCr@SiO_2	2	550	20.0	[25]
4	PtCo@SiO_2	2	550	20.0	[26]
5	PtGa@Al_2O_3	0.67	450	3.6	[27]
6	PtSn@SiO_2	3	500	27.0	[28]
7	Pt@Mg(In)(Al)O	0.7	600	20.4	[29]
8	Pt@Mg(Ga)(Al)O	0.9	600	16.0	[30]
9	PtSn@meso-Al_2O_3	0.4	590	30.0	[31]
10	PtSn@mesoAlSBA-15	0.44	590	28.0	[32]
11	PtSn@$ZnAl_2O_4$	3	600	50.0	[33]
12	PtSn@$MgAl_2O_4$	0.42	580	46.4	[34]
13	PtNa@Sn-ZSM-5	0.5	590	41.7	[35]
14	PtNa@Zn-ZSM-5	0.5	590	40.6	[36]
15	PtIn@Mg(Al)O	0.6	620	61.5	[37]
16	Pt@Mg(Zn)(Al)O	0.28	550	20.0	[38]
17	PtSn@CeO_2	1	680	45.0	[39]
18	PtGa@(Ce)Al_2O_3	0.1	620	58.5	[40]
19	Pt@Mg(Sn)(Al)O	0.5	550	29.5	[41]
20	Pt@Mg(Ga)(Al)O	3	600	13.5	[42]
21	PtIr@Mg(Al)O	1.91	600	24.7	[43]
22	PtSn@MgSBA-15	1	580	43.0	[44]
23	PtGa@SiO_2	4.37	550	40.7	[45]
24	PtSnNaLa@ZSM-5	0.4	590	37.2	[46]
25	PtSnNaCe@ZSM-5	0.5	590	42.0	[47]
26	PtSn@siltSAPO-34	0.45	585	38.2	[48]
27	PtSnNa@$LaAl_2O_3$	0.5	590	41.0	[49]
28	PtSn@Al_2O_3 (A750)	0.5	590	49.0	[50]
29	Pt@Sn-Beta	0.5	570	50.5	[51]
30	Pt@(-OH)Al_2O_3	0.5	550	33.0	[52]
31	Pt@NaHA	1	550	26.0	[53]
32	Pt@ND@G	0.28	600	16.4	[54]
33	Pt@CNT	3.2	600	10.4	[55]
34	Pt@Al_2O_3-nanosheet	0.35	590	48.7	[56]

1.2.2 PDH Mechanism

The most commonly accepted mechanism for the dehydrogenation of alkanes over metal-based catalysts is the reverse Horiuti-Polyani mechanism.[57] The main reaction consists of four steps (**Figure 1.6**): (1) the adsorption of propane on the metal surface by the cleavage of a C-H bond in a dissociative adsorption, resulting in 1-propyl group adsorbed through a Van der Waals interaction,[58,59] (2) the cleavage of the second C-H bond, resulting in a π-mono bonded propylene species or a di-σ-bonded propylene, on two adjacent metallic atoms, (3) propylene desorption; and (4) H_2 desorption from the metallic surface. [24,60,61] The kinetics of the mechanism follow the Langmuir-Hinshelwood expression, since all the surface sites of the catalyst are considered indistinguishable. [14,61] The first C-H activation is accepted as the rate-determining-step (rds).[3,61] However, selectivity is most influenced by the desorption of propylene. The C-H bonds of the alkane have lower reactivity than the ones of analogous olefins. This means that propylene is more reactive than propane, thus implying that side reactions (cracking, deep hydrogenation or even polymerization) may occur during the PDH process, which can easily lead to low selectivity and coke formation.[14,60,62] In the next section, further insights into the possible deactivation mechanisms are provided. Therefore, a valid catalyst must favor the C-H cleavage over the C-C cleavage, and the rational design of the catalysts is of paramount importance.

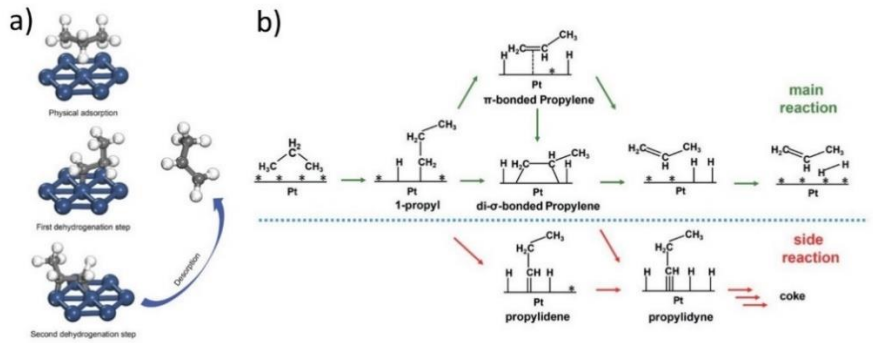

Figure 1.6. a) Proposed structures for the 4 main steps of the mechanism on Pt (111) surface.[59] b) Proposed mechanism for the PDH.[61]

1.2.3 Deactivation mechanisms

The propane dehydrogenation reaction suffers from various side reactions (cracking, hydrogenolysis to lighter hydrocarbons and formation of coke) that all conduct to fast deactivation of the catalyst. For the metal-based and metal-oxide-based catalysts, there are three main causes of deactivation: (i) the coke formation, (ii) the sintering of the particles and (iii) the unsuccessful catalyst regeneration, see **Figure 1.7**.[3]

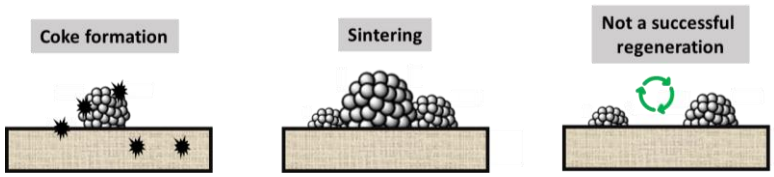

Figure 1.7. Main mechanisms of deactivation for metal-based and metal-oxide-based catalysts.

A first-order deactivation model is accepted to describe the deactivation constant of the catalysts (K_d) at a fixed temperature, where χ_{final} and $\chi_{initial}$, are the final and the initial propane conversion values and "t" represents the duration of the experiment (**Equation 1.1**). [56,63]

$$\ln\left[\frac{(1-\chi_{final})}{\chi_{final}}\right] = k_d \times t + \ln\left[\frac{(1-\chi_{initial})}{\chi_{initial}}\right]$$

Equation 1.1. Deactivation constant (K_d) for PDH.

1.2.3.1 Coke formation

Coke formation is the predominant cause of the catalyst deactivation. Coke deposition refers to the formation of various carbon-rich hydrocarbons and/or macromolecules[5] based on solid carbon at the surface of the catalyst. Coke is the general term for deep dehydrogenation of alkyls or graphitized carbon deposition.[14] In PDH, the coke deposition pathways include four steps: (1) deep dehydrogenation; (2) breaking of C-C bonds, (3) formation of aromatic hydrocarbon

and graphitization.[58,64,65] However, the key intermediates are unknown and the exact mechanism remains ambiguous.[5] Researchers proposed some processes in deep dehydrogenation basis using DFT calculations.[5,58,66] The deep dehydrogenation was studied on Pt (111), propylidene was the intermediate that had the lowest energy and therefore could preferentially adsorb on hollow of three Pt atoms.[67] Other studies indicated that the energy barrier of C-C cleavage decreases continuously and propyne was the most likely intermediate to start the C-C breakage that led to coke deposits.[59] Similar results were obtained by other groups.[68] Additionally, acidic sites also revealed to catalyze the coking process.[14] However, the species that are generally considered being the main precursor of coke depositions are C1 and C2 species, rather than C3, because C1-C2 species have more lone electrons and would attract each other and form aromatic rings through surface-mediated mechanism.[5,58,66] For Pt/Al_2O_3 catalysts, the aromatics formed are derived from C1. The main compounds detected by MS were pyrenes and methyl pyrene and they cannot be formed from C3 species only. Isotopic labeling experiments showed that C3 species would be divided into C1 in the process of coke deposition. In all DFT calculations, the polymerization of C1 or C2 into an aromatic ring is used as the main carbon deposition process.[5,58,66] Once the first aromatic ring is formed, it is expanded continuously to polycyclic aromatic hydrocarbons through a Diels-Alder mechanism. At the end, highly graphitized coke is formed.[5]

Coke prefers to cover the surface of the uncoordinated active sites, explaining the faster decrease in catalytic activity for smaller nanoparticles.[3] For instance, when Pt/Mg(Al)O catalysts were synthesized with various NPs' sizes (from 1 to 10 nm), the highest propylene formation rate corresponded to medium size NPs.[69] When the NP size increased, the selectivity towards propylene increased. However, the conversion rate for propane decreased, obtaining a volcano behavior curve which relates the particle size with the formation of propylene (**Figure 1.8**).[69]

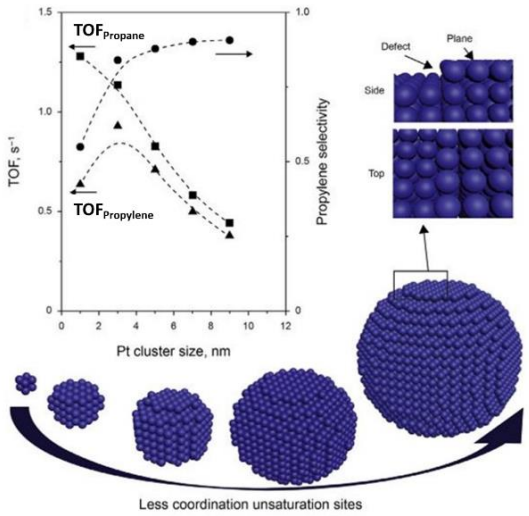

Figure 1.8. The relationship between the propylene selectivity, propane conversion and size of Pt NPs.[69]

The present phenomenon could be associated with the higher proportion of unsaturated step atoms in small Pt NPs. These exhibit higher PDH activity, but at the same time, a higher tendency to cleave the C-C bonds than the corresponding terrace atoms.[70]

For the Pt catalysts, there are two deactivation mechanisms related to the coke deposition. The first consists in the poisoning of the active sites.[71] The second is the limitation of the reagent to access the active sites because of pores blockage by coke.[72] It is possible that both of them occur concurrently. The intermediate C_3H_5*, is taken as a model precursor for the coke deposition. Using DFT calculations, it has been demonstrated that the energy barrier needed to form propylene on flat Pt surface sites is higher (63-72 kJ·mol^{-1}) than on Pt step sites (24-34 kJ·mol^{-1}).[72] However, the propylidene intermediates are generated quite easily and cause the propane to adsorb strongly on such intermediates. Pt/Al_2O_3 and PtSn/Al_2O_3 catalysts have been analyzed by temperature programmed oxidation (TPO) to determine the type of coke formed.[71] The TPO profiles presented different peaks, corresponding to graphitic coke near the metal, and disordered coke on the support.[71]

1.2.3.2 Sintering

Another cause of catalyst deactivation is the sintering, probably due to the high reaction and regeneration temperatures used. In this process, Pt particles' size was related to considerably affect the reaction outcome.[3] The sintering can be caused by: (i) the Ostwald ripening and the (ii) migration-coalescence phenomena. The mechanism of the Ostwald ripening is a spontaneous process that occurs because larger particles are favored thermodynamically over smaller ones (only stable kinetically), this can be explained by the fact that the particle surface is less stable than core of the particle. Therefore, the small NPs tends to stabilize themselves by creating larger particles.[73] Additionally, the migration-coalescence phenomena is implied by Brownian mobility. In PDH, the Ostwald ripening is the predominant mechanism for the sintering of particles, due to the low Tamman temperature of Pt (750 ^{o}C). Tamman temperature can be described as the temperature at which the atoms and/or molecules of a solid acquire enough energy for their bulk mobility to become appreciable. It is estimated to be *ca.* half of the melting point. Nowadays, many efforts have been devoted to fomenting the redispersion of the aggregated nanoparticles during the PDH process and regeneration.[3]

1.2.3.3 Unsuccessful regeneration

The third mechanism of deactivation is related with an unsuccessful regeneration of the catalyst under oxidizing conditions followed by H_2 reduction. Oxychlorination is one of the most typical regeneration conditions which induce the formation of oxychloridic platinum compounds that can induce effectively the redispersion of large Pt particles.[74] Such conditions are efficient for the removal of coke formed during the process and restore the active catalyst. However, a continuous regeneration process might not recover the initial catalytic activity, resulting in an eventual loss of catalytic performance (conversion, selectivity, and stability).[75] The presence of Sn in used $PtSn/Al_2O_3$ catalysts was reported to contribute positively to

the Pt redispersion. Indeed, without Sn, the Pt particles would proceed with the sintering and form larger nanoparticles during the oxidative regeneration process.[75]

1.2.4 Anti-deactivation strategies

Various strategies to prevent catalyst deactivation were described and are summarized in **Figure 1.9**. Generally, these strategies can target the supports or the metal NPs.

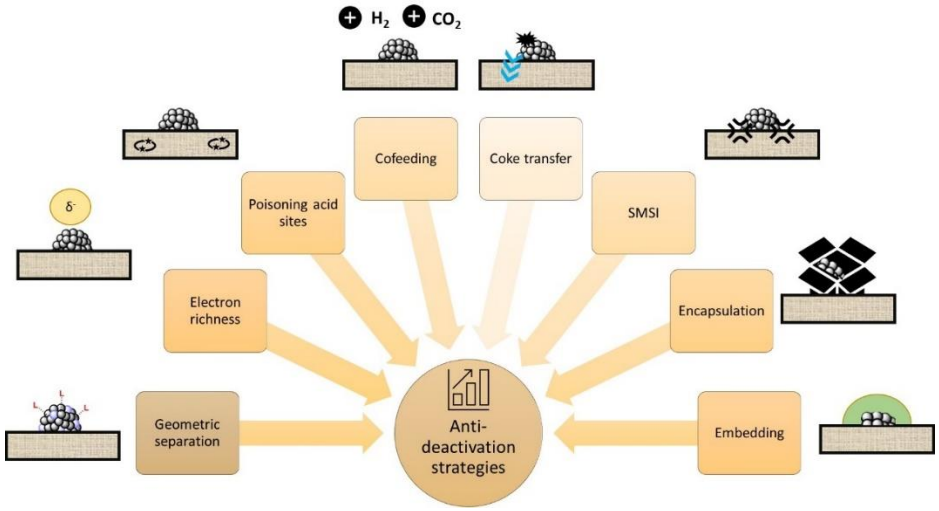

Figure 1.9. Anti-deactivation strategies.

1.2.4.1 Geometric separation

Various studies revealed that the separation of active sites inhibit the structure-sensitive non desired reactions and improve the selectivity to propylene.[14,17] The most typical promoter for particle separation in Pt catalysts is Sn. [14,17] In the section *1.4.1.1 Pt-based catalyst*, the geometric separation achieved by Sn is described. Cu has also been reported as having a promotional effect in Pt/Al_2O_3 catalysts for PDH.[76] The optimal Cu loading content was 0.5 wt.% and the resulting catalyst provided a propylene yield of 36.5% with a selectivity of 90 %. Moreover, the interaction between both metals increased the energy barrier for the C-C bond breaking, thus minimizing the methane formation (**Figure 1.10**). [76] Indium (In) has

also been proved to improve the isolation of the active sites via geometric effects in the PdIn/SiO_2 catalyst for ethane dehydrogenation.[77]

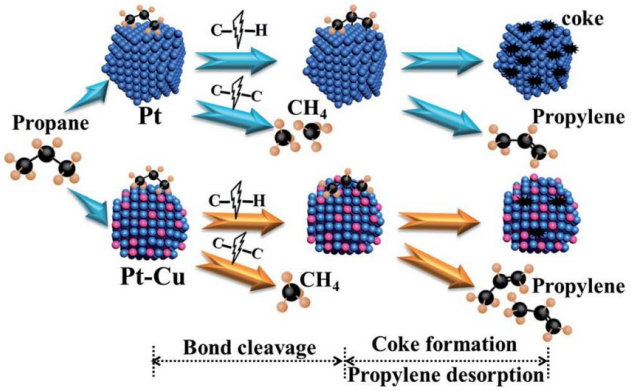

Figure 1.10. Proposed mechanism showing the Cu influence on the catalytic performance of Pt/Al_2O_3 in PDH.[76]

1.2.4.2 Electron richness

The electronic states of the valence d-bands present at the surface of the metal nanoparticles are governing their reactivity, especially the density of states (DOS).[78] With the help of promoters, it is possible to create alloys, which have a direct impact on reactivity increasing the availability of the valence electrons to create chemical bonds with the adsorbates. Therefore, the surface electronic structure is tuned and consequently its reactivity. Modification of the Pt d-band can debilitate the Pt-C-C bond,[20] since the empty d-orbital can be filled with the electrons provided by propylene, that acts as an electron-donor species. With an elevated electron density, further dehydrogenation side reactions, C-C cleavage, and the coke precursors formation are inhibited. Thus, fomenting the desorption of propylene which translates in improved propylene selectivity. Additionally, the introduction of an adequate amount of reducible metal oxide, such as the titanium dioxide (TiO_2), was reported to enhance the catalytic stability and selectivity toward propylene.[79] This improvement can be attributed to the electron transfer from partially reduced TiO_x ($x < 2$) to the Pt species.[79]

1.2.4.3 Poisoning of the acid sites

During the PDH reaction, coke can be deposited on the metal nanoparticles and on the supports. Using non-acidic supports, reduces cracking and polymerization in comparison with acidic supports.[3,14] One of the most applied supports is Al_2O_3 which combines high thermal and mechanical stability with an amphoteric nature. Furthermore, it is possible to decorate it with alkaline promoters (Li^+, Na^+, K^+) to curb support acidity. Other examples using Zn and Mg were reported, leading to a less acidic and more thermally stable spinel phase.[38] Moreover, introducing metal oxides such as TiO_2 or CeO_2 to modify the Al_2O_3 support can also modify the acidity. Indeed, the interaction between the Pt and the support is improved and therefore, the activity, stability and anti-coking behavior is upgraded. At the same time, this type of customization modulates the electronic properties of the main active metal and its dispersion.[3]

1.2.4.4 Cofeeding stream

The modification of the regeneration conditions by the cofeeding streams (i.e., H_2 and/or CO_2) additionally alters the catalyst structure enhancing the elimination of coke.[3] Using a validated simulation model, the H_2/C_3H_8 ratio was varied (from 0 to 4) maintaining the propane and total inlet flow constant while varying only H_2, to analyze its effect on activity in PDH on a Pt-based catalyst.[68] In **Figure 1.11**, the plot of site time yields (STY) of the possible products is showed. At higher values of H_2 pressure, it is possible to decrease the coverage of deeply hydrogenated coke precursors on the surface of the catalyst, such as ethylidene (CCH_3) and methylidyne (CH).[68] Ethylidene and methylidyne are the direct products of the scission reaction of propyne, which is known to be the first C-C scission relevant step for side product formation.[68] A H_2/C_3H_8 ratio of about 3 was found to have the maximum STY.

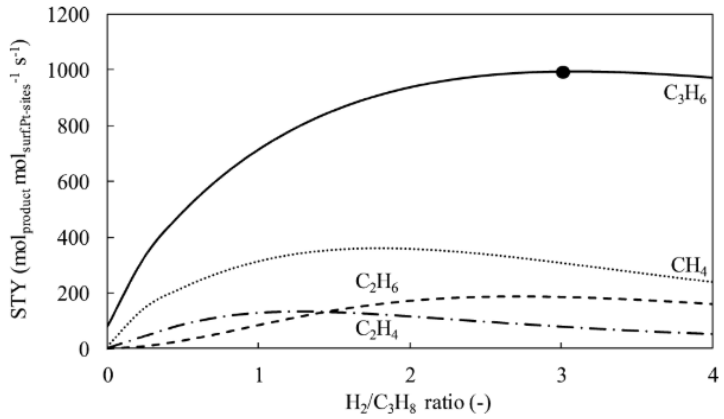

Figure 1.11. Simulation using $2.94 \cdot 10^{-5}$ g of Pt-based catalyst, plotting the Site time yields (STY) of propane dehydrogenation possible products (C_3H_6, C_2H_6, C_2H_4 and CH_4) versus H_2/C_3H_8 ratio.[68]

However, experimental studies showed that the optimum H_2/C_3H_8 ratio was lower, at ca. 1.25.[30] As stated in the literature, the selectivity varying the H_2/C_3H_8 ratio is not influenced at all.[30] Various explanations to explain the positive effect of using H_2 as a cofeeding gas were proposed: (i) H_2 decreases the coverage of coke precursors, (ii) there is a positive dependency of the energy barriers governed by H_2, (iii) a more favored alternative energy pathway is available at high values of H_2 and, (iv) subsurface hydrogen may have an effect.[68]

Additionally, a cofeeding with CO_2,[80,81] acting as a soft oxidant, can decrease the coke formed at high temperature by the reverse Boudouard reaction. The Boudouard reaction, is a redox equilibrium between the mixture of carbon monoxide (CO) and carbon dioxide (CO_2) at a given temperature.[82] The reverse Boudouard reaction can be expressed as follows: $CO_2 + C \leftrightarrow 2\ CO$. At the end, the cofeed with CO_2 increases propane conversion and foments to preserve the perdurability of the catalyst, that has been attributed to a simple dehydrogenation by its coupling with the reverse water gas shift reaction.[80] $FeNi/CeO_2$ and $NiPt/CeO_2$ catalysts have been reported as promising catalysts in the oxidative dehydrogenation of propane using CO_2.[81]

1.2.4.5 Transfer of coke

Redistributing the coke precursors present on the metals and/or supports may also lengthen the catalyst life. The Pt and coke precursor interaction is debilitated by Pt atoms with an elevated electron density, which conduct the coke adducts to relocate from the Pt atoms to the supports, ergo improving the catalyst stability and the resistance to coke deposition.[3] Due to this action, the coke amounts significantly diminished.[83] It is also reported that the Sn modification does not only inhibit the C-C scission but fomenting a migration of the coke precursors from the active metal species to the corresponding support. Pt catalysts supported onto Al_2O_3 were studied in PDH with various TiO_2 loadings. TiO_2 was found to contribute to the electron abstraction from partially reduced TiO_x species to Pt, therefore the less electron-rich Pt particles inhibited the adsorption of propylene and the formation of coke precursors from the metal surface to the support.[83] As well, propylene selectivity and catalytic stability were improved. The optimal content was 10 % wt. loading of TiO_2 onto Pt/Al_2O_3.[83] However, until now the coke transfer pathway has not been proved.[3]

1.2.4.6 Strong metal-support interaction (SMSI)

Strong metal-support interaction (SMSI) can occur from reactions between a metal and an oxide that can be reduced.[3] Cerium oxide (CeO_2), in comparison with the typical alkane dehydrogenation support Al_2O_3, counts with the capacity of trapping the Pt atoms in an ionic form because of the SMSI.[39] Consequently, this catalyst possesses good stability even at high temperature conditions (680 ^oC). and can be regenerated completely without suffering deactivation.[39]

On the other hand, SMSI can also influence non-oxide carriers.[84] For example, thermally stable PtTi intermetallic NPs synthesized via SMSI between Pt and MXenes, (i.e., metal carbides, nitrides…), resulted in a high selective catalyst for light alkane dehydrogenation.[84]

1.2.4.7 Encapsulation

Encapsulation of the active phase can be accomplished using oxides, mesoporous materials, or even carbon layers.[3] There is a situation of confinement by the support, providing an increase in the surface area which promotes the dispersion of the active metals and avoids the sintering.[3] Covering the Pt nuclei with a shell made of oxide can efficiently avoid the Pt NPs aggregation at high reaction temperatures. For instance, Pt@SnO_2/Al_2O_3 presents improved stability during the PDH compared to typical Pt@Al_2O_3 catalyst.[54] This is due to the coated structure which is maintained up to 700 ^oC. Other materials based on carbon such as nanocarbons, nanodiamonds and nanotubes are exceptional supports for PDH.[3] Making the comparison with the alumina-based supports, for instance, a defective graphene nano shell inhibits the agglomeration of Pt-NPs.[54] Additionally, mesoporous supports were reported as a good option due to their confinement effect.[3] Silica-based supports such as the mesoporous SBA-15 were used to support PtFe@Pt/SBA-15 catalyst with a mean-size of *ca.* 7 nm.[85] In contrast, the analogous on SiO_2, possessed a mean size *ca.* 21 nm.[85] It was thus concluded that the mesoporous structure of SBA-15 can confine more efficiently the metal NPs and avoid sintering during catalysis and/or regeneration.[85]

1.2.4.8 Embedding

Another strategy reported by Corma and coworkers consists in the preparation of metal NPs by fixing the metal onto zeolite crystals.[86] The rigid framework of the aluminosilicate has a positive effect in stabilizing the NPs. Their approach consisted in generating Pt NPs and single atoms with improved thermal stability using MCM-22, during the growth of the material from 2D to 3D. Elevated temperatures were applied in the oxidation-reduction treatments and led to the transformation of the encapsulated Pt into small NPs (mean size between 1 and 2 nm).[86] Sn can be added during the Pt synthetic procedure as a promoter. Interestingly, when K was added as a second promoter, differences in stability were observe since after calcination, the PtSn@MFI suffered from agglomeration whereas the K-PtSn@MFI remained unaltered and well-dispersed.[87,88]

1.3 Available commercial technologies for PDH

Due to the paramount importance of the PDH reaction, several technologies were developed. This includes nine technologies: Catofin (ABB Lummus company), Oleflex (Honeywell UOP), FBD-4 (Snamprogetti and Yarsintez), PDH (Linde-BASF-Statoil), STAR (Phillips), ADHO technology (China university of petroleum), FCDh (Dow Chemical Company) and KBRs (K-PRO) and SABIC. [3,14,89,90]

The existing technologies mainly vary in three factors: (i) the mode of operation and regeneration, which can be cyclic or continuous; (ii) the formulation of the catalyst, mainly based either on Pt or Cr, and (iii) the heat regulation, needed to assist the endothermic nature of the propane dehydrogenation. In the following section, a description of the PDH technologies is assessed and an overview in form of a table (for all the technologies except SABIC due to lack of data) can be seen in **Table 1.2.**

Table 1.2. Summary of the commercial technologies for PDH.

Tech.	**Catofin**	**Oleflex**	**STAR**	**Linde-BASF-Statoil**	**FBD-3**	**ADHO**	**FCDh**	**KBR**
Dev.	ABB Lummus	UOP	Phillips	Linde-BASF	Snamprogetti-Yarsintez	China University of Petroleum	Dow Chemical Company	K-PRO
Year	1986	1990	1999	1995	1964	2016	2016	2018
Cat.	K(Na)CrO_x/Al_2O_3	K(Na)$PtSn/Al_2O_3$	$PtSn/ZnAl_2O_4$ /$CaO-Al_2O_3$	$PtSn/ZrO_2$	CrO_x/Al_2O_3	Refractory mixed oxides	PtGa-K/Si-Al_2O_3	Non-Pt Non-Cr
T (^oC)	560 - 650	525 – 705	480 – 620	550 – 650	550 – 600	500 – 650	600	600
P (bar)	0.2 – 0.5	1 – 3	5 – 6	>1	1.1 – 1.5	-	1	1.5
Con. (%)	40 – 45	30 – 40	35	40 – 45	45 – 50	50	45	45
Sel. (%)	82 - 87	85.5 – 88	80 - 90	95	80 - 85	90	93	87 - 90

1.3.1 Catofin process

The Catofin process, licensed by ABB Lummus company, was the first dehydrogenation C_3-C_5 alkene technology developed.[3] It is based on the Houdry Catadiene process, that primarily was devoted to isobutane dehydrogenation. The Catofin process consists of four sections: (i) propane dehydrogenation reaction to obtain propylene, (ii) reactor discharge compression, (iii) product recovery and (iv) refinery units. The present process uses 5-8 parallel adiabatic fixed bed reactors containing a chromium-alumina-based-catalyst promoted with alkali, with a content larger than 18% wt. Cr. It exhibits a stable behavior and provides conversion of propane (45-50%) and good propylene selectivity (87%). The PDH reaction takes place at *ca.* 575 ^{o}C at 0.2-0.5 bar (a) of pressure.[3,14,91] Prior to the catalytic reaction, the hydrocarbons are previously heated at 650 ^{o}C (0.5 bar (a)). Every reactor is continuously running, some of them are devoted to PDH reaction and others to regeneration and purging steps (15-30 min), resulting in a nonstop product generation.[14] In the Catofin process, a dilution of the catalyst with inert material is needed to foment an energy reservoir for the PDH reaction. Nonetheless, this technology is not very efficient since large amount of energy is consumed in each feeding. To overcome this drawback, Clariant patented a technology called “heat generating material (HGM)”, which is described as a new metal-oxide-based material (CuO/Al_2O_3 promoted by Ca and Mn oxides) to foment the improvement of selectivity and yield in the mentioned process by the exothermal reduction of Cu.[90] Introducing the HGM optimizes the catalyst bed temperature profile, decreasing the energy and air consumed during the regeneration process and increasing the life of the catalyst. In 2012 the HGM/Catofin process was used on a commercial scale using the Catofin installations.[92]

1.3.2 Oleflex process

The Oleflex process, licensed by Honeywell UOP and commercialized in late 1990’s, is a propane to propylene technology based on moving bed reactors regenerated

continuously. It consists of three sections: (i) reactor, (ii) product recovery and (iii) regeneration of the catalyst. The reactor section consists of one or more radial flow moving bed reactors, coupled with a pre-heating system, interstage heaters and a feed-effluent gas-gas exchanger.[15] The regeneration section consists of burning the coke generated at the catalyst surface and returning it to the reactor, which is redispersed on the support material by a treatment with a mixture containing chlorine and air. The redispersion of sintered Pt is accomplished with the formation of oxychlorinated species.[90] Dimethyl sulfide is introduced to the bed reactors to suppress the formation of coke and prevent the walls of the reactor to embrittle as a product of the interaction with the formed alkenes.[15] This Pt-Sn-alumina catalyst operates at pressures between 1 and 3 bars and at temperatures of 525 – 705 ^{o}C. This catalyst can convert the feedstock of propane-rich liquefied petroleum gas (LPG) into polymer-grade propylene.[3] More recent catalyst were produced by decreasing the Pt content and increasing the selectivity towards propylene.[3] The propane conversion and propylene selectivity values are estimated to be 29% and 89 % respectively, and the time-on-stream it is of 1000 days.[15]

1.3.3 FBD-3 process

The FBD process, licensed by Snamprogetti and Yarsintez, was developed during the 1960s and can be used for the dehydrogenation of propane (FBD-3) and for isobutane (FBD-4).[3,14,15,90] FBD-3 is based on fluidized bed dehydrogenation. The catalyst is chromium based (15-19%) CrO_x/Al_2O_3, promoted with an alkali metal. The alkane is fed into the reaction tower and the propane dehydrogenation occurs between 1.1- 1.5 bar (a) at 550 - 600 ^{o}C. Subsequently, the catalyst and the gas products are separated by the cyclone separator. The catalysts suffer a deactivation over time, therefore its transportation to a regeneration unit is needed to combust (700 ^{o}C) the carbon deposited on the surface. Afterwards, the regenerated catalysts is transferred to the reaction tower to start the process again. [3,14,15,90]

1.3.4 Linde-BASF-Statoil process

The Linde-BASF-Statoil process also named PDH technology was developed by Linde AG in 1992.[14] Initially, the catalyst was chromium-supported-on alumina oxide with alkali and alkaline promoters. At a later date, they changed to Pt-Sn supported onto hydrotalcite, Mg(Al)O.[3] This PDH technology consists of three gas-fired-steam-reformer-type dehydrogenation reactors. Two of them devoted to dehydrogenation process and the third one used for regeneration purposes under air.[14] The reactors operate at 550 – 650 ^{o}C, and under isothermal regime, the PDH technology can provide > 90 % propylene selectivity and a propane conversion between 40 - 45 %. It is noteworthy that the catalyst life it is estimated to be near 2 years, meaning that little amounts of coke are deposited onto the catalyst. Furthermore, it operates at atmospheric pressure and avoid safety issues in comparison with other technologies. [90]

1.3.5 STAR technology

The STAR (Steam Active Reforming) process, acquired by Uhde and developed in 1999 by Phillips, is a cyclic process used for the dehydrogenation of low paraffins (propane or butanes) into the analogous olefins.[14,15,90] It operates at 5.8 bar (a) and at temperatures between 500 and 600 ^{o}C. First, the feedstock is prepared by separating possible contaminants and the remaining feed is heated up and mixed with oxygen. The STAR technology involves the oxidative propane dehydrogenation. By introducing the oxygen (in an oxyreactor), the latter reacts with hydrogen products and lead to the formation of H_2O. The equilibrium of the reaction reverses the equilibrium of the propane dehydrogenation reaction, and the conversion rate is increased. Furthermore, the exothermic nature of the water formation provides additional heat to the PDH endothermic reaction. [14,15,90] The steam is co-fed with propane to convert the vast majority of coke to CO_2, which translates in increasing the operation time (to *ca.* 7 h) before the regeneration step is required (1 h).[90] Notwithstanding, the resulting olefins must be separated from any residual hydrogen and other side products using separation operation to

improve the yield of the process. The STAR catalyst contains PtSn on Zn-Ca aluminate and exhibit extraordinary dehydrogenation performance. It has been validated and have a life span of more than 5 years. The STAR process provides a conversion of *ca.* 35% and propylene selectivity of 80 - 90%.[3]

1.3.6 ADHO technology

The ADHO technology, recently developed in 2016 by the China University of Petroleum and licensed industrially by Shandong Hengyuan Petrochemical Company Limited, is a propane/butane dehydrogenation technology.[3] It is operated by a non-toxic and non-noble metal catalyst, containing a mixture of refractory mixed oxides. Regeneration of the catalyst is carried out continuously. Furthermore, the catalyst presents good mechanical strength properties and is also valid not only for the PDH and BDH separated but as well for a mixture of propane and butane in the feed. The process operates between 500 and 650 ^{o}C and the propane conversion is around 50 % with a propylene selectivity of 90 %.[3]

1.3.7 FCDh process

The FCDh process, recently developed by the Dow Chemical Company in 2016, consists in a fluidized catalytic dehydrogenation (FCDh) technology. It aims to produce propylene using shale gas, a form of natural gas composed mainly by methane, as the feedstock. The catalyst used is based on Pt-Ga-L/Si-Al_2O_3. It is operated using a fluid catalytic cracking technology. Propylene selectivity achieved is *ca.* 93 % and propane conversion 45 %.[3, 90] The present technology applies a robust reactor/catalyst regeneration that allows the process to be scaled up as needed. Additionally, the FCDh process can be easily integrated within existing ethylene crackers in parallel with furnaces to increase the production of ethylene and propylene.[3]

1.3.8 KBRs technology

The KBRs technology, developed by K-PRO, was launched in 2018.[3] It combines an innovative highly selective dehydrogenation catalyst based on the use of non-precious metals, without chromium.[3] KBRs implements a unique propylene production unit based in FCC reactions. The regeneration is performed in a continuous regime using an orthoflow FCC reactor.

1.3.9 SABIC technology

The main advantage of the SABIC technology, is that the reactor devoted to the propane dehydrogenation is integrated with an internal regenerator.[90] Thus, it is possible to continue to produce propylene with a single unit. The heat produced in the regenerator unit is applied directly to foment the endothermic propane dehydrogenation, with a minor catalyst circulation and therefore abrasion. Besides, it allows more versatility in the selection of the catalyst, which can be Cr or Pt based with their corresponding regeneration frequency times (8-20 min vs 6-12 h, respectively). [90]

1.4 Catalyst development

In the propane dehydrogenation, the rate determining step (rds) is the primary activation of C-H bond of propane.[3,93–95] Besides, the product (propylene) is far more reactive than the reagent (propane), and can suffer side reactions (i.e., cracking, hydrogenolysis or continue with the dehydrogenation). In the past decades, a vast array of heterogeneous catalysts was investigated for PDH purposes and can be classified by three different types: (1) metal-based catalysts; (2) metal-oxide-based catalysts or (3) catalysts with other formulations (**Scheme 1.2**). Concerning the metal-based catalyst, Pt represents the most prominent example; however, insights into the use of other active metals such as Pd, Rh or Ni will be commented. For metal-oxide-based-catalysts, the chromium oxide (CrOx), vanadium oxide (VOx) and gallium oxide (GaOx)-based catalysts can be highlighted as the most important ones. And finally, the group of catalysts with other

formulations includes alternative carbon-based materials, carbides, and nitrides, among others.

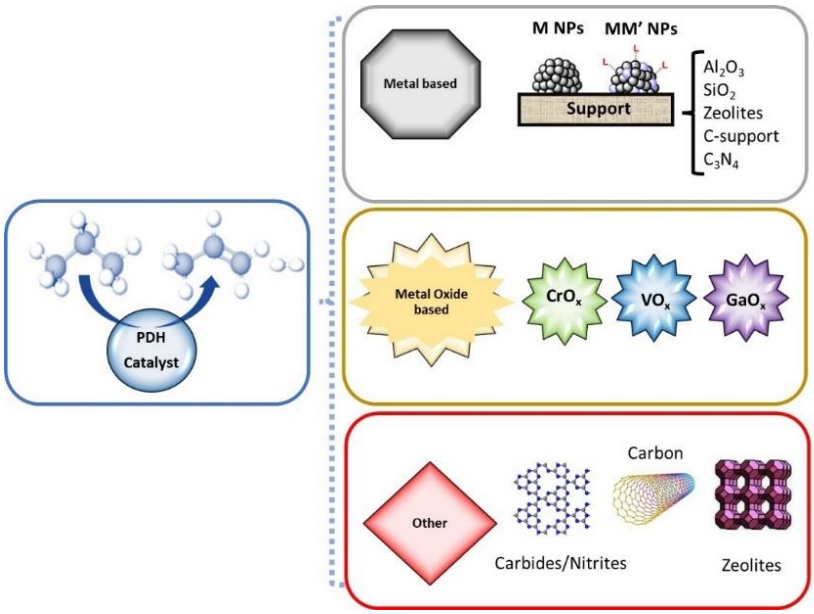

Scheme 1.2. General scheme of various strategies to the catalyst' development for PDH.

In terms of catalyst development, the support and the promoter's choice are considered as important as active metal.

The selection of the support is of paramount importance, and it is not trivial. An adequate support should have high surface area with a homogeneous pore size to foment uniform distribution of the particles, good thermal stability under the PDH reaction conditions, excellent mechanical strength, it should be able to maintain the metal particles well-dispersed and also possesses an adequate acid-base properties.[96] Al_2O_3 could be highlighted as the most typical support for PDH. Other important examples are CeO_2,[39] SiO_2,[28,97] spinel structures ($MgAl_2O_4$),[98] zeolites,[99,100] and carbonaceous materials.[101]

The combination of the active metal, for instance Pt, Pd, Rh or Ni, with another metal (M) as a promoter, permit the formation of alloys or intermetallic substances/composites. The promoter enhances the selectivity toward propylene

and improves the catalytic activity as well as diminishing the active metal loading. The most typical promoter is Sn, but Ga, Zn and In, among other metals are also frequently reported.[3,61] The promoter provides electronic and/or geometric effects that will enhance the catalyst performance in PDH. The promoters can modify electronically the properties of the active metals, but their exact effect on the active phase is still not clear.[3,61] Mainly, it is thought that an electron donation occurs from the promoter to the active metal and as such the d-band energy of the active metal is modified. On the other hand, the introduction of the promoter can remarkably influence geometrically the active metal, inhibiting the structure-sensitive side reactions (hydrogenolysis, coke formation, deep dehydrogenation) and therefore enhance PDH selectivity.[5]

1.4.1 Metal-based catalysts

1.4.1.1 Pt-based catalysts

Pt is the most used metal for propane dehydrogenation due to its outstanding affinity to activate the paraffinic C-H bonds.[3,102,103] However, the Pt-Pt ensembles are also active in side reactions, presenting low selectivity (i.e.; cracking, over-hydrogenation, etc.).[61] It has been shown that Pt three-fold hollow sites possesses large Pt ensembles which are considered to be responsible for the formation of strongly adsorbed alkylidyne species, which are the precursor of hydrogenolysis and coke forming reactions.[65,104,105] To overcome the latter issues, it is necessary to improve the supports, promoters and synthesis methods.[5]

A conventional catalyst for PDH is the Pt-supported onto aluminum oxide ($Pt@Al_2O_3$).[14,61] Nonetheless, electron deficient Pt nanoparticles have a weak interaction with the Al_2O_3.[14] Moreover, the amphoteric nature of this same support, can decrease the selectivity towards the olefins and foment the sintering and the coking, since the Al_2O_3 presents some acidic character.[68] As a direct consequence, efforts in improving the engineering of the supports were implemented so as to foment the metal-support interaction and to induce electronic effects. The addition

of alkaline salts (i.e., Li^+, Na^+ or K^+) was reported to poison the acid sites and therefore restricts the coke formation. [96,98,106,107] As well, a vast array of supports was extensively studied: SiO_2,[108] zeolites,[87,109,110] nanocarbon materials (nanodiamond, carbon nanotubes, carbon nanofibers, graphite).[54,55,111]

Pt is active in PDH in its metallic state Pt (0),[14] and sometimes a reduction step is necessary prior to the reaction. It is described that PDH is not sensitive to the structure of the Pt particles. Only the number of active sites is relevant, therefore small particles are preferred, avoiding the trimers of Pt atoms.[105] Nevertheless, the undesired side reactions (coke formation, hydrogenolysis and isomerization) are reported to be structure sensitive. [14,100,112,113] There is still controversy, because Zhu *et al*., suggests that coke formation is not structure-sensitive, since the coke can be generated by all the Pt facets of the particle, especially in the un-coordinated active Pt sites.[102] They reported that this mentioned phenomena is due to the weakened bond strength of propylene and the higher barrier of energy for dehydrogenation on the Pt (111) domain. For that reason, high coke formation rates were described with the small Pt cluster, since a larger surface area will lead to faster coke formation, and therefore, faster deactivation.

Hence, to obtain good propylene selectivity, various attempts were made to modify the Pt-surface via different strategies that include electronic and/or geometric modifications to the catalyst active phase.[14,27,114]

Several studies revealed that alloys based on Pt and another transition metal (promoter), such as Sn, Ga, Zn, Ti, Cu, enhance the performance in the PDH.[14,78,115–118]

· PtSn catalysts

Tin (Sn) is by far the most extensively studied promoter for Pt catalyst both at industrial and research levels. [3,61] Sn is reported to suppress many side reactions (hydrogenolysis, isomerization), helps to minimize the sintering of the Pt particles,

modifies the acidity of the support, and diffusion of coke adducts from the metal to the support.[14] The promotional role of Sn in Pt catalysts is due to geometric and electronic effects.

The addition of Sn has a structural role because it acts as a site blocking atom, forcing the reaction pathway to the propylene production, because the hydrogenolysis of the adsorbed alkyl through a *γ*-H activation at a neighbouring Pt atom it is not favoured because of Sn (**Figure 1.12**). The alloying of PtSn is also well studied and described and it is reported that its intrinsic effects change the Pt oxophilicity,[103] improving the productivity towards the target molecule, propylene.

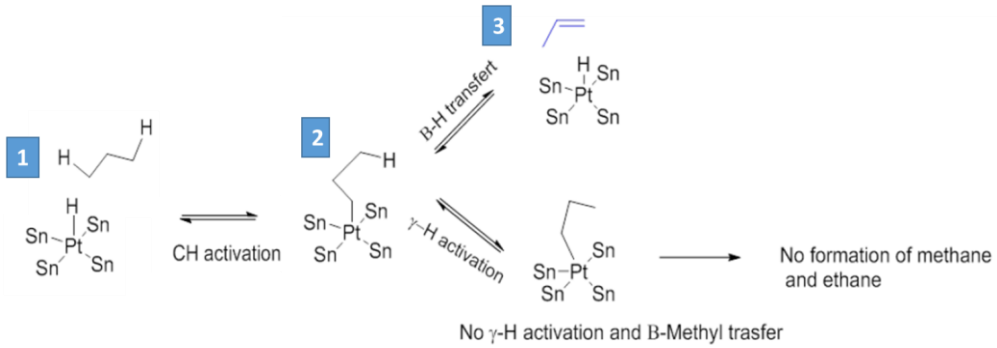

Figure 1.12. PDH mechanism over a bimetallic PtSn-based catalysts. 1,2,3 (blue) are the pathways that lead to the target product, propylene.

· Geometric effect of Sn

Concerning the geometric effect, it has been proposed that the side reactions can be suppressed by minimizing the size of the Pt particles. [14,] The Sn addition will promote the formation of the platinum-tin alloy, covering partially the Pt particles by Sn, which will result in smaller Pt ensembles. [119–121] Olsbye *et al*., [122,123] reported that the Sn is covering selectively the Pt sites that possess low coordination, namely the steps, corners, edges, and defects; the latter ones are responsible for hydrogenolysis. Since PDH reaction is not dependent on structure, small groups of

atoms or, even single atoms of Pt are able to act as catalysts. The Pt-Sn formation will reduce the amount of Pt neighbors, preventing the structure sensitive side reactions, to take place. Moreover, it has been suggested that the sintering of the Pt particles is reduced upon Sn addition.[123] Additionally, the adsorption of coke precursors is preferred on large Pt groups, and this, the use of catalyst can reduce coke deposition.[14]

· Electronic perspective of Sn

Weckhuysen *et al*.,[14] reported that the Sn species alloyed that are in the metallic form Sn (0) or oxidized Sn (2+) are very close to Pt, and therefore are capable of transferring electrons to Pt 5d band, which alters the catalytic characteristics and adsorption properties of Pt. According to previous local density of states (LDOS) studies,[124] it was proved that no hybridization between propane and Pt states is possible. Thus, propane does not covalently adsorb on PtSn surfaces. According to the d-band model,[125] shifting the center of the band to lower values would decrease the interaction strength between the metal surface and the adsorbates. The enrichment of this electronic state rapidly benefits the desorption of propylene due to repel force between electron-rich π bonds in propylene and metal surface.[126,127] Whereas, an upshift of the band center would increase the binding interaction between the surface and the adsorbates.[128] DFT calculations, studied Pt with different Sn loadings (Pt(111), Pt_3Sn/Pt(111), Pt_3Sn(111), Pt_2Sn(111) and Pt_2Sn/Pt(111)).[103] The more Sn, the broader is the d-band (see **Figure 1.13**, a). There is a competition between the propylene dehydrogenation and the propylene desorption, that would affect directly on the propylene selectivity. In **Figure 1.13**, the energy barrier difference (E_{diff}) between propylene dehydrogenation and propylene desorption over the Pt(111) and PtSn surfaces is displayed.[103] It has been observed that the bonding strength of propyl and propylene on alloyed PtSn surfaces is lowered (see **Figure 1.13**, a).[103] Also, the energy barrier for propylene desorption is lowered when more Sn is present, that increases the activation energy

for propylene dehydrogenation, affecting positively the propylene selectivity (see **Figure 1.13**, b).[103] They found that propylene is less stable on $Pt_3Sn(111)$ than Pt(111). However, the best adsorption energy of 1-propylene was achieved when using $Pt_2Sn/Pt(111)$. Nevertheless, a compromise between the propane adsorption and propylene desorption proves that the best candidate was $Pt_3Sn(111)$ alloy.[103]

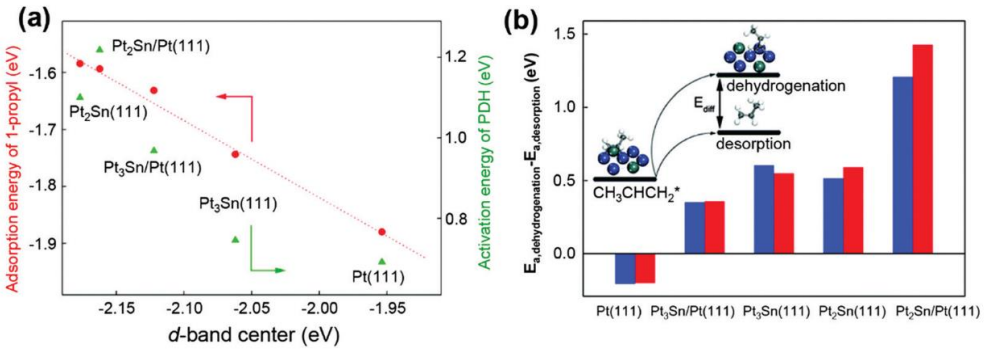

Figure 1.13. (a) Binding energy plot of the 1-propyl (red points) and the energy barriers for PDH to 1-propyl (green points) versus the d-band centers over Pt (111) and PtSn surfaces. (b) Energy barrier difference (E_{diff}) between propylene dehydrogenation and desorption of propylene. The blue and red bars denote the pathways to 1-propenyl or 2-propenyl, respectively.[103]

Supplementary DFT studies described these experimental results revealing an increase of the Pt electron density, which is believed to weaken the adsorption of the ethylidyine on Pt atoms near Sn.[103] Moreover, the selectivity is increased when the energy barrier of the desorption of propylene decreases since deep dehydrogenation and cracking processes will be less favored.[56,70,129] Several studies were performed on such Pt-Sn interactions, verifying previous results.[103,130–134]

· *PtGa catalysts*

Another commonly used promotor for Pt-based systems is gallium (Ga). At high temperatures (> 500 ^{o}C), the alloy Pt-Ga can be formed with various compositions.[61] It is reported that Ga introduction enhances remarkably the selectivity toward propylene and improves the catalytic stability, which was attributed to the geometric and electronic effects.[61]

Series of Pt-Ga/Al_2O_3 were synthesized and used for PDH.[135] By introducing Ga, the propene selectivity increased, and the deactivation and carbon formation were suppressed. This was explained by the ability of Ga to slightly modify the acidity of the support, which the electronic and geometric effects of the Pt-Ga alloy may be the principal motives of the enhancement in the catalytic results. It is also reported that the catalysts stability can also be reinforced using CeO_2-Al_2O_3 as the support, due to the Ga^{3+} cations are incorporated to the cubic structure of CeO_2 and the lattice oxygen storage capacity and surface oxygen mobility are enhanced. As well, the enhanced reducibility of CeO_2 indicates the higher capability to eliminate the coke deposition.[136]

· Other PtM catalysts

Certainly, Sn and Ga are not the unique promoters for Pt-based catalysts. Other highly reported promoters are Zn and In.

PtZn catalysts.

The Pt-Zn alloy was formed after H_2 reduction. In this alloy, notable changes in the electronic, structural, and geometric properties of the Pt catalysts were described. Furthermore, the unalloyed Zn adducts present on the support (i.e., single sites of Zn on SiO_2 or Zn as framework in zeolite) were suggested to have a crucial function in stabilizing the active Pt-Zn alloy.[61,78] As a consequence, the catalytic performances were remarkably enhanced. There is high number of publications on Pt-Zn alloys supported on different zeolitic materials and, in some cases alkali metal ions (i.e., Na^+ and K^+) were added to poison the acid Brønsted sites on zeolites to prevent cracking, oligomerization and coke formation.[137] This includes HZSM5[138,139], NaZSM5[140], Na-Beta[140], Na-Mordenite[140], Na-MCM-22[137], and CIT-6[141], among others. It is reported that Zn addition promotes the Pt dispersion. It is important to mention that the propylene selectivity observed with the silica-aluminum zeolites is lower than with silicious zeolites, probably due to acidity of the silica-aluminum zeolites.[137,142,143] Other supports such as SiO_2[23,78,144] or Mg(Zn)AlO_x hydrotalcites[145]

were also examined and found to possess interesting activities in PDH with selectivity of propylene above 99%.

PtIn catalysts.

Indium (In) is also reported to be a good promoter for Pt-based catalysts. [101,105,146,147,] The Pt-In systems were reported to be more homogeneous in composition, than Pt-Sn and Pt-Ga catalysts.[146,147] With a reduction step under H_2, up to seven different intermetallic alloys could be formed depending on the In loading.[105] However, according to DFT calculations, the Pt_3In alloy is the one that has a comparable activity to pure Pt and Pt_3Sn.[105] Furthermore, Pt_3In can achieve better propylene selectivity than Pt.[148] This is in accordance with some experimental work, concerning Pt-In catalysts on SiO_2 but for ethane dehydrogenation,[105] where Pt_3In phase was far more active than $PtIn_2$. More examples were reported regarding the In promotion in Pt catalysts. In can be introduced onto hydrotalcites, such as Mg(In)(Al)O.[101] The latter catalyst exhibited an increased performance for light dehydrogenation of alkanes in comparison with Pt/Mg(Sn)(Al)O and Pt/Mg(Ga)(Al)O. [101] Nevertheless, the exact structure of Pt-In alloy on hydrotalcites has not been determined yet.[135]

Pt was combined with other metals (M) with different electronegativity such as Cu,[149] Fe,[150] Co,[151] Mn,[24] V,[152] and, Ti,[84] among others to form Pt-M composites, such combinations resulted in the enhancement of the catalyst performance and stability.[153]

1.4.1.2 Other metal-based catalysts

Systems based on Pd, Rh or even Ni were reported as PDH catalysts.

Pd-based catalysts.

In comparison with Pt, Pd shows an increased intrinsic activity towards the cracking of the C-C bond, which translates in inferior selectivity toward propylene.[135]

Additionally, Pd-based catalyst quickly deactivate because of coke formation. To beat these challenges, various promoters were added and the corresponding intermetallic alloys Pd-Sn[154] , Pd-Ga[155] , Pd-Zn[156] , and Pd-In[77] can be formed. They all exhibit higher activity than the monometallic Pd catalysts. The Pd bimetallic catalysts provided promising performance in propane dehydrogenation, although their activity is lower than Pt bimetallic systems.[135] Additionally, the Pd price is much higher than that of Pt, and is thus not an attractive alternative for large scale applications.

Rh and Ni-based catalysts.

Numerous studies revealed that some other metals such as Rh and Ni can be used as active phases.[135,132] Usually, Ga is the chosen promotor and leads to single-atom alloy or intermetallic compounds.[135] These structures produce metal sites that are active for the dissociation of C-H bond.

Interestingly, Ga-Rh/Al_2O_3 catalysts showed high propylene selectivity (>90 %) and a reasonable catalyst stability.[157,158] However, the high price of Rh greatly limit any potential industrial applications.

Ni-based catalysts are a good option to lower the cost of the noble-based catalysts. Ni can activate the alkane molecule; however, Ni alone possesses a high activity towards C-C hydrogenolysis, which increase the production of methane. To improve the selectivity toward olefins, various metal promoters need to be introduced, such as Sn and Ga.[135]

1.4.2 Metal-oxide-based catalysts

In the past decades, a high number of heterogeneous catalysts based on metal-oxide were exploited for PDH. The Lewis acid M-O sites present in metal oxides can efficiently activate the C-H bonds of propane. The most reported systems are based on chromium oxide (CrO_x), vanadium oxide (VO_x) and gallium oxide (GaO_x). They

exhibit substantial activity and good propylene selectivity but experience the loss of oxygen under the reaction conditions, leading to a fast deactivation due to coke deposition. Therefore, regular regeneration cycles are needed to recover the catalyst activity. However, sintering is not completely reversible. For that reason, some challenges remain in terms of coke formation, catalyst stability and environmental problems. [3,14,62]

CrO_x-based catalysts.

Chromium oxides (CrO_x) are commonly applied in the PDH process, especially for the commercial technologies Catofin and FBD-4. Propane reacts at the Cr-O sites. Nevertheless, in comparison with Pt sites is more complex and it is a toxic metal. It is known that the fresh CrO_x catalyst possess a wide range of chromium ions with different oxidation states (Cr^{6+}, Cr^{5+}, Cr^{3+} and Cr^{2+}) which have different roles in the PDH reaction. [159,160] Since the PDH occurs under a reducing atmosphere, the high valence states would be reduced in the process. This was verified using XANES since the reduction of Cr^{6+} species to Cr^{3+} was observed.[161] Moreover, Cr^{3+} is believed to be the active phase of the reaction. In general, CrO_x catalysts have interesting reactivity and selectivity but low stability.[159,160,161]

VO_x-based catalysts.

Vanadium oxide-based catalysts (VO_x) exhibit high selectivity toward propylene. Among VO_x, CrO_x and PtSn-based catalysts for PDH, VO_x catalyst exhibited the best propylene selectivity and stability during the continuous regeneration cycles.[162] Before the PDH reaction, V^{5+} is the predominant specie, but after the H_2 reducing treatment, the V^{5+} ions are partially reduced to V^{4+} and V^{3+}, since part of V^{5+} remain and all the species coexists during the reaction.[162] The active phase is believed to be V^{3+}. Like CrO_x-based catalyst, the carbon deposition is the principal reason for the deactivation of VO_x catalysts, and is believed to be strongly linked with the

dispersion of the present species. [162] However, VO_x is toxic, restricting their application in industry.

GaO_x-based catalysts.

Gallium oxide-based catalysts (GaO_x) were studied in PDH for many years.[122,163,164] There is no quorum about which are the active phase since there is a strong influence of the support, preparation methodology and loading used.[165] The active phase of Ga_2O_3 are the coordinatively unsaturated Ga^{3+} species which is a Lewis acid site.[163,164] For these catalysts, Pt can act as a promoter favoring the desorption of hydrogen and recovering the gallium hydride species and/or the hydroxide species. Upon H_2 pretreatment Ga-H species are fomented, which are reported to possess a higher activity than the Ga^+ sites. [122,166] These types of catalysts also suffer from sintering and a controlled regeneration required to restore their performance.[167]

Other metal oxides formulations reported are based on ZrO_x, InO_x, ZnO, MoO_x, Fe-based and Co-based. [135]

1.4.3 Other catalysts

Apart from metal and metal-oxide-based catalysts for PDH, the transition to a greener chemical industry demanded environmentally friendly and cheaper catalysts. [135] Recently, carbon-based materials or transition metal carbides and nitrides were reported for this process.[62]

Transition metal carbides and nitrides.

By the incorporation of C and N atoms into the interstitial sites of the transition metals, it is possible to create transition metal carbides and nitrides, respectively. [135,180,181] Their formation can significatively affect the physicochemical properties of the metals.[180] Concerning the catalytic perspective, the transition metal carbides (TMC) display similar properties as the noble Pt-catalysts, for instance, Mo_2C,

showing propylene selectivity higher than 95 % in the absence of H_2.[181] Nevertheless, there is a limitation regarding the surface area and the deactivation of the catalysts.[135]

Despite the fact that a myriad of heterogeneous catalysts have proved to possess formidable activities and selectivity in PDH, the exact active site structure of PDH catalysts remain after unclear.[3] A recent review,[128] provided fundamental understanding via DFT calculations and kinetic analysis, into the selectivity towards propylene and coke formation. Computational studies proposed that Pt-based alloys, especially the Pt_3Sn, as the more suitable candidate for the chemical industry as it lowers the desorption energy of the propylene.

To summarize, the state-of-the-art concerning the metal-based, metal-oxide-based, and other catalysts were presented for the non-oxidative dehydrogenation of propane to target propylene, one of the most important value-added chemical building blocks in the chemical industry. Among them, Pt-based catalysts are the most studied, especially when promoted with Sn. Ga, Zn and In are other commonly used promoters for Pt. The promoters cause geometric and electronic effects, improving significatively their catalyst performance. Other active metals are Pd, Rh and Ni. Metal-oxides are another very popular option, especially CrO_x, VO_x or GaO_x. However, these catalysts suffer from deactivation, and a controlled regeneration is required to restore their performance. Due to the demand of more environmentally friendly and cheaper catalysts, other formulations were reported using carbon-based materials or transition metal carbides and nitrides.

Carbon materials.

In the late 70s carbon was found to be active for alkane dehydrogenations.[168] Nanocarbon materials (i.e., graphene, carbon nanotubes, mesoporous carbons, activated carbons, etc.) are interesting as supports for the catalyst since they present a high surface area and, are inexpensive and environmentally friendly. It

has been reported that nanocarbons could be used as a metal-free catalysts for PDH and present catalytic activities comparable with those of the noble metal and metal oxide-based catalysts.[169–173] Furthermore, it is possible to easily tune the surface functionalities through chemical oxidation to carry out the introduction of O groups (such as ketones, carboxylic, lactone, ether or phenol), ii) introduction of N groups (such as pyridine oxide, amide, amine, pyrrole) or, iii) introduction of P groups (such as -P=O, -$PO(OH)_2$, -$OPO(OH)_2$ and -$P(OH)_2$).[169,170,174] The so-mentioned functionalities of activated carbon can catalyze a vast array of reactions.[175] Carbon nanofibers (CNFs) were reported to be active catalysts, and that the existence of radicals formed at the surface of coke favors the dehydrogenation reaction. Additionally, oxygen functionalities on activated carbon and CNFs presented active sites for the oxidative dehydrogenation reactions.[176] Their catalytic performances were related with surface functional groups, defects and electronic properties.[177] Moreover, a mixed nanocarbon made of a diamond core and a graphitic shell presented activity for PDH, which was explained by the presence of either ketone groups or of structural defects in the graphitic part of the material.[178] Recently, non-precious metals (Co and Cu) confined in a carbon matrix which contained nitrogen were also reported to be active in PDH reaction at 773 K.[179]

1.5 Nanochemistry

Nanomaterials present at least have one dimension (1D) in the range from 1-100 nm. Metal NPs (M-NPs) display unique physical and chemical properties that are remarkably different from the bulk materials.[182] NPs possess high surface volume ratio, and as such provide an elevated number of potential active sites exposed.[183] NPs are used in different fields such as biology, medicine, physics, material science and chemistry.[184,185] One of their most popular application is in the field of catalysis.[186] Direct application of colloidal (or unsupported) M-NPs, provide interesting insights into the reactivity of heterogeneous catalysts (hydrogenation, oxidation, C-C bond formation and a long etcetera).[187] Since they are not supported,

they can freely rotate in the three dimensions, meaning the reactants can easily reach the active sites and therefore, high activity is promoted.[188]

The formation of M-NPs is believed to follow the LaMer mechanism (**Figure 1.14**).[189,190]

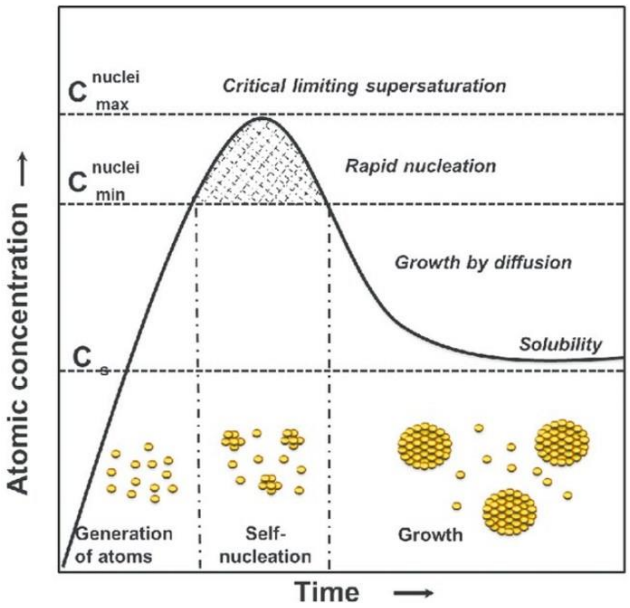

Figure 1.14. LaMer mechanism showing the atomic concentration versus time illustrating the generation of atoms, self-nucleation, and posterior growth. Extracted from [191].

This mechanism consists in three steps: the precursor decomposes and creates (i) a fast increase of the concentration of free and available atoms in solution; that (ii) self-nucleate until reaching the supersaturation giving rise to (iii) the growth nanoparticles/nuclei via homogeneous nucleation.[192] In the latter step, the seed particles are generated in-situ and it is believed that the growth mechanism follow the same process. [193]

1.5.1 Stabilization of metallic NPs

M-NPs are kinetically stable but not thermodynamically, because the minimum energy is the bulk metal.[185] Van der Waals forces will pull two near-by particles to join each other. Therefore, there is a tendency towards aggregation and the use of

a stabilizing agent is required during their synthesis. There are three types of NP stabilization: electrostatic, steric or electrosteric (**Figure 1.15**).

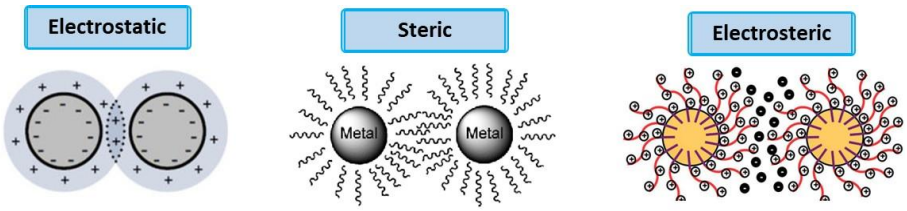

Figure 1.15. Scheme of the electrostatic, steric, and electrostatic stabilization of M-NPs.

Electrostatic stabilization.

The electrostatic stabilization is based on an electrical double layer which creates a Coulombic repulsion that enables, if the electric potential is high enough, the separation of the NPs and thus avoids agglomeration. As an example, we can encounter ions, atoms or groups of atoms that bears one or more positive or negative electrical charges such as halides or carboxylates. Generally, this type of stabilization is performed in an aqueous solutions.[194]

Surfactants can form a monolayer which around the core of the M-NPs. Lipophilic surfactants with positive ions such as methyltrioctylammonium chloride provide very stable NPs.[195]

Steric stabilization.

The steric stabilization consists of the adsorption of sterically demanding molecules on the surface of the metal NP, which act as a protective shield. Polymers and/or organic ligands as steric stabilizers.

Polymers can provide metal-NP stabilization through the steric bulk of their framework. The most used polymer is the poly(n-vinyl-2-pyrrolidone), PVP.[187] The lengths of the PVP and its interaction with the solvent have a role in the particle aggregation.

Dendrimers were also used to stabilize NPs, playing a template role in which, the NPs are formed. Furthermore, since dendrimer's structure is substantially different from the traditional surfactants, this opens new options to vary solubility, functionality, and morphology.[196]

Electrosteric stabilization.

The electrosteric stabilization consists in the combination of the two previous strategies. Amphiphilic compounds, ionic liquids or surfactants provide this form of stabilization.[197] It was reported that NPs can strongly adsorb a layer of anions at the metal surface, that at the same time are surrounded by a layer of countercations to maintain the Pauling's principle of electroneutrality.[198]

Ionic Liquids can be used for the synthesis and dispersion of NPs and as their its surface functionalization.[199]

Small molecules or ligands can also be employed and their structure can affect final morphology and size.[200]

1.5.1.1 Ligands as stabilizers

Multiple types of stabilizing agents were reported for the synthesis of metal NPs[201,202] and can regulate the growth, agglomeration, and physicochemical characteristics in a precise way. These includes polymers, dendrimers, surfactants, ionic liquids, and small molecules.[158] In **Figure 1.16,** various types of stabilizing agents are represented.

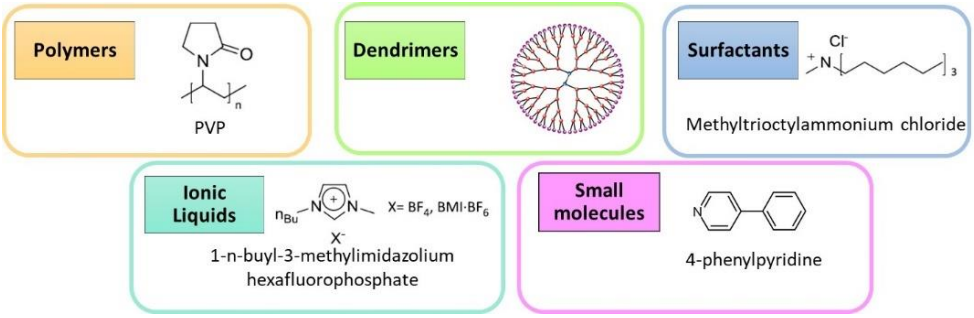

Figure 1.16. Schematic representation of stabilizing agents for NPs used in the literature.

In this context, our group in Tarragona is experienced in the preparation by the *organometallic approach* of colloidal and supported metal nanoparticles (M-NPs) and using organic molecules as stabilizing agents.[203–206] Nanomaterials prepared by this methodology display advantages with respect to materials prepared by classical methods (i.e., wet-impregnation), such as: (a) improved (small) size and shape control, (b) well-defined and more homogeneous compositions, (c) cleaner NP-surfaces, (d) reproducible synthesis under mild reaction conditions (r.t. to 100 °C, and low H_2 pressures, i.e., 1-5 bar), (e) tunable catalytic properties, in some cases controlled by the organic stabilizing agents, and (f) possible one-step preparation of supported monometallic and bimetallic nanoparticles onto porous supports by "in-situ" organometallic complex decomposition.[207]

There are various types of stabilizing ligands according to the donor atom: C-donor,[208] P-donor,[200] S-donor, [209] O-donor, [209] and N-donor ligands.[210]

In this thesis we will focus on the use of C-donor and P-donor ligands. C-donor ligands such as carbene ligands can be rationalized by their σ-donor intrinsic capacity of a sp^2-hybridized lone pair that is available to be donated to a σ-acceptor orbital of the corresponding transition metal. P-donor ligands are strong bases and expected to be σ-donor ligands.[200] Selective coordination of these ligands could modify the steric hindrance at specific sites of the NPs and hence, selectivity. Various P-ligands (i.e., phosphites and phosphines) were used to tune the activity and selectivity of the corresponding nanocatalysts.[206,211]

1.5.2 Synthesis of M-NPs

Generally, NPs synthesis can be carried out by two methodologies: the top-down or the bottom-up approach (**Figure 1.17**). The top-down approach implies mechanical and/or physical methods that decrease the size of a bulk material down to the nanoscale. This can be achieved via simple techniques such as mechanical milling and grinding, but as well through more sophisticated techniques such as laser ablation. This approach introduces structural defects and contaminations and presents the limitation in terms of size control and size distribution.[212,213]

The bottom-up approach involves chemical methods. It starts from atoms through precursor decomposition and ends in bigger nanostructures. It is usually more expensive but in this case, homogeneous particles with controlled size and shape are commonly obtained.[214]

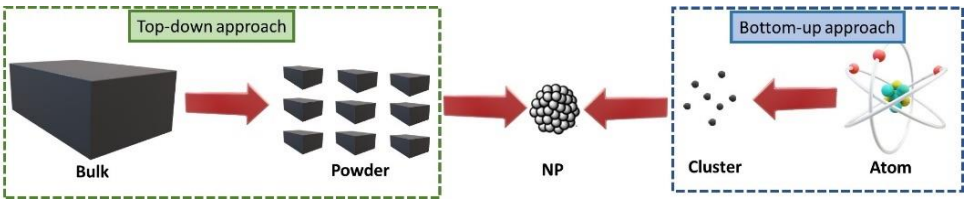

Figure 1.17. Main approaches for the synthesis of M-NPs.

Catalytically active NPs can be synthesized without the presence of a support, giving rise to colloidal NPs, or in presence of a solid support, obtaining supported NPs. Colloidal NPs can be very small and are usually soluble in the reaction media. They present high concentration of metal, facilitating the characterization of the material while supported NPs facilitates the catalyst recyclability and product separation.[215]

Bimetallic NPs have shown also wide applicability especially in the field of catalysis, electrocatalysis, medicine, imaging, etc.[212]

Bimetallic NPs can combine the properties of individual metals but can also exhibit unique properties in terms of electronic, geometric, optical, and even, catalytic.[216,217] Generally, bimetallic NPs are classified according to their structure:

random alloys, core-shell structure, cluster-in-cluster, etc. (**Figure 1.18)**.[174] The final structure will depend on the surface energies of bulk elements and the relative strengths of the metal bond, relative atomic size, and synthetic methodology.

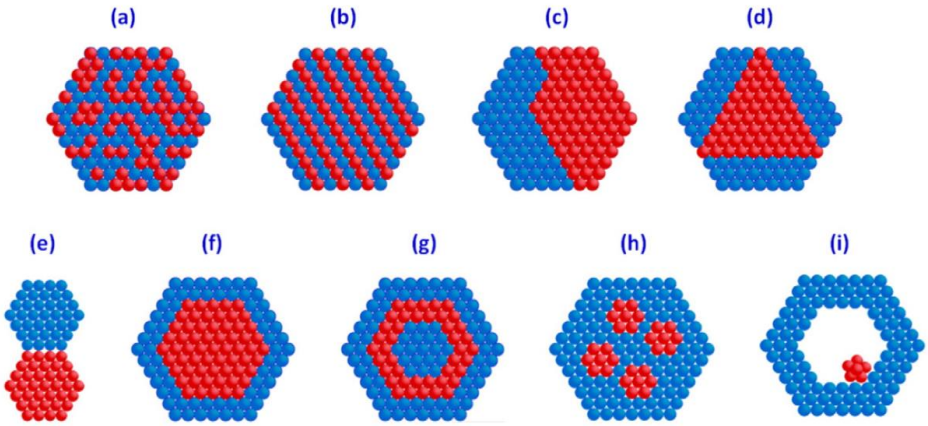

Figure 1.18. Schematic representation of bimetallic NPs (extracted from[174]): (a) mixed alloys; (b) random alloys; subclusters with (c) two interfaces or (d) three interfaces; (e) subcluster with small A-B bonds; (f) core-shell NPs; (g) multishell core-shell NPs; (h) small core materials coated by shell material or (i) movable core within hollow shell material. Based on [218,219].

Immobilization of NPs on supports.

There are different technologies to deposit the NPs on a solid support (**Figure 1.19**). It can be summarized in two main methods: (1) the dispersion of the metal salt precursor by deposition, impregnation, co-precipitation, or adsorption followed by a reductive procedure from the M-NPs,[220] (2) the formation of colloidal NPs, which are subsequently immobilized by grafting or adsorption.[213] This last methodology can be performed in one-pot, meaning that the colloids can be formed in solution where the solid support is also present.

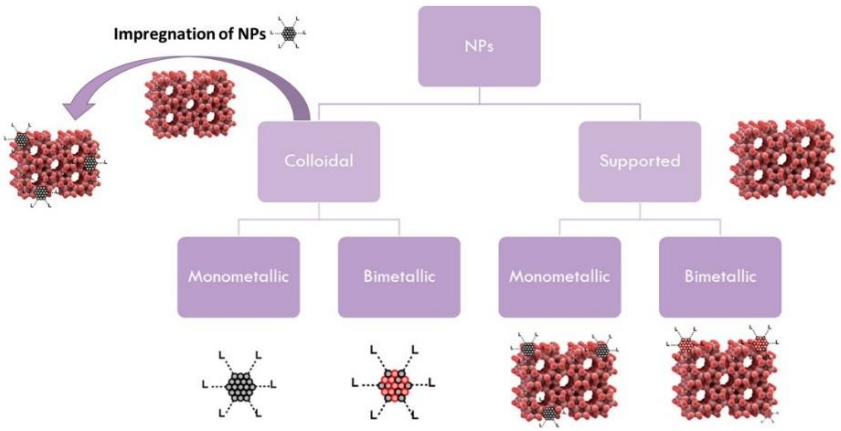

Figure 1.19. Schematic representation of Colloidal NPs and its impregnation and supported NPs.

There is a vast array of synthetic methodologies for the preparation of NPs, such as chemical reduction of transition metal-salts,[221] involving the chemical reduction of a metal salt to a zero-valent naked atom; thermal, photochemical or sonochemical decomposition,[222] (where temperature, light or ultrasound radiation is applied to trigger decomposition of a metal complex); electrochemical reduction, [221] consists in applying a reductive potential to the precursor to cause its decomposition; metal vapor synthesis,[223] (using metal vapors at reduced pressure and condense them at low temperatures). For the preparation of catalysts for propane dehydrogenation, it is noteworthy to mention the following methods: (1) Impregnation and (2) SOMC. Nevertheless, in the present thesis the (3) Organometallic Approach, discovered by Chaudret and coworkers will be studied for the first time in PDH reaction. [207,224]

1.5.2.1 Impregnation methodology

The impregnation methodology is by far the most widely used method to synthesize heterogeneous catalysts. It is popular due to its technical simplicity, limited amount of waste and a low cost.[225] It usually consists of three main steps: (1) the impregnation of a solid support with the corresponding metal precursor; (2) the evaporation of the solvent at high temperatures and (3) reduction of metal precursor (**Figure 1.20**). By capillarity, the solution will be directed into the pores. The maximum loading of metal possible is limited by the solubility of the metal

precursor. There exist two types of impregnations, the wet and the incipient wetness impregnation. The wet impregnation consists in using a higher volume of the metal precursor solution than the total pore volume available in the solid support. Whereas the incipient wetness impregnation volume is exactly the pore volume.[215] However, the impregnation procedures do not lead to the exclusive formation of bimetallic particles, because monometallic phases coexist.[226,227]

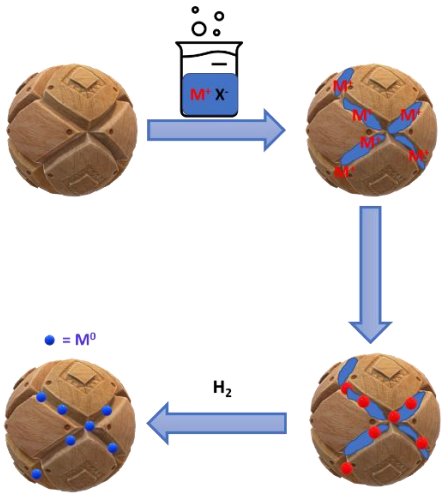

Figure 1.20. Schematic representation of Impregnation methodology.

1.5.2.2 Surface organometallic chemistry (SOMC)

This methodology was pioneered at C2P2-CNRS, Lyon since 1990. Surface Organometallic Chemistry (SOMC) approach is a highly developed area of heterogeneous catalysis.[228] SOMC, with its specific preparation and characterization lead to the obtention of well-defined materials, where the metal sites are introduced by grafting tailored molecular precursors. [229,230] That, can be achieved because all the steps are carefully controlled using the tools of organometallic and coordination chemistry.[230] The key steps of SOMC (**Figure 1.21, a**), consists in (1) Support preparation, where the initial OH density of the solid support is controlled via thermal treatments under vacuum; then (2) grafting of tailored molecular precursors (TMP) to generate the isolated metal sites, usually implying the protonolysis of an anionic ligand of a metal complex (L_nMX_x); then

depending on the post-treatment, single-sites or M-NPs can be obtained. Using SOMC a wide variety of single-sites, supported NPs, isolated metal hydrides or low-coordinate sites can be obtained (**Figure 1.21, b-e**).

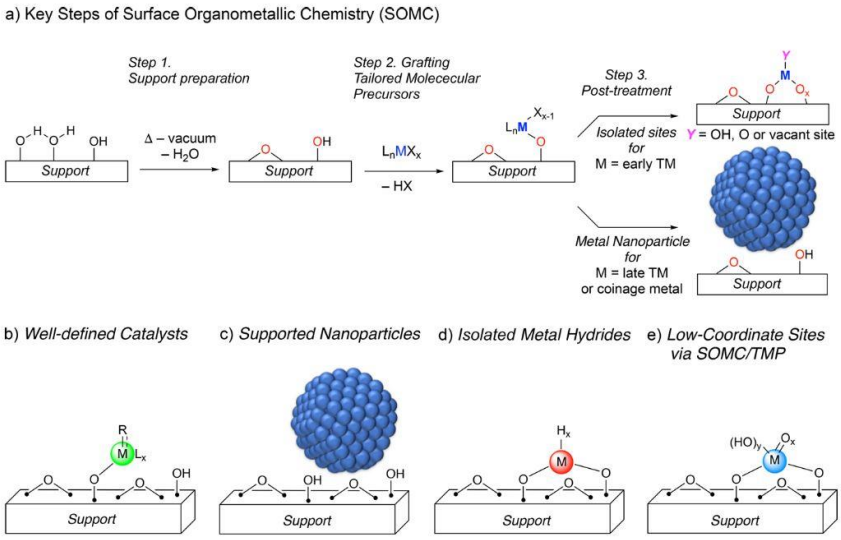

Figure 1.21. General scheme of SOMC. (a) General strategy for the preparation of single-sites or supported NPs. Different supported materials can be obtained such as (b) Well-defined catalysts, (c) Supported NPs, (d) Isolated metal hydrides; or (e) low-coordinate sites via SOMC/TMP.[229]

SOMC catalysts are in a high variety of catalytic reactions as they provide detailed information about the structure of active sites.[229] Basset and co-workers showed that using SOMC, it is possible to generate surface organometallic fragments (SOMFs) or surface coordination fragments (SCFs), which were highly applied in various catalytic mechanisms (**Figure 1.22**).[230]

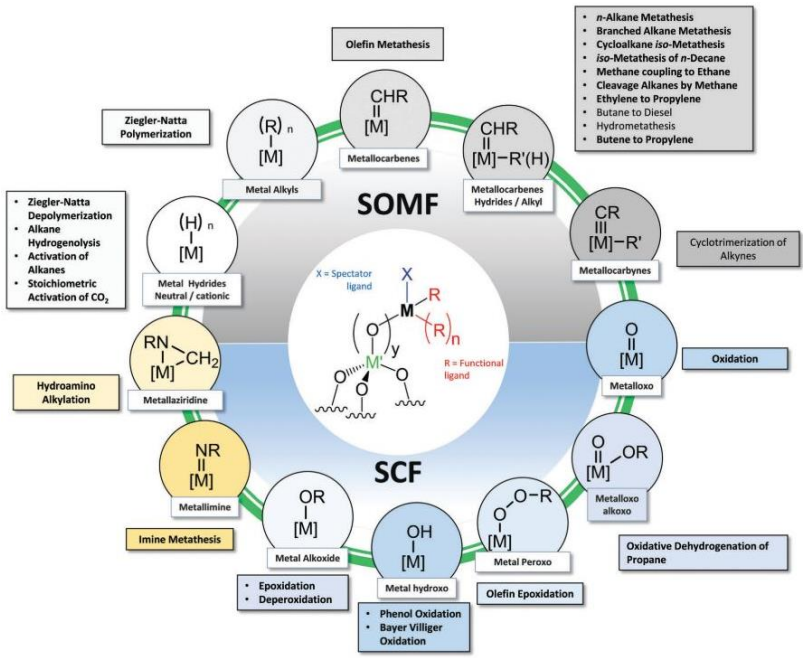

Figure 1.22. SOMF and SCF can be applied in part of reactions for catalytic mechanisms.[230]

SOMC enhances the metal dispersion and can provide homogeneously distributed NPs along a solid oxide support (Al_2O_3, $MgAl_2O_4$, SiO_2 and zeolites).[230,231]

SOMC was used in various applications such as the obtention of 2,3-dimethylbutenes, [232] alkane metathesis (light alkanes, branched and cycloalkanes),[233,234] olefin metathesis,[235] direct oxidative coupling of methane,[233,236] CO_2 conversion with supported metal hydrides,[237] epoxidation of alkenes,[238] Baeyer-Villiger oxidation,[239] phenol oxidation into quinones,[240] and a long etcetera.[230]

1.5.2.3 Organometallic approach (OA)

The organometallic approach (OA) was first reported by Chaudret and co-workers and consists in the decomposition of organometallic precursors (usually zerovalent olefinic metal complexes) under mild conditions in the presence of a reducing gas, usually H_2 or CO (**Figure 1.23**). This approach provides a reproducible methodology

that enables to have a fine control on the size, morphology, and composition of the M-NPs.[207,241]

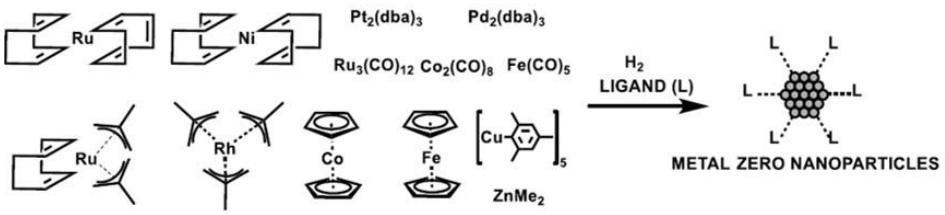

Figure 1.23. Schematic representation of the organometallic approach.

Ideally, the olefinic precursor reacts with dihydrogen to produce an alkane which subsequently will be released creating the naked metallic atoms that will grow to form the NPs with clean and controllable surfaces.[241,242] With this method, it is possible to stabilize the NPs with various types of ligands, which allows to tune their size, shape, and surface environment and consequently their catalytic activity.[243] Chaudret and co-workers also synthesized Ru-NPs protected by weakly coordinating solvents using Ru(COD)(COT) as the organometallic precursor under mild conditions (3 bar H_2). The size and shape of the NPs was influenced by the solvent mixture and the catalytic activity of these NPs was promising in the catalytic hydrogenation of arenes under mild conditions.[224]

The organometallic approach methodology can also be used in the presence of a support to obtain heterogeneous catalysts. This method is thus called one-pot organometallic approach (OPOA). For instance, our group reported the preparation of Ni NPs stabilized by a heterocyclic carbene supported onto carbon nanotubes (CNTs) (Ni-NHC@CNTs) that were used in the semi-hydrogenation of internal alkynes.[204] Bimetallic nanocatalysts NiCu and PdCu stabilized by heterocyclic carbene ligand were supported on CNTs for the selective hydrogenation of alkynes and alkynols, and PdCu/CNTs revealed an efficient catalytic system in the hydrogenation of terminal and internal alkynes.[203] Sala and coworkers reported Ru-

NPs stabilized with 4-phenylpyridime on TiO_2 nanocrystals (Ru@RuO_2PP-TiO_2) for hydrogen evolution using visible light (**Figure 1.24**). [244]

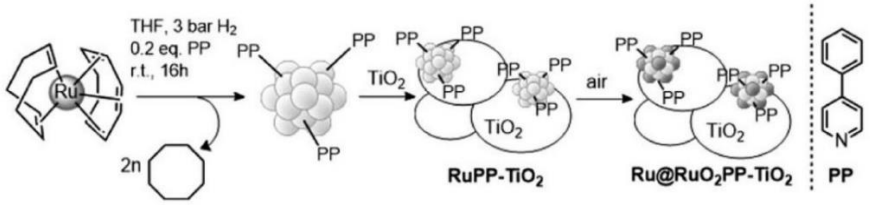

Figure 1.24. Synthesis of Ru@RuO_2PP-TiO_2.[244]

In the present PhD Thesis, metal-based PDH catalysts were synthesized using the SOMC and OPOA synthetic approaches as well as a combination of both. The specific objectives of this thesis are described in Chapter 2.

1.6 References

(1) Ball, D.; W Hill, J.; J Scott, R. *The Basics of General, Organic, and Biological Chemistry*; Saylor Foundation, 2011; Vol. 4.

(2) *Propylene Glycol Market Overview, New Opportunities & SWOT Analysis by 2025*; 2019.

(3) Chen, S.; Chang, X.; Sun, G.; Zhang, T.; Xu, Y.; Wang, Y.; Pei, C.; Gong, J. Propane Dehydrogenation: Catalyst Development, New Chemistry, and Emerging Technologies. *Chem. Soc. Rev.* **2021**, *50* (5), 3315–3354. https://doi.org/10.1039/D0CS00814A.

(4) Lavrenov, A. V; Saifulina, L. F.; Buluchevskii, E. A.; Bogdanets, E. N. Propylene Production Technology: Today and Tomorrow. *Catal. Ind.* **2015**, *7* (3), 175–187. https://doi.org/10.1134/S2070050415030083.

(5) Feng, B.; Wei, Y. C.; Song, W. Y.; Xu, C. M. A Review on the Structure-Performance Relationship of the Catalysts during Propane Dehydrogenation Reaction. *Pet. Sci.* **2021**. https://doi.org/10.1016/J.PETSCI.2021.09.015.

(6) Agency, I. E. CO2 emmisions from fuel combustion https://webstore.iea.org/download/direct/2505?fileName=CO2_Emissions_from_Fuel_Combustion_2019_Overview.pdf.

(7) National Academies of Sciences, E. M.; Studies, D. E. L.; Technology, B. C. S.; Alper, J. *The Changing Landscape of Hydrocarbon Feedstocks for Chemical Production: Implications for Catalysis: Proceedings of a Workshop*; National Academies Press, 2016.

(8) Elvidge, C. D.; Bazilian, M. D.; Zhizhin, M.; Ghosh, T.; Baugh, K.; Hsu, F. The Potential Role of Natural Gas Fl Aring in Meeting Greenhouse Gas Mitigation Targets. *Energy Strateg. Rev.* **2018**, *20*, 156–162. https://doi.org/10.1016/j.esr.2017.12.012.

(9) Weissermel, K.; Arpe, H. J.; Lindley, C. R.; Hawkins, S. *Industrial Organic Chemistry*; Wiley-

VCH, 2003.

(10) Zhong, J.; Han, J.; Wei, Y.; Tian, P.; Guo, X.; Song, C.; Liu, Z. Recent Advances of the Nano-Hierarchical SAPO-34 in the Methanol-to-Olefin (MTO) Reaction and Other Applications. *Catal. Sci. Technol.* **2017**, 4905–4923. https://doi.org/10.1039/c7cy01466j.

(11) Yarulina, I.; Wispelaere, K. De; Bailleul, S.; Goetze, J.; Radersma, M.; Abou-hamad, E.; Vollmer, I.; Goesten, M.; Mezari, B.; Hensen, E. J. M.; Martínez-espín, J. S.; Morten, M.; Mitchell, S.; Perez-ramirez, J.; Olsbye, U.; Weckhuysen, B. M.; Speybroeck, V. Van; Kapteijn, F.; Gascon, J. Structure-Performance Descriptors and the Role of Lewis Acidity in the Methanol-to-Propylene Process. *Nat. Chem.* **2018**, *10*, 804–812. https://doi.org/10.1038/s41557-018-0081-0.

(12) Munnik, P.; Jongh, P. E. De; Jong, K. P. De. Control and Impact of the Nanoscale Distribution of Supported Cobalt Particles Used in Fischer − Tropsch Catalysis. *J. Am. Chem. Soc.* **2014**, *136*, 7333–7340.

(13) Saib, A. M.; Weststrate, C. J.; Niemantsverdriet, J. W. Providing Fundamental and Applied Insights into Fischer − Tropsch Catalysis: Sasol − Eindhoven University of Technology Collaboration. *ACS Catal.* **2016**, *6*, 3840–3855. https://doi.org/10.1021/acscatal.6b00595.

(14) Sattler, J. J. H. B.; Ruiz-Martinez, J.; Santillan-Jimenez, E.; Weckhuysen, B. M. Catalytic Dehydrogenation of Light Alkanes on Metals and Metal Oxides. *Chem. Rev.* **2014**, *114* (20), 10613–10653. https://doi.org/10.1021/cr5002436.

(15) Nawaz, Z. Light Alkane Dehydrogenation to Light Olefin Technologies: A Comprehensive Review. *Rev. Chem. Eng.* **2015**, *31* (5), 413–436. https://doi.org/10.1515/revce-2015-0012.

(16) Al-Zahrani, Abdulrahim, Lachezar, Petrov, Daous, Mohammad, Umar Mohammad, Al-Hazml, Mohammed, Al-hamed, Y. Alkane Dehydrogenation Catalyst and Process for Its Preparation. WO2014016810A1, 2014.

(17) Wang, G.; Zhu, X.; Li, C. Recent Progress in Commercial and Novel Catalysts for Catalytic Dehydrogenation of Light Alkanes. *Chem. Rec.* **2020**, *20* (6), 604–616. https://doi.org/https://doi.org/10.1002/tcr.201900090.

(18) Melott, A. L. Le Châtelier's Principle. *J. Chem. Educ.* **1968**, *45* (6), A519. https://doi.org/10.1021/ed045pA519.2.

(19) Descorme, C.; Gallezot, P.; Geantet, C.; George, C. Heterogeneous Catalysis : A Key Tool toward Sustainability. *ChemCatChem* **2012**, *4*, 1897–1906. https://doi.org/10.1002/cctc.201200483.

(20) Chen, S.; Chang, X.; Sun, G.; Zhang, T.; Xu, Y.; Wang, Y.; Pei, C.; Gong, J. Propane Dehydrogenation: Catalyst Development, New Chemistry, and Emerging Technologies. *Chem. Soc. Rev.* **2021**, *50* (5), 3315–3354. https://doi.org/10.1039/d0cs00814a.

(21) Perego, C.; Peratello, S. Experimental Methods in Catalytic Kinetics. *Catal. Today* **1999**, *52*, 133–145.

(22) Gómez-Quero, S.; Tsoufis, T.; Rudolf, P.; Makkee, M.; Kapteijn, F.; Rothenberg, G. Kinetics of Propane Dehydrogenation over Pt–Sn/Al2O3. *Catal. Sci. Technol.* **2013**, *3* (4), 962–971. https://doi.org/10.1039/C2CY20488F.

(23) Rochlitz, L.; Searles, K.; Alfke, J.; Zemlyanov, D.; Safonova, O. V.; Copéret, C. Silica-

Supported, Narrowly Distributed, Subnanometric Pt-Zn Particles from Single Sites with High Propane Dehydrogenation Performance. *Chem. Sci.* **2020**, *11* (6), 1549–1555. https://doi.org/10.1039/c9sc05599a.

(24) Wu, Z.; Bukowski, B. C.; Li, Z.; Milligan, C.; Zhou, L.; Ma, T.; Wu, Y.; Ren, Y.; Ribeiro, F. H.; Delgass, W. N.; Greeley, J.; Zhang, G.; Miller, J. T. Changes in Catalytic and Adsorptive Properties of 2 Nm Pt3Mn Nanoparticles by Subsurface Atoms. *J. Am. Chem. Soc.* **2018**, *140* (44), 14870–14877. https://doi.org/10.1021/jacs.8b08162.

(25) LiBretto, N. J.; Yang, C.; Ren, Y.; Zhang, G.; Miller, J. T. Identification of Surface Structures in Pt3Cr Intermetallic Nanocatalysts. *Chem. Mater.* **2019**, *31* (5), 1597–1609. https://doi.org/10.1021/acs.chemmater.8b04774.

(26) Cesar, L. G.; Yang, C.; Lu, Z.; Ren, Y.; Zhang, G.; Miller, J. T. Identification of a Pt3Co Surface Intermetallic Alloy in Pt–Co Propane Dehydrogenation Catalysts. *ACS Catal.* **2019**, *9* (6), 5231–5244. https://doi.org/10.1021/acscatal.9b00549.

(27) Bauer, T.; Maisel, S.; Blaumeiser, D.; Vecchietti, J.; Taccardi, N.; Wasserscheid, P.; Bonivardi, A.; Görling, A.; Libuda, J. Operando DRIFTS and DFT Study of Propane Dehydrogenation over Solid- and Liquid-Supported GaxPty Catalysts. *ACS Catal.* **2019**, *9* (4), 2842–2853. https://doi.org/10.1021/acscatal.8b04578.

(28) Deng, L.; Miura, H.; Shishido, T.; Wang, Z.; Hosokawa, S.; Teramura, K.; Tanaka, T. Elucidating Strong Metal-Support Interactions in Pt–Sn/SiO2 Catalyst and Its Consequences for Dehydrogenation of Lower Alkanes. *J. Catal.* **2018**, *365*, 277–291. https://doi.org/10.1016/j.jcat.2018.06.028.

(29) Sun, P.; Siddiqi, G.; Vining, W. C.; Chi, M.; Bell, A. T. Novel Pt/Mg(In)(Al)O Catalysts for Ethane and Propane Dehydrogenation. *J. Catal.* **2011**, *282* (1), 165–174. https://doi.org/10.1016/j.jcat.2011.06.008.

(30) Siddiqi, G.; Sun, P.; Galvita, V.; Bell, A. T. Catalyst Performance of Novel Pt/Mg(Ga)(Al)O Catalysts for Alkane Dehydrogenation. *J. Catal.* **2010**, *274* (2), 200–206. https://doi.org/10.1016/j.jcat.2010.06.016.

(31) Zhang, Y.; Zhou, Y.; Shi, J.; Zhou, S.; Sheng, X.; Zhang, Z.; Xiang, S. Comparative Study of Bimetallic Pt-Sn Catalysts Supported on Different Supports for Propane Dehydrogenation. *J. Mol. Catal. A Chem.* **2014**, *381*, 138–147. https://doi.org/10.1016/j.molcata.2013.10.007.

(32) Duan, Y.; Zhou, Y.; Zhang, Y.; Sheng, X.; Xue, M. Effect of Sodium Addition to PtSn/AlSBA-15 on the Catalytic Properties in Propane Dehydrogenation. *Catal. Letters* **2011**, *141* (1), 120–127. https://doi.org/10.1007/s10562-010-0445-6.

(33) Vu, B. K.; Song, M. B.; Ahn, I. Y.; Suh, Y. W.; Suh, D. J.; Kim, W. Il; Koh, H. L.; Choi, Y. G.; Shin, E. W. Pt-Sn Alloy Phases and Coke Mobility over Pt-Sn/Al2O3 and Pt-Sn/ZnAl2O4 Catalysts for Propane Dehydrogenation. *Appl. Catal. A Gen.* **2011**, *400* (1–2), 25–33. https://doi.org/10.1016/j.apcata.2011.03.057.

(34) Zhu, H.; Anjum, D. H.; Wang, Q.; Abou-Hamad, E.; Emsley, L.; Dong, H.; Laveille, P.; Li, L.; Samal, A. K.; Basset, J.-M. Sn Surface-Enriched Pt-Sn Bimetallic Nanoparticles as a Selective and Stable Catalyst for Propane Dehydrogenation. *J. Catal.* **2014**, *320*, 52–62. https://doi.org/10.1016/j.jcat.2014.09.013 CO - JCTLA5.

(35) Zhang, Y.; Zhou, Y.; Huang, L.; Xue, M.; Zhang, S. Sn-Modified ZSM-5 As Support for Platinum Catalyst in Propane Dehydrogenation. *Ind. Eng. Chem. Res.* **2011**, *50* (13), 7896–

7902. https://doi.org/10.1021/ie1024694.

(36) Zhang, Y.; Zhou, Y.; Huang, L.; Zhou, S.; Sheng, X.; Wang, Q.; Zhang, C. Structure and Catalytic Properties of the Zn-Modified ZSM-5 Supported Platinum Catalyst for Propane Dehydrogenation. *Chem. Eng. J.* **2015**, *270*, 352–361. https://doi.org/10.1016/j.cej.2015.01.008.

(37) Xia, K.; Lang, W. Z.; Li, P. P.; Long, L. L.; Yan, X.; Guo, Y. J. The Influences of Mg/Al Molar Ratio on the Properties of PtIn/Mg(Al)O-x Catalysts for Propane Dehydrogenation Reaction. *Chem. Eng. J.* **2016**, *284*, 1068–1079. https://doi.org/10.1016/j.cej.2015.09.046.

(38) Belskaya, O. B.; Stepanova, L. N.; Gulyaeva, T. I.; Erenburg, S. B.; Trubina, S. V.; Kvashnina, K.; Nizovskii, A. I.; Kalinkin, A. V.; Zaikovskii, V. I.; Bukhtiyarov, V. I.; Likholobov, V. A. Zinc Influence on the Formation and Properties of Pt/Mg(Zn)AlOx Catalysts Synthesized from Layered Hydroxides. *J. Catal.* **2016**, *341*, 13–23. https://doi.org/10.1016/j.jcat.2016.06.006.

(39) Xiong, H.; Lin, S.; Goetze, J.; Pletcher, P.; Guo, H.; Kovarik, L.; Artyushkova, K.; Weckhuysen, B. M.; Datye, A. K. Thermally Stable and Regenerable Platinum–Tin Clusters for Propane Dehydrogenation Prepared by Atom Trapping on Ceria. *Angew. Chemie - Int. Ed.* **2017**, *56* (31), 8986–8991. https://doi.org/10.1002/anie.201701115.

(40) Im, J.; Choi, M. Physicochemical Stabilization of Pt against Sintering for a Dehydrogenation Catalyst with High Activity, Selectivity, and Durability. *ACS Catal.* **2016**, *6* (5), 2819–2826. https://doi.org/10.1021/acscatal.6b00329.

(41) Zhu, Y.; An, Z.; Song, H.; Xiang, X.; Yan, W.; He, J. Lattice-Confined Sn (IV/II) Stabilizing Raft-like Pt Clusters: High Selectivity and Durability in Propane Dehydrogenation. *ACS Catal.* **2017**, *7* (10), 6973–6978. https://doi.org/10.1021/acscatal.7b02264.

(42) Redekop, E. A.; Galvita, V. V.; Poelman, H.; Bliznuk, V.; Detavernier, C.; Marin, G. B. Delivering a Modifying Element to Metal Nanoparticles via Support: Pt-Ga Alloying during the Reduction of Pt/Mg(Al,Ga)Ox Catalysts and Its Effects on Propane Dehydrogenation. *ACS Catal.* **2014**, *4* (6), 1812–1824. https://doi.org/10.1021/cs500415e.

(43) Wu, J.; Mallikarjun Sharada, S.; Ho, C.; Hauser, A. W.; Head-Gordon, M.; Bell, A. T. Ethane and Propane Dehydrogenation over PtIr/Mg(Al)O. *Appl. Catal. A Gen.* **2015**, *506*, 25–32. https://doi.org/10.1016/j.apcata.2015.08.029.

(44) Li, B.; Xu, Z.; Chu, W.; Luo, S.; Jing, F. Ordered Mesoporous Sn-SBA-15 as Support for Pt Catalyst with Enhanced Performance in Propane Dehydrogenation. *Cuihua Xuebao/Chinese J. Catal.* **2017**, *38* (4), 726–735. https://doi.org/10.1016/S1872-2067(17)62805-5.

(45) Searles, K.; Chan, K. W.; Mendes Burak, J. A.; Zemlyanov, D.; Safonova, O.; Copéret, C.; Keith Searles,† Ka Wing Chan,† Jorge Augusto Mendes Burak,† Dmitry Zemlyanov, O. S.; and Christophe Copéret*. Highly Productive Propane Dehydrogenation Catalyst Using Silica-Supported Ga-Pt Nanoparticles Generated from Single-Sites. *J. Am. Chem. Soc.* **2018**, *140* (37), 11674–11679. https://doi.org/10.1021/jacs.8b05378.

(46) Zhang, Y.; Zhou, Y.; Tang, M.; Liu, X.; Duan, Y. Effect of La Calcination Temperature on Catalytic Performance of PtSnNaLa/ZSM-5 Catalyst for Propane Dehydrogenation. *Chem. Eng. J.* **2012**, *181–182*, 530–537. https://doi.org/10.1016/j.cej.2011.11.055.

(47) Xue, M.; Zhou, Y.; Zhang, Y.; Liu, X.; Duan, Y.; Sheng, X. Effect of Cerium Addition on Catalytic Performance of PtSnNa/ZSM-5 Catalyst for Propane Dehydrogenation. *J. Nat. Gas Chem.* **2012**, *21* (3), 324–331. https://doi.org/10.1016/S1003-9953(11)60372-1.

(48) Nawaz, Z.; Baksh, F.; Zhu, J.; Wei, F. Dehydrogenation of C3-C4 Paraffin's to Corresponding Olefins over Slit-SAPO-34 Supported Pt-Sn-Based Novel Catalyst. *J. Ind. Eng. Chem.* **2013**, *19* (2), 540–546. https://doi.org/10.1016/j.jiec.2012.09.024.

(49) Zhang, Y.; Zhou, Y.; Shi, J.; Zhou, S.; Zhang, Z.; Zhang, S.; Guo, M. Propane Dehydrogenation over PtSnNa/La-Doped Al2O3 Catalyst: Effect of La Content. *Fuel Process. Technol.* **2013**, *111*, 94–104. https://doi.org/10.1016/j.fuproc.2013.02.001.

(50) Jang, E. J.; Lee, J.; Jeong, H. Y.; Kwak, J. H. Controlling the Acid-Base Properties of Alumina for Stable PtSn-Based Propane Dehydrogenation Catalysts. *Appl. Catal. A Gen.* **2019**, *572* (October 2018), 1–8. https://doi.org/10.1016/j.apcata.2018.12.024.

(51) Xu, Z.; Yue, Y.; Bao, X.; Xie, Z.; Zhu, H. Propane Dehydrogenation over Pt Clusters Localized at the Sn Single-Site in Zeolite Framework. *ACS Catal.* **2020**, *10* (1), 818–828. https://doi.org/10.1021/acscatal.9b03527.

(52) Mironenko, R. M.; Belskaya, O. B.; Talsi, V. P.; Gulyaeva, T. I.; Kazakov, M. O.; Nizovskii, A. I.; Kalinkin, A. V.; Bukhtiyarov, V. I.; Lavrenov, A. V.; Likholobov, V. A. Effect of γ-Al2O3 Hydrothermal Treatment on the Formation and Properties of Platinum Sites in Pt/γ-Al2O 3 Catalysts. *Appl. Catal. A Gen.* **2014**, *469*, 472–482. https://doi.org/10.1016/j.apcata.2013.10.027.

(53) Im, J.; Shin, H.; Jang, H.; Kim, H.; Choi, M. Maximizing the Catalytic Function of Hydrogen Spillover in Platinum-Encapsulated Aluminosilicates with Controlled Nanostructures. *Nat. Commun.* **2014**, *5*. https://doi.org/10.1038/ncomms4370.

(54) Liu, J.; Yue, Y.; Liu, H.; Da, Z.; Liu, C.; Ma, A.; Rong, J.; Su, D.; Bao, X.; Zheng, H. Origin of the Robust Catalytic Performance of Nanodiamond-Graphene-Supported Pt Nanoparticles Used in the Propane Dehydrogenation Reaction. *ACS Catal.* **2017**, *7* (5), 3349–3355. https://doi.org/10.1021/acscatal.6b03452.

(55) Liu, J.; Li, J.; Rong, J.; Liu, C.; Dai, Z.; Bao, J.; Da, Z.; Zheng, H. Defect-Driven Unique Stability of Pt/Carbon Nanotubes for Propane Dehydrogenation. *Appl. Surf. Sci.* **2019**, *464*, 146–152. https://doi.org/10.1016/j.apsusc.2018.08.260.

(56) Shi, L.; Deng, G. M.; Li, W. C.; Miao, S.; Wang, Q. N.; Zhang, W. P.; Lu, A. H. Al2O3 Nanosheets Rich in Pentacoordinate Al3+ Ions Stabilize Pt-Sn Clusters for Propane Dehydrogenation. *Angew. Chemie - Int. Ed.* **2015**, *54* (47), 13994–13998. https://doi.org/10.1002/anie.201507119.

(57) Horiuti, I.; Polanyi, M. Exchange Reactions of Hydrogen on Metallic Catalysts. *Trans. Faraday Soc.* **1934**, *30*, 1164–1172.

(58) Lian, Z.; Ali, S.; Liu, T.; Si, C.; Li, B.; Su, D. S. Revealing the Janus Character of the Coke Precursor in the Propane Direct Dehydrogenation on Pt Catalysts from a KMC Simulation. *ACS Catal.* **2018**, *8* (5), 4694–4704. https://doi.org/10.1021/acscatal.8b00107.

(59) Yang, M. L.; Zhu, Y. A.; Fan, C.; Sui, Z. J.; Chen, D.; Zhou, X. G. Density Functional Study of the Chemisorption of C1, C2 and C3 Intermediates in Propane Dissociation on Pt(1 1 1). *J. Mol. Catal. A Chem.* **2010**, *321* (1–2), 42–49. https://doi.org/10.1016/j.molcata.2010.01.017.

(60) Lian, Z.; Ali, S.; Liu, T.; Si, C.; Li, B.; Su, D. S. Revealing the Janus Character of the Coke Precursor in the Propane Direct Dehydrogenation on Pt Catalysts from a KMC Simulation. *ACS Catal.* **2018**, *8*, 4694–4705. https://doi.org/10.1021/acscatal.8b00107.

(61) Liu, S.; Zhang, B.; Liu, G. Metal-Based Catalysts for the Non-Oxidative Dehydrogenation of Light Alkanes to Light Olefins. *React. Chem. Eng.* **2021**, 9–26. https://doi.org/10.1039/d0re00381f.

(62) Hu, Z.; Yang, D.; Wang, Z.; Yuan, Z. State-of-the-Art Catalysts for Direct Dehydrogenation of Propane to Propylene. *Chinese J. Catal.* **2019**, *40* (9), 1233–1254. https://doi.org/10.1016/S1872-2067(19)63360-7.

(63) Serrano-Ruiz, J. C.; Sepúlveda-Escribano, A.; Rodríguez-Reinoso, F. Bimetallic PtSn/C Catalysts Promoted by Ceria: Application in the Nonoxidative Dehydrogenation of Isobutane. *J. Catal.* **2007**, *246* (1), 158–165. https://doi.org/10.1016/j.jcat.2006.12.004.

(64) Huš, M.; Kopač, D.; Likozar, B. Kinetics of Non-Oxidative Propane Dehydrogenation on Cr2O3 and the Nature of Catalyst Deactivation from First-Principles Simulations. *J. Catal.* **2020**, *386*, 126–138. https://doi.org/10.1016/j.jcat.2020.03.037.

(65) Zhao, Z. J.; Chiu, C. C.; Gong, J. Molecular Understandings on the Activation of Light Hydrocarbons over Heterogeneous Catalysts. *Chem. Sci.* **2015**, *6* (8), 4403–4425. https://doi.org/10.1039/c5sc01227a.

(66) Larsson, M.; Hulten, M.; Blekkan, E. A.; Andersson, B. The Effect of Reaction Conditions and Time on Stream on the Coke Formed during Propane Dehydrogenation. *J. Catal.* **1997**, *164*, 44–53.

(67) Valcárcel, A.; Ricart, J. M.; Clotet, A.; Illas, F.; Markovits, A.; Minot, C. Theoretical Study of Dehydrogenation and Isomerisation Reactions of Propylene on Pt(111). *J. Catal.* **2006**, *241* (1), 115–122. https://doi.org/10.1016/j.jcat.2006.04.022.

(68) Saerens, S.; Sabbe, M. K.; Galvita, V. V.; Redekop, E. A.; Reyniers, M. F.; Marin, G. B. The Positive Role of Hydrogen on the Dehydrogenation of Propane on Pt(111). *ACS Catal.* **2017**, *7* (11), 7495–7508. https://doi.org/10.1021/acscatal.7b01584.

(69) Zhu, J.; Yang, M. L.; Yu, Y.; Zhu, Y. A.; Sui, Z. J.; Zhou, X. G.; Holmen, A.; Chen, D. Size-Dependent Reaction Mechanism and Kinetics for Propane Dehydrogenation over Pt Catalysts. *ACS Catal.* **2015**, *5* (11), 6310–6319. https://doi.org/10.1021/acscatal.5b01423.

(70) Nykänen, L.; Honkala, K. Selectivity in Propene Dehydrogenation on Pt and Pt3Sn Surfaces from First Principles. *ACS Catal.* **2013**, *3* (12), 3026–3030. https://doi.org/10.1021/cs400566y.

(71) Li, Q.; Sui, Z.; Zhou, X.; Zhu, Y.; Zhou, J.; Chen, D. Coke Formation on Pt-Sn/Al2O3 Catalyst in Propane Dehydrogenation: Coke Characterization and Kinetic Study. *Top. Catal.* **2011**, *54* (13–15), 888–896. https://doi.org/10.1007/s11244-011-9708-8.

(72) Bitter, J. H.; Seshan, K.; Lercher, J. A. Deactivation and Coke Accumulation during CO2/CH4 Reforming over Pt Catalysts. *J. Catal.* **1999**, *183* (2), 336–343. https://doi.org/10.1006/jcat.1999.2402.

(73) Hansen, T. W.; Delariva, A. T.; Challa, S. R.; Datye, A. K. Sintering of Catalytic Nanoparticles: Particle Migration or Ostwald Ripening? *Acc. Chem. Res.* **2013**, *46* (8), 1720–1730. https://doi.org/10.1021/ar3002427.

(74) Kim, G. H.; Jung, K. D.; Kim, W. Il; Um, B. H.; Shin, C. H.; Oh, K.; Koh, H. L. Effect of Oxychlorination Treatment on the Regeneration of Pt-Sn/Al2O3 Catalyst for Propane Dehydrogenation. *Res. Chem. Intermed.* **2016**, *42* (1), 351–365.

https://doi.org/10.1007/s11164-015-2300-2.

(75) Uemura, Y.; Inada, Y.; Bando, K. K.; Sasaki, T.; Kamiuchi, N.; Eguchi, K.; Yagishita, A.; Nomura, M.; Tada, M.; Iwasawa, Y. Core-Shell Phase Separation and Structural Transformation of Pt 3Sn Alloy Nanoparticles Supported on γ-Al2O 3 in the Reduction and Oxidation Processes Characterized by in Situ Time-Resolved XAFS. *J. Phys. Chem. C* **2011**, *115* (13), 5823–5833. https://doi.org/10.1021/jp111286b.

(76) Han, Z.; Li, S.; Jiang, F.; Wang, T.; Ma, X.; Gong, J. Propane Dehydrogenation over Pt – Cu Bimetallic Catalysts : The Nature of Coke Deposition and the Role of Copper. *Nanoscale* **2014**, *6*, 10000. https://doi.org/10.1039/c4nr02143f.

(77) Wu, Z.; Wegener, E. C.; Tseng, H.; Gallagher, J. R.; Harris, J. W.; Diaz, R. E.; Ren, Y.; Ribeiro, F. H.; Miller, J. T. Pd–In Intermetallic Alloy Nanoparticles : Highly Selective Ethane Dehydrogenation Catalysts. *Catal. Sci. Technol.* **2016**, *6*, 6965–6976. https://doi.org/10.1039/c6cy00491a.

(78) Cybulskis, V. J.; Bukowski, B. C.; Tseng, H.-T.; Gallagher, J. R.; Wu, Z.; Wegener, E.; Kropf, A. J.; Ravel, B.; Ribeiro, F. H.; Greeley, J.; Miller, J. T. Zinc Promotion of Platinum for Catalytic Light Alkane Dehydrogenation: Insights into Geometric and Electronic Effects. *ACS Catal.* **2017**, *7* (6), 4173–4181. https://doi.org/10.1021/acscatal.6b03603.

(79) Feng Jiang, Liang Zeng, Shuirong Li, Gang Liu, Shengping Wang, and J. G. Propane Dehydrogenation over Pt/TiO2-Al2O3 Catalysts. *ACS Catal.* **2014**, *5*, 438–447.

(80) Chen, M.; Xu, J.; Cao, Y.; He, H.; Fan, K.; Zhuang, J. Dehydrogenation of Propane over In2O3–Al2O3 Mixed Oxide in the Presence of Carbon Dioxide. *J. Catal.* **2010**, *272* (1), 101–108. https://doi.org/10.1016/j.jcat.2010.03.007.

(81) Gomez, E.; Yan, B.; Kattel, S.; Chen, J. G. Carbon Dioxide Reduction in Tandem with Light-Alkane Dehydrogenation. *Nat. Rev. Chem.* **2019**, *3* (11), 638–649. https://doi.org/10.1038/s41570-019-0128-9.

(82) Wikipedia. Boudard reaction https://en.wikipedia.org/wiki/Boudouard_reaction#cite_note-1 (accessed May 13, 2022).

(83) Jiang, F.; Zeng, L.; Li, S.; Liu, G.; Wang, S.; Gong, J. Propane Dehydrogenation over Pt / TiO2 – Al2O3 Catalysts. *ACS Catal.* **2015**.

(84) Li, Z.; Yu, L.; Milligan, C.; Ma, T.; Zhou, L.; Cui, Y.; Qi, Z.; Libretto, N.; Xu, B.; Luo, J.; Shi, E.; Wu, Z.; Xin, H.; Delgass, W. N.; Miller, J. T.; Wu, Y. Two-Dimensional Transition Metal Carbides as Supports for Tuning the Chemistry of Catalytic Nanoparticles. *Nat. Commun.* **2018**, *9* (1), 5258. https://doi.org/10.1038/s41467-018-07502-5.

(85) Cai, W.; Mu, R.; Zha, S.; Sun, G.; Chen, S.; Zhao, Z.; Tian, H.; Tang, Y.; Tao, F. (Feng); Zeng, L.; Gong, J. Subsurface Catalysis-Mediated Selectivity of Dehydrogenation Reaction. *Sci. Adv.* **2018**, *4*, 1–9.

(86) Joo, S. H.; Park, J. Y.; Tsung, C.; Yamada, Y.; Yang, P.; Somorjai, G. A. Thermally Stable Pt/Mesoporous Silica Core-Shell Nanocatalysts for High-Temperature Reactions. *Nat. Mater.* **2008**, *8* (2), 126–131. https://doi.org/10.1038/nmat2329.

(87) Liu, L.; Lopez-haro, M.; Lopes, C. W.; Rojas-buzo, S.; Concepcion, P.; Manzorro, R.; Simonelli, L.; Sattler, A.; Serna, P.; Calvino, J. J.; Corma, A. Structural Modulation and Direct Measurement of Subnanometric Bimetallic PtSn Clusters Confined in Zeolites. *Nat. Catal.*

2020, *3*, 628–638. https://doi.org/10.1038/s41929-020-0472-7.

(88) Liu, L.; Lopez-haro, M.; Lopes, C. W.; Li, C.; Concepcion, P.; Simonelli, L.; Calvino, J. J.; Corma, A. Regioselective Generation and Reactivity Control of Subnanometric Platinum Clusters in Zeolites for High-Temperature Catalysis. *Nat. Mater.* **2019**, *18*, 866–873. https://doi.org/10.1038/s41563-019-0412-6.

(89) Nawaz, Z. Light Alkane Dehydrogenation to Light Olefin Technologies: A Comprehensive Review. *Rev. Chem. Eng.* **2015**, *31* (5), 413–436. https://doi.org/doi:10.1515/revce-2015-0012.

(90) Monai, M.; Gambino, M.; Weckhuysen, B. M. Propane to Olefins Tandem Catalysis : A Selective Route towards Light Olefins Production. *Chem. Soc. Rev.* **2021**, *50*, 11503–11529. https://doi.org/10.1039/d1cs00357g.

(91) Bhasin, M. M.; Mccain, J. H.; Vora, B. V; Imai, T.; Pujado, P. R. Dehydrogenation and Oxydehydrogenation of Paraffins to Olefins. *Appl. Catal. A Gen.* **2001**, *221*, 397–419.

(92) Council, A. C. *Shale Gas, Competitiveness, and New US Chemical Industry Investment: An Analysis Based on Annouced Projects*; 2013; Vol. 6.

(93) Chen, K.; Bell, A. T.; Iglesia, E. The Relationship between the Electronic and Redox Properties of Dispersed Metal Oxides and Their Turnover Rates in Oxidative Dehydrogenation Reactions. *J. Catal.* **2002**, *209* (1), 35–42. https://doi.org/10.1006/jcat.2002.3620.

(94) Latimer, A. A.; Kulkarni, A. R.; Aljama, H.; Montoya, J. H.; Yoo, J. S.; Tsai, C.; Abild-Pedersen, F.; Studt, F.; Nørskov, J. K. Understanding Trends in C-H Bond Activation in Heterogeneous Catalysis. *Nat. Mater.* **2017**, *16* (2), 225–229. https://doi.org/10.1038/nmat4760.

(95) Zeng, L.; Cheng, Z.; Fan, J. A.; Fan, L. S.; Gong, J. Metal Oxide Redox Chemistry for Chemical Looping Processes. *Nat. Rev. Chem.* **2018**, *2* (11), 349–364. https://doi.org/10.1038/s41570-018-0046-2.

(96) Bocanegra, S. A.; Castro, A. A.; Guerrero-Ruíz, A.; Scelza, O. A.; de Miguel, S. R. Characteristics of the Metallic Phase of Pt/Al2O3 and Na-Doped Pt/Al2O3 Catalysts for Light Paraffins Dehydrogenation. *Chem. Eng. J.* **2006**, *118* (3), 161–166. https://doi.org/10.1016/j.cej.2006.02.004.

(97) Zhu, Y.; Kong, X.; Yin, J.; You, R.; Zhang, B.; Zheng, H.; Wen, X.; Zhu, Y.; Li, Y. W. Covalent-Bonding to Irreducible SiO2 Leads to High-Loading and Atomically Dispersed Metal Catalysts. *J. Catal.* **2017**, *353*, 315–324. https://doi.org/10.1016/j.jcat.2017.07.030.

(98) De Miguel, S. R.; Bocanegra, S. A.; Vilella, I. M. J.; Guerrero-Ruiz, A.; Scelza, O. A. Characterization and Catalytic Performance of PtSn Catalysts Supported on Al2O3 and Na-Doped Al2O3 in n-Butane Dehydrogenation. *Catal. Letters* **2007**, *119* (1–2), 5–15. https://doi.org/10.1007/s10562-007-9215-5.

(99) Silvestre-Albero, J.; Serrano-Ruiz, J. C.; Sepúlveda-Escribano, A.; Rodríguez-Reinoso, F. Zn-Modified MCM-41 as Support for Pt Catalysts. *Appl. Catal. A Gen.* **2008**, *351* (1), 16–23. https://doi.org/10.1016/j.apcata.2008.08.021.

(100) Santhosh Kumar, M.; Chen, D.; Holmen, A.; Walmsley, J. C. Dehydrogenation of Propane over Pt-SBA-15 and Pt-Sn-SBA-15: Effect of Sn on the Dispersion of Pt and Catalytic Behavior. *Catal. Today* **2009**, *142* (1–2), 17–23.

https://doi.org/10.1016/j.cattod.2009.01.002.

(101) Zhang, J.; Deng, Y.; Cai, X.; Chen, Y.; Peng, M.; Jia, Z.; Jiang, Z.; Ren, P.; Yao, S.; Xie, J.; Xiao, D.; Wen, X.; Wang, N.; Liu, H.; Ma, D. Tin-Assisted Fully Exposed Platinum Clusters Stabilized on Defect-Rich Graphene for Dehydrogenation Reaction. *ACS Catal.* **2019**, *9* (7), 5998–6005. https://doi.org/10.1021/acscatal.9b00601.

(102) Zhu, J.; Yang, M.; Yu, Y.; Zhu, Y.; Sui, Z.; Zhou, X.; Holmen, A.; Chen, D. Size-Dependent Reaction Mechanism and Kinetics for Propane Dehydrogenation over Pt Catalysts. *ACS Catal.* **2015**, *5*, 6310–6319. https://doi.org/10.1021/acscatal.5b01423.

(103) Yang, M.-L.; Zhu, Y.-A.; Zhou, X.-G.; Sui, Z.-J.; Chen, D. First-Principles Calculations of Propane Dehydrogenation over PtSn Catalysts. *ACS Catal.* **2012**, *2* (6), 1247–1258. https://doi.org/10.1021/cs300031d.

(104) Purdy, S. C.; Seemakurthi, R. R.; Mitchell, G. M.; Davidson, M.; Lauderback, B. A.; Deshpande, S.; Wu, Z.; Wegener, E. C.; Greeley, J.; Miller, J. T. Structural Trends in the Dehydrogenation Selectivity of Palladium Alloys. *Chem. Sci.* **2020**, *11* (19), 5066–5081. https://doi.org/10.1039/d0sc00875c.

(105) Wegener, E. C.; Wu, Z.; Tseng, H.-T.; Gallagher, J. R.; Ren, Y.; Diaz, R. E.; Ribeiro, F. H.; Miller, J. T. Structure and Reactivity of Pt–In Intermetallic Alloy Nanoparticles: Highly Selective Catalysts for Ethane Dehydrogenation. *Catal. Today* **2018**, *299*, 146–153. https://doi.org/https://doi.org/10.1016/j.cattod.2017.03.054.

(106) Cano, I.; Martinez-Prieto, L. M.; Fazzini, P. F.; Coppel, Y.; Chaudret, B.; van Leeuwen, P. W. N. M. Characterization of Secondary Phosphine Oxide Ligands on the Surface of Iridium Nanoparticles. *Phys. Chem. Chem. Phys.* **2017**, *19* (32), 21655–21662. https://doi.org/10.1039/c7cp03439c CO - PPCPFQ.

(107) Casella, M. L.; Siri, G. J.; Santori, G. F.; Ferreti, O. A.; Ramírez-Corredores, M. M. Surface Characterization of Li-Modified Platinum/Tin Catalysts for Isobutane Dehydrogenation. *Langmuir* **2000**, *16* (13), 5639–5643. https://doi.org/10.1021/la991437r.

(108) Santhosh Kumar, M.; Chen, D.; Holmen, A.; Walmsley, J. C. Dehydrogenation of Propane over Pt-SBA-15 and Pt-Sn-SBA-15: Effect of Sn on the Dispersion of Pt and Catalytic Behavior. *Catal. Today* **2009**, *142* (1), 17–23. https://doi.org/https://doi.org/10.1016/j.cattod.2009.01.002.

(109) Santhosh Kumar, M.; Holmen, A.; Chen, D. The Influence of Pore Geometry of Pt Containing ZSM-5, Beta and SBA-15 Catalysts on Dehydrogenation of Propane. *Microporous Mesoporous Mater.* **2009**, *126* (1–2), 152–158. https://doi.org/10.1016/j.micromeso.2009.05.031.

(110) Liu, L.; Lopez-Haro, M.; Lopes, C. W.; Rojas-Buzo, S.; Concepcion, P.; Manzorro, R.; Simonelli, L.; Sattler, A.; Serna, P.; Calvino, J. J.; Corma, A. Structural Modulation and Direct Measurement of Subnanometric Bimetallic PtSn Clusters Confined in Zeolites. *Nat. Catal.* **2020**, *3* (8), 628–638. https://doi.org/10.1038/s41929-020-0472-7.

(111) Volynkin, A.; Rønning, M.; Blekkan, E. A. The Role of Carbon Support for Propane Dehydrogenation Over Platinum Catalysts. *Top. Catal.* **2015**, *58* (14–17), 854–865. https://doi.org/10.1007/s11244-015-0452-3.

(112) Song, H.; Rioux, R. M.; Hoefelmeyer, J. D.; Komor, R.; Niesz, K.; Grass, M.; Yang, P.; Somorjai, G. A. Hydrothermal Growth of Mesoporous SBA-15 Silica in the Presence of PVP-Stabilized

Pt Nanoparticles: Synthesis, Characterization, and Catalytic Properties. *J. Am. Chem. Soc.* **2006**, *128* (9), 3027–3037. https://doi.org/10.1021/ja057383r.

(113) Rioux, R. M.; Song, H.; Hoefelmeyer, J. D.; Yang, P.; Somorjai, G. A. High-Surface-Area Catalyst Design: Synthesis, Characterization, and Reaction Studies of Platinum Nanoparticles in Mesoporous SBA-15 Silica. *J. Phys. Chem. B* **2005**, *109* (6), 2192–2202. https://doi.org/10.1021/jp048867x.

(114) Santhosh Kumar, M.; Chen, D.; Walmsley, J. C.; Holmen, A. Dehydrogenation of Propane over Pt-SBA-15: Effect of Pt Particle Size. *Catal. Commun.* **2008**, *9* (5), 747–750. https://doi.org/10.1016/j.catcom.2007.08.015.

(115) Holmen, A.; Blekkan, E. A. Propane Dehydrogenation over Supported Pt and Pt – Sn Catalysts : Catalyst Preparation , Characterization , and Activity Measurements. **1996**, *12* (158), 1–12.

(116) Han, Z.; Li, S.; Jiang, F.; Wang, T.; Ma, X.; Gong, J. Propane Dehydrogenation over Pt – Cu Bimetallic Catalysts : The Nature of Coke Deposition and the Role of Copper. *Nanoscale* **2014**, *6*. https://doi.org/10.1039/c4nr02143f.

(117) Xia, K.; Lang, W.; Li, P.; Yan, X.; Guo, Y. The Properties and Catalytic Performance of PtIn / Mg (Al) O Catalysts for the Propane Dehydrogenation Reaction : Effects of PH Value in Preparing Mg (Al) O Supports by the Co-Precipitation Method. *J. Catal.* **2016**, *338*, 104–114. https://doi.org/10.1016/j.jcat.2016.02.028.

(118) Furukawa, S.; Komatsu, T. Intermetallic Compounds : Promising Inorganic Materials for Well- Structured and Electronically Modi Fi Ed Reaction Environments for E Ffi Cient Catalysis. *ACS Catal.* **2017**, *7*. https://doi.org/10.1021/acscatal.6b02603.

(119) Hill, J. M.; Cortright, R. .; Dumesic, J. . Silica- and L-Zeolite-Supported Pt, Pt/Sn and Pt/Sn/K Catalysts for Isobutane Dehydrogenation. *Appl. Catal. A Gen.* **1998**, *168* (1), 9–21. https://doi.org/10.1016/S0926-860X(97)00338-4.

(120) Cortright, R. D.; Hill, J. M.; Dumesic, J. A. Selective Dehydrogenation of Isobutane over Supported Pt/Sn Catalysts. *Catal. Today* **2000**, *55* (3), 213–223. https://doi.org/10.1016/S0920-5861(99)00249-7.

(121) Wu, J.; Peng, Z.; Bell, A. T. Effects of Composition and Metal Particle Size on Ethane Dehydrogenation over PtxSn100−x/Mg(Al)O (70⩽x⩽100). *J. Catal.* **2014**, *311*, 161–168. https://doi.org/10.1016/j.jcat.2013.11.017.

(122) Virnovskaia, A.; Morandi, S.; Rytter, E.; Ghiotti, G.; Olsbye, U. Characterization of Pt,Sn/Mg(Al)O Catalysts for Light Alkane Dehydrogenation by FT-IR Spectroscopy and Catalytic Measurements. *J. Phys. Chem. C* **2007**, *111* (40), 14732–14742. https://doi.org/10.1021/jp074686u.

(123) Nagaraja, B. M.; Shin, C.-H.; Jung, K.-D. Selective and Stable Bimetallic PtSn/θ-Al2O3 Catalyst for Dehydrogenation of n-Butane to n-Butenes. *Appl. Catal. A Gen.* **2013**, *467*, 211–223. https://doi.org/10.1016/j.apcata.2013.07.022.

(124) Nykänen, L.; Honkala, K. Density Functional Theory Study on Propane and Propene Adsorption on Pt(111) and PtSn Alloy Surfaces. *J. Phys. Chem.* **2011**, *115* (19), 9578–9586.

(125) Hammer, B.; Norksov, J. K. Theoretical Surface Science and Catalysis — Calculations and Concepts. *Adv. Catal.* **2000**, *45*, 71–129.

(126) LL, L.; WZ, L.; X, Y.; K, X.; YJ, G. Ytrium-Modified Alumina as Support for Trimetallic PtSnIn Catalysts with Improved Catalytic Performance in Propane Dehydrogenation. *Fuel Process. Technol.* **2016**, *146*, 48–55.

(127) Deng, L.; Miura, H.; Shishido, T.; Wang, Z.; Hosokawa, S.; Teramura, K.; Tanaka, T. Elucidating Strong Metal-Support Interactions in Pt-Sn/SiO2 Catalysts and Its Consequences for Dehydrogenation of Lower Alkanes. *J. Catal.* **2018**, *365*, 277–291.

(128) Wang, Y.; Hu, P.; Yang, J.; Zhu, Y. A.; Chen, D. C-H Bond Activation in Light Alkanes: A Theoretical Perspective. *Chem. Soc. Rev.* **2021**, *50* (7), 4299–4358. https://doi.org/10.1039/d0cs01262a.

(129) Gao, J.; Zhao, H.; Yang, X.; Koel, B. E.; Podkolzin, S. G. Geometric Requirements for Hydrocarbon Catalytic Sites on Platinum Surfaces. *Angew. Chemie - Int. Ed.* **2014**, *53* (14), 3641–3644. https://doi.org/10.1002/anie.201309043.

(130) Chen, D.; Sharma, S.; Cardona-Martínez, N.; Dumesic, J. A.; Bell, V. A.; Hodge, G. D.; Madon, R. J. Acidity Studies of Fluid Catalytic Cracking Catalysts by Microcalorimetry and Infrared Spectroscopy. *J. Catal.* **1992**, *136* (2), 392–402. https://doi.org/10.1016/0021-9517(92)90070-X.

(131) Ruiz-Martínez, J.; Sepúlveda-Escribano, A.; Anderson, J. A.; Rodríguez-Reinoso, F. Influence of the Preparation Method on the Catalytic Behaviour of PtSn/TiO2 Catalysts. *Catal. Today* **2007**, *123* (1–4), 235–244. https://doi.org/10.1016/j.cattod.2007.02.013.

(132) Ruiz-Martínez, J.; Coloma, F.; Sepúlveda-Escribano, A.; Anderson, J. A.; Rodríguez-Reinoso, F. Effect of Tin Content and Reduction Temperature on the Catalytic Behaviour of PtSn/TiO2 Catalysts in the Vapour-Phase Hydrogenation of Crotonaldehyde. *Catal. Today* **2008**, *133–135* (1–4), 35–41. https://doi.org/10.1016/j.cattod.2007.11.053.

(133) Ruiz-Martínez, J.; Sepúlveda-Escribano, A.; Anderson, J. A.; Rodríguez-Reinoso, F. Spectroscopic and Microcalorimetric Study of a TiO2-Supported Platinum Catalyst. *Phys. Chem. Chem. Phys.* **2009**, *11* (6), 917–920. https://doi.org/10.1039/b816601c.

(134) Soares, O. S. G. P.; Órfão, J. J. M.; Ruiz-Martínez, J.; Silvestre-Albero, J.; Sepúlveda-Escribano, A.; Pereira, M. F. R. Pd-Cu/AC and Pt-Cu/AC Catalysts for Nitrate Reduction with Hydrogen: Influence of Calcination and Reduction Temperatures. *Chem. Eng. J.* **2010**, *165* (1), 78–88. https://doi.org/10.1016/j.cej.2010.08.065.

(135) Liu, S.; Zhang, B.; Liu, G. Metal-Based Catalysts for the Non-Oxidative Dehydrogenation of Light Alkanes to Light Olefins. *React. Chem. Eng.* **2020**. https://doi.org/10.1039/d0re00381f.

(136) Wang, T.; Jiang, F.; Liu, G.; Zeng, L.; Zhao, Z.; Gong, J. Effects of Ga Doping on Pt/CeO2-Al2O3 Catalysts for Propane Dehydrogenation. *AIChE* **2016**, *62* (12). https://doi.org/10.1002/aic.

(137) Kley, I.; Traa, Y. Influence of Acid Sites on the Propene Selectivity during Propane Dehydrogenation on Zeolite Pt / Zn , Na-MCM-22. *Microporous Mesoporous Mater.* **2012**, *164*, 145–147. https://doi.org/10.1016/j.micromeso.2012.06.058.

(138) Nawaz, Z.; Wei, F. Hydrothermal Study of Pt – Sn-Based SAPO-34 Supported Novel Catalyst Used for Selective Propane Dehydrogenation to Propylene. *J. Ind. Eng. Chem.* **2010**, *16* (5), 774–784. https://doi.org/10.1016/j.jiec.2010.07.002.

(139) Chen, C.; Sun, M.; Hu, Z.; Ren, J.; Zhang, S.; Yuan, Z. New Insight into the Enhanced Catalytic

Performance of ZnPt / HZSM-5 Catalysts for Direct Dehydrogenation of Propane to Propylene †. *Catal. Sci. Technol.* **2019**, *9*, 1979–1988. https://doi.org/10.1039/c9cy00237e.

(140) Cola, P. L. De; Gla, R.; Weitkamp, J. Non-Oxidative Propane Dehydrogenation over Pt – Zn-Containing Zeolites. *Appl. Catal. A Gen.* **2006**, *306*, 85–97. https://doi.org/10.1016/j.apcata.2006.03.028.

(141) Andy, P.; Davis, M. E. Dehydrogenation of Propane over Platinum Containing CIT-6. *Ind. Eng. Chem. Res.* **2004**, No. 3, 2922–2928.

(142) Sun, Q.; Wang, N.; Fan, Q.; Zeng, L.; Mayoral, A.; Miao, S.; Yang, R.; Jiang, Z.; Zhou, W.; Zhang, J.; Zhang, T.; Xu, J.; Zhang, P.; Cheng, J.; Yang, D.-C.; Jia, R.; Li, L.; Zhang, Q.; Wang, Y.; Terasaki, O.; Yu, J. Subnanometer Bimetallic Pt-Zn Clusters in Zeolites for Propane Dehydrogenation. *Angew. Chemie - Int. Ed.* **2020**, *59* (44), 19450–19459. https://doi.org/10.1002/ange.202003349.

(143) Wang, Y.; Hu, Z.; Lv, X.; Chen, L.; Yuan, Z. Ultrasmall PtZn Bimetallic Nanoclusters Encapsulated in Silicalite-1 Zeolite with Superior Performance for Propane Dehydrogenation. *J. Catal.* **2020**, *385*, 61–69. https://doi.org/10.1016/j.jcat.2020.02.019.

(144) Camacho-bunquin, J.; Ferrandon, M. S.; Sohn, H.; Kropf, A. J.; Yang, C.; Wen, J.; Hackler, R. A.; Liu, C.; Celik, G.; Marshall, C. L.; Stair, P. C.; Delferro, M. Atomically Precise Strategy to a PtZn Alloy Nanocluster Catalyst for the Deep Dehydrogenation of n - Butane to 1,3-Butadiene. *ACS Catal.* **2018**, *8*, 10058–10063. https://doi.org/10.1021/acscatal.8b02794.

(145) Belskaya, O. B.; Stepanova, L. N.; Gulyaeva, T. I.; Erenburg, S. B.; Trubina, S. V; Kvashnina, K.; Nizovskii, A. I.; Kalinkin, A. V; Zaikovskii, V. I.; Bukhtiyarov, V. I.; Likholobov, V. A. Zinc Influence on the Formation and Properties of Pt/Mg(Zn)AlOx Catalysts Synthesized from Layered Hydroxides. *J. Catal.* **2016**, *341*, 13–23. https://doi.org/10.1016/j.jcat.2016.06.006.

(146) Sun, P.; Siddiqi, G.; Vining, W. C.; Chi, M.; Bell, A. T. Novel Pt/Mg(In)(Al)O Catalysts for Ethane and Propane Dehydrogenation. *J. Catal.* **2011**, *282* (1), 165–174. https://doi.org/10.1016/j.jcat.2011.06.008.

(147) Roma, M. C.; Vilella, I. M. J.; Cazorla-amoro, D.; Yamashita, H. State of Pt in Dried and Reduced PtIn and PtSn Catalysts Supported on Carbon. *J. Phys. Chem. C.* **2007**, *111*, 4710–4716.

(148) Wu, J.; Peng, Z.; Sun, P.; Bell, A. T. N -Butane Dehydrogenation over Pt/Mg(In)(Al)O. *Appl. Catal. A, Gen.* **2014**, *470*, 208–214. https://doi.org/10.1016/j.apcata.2013.10.058.

(149) Marcinkowski, M. D.; Darby, M. T.; Liu, J.; Wimble, J. M.; Lucci, F. R.; Lee, S.; Michaelides, A.; Flytzani-Stephanopoulos, M.; Stamatakis, M.; Sykes, E. C. H. Pt/Cu Single-Atom Alloys as Coke-Resistant Catalysts for Efficient C–H Activation. *Nat. Chem.* **2018**, *10* (3), 325–332. https://doi.org/10.1038/nchem.2915.

(150) Wegener, E. C.; Bukowski, B. C.; Yang, D.; Wu, Z.; Kropf, A. J.; Delgass, W. N.; Greeley, J.; Zhang, G.; Miller, J. T. Intermetallic Compounds as an Alternative to Single-Atom Alloy Catalysts: Geometric and Electronic Structures from Advanced X-Ray Spectroscopies and Computational Studies. *ChemCatChem* **2020**, *12* (5), 1325–1333. https://doi.org/https://doi.org/10.1002/cctc.201901869.

(151) Cesar, L. G.; Yang, C.; Lu, Z.; Ren, Y.; Zhang, G.; Miller, J. T. Identification of a Pt3Co Surface Intermetallic Alloy in Pt-Co Propane Dehydrogenation Catalysts. *ACS Catal.* **2019**, *9* (6), 5231–5244. https://doi.org/10.1021/acscatal.9b00549.

(152) Purdy, S. C.; Ghanekar, P.; Mitchell, G.; Kropf, A. J.; Zemlyanov, D. Y.; Ren, Y.; Ribeiro, F.; Delgass, W. N.; Greeley, J.; Miller, J. T. Origin of Electronic Modification of Platinum in a Pt3V Alloy and Its Consequences for Propane Dehydrogenation Catalysis. *ACS Appl. Energy Mater.* **2020**, *3* (2), 1410–1422. https://doi.org/10.1021/acsaem.9b01373.

(153) Gorczyca, A.; Raybaud, P.; Moizan, V.; Joly, Y.; Chizallet, C. Atomistic Models for Highly-Dispersed PtSn/γ-Al2O3 Catalysts: Ductility and Dilution Affect the Affinity for Hydrogen. *ChemCatChem* **2019**, *11* (16), 3941–3951. https://doi.org/https://doi.org/10.1002/cctc.201900429.

(154) Zhang, G.; Ye, C.; Liu, W.; Zhang, X.; Su, D.; Yang, X.; Chen, J. Z.; Wu, Z.; Miller, J. T. Diffusion-Limited Formation of Nonequilibrium Intermetallic Nanophase for Selective Dehydrogenation. *Nanoletters* **2019**, *19*, 4380–4383. https://doi.org/10.1021/acs.nanolett.9b00994.

(155) Romero, D.; Rodrı, D.; Sa, J.; Domı, F. Dehydrogenation of N-Butane over Pd –Ga/Al2O3 Catalysts. *Appl. Catal. A, Gen.* **2010**, *373*, 66–70. https://doi.org/10.1016/j.apcata.2009.10.040.

(156) Gallagher, J. R.; Childers, D. J.; Zhao, H.; Winans, R. E.; Meyer, R. J.; Miller, J. T. Structural Evolution of an Intermetallic Pd – Zn Catalyst Selective for Propane Dehydrogenation. *Phys. Chem. Chem. Phys.* **2015**, *17*, 28144–28153. https://doi.org/10.1039/c5cp00222b.

(157) Wolf, M.; Raman, N.; Taccardi, N.; Haumann, M. Coke Formation during Propane Dehydrogenation over Ga-Rh Supported Catalytically Active Liquid Metal Solutions. *ChemCatChem* **2020**, *12*, 1085–1094. https://doi.org/10.1002/cctc.201901922.

(158) Bauer, T.; Wu, M.; Haumann, M.; Wolf, M.; Wittka, H.; Papp, C.; Go, A.; Spiecker, E.; Libuda, J.; Steinru, H.; Wasserscheid, P. Highly Effective Propane Dehydrogenation Using Ga − Rh Supported Catalytically Active Liquid Metal Solutions. *ACS Catal.* **2019**, *9*, 949–9507. https://doi.org/10.1021/acscatal.9b02459.

(159) Fridman, V. Z.; Xing, R. Investigating the CrOx/Al2O3 Dehydrogenation Catalyst Model : II . Relative Activity of the Chromium Species on the Catalyst Surface. *"Applied Catal. A, Gen.* **2017**, *530*, 154–165. https://doi.org/10.1016/j.apcata.2016.11.024.

(160) Fridman, V. Z.; Xing, R.; Severance, M. Investigating the CrOx/Al2O3 Dehydrogenation Catalyst Model:I . Identification and Stability Evaluation of the Cr Species on the Fresh and Equilibrated Catalysts. *"Applied Catal. A, Gen.* **2016**, *523*, 39–53. https://doi.org/10.1016/j.apcata.2016.05.008.

(161) Sattler, J. J. H. B.; Mens, A. M.; Weckhuysen, B. M. Real-Time Quantitative Operando Raman Spectroscopy of a CrO x / Al 2 O 3 Propane Dehydrogenation Catalyst in a Pilot- Scale Reactor. *ChemCatChem* **2014**, *66*, 3139–3145. https://doi.org/10.1002/cctc.201402649.

(162) Sokolov, S.; Bychkov, Y.; Stoyanova, M.; Rodemerck, U.; Bentrup, U.; Linke, D.; Tyulenin, Y. P.; Korchak, V. N.; Kondratenko, E. V. Effect of VO x Species and Support on Coke Formation and Catalyst Stability in Nonoxidative Propane Dehydrogenation. *ChemCatChem* **2015**, *7*, 1691–1700. https://doi.org/10.1002/cctc.201500151.

(163) Schreiber, M. W.; Plaisance, C. P.; Baumga, M.; Reuter, K.; Jentys, A.; Bermejo-deval, R.; Lercher, J. A. Lewis − Brønsted Acid Pairs in Ga /H-ZSM-5 To Catalyze Dehydrogenation of Light Alkanes. *J. Am. Chem. Soc.* **2018**, *140*, 4898–4859. https://doi.org/10.1021/jacs.7b12901.

(164) Zheng, B.; Hua, W.; Yue, Y.; Gao, Z. Dehydrogenation of Propane to Propene over Different Polymorphs of Gallium Oxide. *J. Catal.* **2005**, *232*, 143–151. https://doi.org/10.1016/j.jcat.2005.03.001.

(165) Shao, C.; Lang, W.; Yan, X.; Guo, Y. Catalytic Performance of Gallium Oxide Based- Catalysts for the Propane Dehydrogenation Reaction : E Ff Ects of Support and Loading Amount. *RSC Adv.* **2017**, *7*, 4710–4723. https://doi.org/10.1039/c6ra27204e.

(166) Searles, K.; Siddiqi, G.; Safonova, O. V; Copéret, C. Silica-Supported Isolated Gallium Sites as Highly Active, Selective and Stable Propane Dehydrogenation Catalysts. *Chem. Sci.* **2017**, *8*, 2661–2666. https://doi.org/10.1039/c6sc05178b.

(167) Pidko, E. A.; Santen, R. A. van; Hensen, E. J. M. Multinuclear Gallium-Oxide Cations in High-Silica Zeolites. *Phys. Chem. Chem. Phys.* **2009**, *11*, 2893–2902. https://doi.org/10.1039/b905015a.

(168) Qi, W.; Yan, P.; Su, D. S. Oxidative Dehydrogenation on Nanocarbon : Insights into the Reaction Mechanism and Kinetics via in Situ Experimental Methods. *Acc. Chem. Res.* **2018**, *51*, 640–648. https://doi.org/10.1021/acs.accounts.7b00475.

(169) Liu, L.; Zhu, Y.; Su, M.; Yuan, Z. Metal-Free Carbonaceous Materials as Promising Heterogeneous Catalysts. *ChemCatChem* **2015**, *7*, 2765–2787. https://doi.org/10.1002/cctc.201500350.

(170) Zhao, Z.; Ge, G.; Li, W.; Guo, X.; Wang, G. Modulating the Microstructure and Surface Chemistry of Carbocatalysts for Oxidative and Direct Dehydrogenation : A Review. *Chinese J. Catal.* **2016**, *37* (5), 644–670. https://doi.org/10.1016/S1872-2067(15)61065-8.

(171) Liu, L.; Deng, Q.; Agula, B.; Zhao, X.; Ren, T.; Yuan, Z. Ordered Mesoporous Carbon Catalyst for Dehydrogenation of Propane to Propylene. *Chem. Commun.* **2011**, *47*, 8334–8336. https://doi.org/10.1039/c1cc12806j.

(172) Hu, Z.; Zhao, H.; Chen, C.; Yuan, Z. Castanea Mollissima Shell-Derived Porous Carbons as Metal-Free Catalysts for Highly Efficient Dehydrogenation of Propane to Propylene. *Catal. Today* **2018**, *316*, 214–222. https://doi.org/10.1016/j.cattod.2018.01.010.

(173) Hu, Z.; Chen, C.; Ren, J.; Yuan, Z. Direct Dehydrogenation of Propane to Propylene on Surface-Oxidized Multiwall Carbon Nanotubes. *Appl. Catal. A, Gen.* **2018**, *559*, 85–93. https://doi.org/10.1016/j.apcata.2018.04.017.

(174) Zhu, Y.; Liu, Y.; Liu, Y.; Ren, T.; Du, G.; Chen, T.; Yuan, Z. Heteroatom-Doped Hierarchical Porous Carbons as High-Performance Metal-Free Oxygen Reduction Electrocatalysts. *J. Mater. Chem. A* **2015**, *3*, 11725–11729. https://doi.org/10.1039/c5ta01611h.

(175) Shimada, H.; Akazawa, T.; Ikenaga, N.; Suzuki, T. Dehydrogenation of Isobutane to Isobutene with Iron-Loaded Activated Carbon Catalyst. *Appl. Catal.* **1998**, *168*, 243–250.

(176) Pereira, M. F. R.; Orfao, J. J. .; Figueiredo, J. L. Oxidative Dehydrogenation of Ethylbenzene on Activated Carbon Catalysts . I . In ¯ Uence of Surface Chemical Groups. *Appl. Catal. A, Gen.* **1999**, *184*, 153–160.

(177) Baquero, E. A.; Tricard, S.; Flores, J. C.; de Jesus, E.; Chaudret, B. Highly Stable Water-Soluble Platinum Nanoparticles Stabilized by Hydrophilic N-Heterocyclic Carbenes. *Angew. Chemie, Int. Ed.* **2014**, *53* (48), 13220–13224. https://doi.org/10.1002/anie.201407758 CO - ACIEF5.

(178) Wang, R.; Sun, X.; Zhang, B.; Sun, X.; Su, D. Hybrid Nanocarbon as a Catalyst for Direct Dehydrogenation of Propane : Formation of an Active and Selective Core – Shell Sp2/Sp Nanocomposite Structure. *Chem. - A Eur. J.* **2014**, *20*, 6324–6331. https://doi.org/10.1002/chem.201400018.

(179) Xie, J.; Kammert, J. D.; Kaylor, N.; Zheng, J. W.; Choi, E.; Pham, H. N.; Sang, X.; Stavitski, E.; Attenkofer, K.; Unocic, R. R.; Datye, A. K.; Davis, R. J. Atomically Dispersed Co and Cu on N - Doped Carbon for Reactions Involving C − H Activation. *ACS Catal.* **2018**, *8*, 3875–3884. https://doi.org/10.1021/acscatal.8b00141.

(180) Wan, W.; Tackett, B. M.; Chen, J. G. Reactions of Water and C1 Molecules on Carbide and Metal-Modified Carbide Surfaces. *Chem. Soc. Rev.* **2017**, *46*, 1807. https://doi.org/10.1039/c6cs00862c.

(181) Sullivan, M. M.; Bhan, A. Effects of Oxygen Coverage on Rates and Selectivity of Propane-CO 2 Reactions on Molybdenum Carbide. *J. Catal.* **2018**, *357*, 195–205. https://doi.org/10.1016/j.jcat.2017.11.004.

(182) Auffan, M.; Rose, J.; Bottero, J. Y.; Lowry, G. V.; Jolivet, J. P.; Wiesner, M. R. Towards a Definition of Inorganic Nanoparticles from an Environmental, Health and Safety Perspective. *Nat. Nanotechnol.* **2009**, *4* (10), 634–641. https://doi.org/10.1038/nnano.2009.242.

(183) Coq, B.; Figueras, F. Structure - Activity Relationships in Catalysis by Metals: Some Aspects of Particle Size, Bimetallic and Supports Effects. *Coord. Chem. Rev.* **1998**, *178–180* (PART 2), 1753–1783. https://doi.org/10.1016/s0010-8545(98)00058-7.

(184) Schmid, G. *Nanoparticles: From Theory to Application*; Wiley-VCH, 2004.

(185) Aiken, J. D.; Finke, R. G. A Review of Modern Transition-Metal Nanoclusters: Their Synthesis, Characterization, and Applications in Catalysis. *J. molecu* **1999**, *145*, 1–44. https://doi.org/10.1039/c8nr04414g.

(186) Ahmadi, T. S.; Wang, Z. L.; Green, T. C.; Henglein, A.; El-sayed, M. A. Shape - Controlled Synthesis of Colloidal Platinum Nanoparticles. *Science (80-.).* **1996**, *272*.

(187) Astruc, D.; Lu, F.; Aranzaes, J. R. Nanoparticles as Recyclable Catalysts: The Frontier between Homogeneous and Heterogeneous Catalysis. *Angew. Chemie - Int. Ed.* **2005**, *44* (48), 7852–7872. https://doi.org/10.1002/anie.200500766.

(188) Wassersheid, P.; Keim, W. Ionic Liquids New Solutions for Transition Metal Catalysis. *Angew. Chemie - Int. Ed.* **2000**, *39*, 3772–3789.

(189) La Mer, V. K.; Robert H Dinegar. Theory, Production and Mechanism of Formation of Monodispersed Hydrosols. *J. Am. Chem. Soc.* **1950**, *72*. https://doi.org/10.1097/00007611-192203000-00016.

(190) La Mer, V. K.. Nucleation in Phase Transitions. *Ind. Eng. Chem.* **1952**, *44* (6), 1270–1277. https://doi.org/10.1021/ie50510a027.

(191) Khan, R.; Rehman, A.; Hayat, A.; Andreescu, S. Magnetic Particles-Based Analytical Platforms for Food Safety Monitoring. *Magnetochemistry* **2019**, *5* (4), 1–20. https://doi.org/10.3390/magnetochemistry5040063.

(192) Xia, Y.; Xiong, Y.; Lim, B.; Skrabalak, S. E. Shape-Controlled Synthesis of Metal Nanocrystals:

Simple Chemistry Meets Complex Physics? *Angew. Chemie - Int. Ed.* **2009**, *48* (1), 60–103. https://doi.org/10.1002/anie.200802248.

(193) Tao, A. R.; Habas, S.; Yang, P. Shape Control of Colloidal Metal Nanocrystals. *Small* **2008**, *4* (3), 310–325. https://doi.org/10.1002/smll.200701295.

(194) Roucoux, A.; Schulz, J.; Patin, H. Reduced Transition Metal Colloids: A Novel Family of Reusable Catalysts? *Chem. Rev.* **2002**, *102* (10), 3757–3778. https://doi.org/10.1021/cr010350j.

(195) Reetz, M. T.; Breinbauer, R.; Wanninger, K. Suzuki and Heck Reactions Catalyzed by Preformed Palladium Clusters and Palladium/Nickel Bimetallic Clusters. *Tetrahedron Lett.* **1996**, *37* (26), 4499–4502. https://doi.org/10.1016/0040-4039(96)00924-0.

(196) Bronstein, L. M.; Shifrina, Z. B. Nanoparticles in Dendrimers: From Synthesis to Application. *Nanotechnologies Russ.* **2009**, *4* (9–10), 576–608. https://doi.org/10.1134/S1995078009090031.

(197) Cookson, J. The Preparation of Palladium Nanoparticles. *Platin. Met. Rev.* **2012**, *56* (2), 83–98. https://doi.org/10.1595/147106712X632415.

(198) Pauling, L. *The Nature of the Chemical Bond*, 3rd editio.; Cornell University Press, 1960.

(199) He, Z.; Alexandridis, P. Nanoparticles in Ionic Liquids: Interactions and Organization. *Phys. Chem. Chem. Phys.* **2015**, *17* (28), 18238–18261. https://doi.org/10.1039/c5cp01620g.

(200) Heuer-Jungemann, A.; Feliu, N.; Bakaimi, I.; Hamaly, M.; Alkilany, A.; Chakraborty, I.; Masood, A.; Casula, M. F.; Kostopoulou, A.; Oh, E.; Susumu, K.; Stewart, M. H.; Medintz, I. L.; Stratakis, E.; Parak, W. J.; Kanaras, A. G. The Role of Ligands in the Chemical Synthesis and Applications of Inorganic Nanoparticles. *Chem. Rev.* **2019**, *119* (8), 4819–4880. https://doi.org/10.1021/acs.chemrev.8b00733.

(201) Javed, R.; Zia, M.; Naz, S.; Aisida, S. O.; Ain, N. ul; Ao, Q. Role of Capping Agents in the Application of Nanoparticles in Biomedicine and Environmental Remediation: Recent Trends and Future Prospects. *J. Nanobiotechnology* **2020**, *18* (1), 1–15. https://doi.org/10.1186/s12951-020-00704-4.

(202) Niu, Z.; Li, Y. Removal and Utilization of Capping Agents in Nanocatalysis. *Chem. Mater.* **2014**, *26* (1), 72–83. https://doi.org/10.1021/cm4022479.

(203) Lomelí-Rosales, D. A.; Delgado, J. A.; Díaz de los Bernardos, M.; Pérez-Rodríguez, S.; Gual, A.; Claver, C.; Godard, C. A General One-Pot Methodology for the Preparation of Mono- and Bimetallic Nanoparticles Supported on Carbon Nanotubes: Application in the Semi-Hydrogenation of Alkynes and Acetylene. *Chem. - A Eur. J.* **2019**, *25* (35), 8321–8331. https://doi.org/10.1002/chem.201901041.

(204) De Los Bernardos, M. D.; Pérez-Rodríguez, S.; Gual, A.; Claver, C.; Godard, C. Facile Synthesis of NHC-Stabilized Ni Nanoparticles and Their Catalytic Application in the: Z -Selective Hydrogenation of Alkynes. *Chem. Commun.* **2017**, *53* (56), 7894–7897. https://doi.org/10.1039/c7cc01779k.

(205) Castelbou, J. L.; Gual, A.; Mercadé, E.; Claver, C.; Godard, C. Ligand Effect in the Rh-NP Catalysed Partial Hydrogenation of Substituted Arenes. *Catal. Sci. Technol.* **2013**, *3* (10), 2828–2833. https://doi.org/10.1039/c3cy00388d.

(206) Llop Castelbou, J.; Szeto, K. C.; Barakat, W.; Merle, N.; Godard, C.; Taoufik, M.; Claver, C. A New Approach for the Preparation of Well-Defined Rh and Pt Nanoparticles Stabilized by Phosphine-Functionalized Silica for Selective Hydrogenation Reactions. *Chem. Commun.* **2017**, *53* (22), 3261–3264. https://doi.org/10.1039/c6cc10338c.

(207) Amiens, C.; Chaudret, B.; Ciuculescu-Pradines, D.; Collière, V.; Fajerwerg, K.; Fau, P.; Kahn, M.; Maisonnat, A.; Soulantica, K.; Philippot, K. Organometallic Approach for the Synthesis of Nanostructures. *New J. Chem.* **2013**, *37* (11), 3374–3401. https://doi.org/10.1039/c3nj00650f.

(208) Hopkinson, M. N.; Richter, C.; Schedler, M.; Glorius, F. An Overview of N-Heterocyclic Carbenes. *Nat. Rev. Chem.* **2014**, *510* (7506), 485–496. https://doi.org/10.1038/nature13384.

(209) Lara, P.; Martínez-Prieto, L. M.; Roselló-Merino, M.; Richter, C.; Glorius, F.; Conejero, S.; Philippot, K.; Chaudret, B. NHC-Stabilized Ru Nanoparticles: Synthesis and Surface Studies. *Nano-Structures and Nano-Objects* **2016**, *6*, 39–45. https://doi.org/10.1016/j.nanoso.2016.03.003.

(210) Ramirez, E.; Eradès, L.; Philippot, K.; Lecante, P.; Chaudret, B. Shape Control of Platinum Nanoparticles. *Adv. Funct. Mater.* **2007**, *17* (13), 2219–2228. https://doi.org/10.1002/adfm.200600633.

(211) Favier, I.; Gómez, M.; Muller, G.; Axet, M. R.; Castillón, S.; Claver, C.; Jansat, S.; Chaudret, B.; Philippot, K. Palladium Catalytic Species Containing Chiral Phosphites: Towards a Discrimination between Molecular and Colloidal Catalysts. *Adv. Synth. Catal.* **2007**, *349* (16), 2459–2469. https://doi.org/10.1002/adsc.200700200.

(212) Loza, K.; Heggen, M.; Epple, M. Synthesis, Structure, Properties, and Applications of Bimetallic Nanoparticles of Noble Metals. *Adv. Funct. Mater.* **2020**, *30* (21). https://doi.org/10.1002/adfm.201909260.

(213) Jia, C. J.; Schüth, F. Colloidal Metal Nanoparticles as a Component of Designed Catalyst. *Phys. Chem. Chem. Phys.* **2011**, *13* (7), 2457–2487. https://doi.org/10.1039/c0cp02680h.

(214) Toshima, N.; Yonezawa, T. Bimetallic Nanoparticles - Novel Materials for Chemical and Physical Applications. *New J. Chem.* **1998**, *22* (11), 1179–1201. https://doi.org/10.1039/a805753b.

(215) H, B. E. Pd and Pt NPs as Selective Hydrogenation Catalysts, Technische Universiteit Eindhoven, 2015.

(216) Zaleska-Medynska, A.; Marchelek, M.; Diak, M.; Grabowska, E. Noble Metal-Based Bimetallic Nanoparticles: The Effect of the Structure on the Optical, Catalytic and Photocatalytic Properties. *Adv. Colloid Interface Sci.* **2016**, *229*, 80–107. https://doi.org/10.1016/j.cis.2015.12.008.

(217) Sharma, G.; Kumar, A.; Sharma, S.; Naushad, M.; Prakash Dwivedi, R.; ALOthman, Z. A.; Mola, G. T. Novel Development of Nanoparticles to Bimetallic Nanoparticles and Their Composites: A Review. *J. King Saud Univ. - Sci.* **2019**, *31* (2), 257–269. https://doi.org/10.1016/j.jksus.2017.06.012.

(218) Ferrando, R.; Jellinek, J.; Johnston, R. L. Nanoalloys: From Theory to Applications of Alloy Clusters and Nanoparticles. *Chem. Rev.* **2008**, *108* (3), 845–910. https://doi.org/10.1021/cr040090g.

(219) Ghosh Chaudhuri, R.; Paria, S. Core/Shell Nanoparticles: Classes, Properties, Synthesis Mechanisms, Characterization, and Applications. *Chem. Rev.* **2012**, *112* (4), 2373–2433. https://doi.org/10.1021/cr100449n.

(220) Burda, C.; Chen, X.; Narayanan, R.; El-Sayed, M. A. Chemistry and Properties of Nanocrystals of Different Shapes. *Chem. Rev.* **2005**, *105* (4), 1025–1102. https://doi.org/10.1021/cr030063a.

(221) Bönnemann, H.; Braun, G.; Brijoux, W.; Brinkmann, R.; Tilling, A. S.; Seevogel, K.; Siepen, K. Nanoscale Colloidal Metals and Alloys Stabilized by Solvents and Surfactants: Preparation and Use as Catalyst Precursors. *J. Organomet. Chem.* **1996**, *520* (1–2), 143–162. https://doi.org/10.1016/0022-328X(96)06273-0.

(222) Belapurkar, A. D.; Kapoor, S.; Kulshreshtha, S. K.; Mittal, J. P. Radiolytic Preparation and Catalytic Properties of Platinum Nanoparticles. *Mater. Res. Bull.* **2001**, *36* (1–2), 145–151. https://doi.org/10.1016/S0025-5408(01)00499-8.

(223) Benfield, F. W. S.; Green, M. L. H.; Ogden, J. S.; Young, D. Synthesis of Bis-π-Benzene-Titanium and -Molybdenum Using Metal Vapours. *J. Chem. Soc. Chem. Commun.* **1973**, No. 22, 866–867. https://doi.org/10.1039/C39730000866.

(224) Pelzer, K.; Vidoni, O.; Philippot, K.; Chaudret, B.; Collière, V. Organometallic Synthesis of Size-Controlled Polycrystalline Ruthenium Nanoparticles in the Presence of Alcohols. *Adv. Funct. Mater.* **2003**, *13* (2), 118–126. https://doi.org/10.1002/adfm.200390017.

(225) Zhu, J. Synthesis of Precious Metal NPs Supported on Bacterial Biomass for Catalytic Applications in Chemical Transformations, University of Birmingham, 2014.

(226) Sexton, B. A.; Hughes, A. E.; Foger, K. An X-Ray Photoelectron Spectroscopy and Reaction Study of PtSn Catalysts. *J. Catal.* **1984**, *88* (2), 466–477. https://doi.org/10.1016/0021-9517(84)90024-1.

(227) Meitzner, G.; Via, G. H.; Lytle, F. W.; Fung, S. C.; Sinfelt, J. H. Extended X-Ray Absorption Fine Structure (EXAFS) Studies of Platinum-Tin Catalysts. *J. Phys. Chem.* **1988**, *92* (10), 2925–2932. https://doi.org/10.1021/j100321a042.

(228) Basset, J. M.; Ugo, R. *Modern Surface Organometallic Chemistry*; Psaro, R., Basset, J. M., Roberto, D., Ugo, R., Eds.; Wiley-VCH Verlag GmbH & Co. KGaA, 2009. https://doi.org/10.1002/9783527627097.

(229) Copéret, C. Single-Sites and Nanoparticles at Tailored Interfaces Prepared via Surface Organometallic Chemistry from Thermolytic Molecular Precursors. *Acc. Chem. Res.* **2019**, *52* (6), 1697–1708. https://doi.org/10.1021/acs.accounts.9b00138.

(230) Samantaray, M. K.; D'Elia, V.; Pump, E.; Falivene, L.; Harb, M.; Ould Chikh, S.; Cavallo, L.; Basset, J.-M. The Comparison between Single Atom Catalysis and Surface Organometallic Catalysis. *Chem. Rev.* **2020**, *120* (2), 734–813. https://doi.org/10.1021/acs.chemrev.9b00238 CO - CHREAY.

(231) Copéret, C. Fuels and Energy Carriers from Single-Site Catalysts Prepared via Surface Organometallic Chemistry. *Nat. Energy* **2019**, *4* (12), 1018–1024. https://doi.org/10.1038/s41560-019-0491-2.

(232) Rouge, P.; Garron, A.; Norsic, S.; Larabi, C.; Merle, N.; Delevoye, L.; Gauvin, R. M.; Szeto, K. C.; Taoufik, M. A Smarter Approach to Catalysts by Design: Combining Surface

Organometallic Chemistry on Oxide and Metal Gives Selective Catalysts for Dehydrogenation of 2,3-Dimethylbutane. *Mol. Catal.* **2019**, *471*, 21–26. https://doi.org/10.1016/j.mcat.2019.04.011.

(233) Basset, J. M.; Copéret, C.; Soulivong, D.; Taoufik, M.; Thivolle Cazat, J. Metathesis of Alkanes and Related Reactions. *Acc. Chem. Res.* **2010**, *43* (2), 323–334. https://doi.org/10.1021/ar900203a.

(234) Basset, J. M.; Chakka, S.; Taoufik, M.; Thivolle-Cazat, J. No Title. Eur. Pat. EP2022772A1, 2009.

(235) Chabanas, M.; Baudouin, A.; Copéret, C.; Basset, J. A Highly Active Well-Defined Rhenium Heterogeneous Catalyst for Olefin Metathesis Prepared via Surface Organometallic Chemistry. *J. Am. Chem. Soc.* **2001**, *123*, 2062–2063.

(236) Xu, Y.; Bao, X.; Lin, L. Direct Conversion of Methane under Nonoxidative Conditions. *J. Catal.* **2003**, *216* (1–2), 386–395.

(237) Rataboul, F.; Baudoin, A.; Thieuleux, C.; Veyre, L.; Copéret, C.; Thivolle-Cazat, J.; Basset, J.; Lesage, A.; Emsley, L. Molecular Understanding of the Formation of Surface Zirconium Hydrides upon Treatment under Hydrogen of [(≡SiO)Zr(CH2tBu)3] by Using Advanced Solid-State NMR Techniques. *J. Am. Chem. Soc.* **2004**, *126* (39), 12541–12550.

(238) Copéret, C.; Chabanas, M.; Saint-Arroman, R. P.; Basset, J. Homogeneous and Heterogeneous Catalysis: Bridging the Gap through Surface Organometallic Chemistry. *Angew. Chemie Int. Ed.* **2003**, *43*, 156–181.

(239) Corma, A.; Navarro, M. T.; Michael Renz. Lewis Acidic Sn(IV) Centers—Grafted onto MCM-41—as Catalytic Sites for the Baeyer–Villiger Oxidation with Hydrogen Peroxide. *J. Catal.* **2003**, *219* (1), 242–246.

(240) Kim, N.-K.; Kim, G.-J.; Wha-Seung Ahn. Synthesis, Characterization, and Catalytic Properties of Ti, V, and Zr-HMS Prepared by Metallocene Grafting. *React. Kinet. Catal. Lett.* **2000**, *71*, 273–279.

(241) Philippot, K.; Chaudret, B. Organometallic Approach to the Synthesis and Surface Reactivity of Noble Metal Nanoparticles. *Comptes Rendus Chim.* **2003**, *6* (8–10), 1019–1034. https://doi.org/10.1016/j.crci.2003.07.010.

(242) Chaudret, B. Organometallic Approach to Nanoparticles Synthesis and Self-Organization. *Comptes Rendus Phys.* **2005**, *6*, 117–131. https://doi.org/10.1016/j.crhy.2004.11.008.

(243) Ely, T. O.; Amiens, C.; Chaudret, B.; Snoeck, E.; Verelst, M.; Respaud, M.; Broto, J. Synthesis of Nickel Nanoparticles . Influence of Aggregation Induced by Modification of Poly (Vinylpyrrolidone) Chain Length on Their Magnetic Properties Attracting Increasing Interest , Because They May Differ Surface or Quantum Size Effects . 1 Howeve. *Chem. Mater.* **1999**, *11* (l), 526–529.

(244) Romero, N.; Guerra, R. B.; Gil, L.; Drouet, S.; Salmeron-Sànchez, I.; Illa, O.; Philippot, K.; Natali, M.; García-Antón, J.; Sala, X. TiO2-Mediated Visible-Light-Driven Hydrogen Evolution by Ligand-Capped Ru Nanoparticles. *Sustain. Energy Fuels* **2020**, *4* (8), 4170–4178. https://doi.org/10.1039/d0se00446d.

UNIVERSITAT ROVIRA I VIRGILI
INNOVATIVE NANOCATALYSTS FOR SUSTAINABLE NON-OXIDATIVE DEHYDROGENATION OF PROPANE
Laia Gil Jiménez

2

Objectives

The main objective of this PhD thesis is the development of efficient and innovative catalysts for the propane dehydrogenation (PDH) reaction.

For this purpose, the present thesis includes three different strategies to synthesize the supported catalysts including: (1) the surface-organometallic chemistry (SOMC) (2) the one-pot organometallic approach (OPOA) and (3) a mixed approach combining OPOA and SOMC.

The work described in Chapter 3 aims at the study of novel PtSn catalysts prepared by Surface Organometallic Chemistry (SOMC) approach. The resulting catalysts will be characterized and their performance in PDH will be evaluated. Moreover, an exhaustive study of the PDH operation conditions will be performed and a benchmark catalyst (Linde-BASF-Statoil) will be tested for comparison purposes.

The investigation detailed in Chapter 4 aims at the study of novel PtSn catalysts synthesized by One-Pot Organometallic Approach (OPOA). The catalysts will be characterized and their performance in the PDH reaction will be reported for the first time. When necessary, the colloidal analogues will be synthesized and characterized to obtain further information on the catalyst active phase.

The objective of the research described in Chapter 5 is the preparation of PDH catalysts based on alternative metals (NiSn and PtGa) using the OPOA as synthetic methodology. Characterization and catalytic testing will also be carried out.

PtGa and PtSn catalysts will also be prepared using an innovative mixed approach combining OPOA and SOMC. Their characterization and evaluation in the PDH reaction will also be performed.

2

UNIVERSITAT ROVIRA I VIRGILI
INNOVATIVE NANOCATALYSTS FOR SUSTAINABLE NON-OXIDATIVE DEHYDROGENATION OF PROPANE
Laia Gil Jiménez

3

Pt and PtSn catalysts for PDH prepared by Surface Organometallic Chemistry

3.1 Introduction

As in most catalytic reactions, the performance of catalysts based on PtSn in PDH depends on their structural features,[1,2] and therefore the development of synthetic approaches to achieve well defined active species is highly desired.[3] As previously discussed in Chapter 1, wet-chemistry methodologies such as impregnation, sol-gel and colloidal syntheses were used to synthesize such catalysts.[4,5] However, several issues are often encountered such as (1) particle size > 1 nm, decreases the catalyst efficiency; (2) separation between Pt and Sn results in low synergy;[4,5] and (3) ill-defined catalyst structures,[6] results in the presence of various catalytically active species and therefore in complex analysis. The development of synthetic methods for the preparation of catalyst with small size in which the bimetallic structure is well defined and homogeneously distributed over the support is therefore of high interest. In this context, Surface Organometallic Chemistry (SOMC) appears as an interesting approach to overcome these current issues.[7]

SOMC provides well-defined materials, as initially demonstrated in the late 1970's by Yermankov.[8,9] SOMC can be performed either on an oxide (SOMC/Oxide) or on a metal (SOMC/M). SOMC/Oxide consists in the grafting of the organometallic precursor onto highly dehydroxylated metal-oxide supports whereas, SOMC/M is the selective grafting of a promoter onto the surface hydrides present at the surface of a metal.[10] SOMC is carried out under inert atmosphere and generate identical and homogeneously dispersed catalytic sites. It is important to avoid the presence of water as it may accelerate the mobility of different elements on the surface.[11]

3.1.1 Surface Organometallic Chemistry in alkane dehydrogenation reactions

As discussed in Chapter 1, PtSn bimetallic catalysts exhibit enhanced selectivity and stability in PDH compared to Pt catalysts, mainly due to geometric and electronic effects.[12,13] Several bimetallic catalysts were previously reported using the SOMC approach and applied in alkane dehydrogenation processes.[14–17]

For instance, it was described that $SnBu_4$ selectively reacts at 50 °C (under H_2) with reduced surface Pt atoms to produce $Pt_s[Sn(n\text{-}C_4H_9)_x]_y$.[18] These species experimented a complete hydrogenolysis at high temperatures (*ca.* 100 °C) and tin adatoms could be introduced.[19] Pt-Sn surface alloy can be subsequently formed by a treatment above 450 °C (**Figure 3.1**).[18]

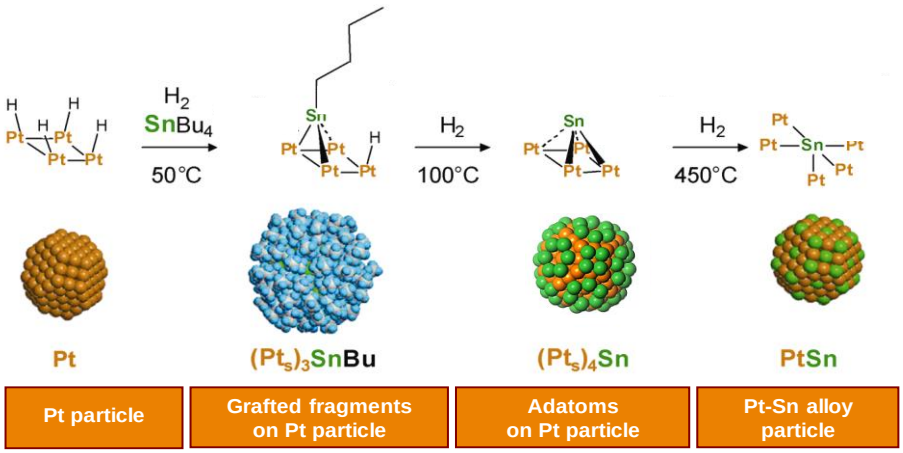

Figure 3.1. Scheme concerning SOMC/M approach for PtSn particles.

Basset and co-workers reported the preparation of monometallic catalysts Pt/Al_2O_3, which, upon addition of $SnBu_4$, produced the bimetallic $PtSn/Al_2O_3$ with a Sn/Pt=0.7.[20] In this study, the Sn fragments were grafted on both the metallic surface ($Pt_s[Sn(n\text{-}C_4H_9)_x]_y$) and the support ($Al\text{-}O\text{-}Sn(n\text{-}C_4H_9)_3$). However, when traces of water were added, the grafting on the support was avoided. Prior to catalytic testing, the samples were reduced at 550 °C under hydrogen that led to the loss of the remaining butyl groups. The catalysts were tested in isobutane dehydrogenation. When no Sn is present, low initial selectivity toward isobutene is observed (<95%) and it slightly increases at higher TOS. This effect was attributed to coke formation on the Pt surface that poisons the catalyst. Whereas, when Sn is present, the selectivity toward isobutene increases (>99%). Similar effect of Sn were reported by other authors.[21,22] These results revealed that this $PtSn/Al_2O_3$ catalyst was highly selective in the isobutane dehydrogenation.[19,20]

In another study, a series of Sn surface enriched PtSn NPs supported on $MgAl_2O_4$ ($PtSn/MgAl_2O_4$) were synthesized by SOMC by Basset and coworkers.[14] They reported that the Sn precursor selectively reacted with the Pt-hydrides formed at the surface of Pt-NPs. ^1H MAS and ^{13}C CP/MAS solid-state NMR indicated that organo-tin moieties $Sn(n\text{-}C_4H_9)$ were chemically bonded to the Pt-NPs surface. Next, the removal of most of the butyl fragments led to bimetallic PtSn-NPs. The remaining groups were suggested to play the role of stabilizers in the synthesized NPs. A total of seven PtSn samples were synthesized at Sn/Pt molar ratios of 0, 1:12, 1:9, 1:6, 1:3, 1:1 and 2:1. XPS analyses revealed that the Pt(δ+)/Pt(0) ratio decreased when Sn concentration increased. The authors commented that it was a consequence of the Pt coverage by surface SnO_2. HAADF and STEM analyses revealed a non-homogeneous structure with Sn species located on the edges and core of Pt (**Figure 3.2**, right). Prior to PDH tests, the catalysts were reduced 2 h at 580 ^oC with 10% H_2. 10% in volume of C_3H_8 was used in the fixed-bed reactor with 10 % H_2 and 80% was He. With an increase of Sn, the NPs surface gradually appears to form a shell-like structure while the NP size remained unchanged. XRD diffractograms revealed identical Pt structures with diffraction peaks corresponding to the corresponding to (111), (200), (220), (311) and (222) planes of Pt, which indicated that the formed PtSn NPs had identical metallic Pt crystals. These observations also indicated that almost no bulk alloy (Pt_xSn_y) was formed during the synthesis. At higher Sn/Pt ratio, the diffraction peaks did not shift, suggesting again the Sn was not incorporated into the crystal network. The crystallite size extracted with the Rietveld analysis showed a dependence on Sn/Pt ratio where the crystallite size decreased with more Sn added to the catalysts. This was in agreement with HAADF and STEM observations. That aspect was attributed to the steric hindrance induced by "$Sn\text{-}(CH_2CH_2CH_2CH_3)$" fragments or to a decrease in the Pt coordination number that limited the growth of the crystals. The introduction of Sn increased the selectivity and conversion in PDH, that was tested at 580^o C. The enhanced activity was associated with high concentration of inactive Sn at the surface of Pt NPs which isolates the active Pt atoms. The catalyst with the

highest conversion (38.9%) and propylene selectivity (99.7%) contained a Sn/Pt theoretical molar ratio of 1:0.5.[14]

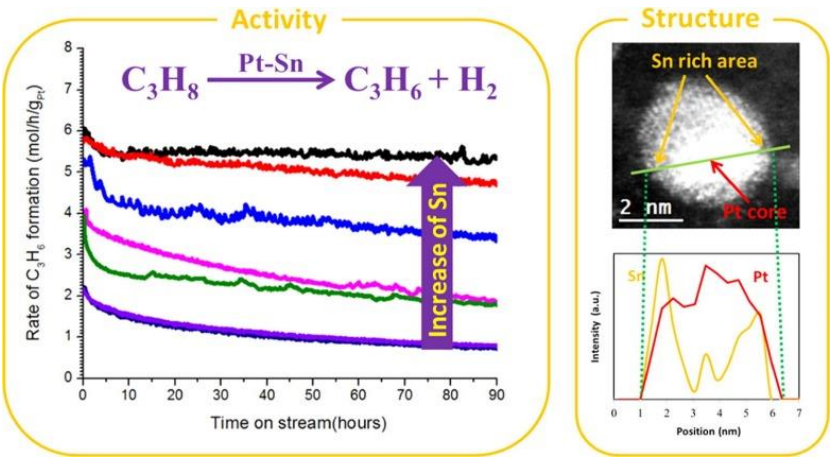

Figure 3.2. (Left) Activity in PDH of $PtSn/MgAl_2O_4$ with different Sn values. (Right) HAADF-STEM and EDS mapping.[14]

Pt catalysts supported on alumina and promoted by tin were reported ($PtSn/Al_2O_3$) and prepared using SOMC by Fierro and coworkers for isobutane dehydrogenation,[23] with Sn/Pt atomic ratio ranging from 0 to 1.6. By FTIR, the peak of CO chemisorbed on Pt at 2074 cm^{-1} was shifted to higher wavenumbers upon Sn incorporation. Thus, indicated the electronic interaction Sn-Pt weakened the Pt-CO bond resulting in an increase of the catalyst stability. Moreover, NH_3 adsorption by FTIR indicated that Bronsted sites were partially poisoned. The oxidation state of the metals was checked by XPS: Pt was present in Pt (0) form and Sn was present in both Sn (0) and Sn (n+). The metallic Sn fraction decreased at higher Sn loading. Upon addition of Sn, the stability of the catalysts increased substantially. In addition, the selectivity towards isomerization and cracking side reactions diminished and dehydrogenation selectivity increased. The highest conversion and selectivity to isobutene (*ca*. 90%) was achieved when Sn/Pt atomic ratio was 1.6 at 823 K in a fixed bed flow reaction at atmospheric pressure.[23]

Ferreti and co-workers prepared a series of Pt-supported catalysts modified with lithium (Li(OH)) and/or tin (Sn/Pt atomic ratio of 0.45) by SOMC that were tested in

isobutane dehydrogenation.[24] They reported that the order of addition of Li was important. Indeed, when Li was impregnated onto the supported metallic phases, the isomerization reactions were minimized, whereas when Li was added on the support (γ-Al_2O_3), both isomerization and cracking side reactions were inhibited. Tin incorporation notably improved selectivity toward isobutene, minimizing side reactions.[24] The isobutane dehydrogenation was carried out at 823 K, and for Pt catalysts, high conversion (*ca.* 25%) was obtained but low selectivity to isobutene (*ca.* 50%) and the rest was contributing to the cracking and isomerization side reactions. Once Sn was added (PtSn), the selectivity to isobutene increased to *ca*. 88%, but the conversion was lower (21%). Finally, the catalyst that possessed a good balance between conversion (19%) and excellent selectivity to isobutene (97%) was PtSn with Li.

Taoufik and coworkers prepared a trimetallic Pt-Sn-Li material with metal loadings of 2 wt.% Pt, 1.3 wt.% Sn and 2.8 wt.% Li, supported onto lithiated alumina (PtSn/Li-Al_2O_3) that was active in the conversion of 2,3-dimethylbutane into 2,3-dimethylbutene.[15] Prior to the synthesis, the dehydroxylated γ-Al_2O_3 was treated with BuLi to quench the Bronsted acidity and as such, suppress the side reactions. Using SOMC/Oxide approach, $LiAl_2O_3$ was treated with $Pt(acac)_2$ and after a calcination under air at 400^o C, Pt NPs were obtained. Next, $SnBu_4$ was reacted in the presence of H_2 (550 mbar) with the hydrides present at the surface of Pt-NPs. Subsequently, after a treatment under 1 atm H_2 at 550 ^{o}C for 2h, the PtSn/Li-Al_2O_3 catalyst was obtained (**Figure 3.3**).[15] DRIFT spectroscopy was used as a qualitative tool to monitor the grafting of the Pt species using the bands at 1400, 1530 and 1600 cm^{-1} assigned to δ(C-H), ν(C-C) and ν(C=O) for grafted and physiosorbed acac ligands.[25] Pt/Al_2O_3 and Pt/Li-Al_2O_3 were synthesized for comparative purposes. Li had a beneficial role in increasing the Pt dispersion. The 2,3-dimethylbutane dehydrogenation was studied at 500 ^{o}C in a dynamic flow reactor with a total pressure of 1 bar. The reaction using Pt/Al_2O_3 revealed an initial conversion of 28% that decreased to 18% after 30h on stream. The main product obtained were

branched alkenes (*ca*. 40%), branched hexanes (*ca*. 25%) and methane (*ca*. 10%). $Pt/LiAl_2O_3$ provided an initial conversion of 42% with *ca.* 45% for DMB1 and *ca*. 51% to DMB2, the rest was detected as DMBD. Finally, $PtSn/LiAl_2O_3$ was also tested and exhibited a conversion near 40% that was maintained over time. The selectivity towards desired products (DMB-1 and DMB-2) was high (77%). These results showed that the Li and Sn modifications increased the selectivity towards the target products providing a good stability over time (**Figure 3.4**).

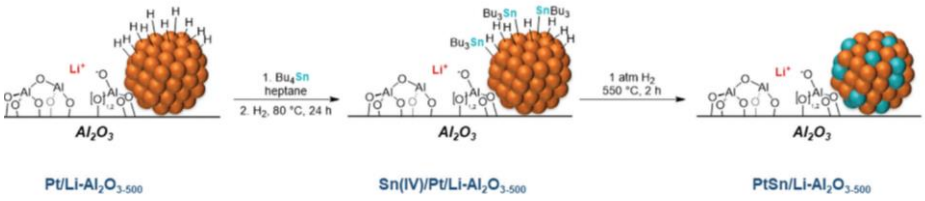

Figure 3.3. Synthesis scheme for generation of PtSn catalyst onto Li-Al_2O_3 using SOMC/M approach.[15,10]

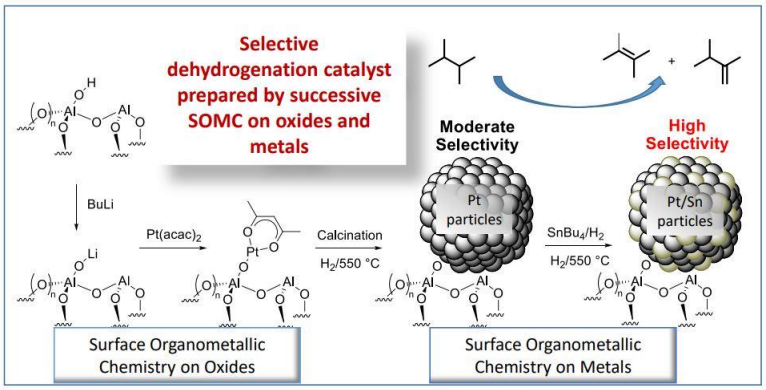

Figure 3.4. Scheme with selective dehydrogenation catalyst prepared by successive SOMC/Oxides and metals. $Pt/LiAl_2O_3$ provided moderate selectivity versus $PtSn/LiAl_2O_3$ that displayed high selectivity in DMBs. [15]

Recently, Basset also reported the synthesis of bimetallic PtSn nanoclusters supported on ɵ-Al_2O_3 with a size below 1 nm (**Figure 3.5**).[3] First, the grafting of $Pt(COD)Me_2$ and $HSnPh_3$ at the surface of the dehydroxylated ɵ-Al_2O_3 led to the formation of a well-defined material containing [(≡AlO-)Pt(COD)Me] and [(≡AlO-)$SnPh_3$] fragments; then, the hydrogenolysis of these surface compounds under mild conditions generated ultra-small PtSn/ɵ-Al_2O_3 clusters with Pt loading kept

constant at 0.50 wt%.[3] Various Sn loadings were added, and various Sn/Pt mol/mol ratio of 0, 1/3, ½, 1, 2, 3 and 4 were obtained. XRD analysis only displayed the support pattern, suggesting that the formed PtSn NPs were highly dispersed. STEM-HAADF revealed that bimetallic nanoclusters were homogeneously distributed, all of them possessing a mean size below 1 nm. A comparative catalyst using a Sn/Pt mol ratio of 3, was synthesized by impregnation and revealed a wide size distribution (from 1 to 5 nm) and agglomeration. Surface area and pore volume were unchanged after Sn addition. XPS measurements revealed that Sn was present in three forms: Sn(0), Sn(II) and Sn(IV), although the exact contribution of each species and Pt oxidation states were not included in the paper. However, a general tendency indicated that increasing the Sn/Pt ratio increased the Sn oxidized species. Nevertheless, the role of Sn in PtSn catalyst remains a matter of debate.[26] It is believed that the presence of oxidized Sn can significatively prevent the sintering of Pt NPs under reaction conditions, which explains the enhanced stability of these catalysts in PDH.[27]

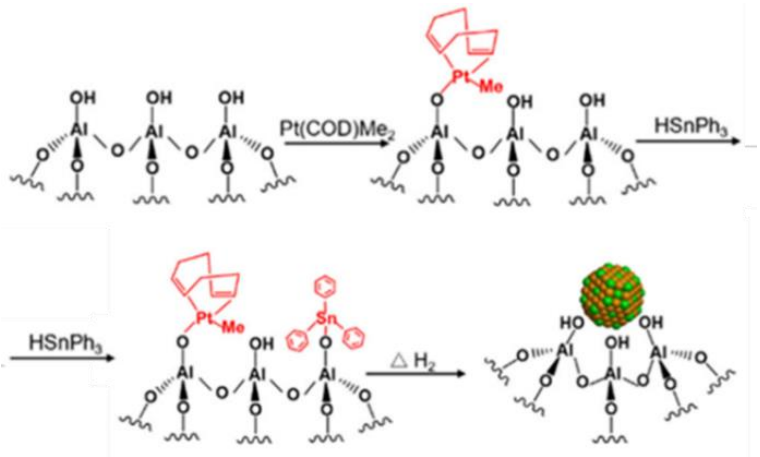

Figure 3.5. Synthesis scheme of PtSn/ɵ-Al_2O_3 by SOMC. [3]

Then, the PtSn/ɵ-Al_2O_3 catalysts prepared at different Sn/Pt ratios were tested in PDH at 550 ^oC using 10 % propane, 10 % hydrogen and He in the feed (equilibrium conversion 45 %). The best catalysts was PtSn(3.0)/ɵ-Al_2O_3 exhibiting good stability for 16 h and a propane conversion of 37% and a propylene selectivity of 99%.[3]

Other examples based on PtM (M ≠ Sn) were described in alkane dehydrogenation, such as PtZn,[28,29] PtB,[30] PtGa,[16,31] (111) using SOMC but these reports lie out of the scope of this thesis.

Various parameters such as the cofeeding steam, hydrogen, O_2 or CO_2, were reported to have a positive effect on the catalytic performance in PDH.[32–37] Recently, experiments showed that for alkane dehydrogenation the cofeeding with hydrogen has a counterintuitive effect that results in improving the activity of Pt-based catalyst.[35,37,38] Upon increasing of the H_2/C_3H_8 ratios, higher turnover frequencies (TOF) to propylene were measured, reaching a maximum for a ratio of 1.25.[37] Nevertheless, the exact cause of the positive effect of hydrogen is still under debate.[39] Various explanations are suggested such as (i) H_2 is reducing the coverage of coke precursors; (ii) an alternative pathway produces propylene at higher H_2 coverage;[38] iii) the reaction energies and barriers are dependent on H_2 coverage in a positive manner;[1,40] and (iv) the subsurface hydrogen could have an effect as well. Other studies indicated that an increased hydrogen coverage is likely to minimize the energy of adsorption of propylene at the surface of the catalyst, thus favouring the process of desorption.[41]

In the present chapter, the SOMC approach (SOMC/Oxide and SOMC/M) was used to produce PDH catalysts using various Pt contents, Sn/Pt ratios onto $LiAl_2O_3$ with as well, various loadings of Li. These catalysts were tested in the Propane Dehydrogenation reaction using different reaction conditions and the effects of H_2 in the feed, temperature, pressure, contact time and oxygen poisoning were particularly looked at. The performance of the best catalyst was also compared with that of a benchmark catalyst for stability studies.

This work was performed in collaboration with the research group of Dr. M. Taoufik (C2P2, CPE Lyon, France), and Dr. Isaias Barbosa Aragao, who was postdoctoral fellow in this group, contributed to the work described in this chapter.

3.2 Results and discussion

In the following sections, the synthesis and characterization of supported Pt-NPs and PtSn-NPs using the Surface Organometallic Chemistry (SOMC) on metals (SOMC/M) and oxides (SOMC/Oxide) will be described as well as their performance in PDH.

3.2.1 Synthesis and characterization of catalysts by SOMC

γ-Al_2O_3 from EVONIK, with a surface area of 100 $m^2 g^{-1}$, was partially dehydroxylated at 500 °C under high vacuum (10^{-5} mbar) to lessen the effect of neighboring -OH groups. n-butyllithium was the Li precursor and readily reacted with the -OH surface groups present in the alumina. A Li loading of 0.45wt% was introduced and verified by ICP-OES. This synthesis was reproduced following a reported procedure.[15] DRIFT spectra revealed the consumption of various Al-OH groups and, the appearance of new peaks from the aliphatic C-H fragments. In the corresponding ^{1}H MAS NMR spectra, signals at 0.1, 0.8 and 1.2 ppm assigned to CH_3, CH_2-Li and CH_2, respectively. In the ^{13}C CP MAS NMR spectra, the corresponding C resonances appeared at -1.1, 11.4, 18.5 and 28.8 ppm were observed and. ^{7}Li MAS NMR spectra displayed a main peak at 0.6 ppm, which was attributed to ≡Al-O-Li (**Figure 3.6)**. Therefore, the presence of physiosorbed BuLi species was confirmed.[42,43]

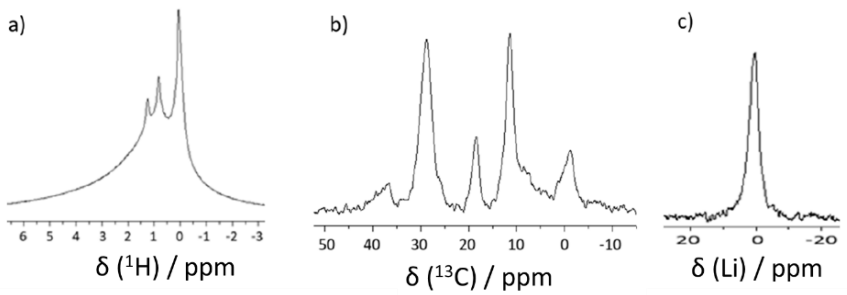

Figure 3.6. NMR characterization of Li(0.45)Al_2O_3. (a) ^{1}H MAS NMR (500 MHz, spinning speed 10 KHz). (b) ^{13}C MAS NMR (125.7 MHz, spinning speed 10 KHz). (c) ^{7}Li CP MAS NMR (194.4 MHz, spinning speed 10 kHz).

Two more loadings of Li were prepared, 0.89 and 1.45 wt% Li (verified by ICP-OES), to study the degree of the alkaline metal promotion.

· Monometallic supported Pt-NPs (SOMC)

First, the grafting of the Pt precursor, $Pt(acac)_2$, onto a dehydroxylated lithiated mesoporous alumina (Li-Al_2O_3) (see experimental section) was performed. A Pt loading of 2 or 0.5 wt.% Pt was targeted.

$Pt(acac)_2$ reacted at r.t. in toluene with the Al-OH groups present on the support, which can be monitored by DRIFT spectroscopy (**Figure 3.7**), revealing a gradual consumption of the Al-OH groups and the appearance of new peaks in the 3000-2800 cm^{-1} region, which are typical of the C-H stretching frequencies of the organic ligand. The broad absorption at 3800-3400 cm^{-1} indicated the presence of Al-OH groups interacting with the surface of the organometallic fragment. Additionally, C-C and C=O stretching, at *ca.* 1530 and 1600 cm^{-1}, respectively, could be observed and assigned to the acetylacetonate ligand (acac) bonded to Pt atoms, which indicated a successful grafting.[15] After calcination and reduction, the previous bands could not be detected, indicating that the ligand had been removed. Only residual Al-OH bands could be observed, and Pt-NPs were formed. The final Pt loading was measured by ICP-OES, showing 1.7 wt.% Pt (from the theoretical 2%). For comparison purposes, a Pt loading of 0.5 wt.% in Pt was also synthesized.

To gain further information about the availability of the Pt active sites for catalysis, H_2 chemisorption experiments were carried out (**Figure 3.8 a**). The irreversible adsorption of H_2 was measured by subtraction of the total adsorption curve and the reversible curve at their plateau. The number of exposed Pt atoms corresponds to the number of H atoms adsorbed. For the sample Pt/Li(0.45)Al_2O_3, a total of 35.6 $\mu molPt \cdot gcat^{-1}$ was obtained. This result was in very good agreement with the mean size distribution of 1.77 ± 0.37 nm observed by TEM (**Figure 3.8 b,c**), when an homogeneous distribution of Pt-NPs along the support was accomplished.

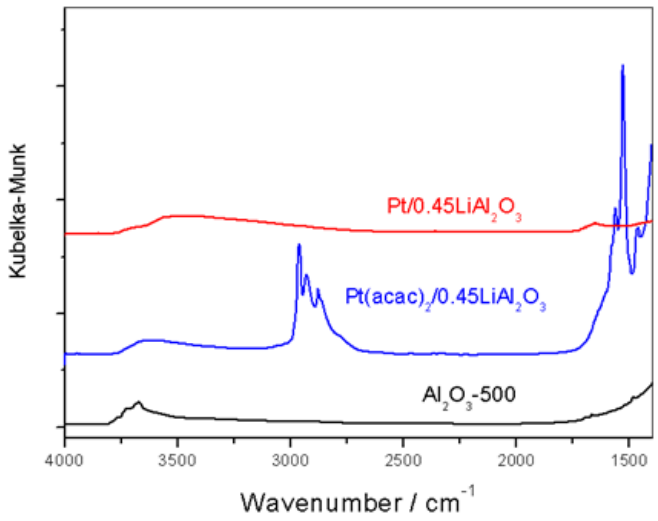

Figure 3.7. DRIFT spectra of the stepwise synthesis of Pt/Li(0.45)Al_2O_3. Bare support (black), sample after grafting the precursor, $Pt(acac)_2$ (blue) and, sample after calcination and reduction treatment to obtain the supported Pt-NPs as Pt/Li(0.45)Al_2O_3. (red).

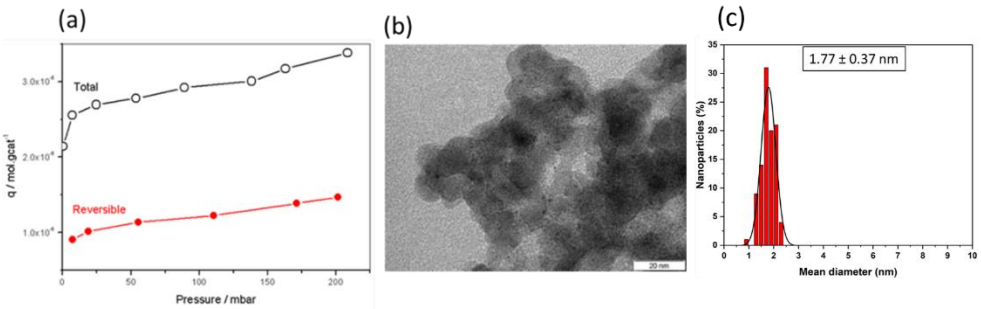

Figure 3.8. Pt/Li(0.45)Al_2O_3 characterized by (a) H_2 chemisorption showing the total adsorption curve (black) and the reversible adsorption curve (red). (b) TEM image and (c) size histogram.

X-Ray Diffraction (XRD) was also carried out (**Figure 3.9**). However, only the support pattern was observed due to the low metal loading. No other diffraction peaks were observed, suggesting that small Pt-NPs were well dispersed onto the surface of the support, in agreement with what Basset and coworkers observed for other supported catalysts onto alumina.[3]

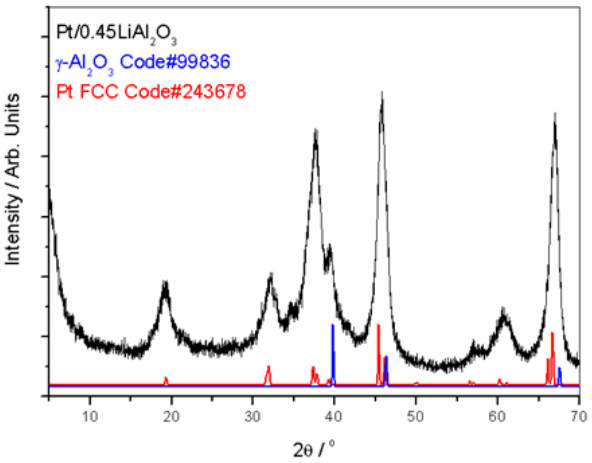

Figure 3.9. XRD diffractogram of Pt/Li(0.45)Al_2O_3 (black) and the standards for Pt (red) and Al_2O_3 (blue) in bands are shown for comparison. Radiation CuKα.

· Bimetallic supported PtSn (SOMC)

Once the Pt-NPs were synthesized by SOMC/Oxide, the next step consisted in applying the SOMC/M with $SnBu_4$ to obtain the supported bimetallic PtSn-NPs.

The monometallic catalyst with a theoretical 2 wt.% Pt, Pt/Li(0.45)Al_2O_3, was modified with $SnBu_4$ in the presence of H_2 at 80 ^oC, targeting a Sn/Pt (mol/mol) ratio of 0.7. After a reductive treatment at high temperature under H_2, the remaining organic fragments were removed and PtSn(0.7)/Li(0.45)Al_2O_3 was formed. ICP-OES revealed a 1.64 wt.% Pt and 0.73 wt.% Sn, corresponding to a molar ratio of Sn/Pt of 0.73. The slightly lower Pt loading in this catalyst is typically observed since the Sn adds to the total weight of the catalyst. The grafting was monitored by DRIFT (**Figure 3.10**). After grafting of the Sn precursor ($PtSnBu_4$/0.45Li-Al_2O_3 (pink line)), new peaks appeared in the 3000-2800 cm^{-1} region. These peaks are characteristic of the C-H stretching frequencies arising from $SnBu_4$. After calcination and reduction, the final catalyst PtSn(0.7)/Li(0.45)Al_2O_3 (purple line) was obtained, the fading of the previous peaks was clearly observed. Regarding the grafting process, the Sn modification was also monitored and quantified by GC, where butane formed from $SnBu_4$ was the only product observed after 24 h, with a typical value

of 3 moles of butanes per mole of Pt. These results are in agreement with those previously reported.[18]

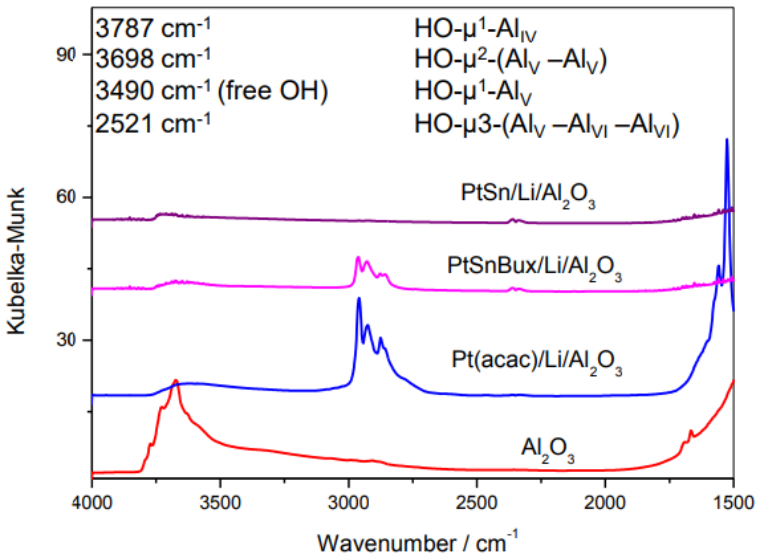

Figure 3.10. DRIFT spectra of (red) Al_2O_3 support, (blue) first grafting Pt(acac)/$LiAl_2O_3$, (pink) second grafting $PtSnBu_x/LiAl_2O_3$ and (purple) final catalyst $PtSn/LiAl_2O_3$.

H_2-Chemisorption experiments were also performed to measure the metallic dispersion (**Table 3.1**). The monometallic catalyst adsorbed 35.6 μmolH $gcat^{-1}$ and after Sn addition, the H_2 adsorption decreased to 14.3 μmolH $gcat^{-1}$, yielding to a Pt dispersion of 16%, due to Sn was deposited on Pt surface.

Table 3.1. H_2-Chemisorption results.

Catalyst	Mmol H $gcat^{-1}$	Dispersion / %
$Pt/Li(0.45)Al_2O_3$	35.6	41
$PtSn(0.7)/Li(0.45)Al_2O_3$	14.3	16

Unless stated theoretical Pt loading is 2 wt.%

HAADF-STEM image and size distribution were obtained (**Figure 3.11**), providing a mean size of 1.8 ± 0.3 nm. The NPs were well-dispersed on the supports and no aggregates were detected. The mean size of the bimetallic NPs was thus identical to that of monometallic NPs.

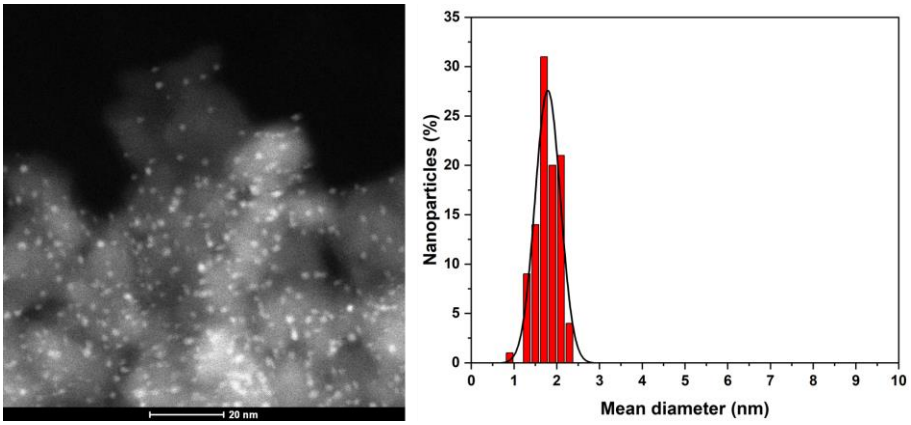

Figure 3.11. HAADF-STEM image and size distribution histogram of PtSn(0.7)/Li(0.45)Al_2O_3.

To gain further information on the composition and distribution of PtSn-NPs, analysis by energy dispersive spectroscopy coupled to scanning-transmission electron microscopy (EDS-STEM) was performed (**Figure 3.12**). In the EDS-STEM mapping, Pt and Sn can be observed in the selected regions. If we focus on the EDS-STEM line scan of a single particle, which allows more accurate measurements the presence of Sn was only observed onto the Pt-NPs. This confirmed that SOMC/M method is a very good approach to selectively graft Sn onto Pt.[18]

By XRD analysis, only the pattern of the support was detected as for monometallic catalyst. This suggested that small Pt-NPs were well dispersed onto the surface of the support and that the structure of the support was maintained, in agreement with previous reports.[3]

Atomic composition and oxidation state of Pt and Sn were assessed by X-Ray Photoelectron Spectroscopy (XPS). The typical band for Pt is the 4f, with two peaks at $Pt4f_{5/2}$ and $Pt4f_{7/2}$ described at binding energies of 74.7 eV and 71.53 eV for Pt(0), with the possibility to have additional peaks due to the existence of other phases of Pt such as Pt(II) and/or Pt(IV).[44] In our case the Pt 4f band could not be used due to an overlapping with the Al 2p arising from Al_2O_3. Therefore, the Pt 4d line, that was weaker but not overlapped, was used instead. [45] Concerning Sn, the Sn 3d

bands used ($Sn3d_{1/2}$ and $Sn3d_{3/2}$).[14] The binding energies used are detailed in **Table 3.2**.

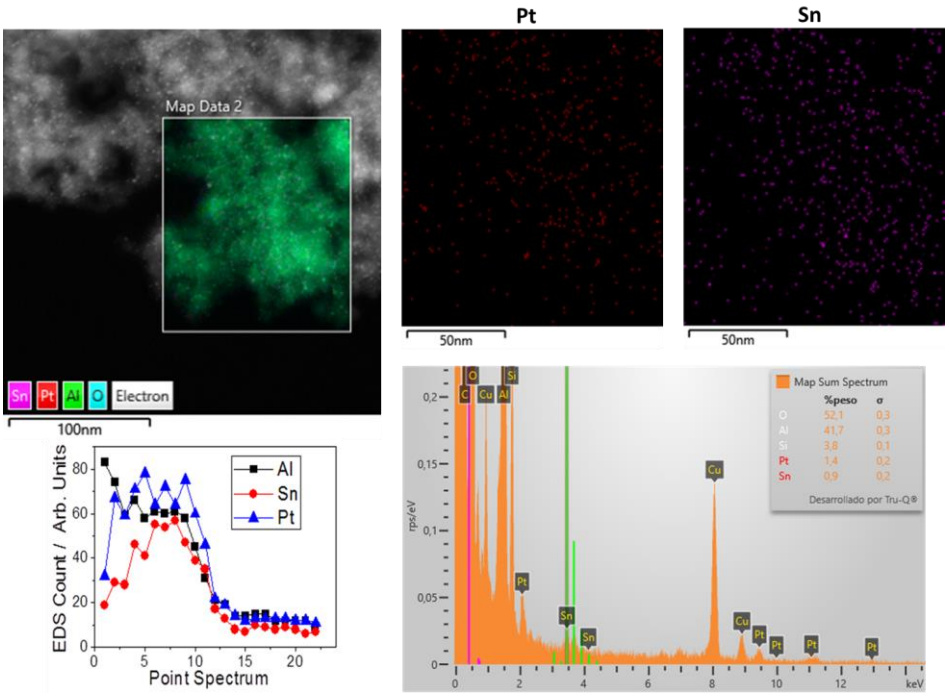

Figure 3.12. EDS-STEM mapping of $PtSn(0.7)/Li(0.45)Al_2O_3$, a general view, Pt and Sn. EDS-STEM line scan of a single particle and EDS mapping of zone selected in first picture.

Table 3.2. Deconvolution binding energies used in CASAXPS for Pt and Sn in supported catalysts.

	$Pt4d_{1/2}$	**$Pt4d_{3/2}$**
Pt (0)	314.4-314.7 eV	331.4-331.7 eV
Pt (δ+)	317.7-318.2 eV	334.6-335.2 eV
	$Sn3d_{1/2}$	**$Sn3d_{3/2}$**
Sn (0)	485.2 eV	493.9 eV
Sn (II)	486.4 eV	494.8 eV
Sn (IV)	487.2 eV	495.2 eV

XPS measurements confirmed that the presence of metallic Pt (0) was predominant, with Pt (70%) *vs.* Pt (δ^+) (30%). The oxidized Pt species are attributed to the oxidation of the surface by O_2 while metallic Pt (0) is located in the core of the PtSn.[14] Regarding Sn, the proportion of Sn(IV)/Sn(II)/Sn(0) was 86/0/14. According to Basset and coworkers, all the Sn (0) and Pt (0) observed should be forming an alloy PtSn,[14] since Sn and Pt component must be in metallic form to produce an alloy.[46] Regarding Sn (IV) and Sn (II) species there could be in a "Sn^{x+}-O-M" form, similarly to what was reported by Corma and co-workers.[47] However, it was not possible to confirm whether metallic Sn enters Pt structure to form the alloy architecture by XPS, XRD (where we only observed the support) nor TEM. The Sn/Pt ratio calculated by XPS was 1.0, thus slightly higher than the ratio obtained by ICP-OES. Sn/Pt ratios within the same order of magnitude (*ca.* 0.52) were previously measured by the XPS using comparable experimental Sn/Pt ratios (between 1:1 and 2:1).[14] Since the ratio was here slightly higher, Sn segregation on the surface could be indicated in agreement with Sn located at the surface of PtSn.[14] Our hypothesis according to the data provided is that the SnO_{2-x} can interact with PtSn in three different manners: as a core shell, as interacting with the support, or even on top of the PtSn NP (**Figure 3.13**).

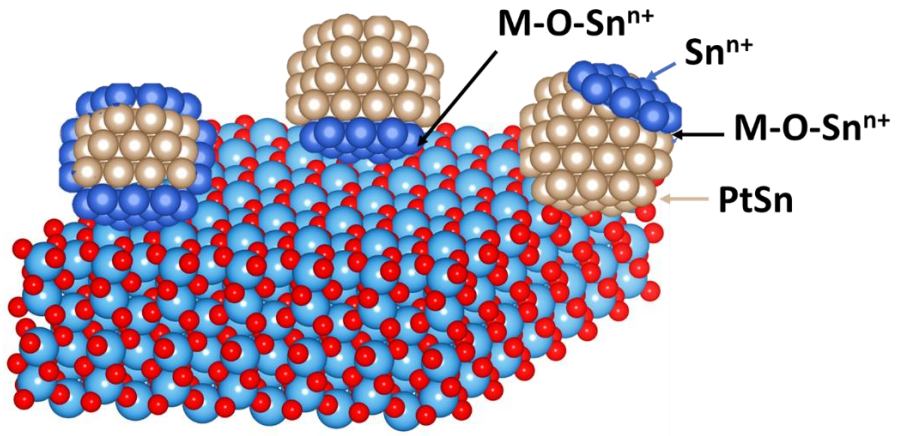

Figure 3.13. Proposal of SnO_{2-x} structures in the PtSn catalyst supported on Al_2O_3.

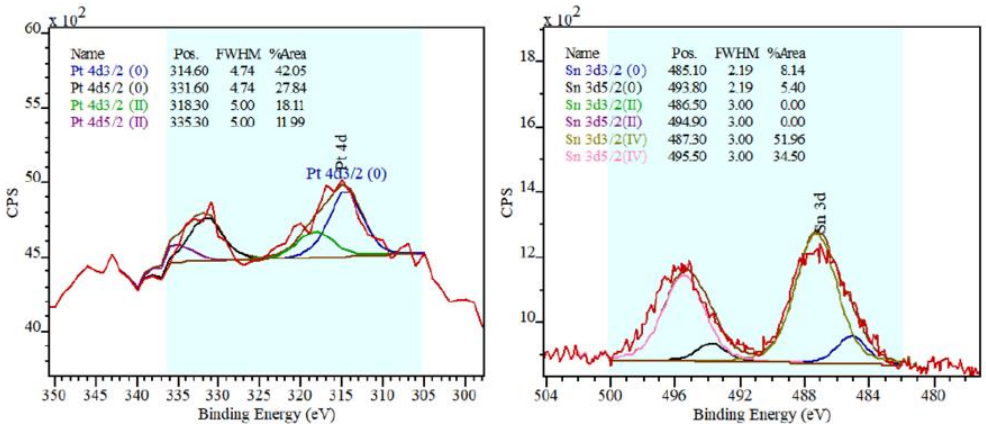

Figure 3.14. XPS analysis of (left) Pt 4d and (right) Sn 3d of PtSn(0.7)/Li(0.45)Al_2O_3.

A total of 6 bimetallic catalysts supported onto lithiated alumina were synthesized and characterized following the procedure above described. The Sn/Pt ratio was varied to 0.5 and 1.0 on the Li(0.45)Al_2O_3 support. It is important to highlight that H_2 chemisorption experiments revealed that at higher Sn loading, less Pt was located at the surface because less H_2 was adsorbed, with values of 12.1 and 6.2 µmol H $gcat^{-1}$ for 0.5 and 1.0 Sn/Pt ratios, respectively. Moreover, the average NPs diameters for PtSn catalyst supported onto Li(0.45)Al_2O_3 **(Figure 3.15**) were slightly greater after Sn addition. In all cases, no agglomeration was detected.

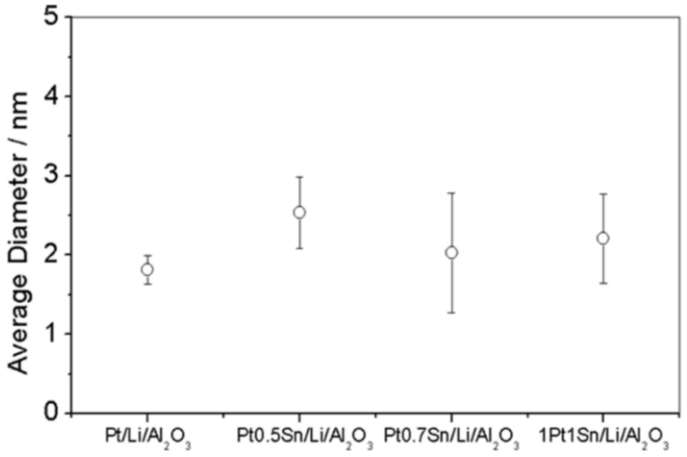

Figure 3.15. NPs average diameter supported onto Li(0.45)Al_2O_3 of the monometallic (Pt) and bimetallic (PtSn) NPs, changing the Sn/Pt ratio to 0, 0.5, 0.7 and 1.0.

Various Li loadings were tested (0.8 and 1.5Li wt.%) with the Sn/Pt ratio of 0.7. The Pt and Sn loadings and Sn/Pt ratios are listed in **Table 3.3**.

Table 3.3. Bimetallic PtSn supported catalyst synthesized by SOMC approach.

Catalyst [a]	Pt(Sn) wt.% [b]	Sn/Pt
PtSn(0.5)/Li(0.45)Al_2O_3	1.70 (0.57)	0.55
PtSn(0.7)/Li(0.45)Al_2O_3	1.64 (0.73)	0.73
PtSn(1.0)/Li(0.45)Al_2O_3	1.67 (1.14)	0.70
PtSn(0.7)/Li(0.80)Al_2O_3	1.89 (0.78)	0.67
PtSn(0.7)/Li(1.5)Al_2O_3	1.92 (0.54)	0.46
0.5PtSn(0.7)/ Li(0.45)Al_2O_3	0.5	0.70

a = Unless stated, theoretical content of Pt is 2 wt.% b = Measured by ICP-OES.

Therefore, it can be concluded that a series of catalysts based on Pt and Sn supported on $LiAl_2O_3$ was successfully synthesized using SOMC methodology. These catalysts contain well-dispersed NPs with mean sizes of *ca.* 1.7-2.0 nm. In the next section, their catalytic performance in PDH is described.

3.2.3 Catalytic evaluation in PDH

Various effects were studied in PDH reaction: (1) the influence of the Sn/Pt ratio; (2) the additive content, and (3) the Pt loading. Furthermore, a study of the operation conditions of PDH reaction regarding the effect of (i) H_2; (ii) temperature and pressure; (iii) contact time; and (iv) oxygen poisoning was assessed.

Unless stated differently, the catalytic tests were carried out inside a stainless-steel fixed bed reactor at 530 ^oC and 1 bar of pressure, using a Gas Hourly Space Velocity (GHSV) of 15.000 $mL \cdot g^{-1} \cdot h^{-1}$, 25 mg of catalyst dispersed in SiC and the feed gases applied where 3 C_3H_8 / 1 H_2 / 21 Ar (expressed in mL/min). In the Experimental section of the present chapter, all the details concerning conversion and selectivity calculations are described.

(1) Influence of Sn/Pt ratio.

With a loading of 2 wt.% Pt and using Li(0.45)Al_2O_3 as support, the effect of various Sn/Pt ratios (0, 0.5, 0.7 and 1.0) was evaluated in PDH reaction. When the monometallic catalyst Pt/Li(0.45)Al_2O_3 was tested in PDH at 560°C and 1 bar (**Figure 3.16**), the propane conversion was initially near 25% and decreased to 15% after 10h of TOS. Concerning the selectivity, the main product obtained was propylene (*ca.* 90%) and the main by-products were methane (C1) and ethane (C2).

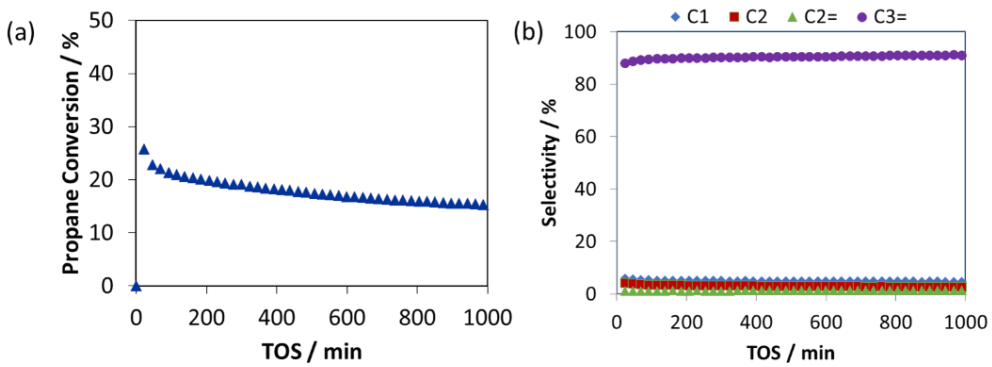

Figure 3.16.(a) Propane conversion of Pt/Li(0.45)Al_2O_3 and (b) selectivity. PDH Conditions: 560 °C, 1 bar, $3C_3H_8$/1 H_2/21 Ar (mL/min), GHSV = 15000 mL·$gcat^{-1}$·h^{-1}

Then, the bimetallic catalysts with various Sn/Pt (mol/mol) ratios of 0.5, 0.7 and 1.0 were tested in PDH at 560°C and 1 bar (**Figure 3.17**). The propane conversion, was enhanced when Sn/Pt ratios of 0.5 and 0.7 were used, reaching an initial propane conversion of 34% and 33%, respectively; and after 600 min of TOS the conversion was 24% and 32%, respectively. However, when Sn/Pt 1 was used, the propane conversion decreased to 7%. This suggested that the surface was saturated. H_2 chemisorption measurements indicated above, where the µmolH $gcat^{-1}$ of Sn/Pt ratios of 0, 0.5, 0.7 and 1 were: 35.6, 12.1, 14.3 and 6.2, respectively with a dispersion of 41%, 13%, 16% and 7%, respectively. Concerning selectivity, independently of the Sn/Pt ratio, all the catalysts were selective to propylene with *ca.* 99%. This clearly indicated the promoting effect of Sn that geometrically affected the surface of Pt-NPs, inhibiting hydrogenolysis pathways.

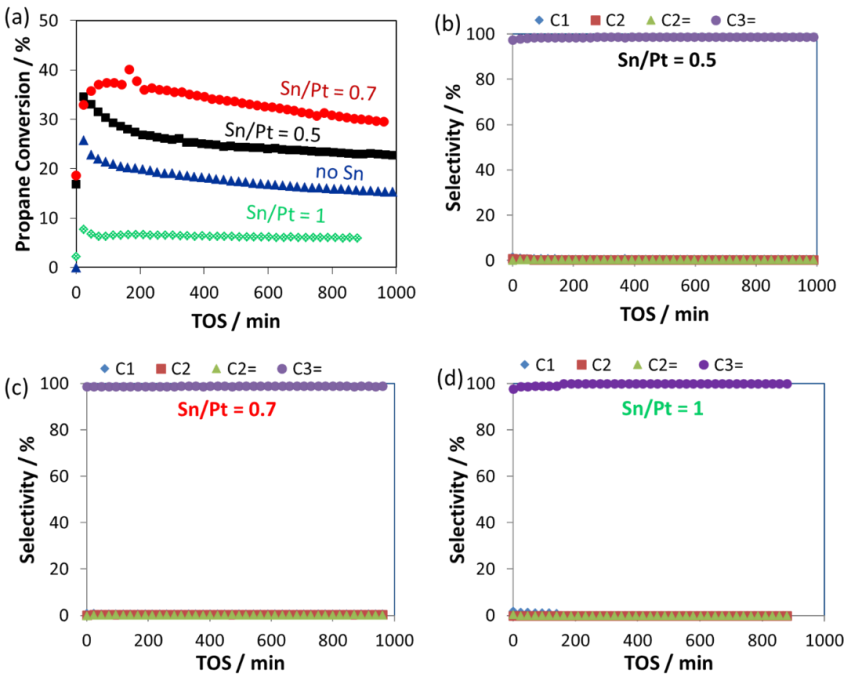

Figure 3.17.(a) Propane conversion of PtSnx/Li(0.45)Al_2O_3 catalysts with various Sn/Pt ratios (x = 0, 0.5, 0.7 and 1.0). Selectivity of (b) PtSn(0.5)/Li(0.45)Al_2O_3, (c) PtSn(0.7)/Li(0.45)Al_2O_3 and (d) PtSn(1)/Li(0.45)Al_2O_3. PDH Conditions: 560ºC, 1 bar, $3C_3H_8$/1 H_2/21 Ar (mL/min), GHSV = 15000 mL·gcat^{-1}·h^{-1}

In **Figure 3.18**, a volcano-like behaviour can be observed as the addition of Sn improves activity but, at the same time, poisons the Pt sites. Therefore, it is of uppermost importance to pay attention to the Sn/Pt ratio to minimize the side reactions and therefore maximize activity and selectivity.

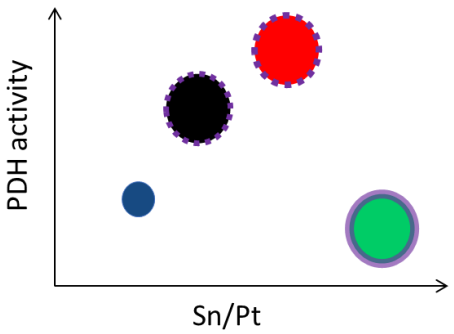

Figure 3.18. Volcano-like behavior in PDH activity of PtSnx/Li(0.45)Al_2O_3 catalysts with various Sn/Pt ratios (x = 0, 0.5, 0.7 and 1.0).

The Sn/Pt ratio showing the best compromise was 0.7, achieving a propane conversion of 33% and a propylene selectivity of 99% at 560 ^{o}C. Comparing to the literature in PDH, PtSn(3.0)/ɵ-Al_2O_3 displayed similar conversion (37%) and propylene selectivity of 99% at 550 ^{o}C.[3] When another support such as $MgAl_2O_4$ was used, the best Sn/Pt molar ratio was 1:0.5 to reach a conversion of 38.9% and a selectivity of 99.7%, at higher temperature (580 ^{o}C).[14] In another study based on the isobutane dehydrogenation at 550 ^{o}C, the optimum Sn/Pt ratio was also 0.7.[19]

(2) Effect of Li loading on Al_2O_3.

The Li loading (0.45, 0.8 and 1.5 wt.% Li) on Al_2O_3 was studied maintaining the Sn/Pt ratio at 0.7 (with 2 wt.% Pt). The performance of these catalysts in PDH at 560^{o}C and 1 bar (**Figure 3.19**) followed the order: 0.45 ≥ 0.8 > 1.5 % Li, with a propane conversion at 800 min of 32%, 29% and 11%, respectively. The 0.45 and 0.8 Li loadings had a similar behaviour, but the sample with less Li (0.45 wt.% Li) was selected as the most promising catalyst. A notable difference in activity was observed when a loading of 1.5 wt.% Li was used. This could be assigned to the presence of lithium oxides at the surface of the catalyst due to an excess of BuLi. The propylene selectivity was high in all cases (*ca.* 98%). Therefore, these results show the importance of optimizing not only the Sn content but also the Li content. A previous study showed the importance of Li in PDH.[48] The presence of Li improved the activity and stability of the catalyst in the conversion of 2,3-dimethylbutane into 2,3-dimethylbutene, although in this case, the Li content was not optimized and a loading of 2.8 wt.% Li was used.[15]

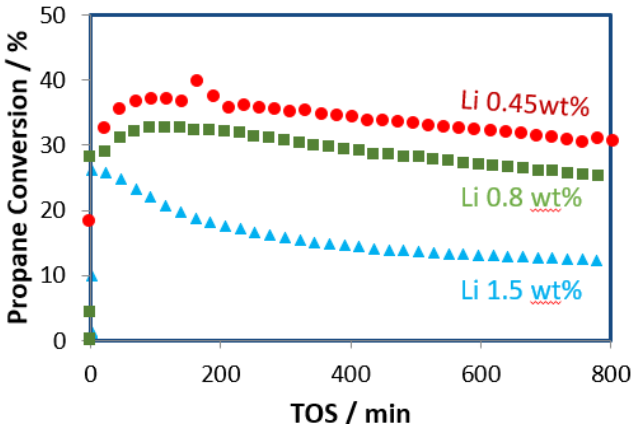

Figure 3.19. Catalytic activity of bimetallic PtSn(0.7)/Li(x)Al_2O_3 with x = 0.45, 0.80 or 1.50wt.%Li. PDH Conditions: 560 ^oC, 1 bar, $3C_3H_8$/1 H_2/21 Ar (mL/min), GHSV = 60.000 mL·$gcat^{-1}$·h^{-1}

(3) Loading of Pt.

Next, the effect of Pt loading was looked at. Indeed, lowering the metal loading of a noble transition metal such as Pt is not only interesting economically but could also affect the size of the NPs. Regarding the monometallic catalysts, 0.5 and 2.0 wt.% Pt loadings were studied with Li(0.45)Al_2O_3 as a support in PDH reaction at 560^{o}C and 1 bar (**Figure 3.20 a**). The propane conversion for the catalyst with 0.5% is lower than for 2 wt.% Pt when using the same amount of catalyst. When the mass of the weighted catalysts (0.5 wt.% Pt) was increased 4 times to have the same Pt content, the propane conversion increased from 16 to 21%. Concerning the bimetallic catalysts (**Figure 3.20 b**), 0.5 wt.% Pt was tested with Sn/Pt ratio of 0.7. In that case, the propane conversion increased from 8% to 15%. However, the rest of this study was conducted with 2 wt.% Pt since very low metal contents difficult the characterization of the samples.

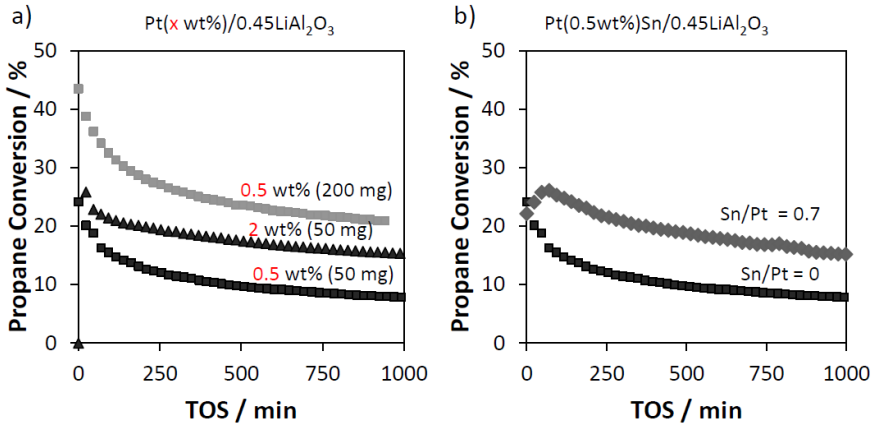

Figure 3.20. Catalytic activity of (a) monometallic and (b) bimetallic catalysts based on Pt variation supported onto $Li(0.45)Al_2O_3$. PDH Conditions: 560 ◦C, 1 bar, $3C_3H_8/1\ H_2/21$ Ar (mL/min), GHSV = 15.000 $mL{\cdot}gcat^{-1}{\cdot}h^{-1}$

Study of the operation conditions.

The optimization of the operational parameters is not trivial in PDH reaction.[32–37] In the following sections, the effect of various parameters such as (i) partial H_2 pressure; (ii) temperature and pressure; (iii) contact time; (iv) oxygen poisoning; (v) propane concentration will be assessed. Moreover, the best catalyst will be (vi) compared with a benchmark technology; (vii) subjected to a stability test and (viii) tested under CO_2 poisoning.

(i) Study of H_2 partial pressure in the feed.

The stability of a catalyst is usually directly affected by the modification of the gas composition of the feed. The presence of hydrogen (H_2) in the stream could lower the conversion at equilibrium due to the thermodynamics, but also lead to a more stable catalyst. Here, two ratios of C_3H_8/H_2 were tested with $PtSn(0.7)/Li(0.45)Al_2O_3$ obtained: (1) C_3H_8/H_2= 3 and, (2) C_3H_8/H_2= 1 (see **Figure 3.21**). However, practically no difference in conversion nor propane selectivity (*ca.* 99 %) could be observed. Since a slightly better conversion and stability was achieved with the C_3H_8/H_2= 3 ratio, this proportion was maintained in subsequent tests. Previous report

described that with at higher H_2/C_3H_8 ratio, an increase in the turnover frequency (TOF) in propylene during PDH was observed, reaching a maximum at 1.25 ratio.[37,39]

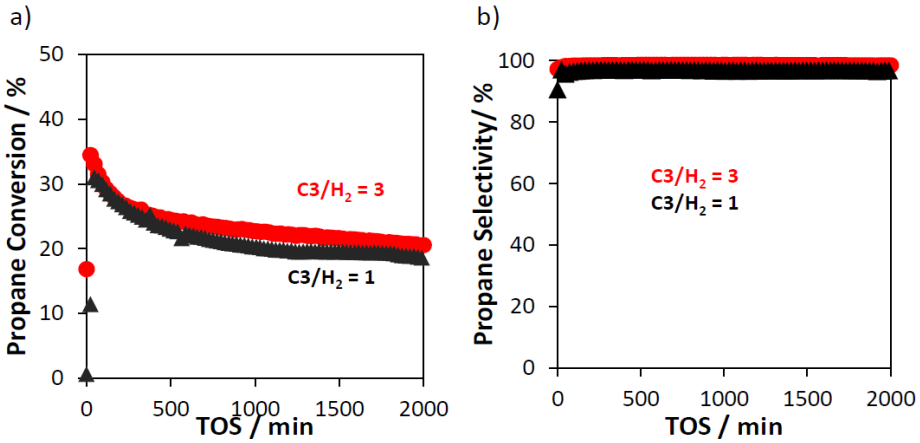

Figure 3.21. Study of the C_3H_8/H_2 ratio variation of 1 (black) or 3 (red) using bimetallic PtSn(0.7)/Li(0.45)Al_2O_3 and its (a) Catalytic activity and (b) Propane Selectivity in PDH reaction. PDH Conditions: 560 ◦C, 1 bar, $3C_3H_8/x\ H_2/21$ Ar (mL/min) where x = 1 or 3, GHSV = 15.000 $mL{\cdot}gcat^{-1}{\cdot}h^{-1}$

3

(ii) Study of the temperature and pressure.

The temperature and pressure have a direct effect on the PDH conversion since it affects the thermodynamics of the reaction.[49] The variation of the equilibrium propane conversion was discussed in Chapter 1. Since the PDH is endothermic, conversion is favoured at high temperatures and low pressures. The effect of temperature was evaluated at 500 ^oC, 530 ^oC and 560 ^oC using PtSn(0.7)/Li(0.45)Al_2O_3 as catalyst (**Figure 3.22**). As expected, it was observed that the higher the temperature, the higher the propane conversion, achieving a propane conversion of 33% at 560 ^oC. At that temperature (**Figure 3.22**), the selectivity was maintained at *ca.* 90% of propylene. In contrast, at 530 ^oC, the selectivity to propylene was above 98%, showing a good compromise in terms of selectivity and activity. At lower temperature, lower conversion was obtained but high selectivity to propylene was obtained. Thus, the selected temperature was 530 ^oC for the subsequent experiments.

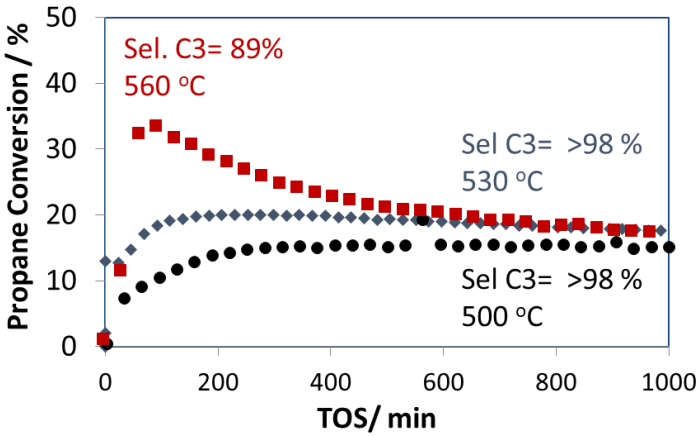

Figure 3.22. Effect of temperature at 500 °C, 530 °C and 560 °C with PtSn(0.7)/Li(0.45)Al_2O_3 in the Propane Conversion, propylene selectivity is indicated. PDH Conditions: T (500 °C, 530 °C and 560 °C), 1 bar, $3C_3H_8$/1 H_2/21 Ar (mL/min), GHSV = 60.000 mL·gcat^{-1}·h^{-1}

The effect of the pressure (1 or 3 bar) was also evaluated (**Figure 3.23**). At high pressure values (3 bar) low conversion was obtained (*ca.* 5%) due to thermodynamic limitations. In terms of selectivity to propylene, 80% was measured. On the other hand, when 1 bar of pressure was used, a propane conversion of 30% and a propylene selectivity of 95% were obtained. These results show as expected that at higher pressure, there is a negative effect on the performance of the catalyst.

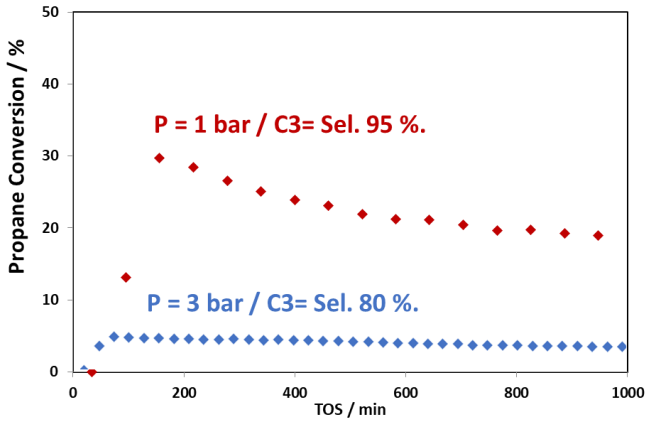

Figure 3.23. Effect of pressure (1 or 3 bar) with PtSn(0.7)/Li(0.45)Al_2O_3 in the Propane Conversion, propylene selectivity indicated. PDH Conditions: 560 °C, P = 1 or 3 bar, $3C_3H_8$/1 H_2/21 Ar (mL/min), GHSV = 60.000 mL·gcat^{-1}·h^{-1}

(iii) Study of the contact time.

The contact time refers to the Gas Hourly Space Velocity (GHSV):

$$GHSV = \frac{Total\ flow\ (\frac{mL}{h})}{g{\cdot}catalyst}$$

Three different values of GHSV were studied: 15.000, 60.000 and 120.000 $mL{\cdot}g_{cat}^{-1}{\cdot}h^{-1}$ (**Figure 3.24**). Concerning the initial propane conversion, a higher value was obtained with at lower GHSV: 35%, 20% an 10% for 15.000, 60.000 and 120.000 $mL{\cdot}g_{cat}^{-1}{\cdot}h^{-1}$, respectively. Moreover, the conversion after 10h (600min of TOS), was maintained. In terms of propylene selectivity, no effect was observed (> 98% in all cases). Thus, it can be concluded that increasing the GHSV lowers the conversion.

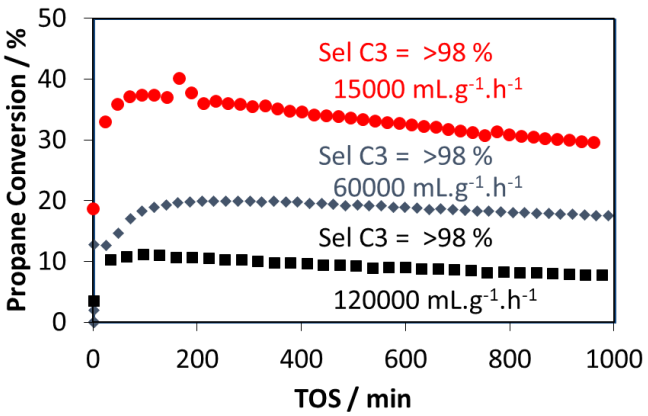

Figure 3.24. Effect of GHSV (15000, 60000 or 120000 $mL{\cdot}gcat^{-1}{\cdot}h^{-1}r$) with $PtSn(0.7)/Li(0.45)Al_2O_3$ in the Propane Conversion, propylene selectivity indicated. PDH Conditions: 560 ◦C, P = 1 bar, $3C_3H_8/1\ H_2/21$ Ar (mL/min), GHSV = 15.000, 60.000 or 120.000 $mL{\cdot}gcat^{-1}{\cdot}h^{-1}$

(iv) Study of oxygen poisoning.

The oxygen poisoning is another parameter to consider since all the catalysts were prepared under inert conditions using glove box techniques. The performance of $PtSn(0.7)/Li(0.45)Al_2O_3$ was compared when the catalyst sample was charged in the glove box and when charged outside, thus exposed to air. In the experiments, its catalytic activity (**Figure 3.25**) and the selectivity remained unchanged. Therefore,

the present catalyst could be easily stored and packed under air, which could be of interest for possible industrial applications.

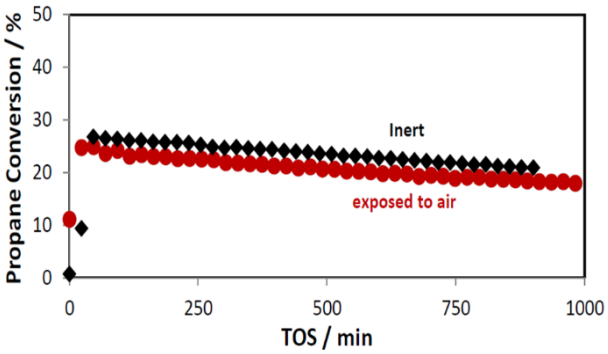

Figure 3.25. Catalytic activity of PtSn(0.7)/Li(0.45)Al_2O_3 tested with inert handling (black diamonds) and under air exposure (red balls). PDH Conditions: 530 ◦C, 1 bar, 3C_3H_8/1 H_2/21 Ar (mL/min), GHSV = 60.000 mL·gcat^{-1}·h^{-1}

(v) Comparison with a benchmark catalyst.

Linde-BASF-Statoil catalyst Pt(0.3 wt.%)Sn/Mg(Al)O was used as a benchmark catalyst and its performance was compared to PtSn(0.7)/Li(0.45)Al_2O_3. The catalyst weight was increased to ensure similar Pt content. Using the same conditions, the catalytic activity of Linde-BASF-Statoil catalyst (**Figure 3.26 a**), displayed very low conversion values (stabilizing near 3.5%) in comparison with PtSn(0.7)/Li(0.45)Al_2O_3 (stabilizing near >30%).

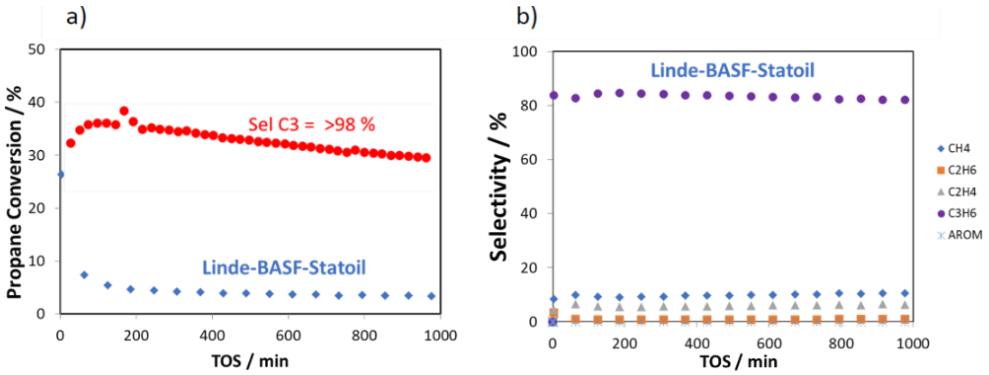

Figure 3.26. (a) Catalytic activity of PtSn(0.7)/Li(0.45)Al_2O_3 (red balls) and Linde-BASF-Statoil (blue diamonds). (b) Selectivity of Linde-BASF-Statoil catalyst (Pt(0.3)Sn/Mg(Al)O). PDH Conditions: 560 ◦C, 1 bar, 3C_3H_8/1 H_2/21 Ar (mL/min), GHSV = 60.000 mL·gcat^{-1}·h^{-1}

Moreover, the propylene selectivity provided by the benchmark catalyst (**Figure 3.26 b**) was only 80%, far from the >98% obtained with the synthesized PtSn catalyst. Therefore, it was concluded that, under the same conditions, the catalyst prepared in this work is more active and selective than the benchmark Linde-BASF-Statoil.

(vi) Stability test against time.

To test the stability of PtSn(0.7)/Li(0.45)Al_2O_3 a 3000min test was performed at 530^o C. As shown in (**Figure 3.27**), almost no deactivation was observed over time with an initial propane conversion of 20% and 14% after 3000min.

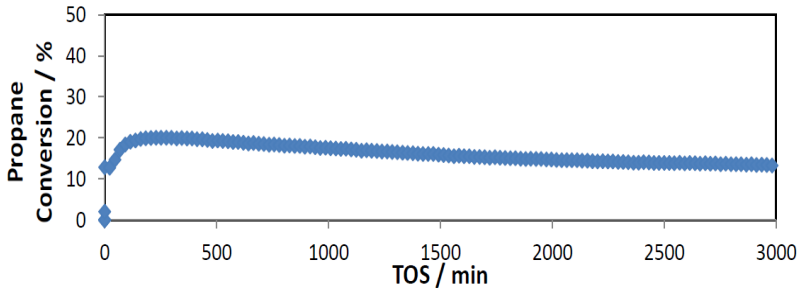

Figure 3.27. Long runs for the best PtSn catalyst synthesized by SOMC PtSn(0.7)/Li(0.45)Al_2O_3. PDH Conditions: 530 ◦C, 1 bar, $3C_3H_8$/1 H_2/21 Ar (mL/min), GHSV = 15.000 mL·gcat^{-1}·h^{-1}

The deactivation constant (K_d) was calculated at time 10h and 50h and was 0.0031 and 0.0085 h^{-1}, respectively.

3.3 Conclusions

A series of Pt and PtSn-NPs supported onto $LiAl_2O_3$ were prepared by SOMC/Oxide followed by SOMC/M and tested in the PDH reaction. The catalysts were characterized by various techniques such as TEM, HAADF-STEM, N_2-adsorption/desorption isotherms, H_2-chemisorption, DRIFT and XRD, which revealed the presence of small and well-dispersed bimetallic NPs, crucial to obtain highly active and selective catalysts for PDH.

Moreover, an exhaustive study of the operation conditions of PDH concerning the effect of H_2, temperature and pressure, contact time, oxygen poisoning and long-time studies for stability was performed. Finally, the operation conditions were optimized to a propane/H_2 ratio of 3, feed composition of 3 C_3H_8/1 H_2/21 Ar (mL/min), 530 ^oC and 1 bar, inert preparation of the reactor inside the glovebox and, GHSV = 15.000 $mL \cdot gcat^{-1} \cdot h^{-1}$.

The influence of the Sn/Pt ratio, the loading of Li on the support and the Pt loading of the catalyst were also studied. The most promising Sn/Pt ratio was 0.7 (mol/mol), with a Li loading on the Al_2O_3 support of 0.45 wt.% Li. An initial propane conversion of 20% was obtained, still providing 18% and 14% conversion after 900 min and 3000 min of TOS. The selectivity of the optimized catalyst to propylene was always >98%, displaying an excellent performance in PDH, superior to that of the benchmark catalyst (Linde-BASF-Statoil).

3.4 Experimental Details

3.4.1 General Methods.

$Pt(acac)_2$ was purchased from Aldrich and used without further purification. $SnBu_4$ precursor was purchased from Aldrich, degassed, and stored under molecular sieves 4Å before use. Solvents (n-hexane and toluene) were dried under a NaK alloy and degassed by freeze-pump-thaw cycles prior use. Gases were purchased from Air liquide. All experiments were carried out under controlled atmosphere, using Schlenk and glove box techniques for organometallic synthesis. The synthesis and handling of supported species were carried out using high-vacuum lines (*ca.* 1 mPa) and glove boxes. Calcination of the supports and catalyst was performed using in-house produced furnaces (C2P2, CPE) with the following general conditions, 80 mL min^{-1} oxygen flow and 250-500^o C temperature for 16 h. The evolved gases during the grafting reaction were analyzed on a Hewlett-Packard 5890 series II gas chromatograph (GC), equipped with a flame ionization detector (FID) and an HP PLOT KCl/Al_2O_3 column (50 m × 0.32 mm).

3.4.2 Support pre-treatment.

(1) Al_2O_3.

Pyrogenic Al_2O_3 from EVONIK (100 $m^2\ g^{-1}$) was pretreated before use. γ-Al_2O_3 (10 g) was hydrated and compacted by slurring with deionized water and completely dried at 110° C. Later, Al_2O_3 was sieved, calcined under synthetic air at 500° C overnight, and then dehydroxylated under 10^{-5} mbar at 500° C overnight. The solid, labelled as Al_2O_3-500, is stored inside an argon filled glovebox. OH titration was performed by reaction between the support and excess Al*i*Bu_3, which reacts quantitatively with hydroxyl groups from Al_2O_3-500, and quantification of released isobutane by GC. Al_2O_3 samples were characterized by TEM analysis, N_2 adsorption/desorption isotherms, DRIFT and solid-state NMR.

(2) Li-Al_2O_3.

Al_2O_3-500 (3.0 g) was lithiated with BuLi (0.8 mL, 2.5 mol L^{-1} in hexanes) at room temperature in hexane (10 mL) for a minimum of 2 h, then it was filtered, washed (3x hexane 10 mL) and dried under vacuum (10^{-5} mbar), yielding 0.45 wt.% Li, which was called Li(0.45)Al_2O_3. Li content was studied and two other Li-Al_2O_3 were prepared. Sample with 1.5 wt.% Li, was prepared without washing steps, the sample was dried directly after the reaction, which yielded the sample Li(1.5)Al_2O_3. The second, an excess of BuLi was used (eq. to 4 wt% of Li) but the solid was thoroughly washed, which yielded the sample labelled Li(0.89)Al_2O_3. Li-Al_2O_3 samples were characterized by TEM analysis, N_2-adsorption/desorption isotherms, DRIFT and solid-state NMR.

3.4.3 Catalyst Preparation by SOMC.

PtSn-catalysts were prepared by a two-step grafting. First, $Pt(acac)_2$ (205 µmol, 81 mg) is grafted on 2 g of the oxide support (LiAl_2O_3) at room temperature, overnight, using the desired amount of precursor on toluene to achieve 2wt% of Pt. Then, the Pt nanoparticles (Pt-NPs) were formed by calcination at 400 °C, 4°C min^{-1}, for 4 h

followed by reduction at 500 °C, 1°C min^{-1}, for 4 h under pure H_2. The monometallic materials were stored inside an Ar filled glovebox.

The second grafting is the reaction of the organotin precursor on the hydride covered Pt-NPs. Briefly, on a double Schlenck, the desired amount of $SnBu_4$ (Sn/Pt ratios of 0.5, 0.7, and 1) is stirred at 80°C in heptane (15 mL) with the monometallic catalyst (max. of 1.2 g per batch) under 500 mbar of pure H_2 overnight. After that, the solid is washed 3 to 5 times with the same solvent to remove the unreacted Sn precursor. Gases and liquid are collected for butane analysis. The powder is dried under vacuum (10^{-5} mbar), and, finally, it is treated under H_2 at 550°C, 1°Cmin^{-1}, 4 h for the hydrogenolysis of the grafted organometallic species and formation of the desired PtSn-NPs. Catalyst samples were characterized by TEM, HAADF-STEM experiments, N_2-adsorption/desorption isotherms, H_2-chemisorption, DRIFT, XRD and solid-state NMR.

3.4.4 Catalyst Characterization.

Transmission Electron Microscopy (TEM) experiments were performed at the "Unitat de Microscopia dels Serveis Cientificotècnics de la Universitat Rovira i Virgili" in Tarragona with a JEOL model 1011 electron microscope operating at 100 kV with resolution of 3 Å. The particle size distributions were determined by a manual analysis of enlarged images. At least 200 particles on a given grid were measured to obtain a statistical size distribution and a mean diameter.

Scanning Transmission Electron Microscopy - High Angle Annular Dark Field (STEM-HAADF) images were obtained in a probe-corrected Titan Low Base (FEI) at a working voltage of 300 kV, coupled with a HAADF detector (Fischione), available in the "Advanced Microscopy Laboratory of Instituto de Nanociencia de Aragón" in Zaragoza. X-ray Energy Dispersive Spectra (EDS) were obtained with an EDAX detector. The samples were dispersed in THF, and a small amount of solution was then deposited on a Cu-carbon grid.

N_2 adsorption/desorption isotherms were acquired in a Micrometrics ASAP 2020 instrument. N_2 adsorption/desorption isotherms were acquired after dehydroxylation, under air-free conditions and without further pretreatments.

Elemental analyses were carried out by inductive plasma coupled atomic emission spectroscopy (ICP-AES) under air-free conditions by Mikroanalytisches Labor Pascher, Remagen (Germany).

Diffuse reflectance infrared - Fourier transform spectroscopy (DRIFTS) was taken at room temperature in a Nicolet 6700 FTIR spectrophotometer equipped with a MCT detector and the SMART accessory DRIFT module in an airtight cell with CaF_2 windows.

Solid-state NMR spectra were acquired on Bruker Advance 500. For Chemical shifts are given in ppm with respect to TMS as external reference. The ^{13}C CP-MAS NMR spectrum was obtained at 11.74 T using the CP-MAS pulse sequence and a high power ^{1}H decoupling at RF field amplitude of 70 kHz. Chemical shifts are given in ppm with respect to TMS as external reference for ^{1}H and ^{13}C.

Powder X-Ray Diffraction (PXRD) patterns were collected on a Bruker D8 Advance diffractometer with Bragg-Brentano geometry goniometer in Theta-Theta mode and Cu Kα1,2 X-Ray source. Diffractograms were collected in 10–70° 2θ range by ethanol dispersion over Silicon support and treated using DIFFRAC.EVA Bruker software.

H_2 chemisorption was measured manually on the high-vacuum lines using high purity H_2, an Edwards 655AB TRANS 1000 MB sensor, and an Edwards model 1575 pressure display. Around 1 g of each sample was reduced in situ at 500ºC for 30 min, the surface is cleaned for 60 min under 10^{-5} mbar at 500ºC, and the measurements are performed at room temperature. Total adsorption is measured stepwise, and after the sample is submitted to 60 mins the irreversible adsorption is measured as well as the total volume of the cell.

3.4.5 Catalyst Activity Measurements.

Propane dehydrogenation (PDH) experiments were carried under O_2 and H_2O exclusion conditions, unless stated differently. All gases were purchased from Air Liquide and further purified in line with molecular sieves and BTS catalysts traps (is a copper oxide/aluminium oxide/zinc oxide mixture used as a highly efficient oxygen scavenger in gas purification) to assure high purity. A stainless-steel tubing of a ½ inch was used as a continuous flow reactor, containing a thermocouple that is heated by a vertical furnace (P_{total} = 1 bar, T = 530 °C) and it was packed inside an Ar filled glovebox. A 4-way valve system allowed the inert handling and various stainless-steel fillers were used to reduce the dead volume. Typically, 25 mg of catalyst were diluted to 2.5 g with SiC. A reductive pre-treatment of 16 h at 550 ^oC (1 °C/min) was carried out with pure hydrogen flow, prior to start the catalytic tests, the system reached room temperature and it was purged with Ar. A 3 C_3H_8: 1 H_2: 21 Ar (mL/min) gas composition was used and controlled by Brooks mass flow controllers. The Gas hourly space velocity (GSHV) was kept to 60.000 $mL{\cdot}gcat^{-1}{\cdot}h^{-1}$, unless stated differently. The products were determined by an online HP 6890 GC equipped with 50 m KCl/Al_2O_3 column and FID detector. Propane conversion was calculated typically by carbon balance. Selectivity to each product was similarly obtained.

$$Propane\ conversion\ (\%) = \frac{Total\ Propane_{out}}{Total\ Propane_{in}}\ x\ 100$$

$$Propylene\ selectivity\ (\%) = \frac{Total\ propylene_{out}}{Total\ propane_{in} - Total\ propane_{out}}\ x\ 100$$

The deactivation constant (k_d) was calculated at the reaction temperature (i.e., 530 ^oC) according to the following formula:

$$\ln\left[\frac{(1-\chi_{final})}{\chi_{final}}\right] = k_d \times t + \ln\left[\frac{(1-\chi_{initial})}{\chi_{initial}}\right]$$

Where χ_{final} and $\chi_{initial}$, are the final and the initial propane conversion values and "t" represents the lifetime of the catalyst.

3.5 References

(1) Nykänen, L.; Honkala, K. Selectivity in Propene Dehydrogenation on Pt and Pt3Sn Surfaces from First Principles. *ACS Catal.* **2013**, *3* (12), 3026–3030. https://doi.org/10.1021/cs400566y.

(2) Zhu, J.; Yang, M. L.; Yu, Y.; Zhu, Y. A.; Sui, Z. J.; Zhou, X. G.; Holmen, A.; Chen, D. Size-Dependent Reaction Mechanism and Kinetics for Propane Dehydrogenation over Pt Catalysts. *ACS Catal.* **2015**, *5* (11), 6310–6319. https://doi.org/10.1021/acscatal.5b01423.

(3) Xu, Z.; Xu, R.; Yue, Y.; Yuan, P.; Bao, X.; Abou-Hamad, E.; Basset, J. M.; Zhu, H. Bimetallic Pt-Sn Nanocluster from the Hydrogenolysis of a Well-Defined Surface Compound Consisting of [(AlO-)Pt(COD)Me] and [(AlO-)SnPh3] Fragments for Propane Dehydrogenation. *J. Catal.* **2019**, *374*, 391–400. https://doi.org/10.1016/j.jcat.2019.04.035.

(4) Gould, T. D.; Lubers, A. M.; Corpuz, A. R.; Weimer, A. W.; Falconer, J. L.; Medin, J. W. Controlling Nanoscale Properties of Supported Platinum Catalysts through Atomic Layer Deposition. *ACS Catal.* **2015**, *5*, 1344–1352.

(5) Sun, P.; Siddiqi, G.; Vining, W. C.; Chi, M.; Bell, A. T. Novel Pt/Mg(In)(Al)O Catalysts for Ethane and Propane Dehydrogenation. *J. Catal.* **2011**, *282* (1), 165–174. https://doi.org/10.1016/j.jcat.2011.06.008.

(6) Zaera, F. Molecular Approaches to Heterogeneous Catalysis. *Coord. Chem. Rev.* **2021**, *448* (1), 21419.

(7) Basset, J. M.; Ugo, R. *Modern Surface Organometallic Chemistry*; Psaro, R., Basset, J. M., Roberto, D., Ugo, R., Eds.; Wiley-VCH Verlag GmbH & Co. KGaA, 2009. https://doi.org/10.1002/9783527627097.

(8) I, Y. Y.; Kuznetsov, B. N. Supported Metallic Catalysts Prepared by Decomposition of Surface Ornagometallic Complexes. *J. Mol. Catal. A Chem.* **1980**, *9*, 13–40.

(9) Yu I Yermakov. Supported Catalysts Obtained by Interaction of Organometallic Compounds of Transition Elements with Oxide Supports. *Catal. Rev.* **1976**, *13*, 77–120.

(10) Docherty, S. R.; Rochlitz, L.; Payard, P.-A.; Copéret, C. Heterogeneous Alkane Dehydrogenation Catalysts Investigated via a Surface Organometallic Chemistry Approach. *Chem. Soc. Rev.* **2021**, *50*, 5806–5822. https://doi.org/10.1039/d0cs01424a.

(11) Samantaray, M. K.; D'Elia, V.; Pump, E.; Falivene, L.; Harb, M.; Ould Chikh, S.; Cavallo, L.; Basset, J.-M. The Comparison between Single Atom Catalysis and Surface Organometallic Catalysis. *Chem. Rev.* **2020**, *120* (2), 734–813. https://doi.org/10.1021/acs.chemrev.9b00238 CO - CHREAY.

(12) Sattler, J. J. H. B.; Ruiz-Martinez, J.; Santillan-Jimenez, E.; Weckhuysen, B. M. Catalytic Dehydrogenation of Light Alkanes on Metals and Metal Oxides. *Chem. Rev.* **2014**, *114* (20), 10613–10653. https://doi.org/10.1021/cr5002436.

(13) Hill, J. M.; Cortright, R. .; Dumesic, J. . Silica- and L-Zeolite-Supported Pt, Pt/Sn and Pt/Sn/K

Catalysts for Isobutane Dehydrogenation. *Appl. Catal. A Gen.* **1998**, *168* (1), 9–21. https://doi.org/10.1016/S0926-860X(97)00338-4.

(14) Zhu, H.; Anjum, D. H.; Wang, Q.; Abou-hamad, E.; Emsley, L.; Dong, H.; Laveille, P.; Li, L.; Samal, A. K.; Basset, J. M. Sn Surface-Enriched Pt-Sn Bimetallic Nanoparticles as a Selective and Stable Catalyst for Propane Dehydrogenation. *J. Catal.* **2014**, *320* (1), 52–62. https://doi.org/10.1016/j.jcat.2014.09.013.

(15) Rouge, P.; Garron, A.; Norsic, S.; Larabi, C.; Merle, N.; Delevoye, L.; Gauvin, R. M.; Szeto, K. C.; Taoufik, M. A Smarter Approach to Catalysts by Design: Combining Surface Organometallic Chemistry on Oxide and Metal Gives Selective Catalysts for Dehydrogenation of 2,3-Dimethylbutane. *Mol. Catal.* **2019**, *471*, 21–26. https://doi.org/10.1016/j.mcat.2019.04.011.

(16) Searles, K.; Chan, K. W.; Mendes Burak, J. A.; Zemlyanov, D.; Safonova, O.; Copéret, C. Highly Productive Propane Dehydrogenation Catalyst Using Silica-Supported Ga-Pt Nanoparticles Generated from Single-Sites. *J. Am. Chem. Soc.* **2018**, *140* (37), 11674–11679. https://doi.org/10.1021/jacs.8b05378.

(17) Samantaray, M. K.; Pump, E.; Bendjeriou-Sedjerari, A.; D'Elia, V.; Pelletier, J. D. A.; Guidotti, M.; Psaro, R.; Basset, J. M. Surface Organometallic Chemistry in Heterogeneous Catalysis. *Chem. Soc. Rev.* **2018**, *47* (22), 8403–8437. https://doi.org/10.1039/c8cs00356d.

(18) Humblot, F.; Didillon, D.; Lepeltier, F.; Candy, J. P.; Corker, J.; Clause, O.; Bayard, F.; Basset, J. M. Surface Organometallic Chemistry on Metals: Formation of a Stable ≡ Sn(n-C4H9) Fragment as a Precursor of Surface Alloy Obtained by Stepwise Hydrogenolysis of Sn(n-C4H9)4 on a Platinum Particle Supported on Silica. *J. Am. Chem. Soc.* **1998**, *120* (1), 137–146. https://doi.org/10.1021/ja964405o.

(19) Bentahar, F. Z.; Bayard, F.; Candy, J. P.; Basset, J. M. CHEMICAL MODIFICATION OF PLATINUM CATALYST SURFACE BY REACTION WITH TETRABUTYLTIN; APPLICATION TO THE SELECTIVE DEHYDROGENATION OF ISOBUTANE TO ISOBUTENE. In *Fundamental and applied aspects of chemically modified surfaces*; Woodhead publishing series in metals and surface engineering, 1999; pp 235–245. https://doi.org/10.1533/9781845698591.235.

(20) Nedez, C.; Theolier, A.; Lefebvre, F.; Choplin, A.; Basset, J.; J F Joly. Surface Organometallic Chemistry of Tin: Reactivity of Tetraalkyltin Complexes and Tributyltin Hydride toward Silica. *J. Am. Chem. Soc.* **1993**, *115* (2), 722–729.

(21) R.D, C.; Dumesic J.A. Microcalorimetric, Spectroscopic, and Kinetic Studies of Silica Supported Pt and Pt/Sn Catalysts for Isobutane Dehydrogenation. *J. Catal.* **1994**, *2*, 771–778.

(22) Kappenstein, C.; Saouabe, M.; Guérin, M.; Marecot, P.; Uszkurat, I.; Paál, Z. Characterization and Activity of Pt-Sn/Al2O3 Catalysts of Different Preparation: Coimpregnation and New Pt-Sn Precursor. *Catal. Letters* **1995**, *31*, 9–17.

(23) Santorini, G. F.; Casella, M. L.; Siri, G. J.; Ferretti, O. A.; Fierro, J. L. G. An Organometallic Approach for Tin Promotion Enhancement over Pt/γ-Al2O3 Alkane Dehydrogenation Catalysts. *Stud. Surf. Sci. Catal.* **2000**, *130*, 3897–3902.

(24) Siri, G. J.; Casella, L.; Santori, G. F. Tin/Platinum on Alumina as Catalyst for Dehydrogenation of Isobutane . Influence of the Preparation Procedure and of the Addition of Lithium on the Catalytic Properties. *Ind. Eng. Chem. Res.* **1997**, *36*, 4821–4826.

(25) Womes, M.; Cholley, T.; Peltier, F. Le; Morin, S.; Didillon, B.; Szydlowski-Shildknecht, N. Study of the Reaction Mechanisms between Pt(Acac)2 and Alumina Surface Sites: Application to a

New Refilling Technique for the Controlled Variation of the Particle Size of Pt/Al2O3 Catalysts. *Appl. Catal. A, Gen.* **2005**, *283* (1–2), 9–22.

(26) Pham, H. N.; Sattler, J. J. H. B. H. B.; Weckhuysen, B. M.; Datye, A. K. Role of Sn in the Regeneration of Pt/γ-Al2O3 Light Alkane Dehydrogenation Catalysts. *ACS Catal.* **2016**, *6* (4), 2257–2264. https://doi.org/10.1021/acscatal.5b02917.

(27) Zhu, Y.; An, Z.; Song, H.; Xiang, X.; Yan, W.; He, J. SI Lattice-Confined Sn (IV/II) Stabilizing Raft-like Pt Clusters: High Selectivity and Durability in Propane Dehydrogenation. *ACS Catal.* **2017**, *7* (10), 6973–6978. https://doi.org/10.1021/acscatal.7b02264.

(28) Camacho-bunquin, J.; Ferrandon, M. S.; Sohn, H.; Kropf, A. J.; Yang, C.; Wen, J.; Hackler, R. A.; Liu, C.; Celik, G.; Marshall, C. L.; Stair, P. C.; Delferro, M. Atomically Precise Strategy to a PtZn Alloy Nanocluster Catalyst for the Deep Dehydrogenation of n - Butane to 1,3-Butadiene. *ACS Catal.* **2018**, *8*, 10058–10063. https://doi.org/10.1021/acscatal.8b02794.

(29) Sun, Q.; Wang, N.; Fan, Q.; Zeng, L.; Mayoral, A.; Miao, S.; Yang, R.; Jiang, Z.; Zhou, W.; Zhang, J.; Zhang, T.; Xu, J.; Zhang, P.; Cheng, J.; Yang, D.-C.; Jia, R.; Li, L.; Zhang, Q.; Wang, Y.; Terasaki, O.; Yu, J. Subnanometer Bimetallic Pt-Zn Clusters in Zeolites for Propane Dehydrogenation. *Angew. Chemie - Int. Ed.* **2020**, *59* (44), 19450–19459. https://doi.org/10.1002/ange.202003349.

(30) C. Byron; Bai, S.; Celik, G.; Ferrandon, M. S.; Liu, C.; Ni, C.; Mehdad, A.; Delferro, M.; Lobo, R. F.; A. V. Teplyakov. Role of Boron in Enhancing the Catalytic Performance of Supported Platinum Catalysts for the Nonoxidative Dehy- Drogenation of n-Butane. *ACS Catal.* **2020**, *10*, 1500–1510.

(31) Searles, K.; Siddiqi, G.; Safonova, O. V; Copéret, C. Silica-Supported Isolated Gallium Sites as Highly Active, Selective and Stable Propane Dehydrogenation Catalysts. *Chem. Sci.* **2017**, *8*, 2661–2666. https://doi.org/10.1039/c6sc05178b.

(32) Zhao, Z. J.; Chiu, C. C.; Gong, J. Molecular Understandings on the Activation of Light Hydrocarbons over Heterogeneous Catalysts. *Chem. Sci.* **2015**, *6* (8), 4403–4425. https://doi.org/10.1039/c5sc01227a.

(33) Li, Q.; Sui, Z.; Zhou, X.; Zhu, Y.; Zhou, J.; Chen, D. Coke Formation on Pt-Sn/Al2O3 Catalyst in Propane Dehydrogenation: Coke Characterization and Kinetic Study. *Top. Catal.* **2011**, *54* (13–15), 888–896. https://doi.org/10.1007/s11244-011-9708-8.

(34) Sattler, J. J. H. B.; Beale, A. M.; Weckhuysen, B. M. Operando Raman Spectroscopy Study on the Deactivation of Pt/Al 2O3 and Pt-Sn/Al2O3 Propane Dehydrogenation Catalysts. *Phys. Chem. Chem. Phys.* **2013**, *15* (29), 12095–12103. https://doi.org/10.1039/c3cp50646k.

(35) Sattler, J. J. H. B.; Gonzalez-Jimenez, I. D.; Luo, L.; Stears, B. A.; Malek, A.; Barton, D. G.; Kilos, B. A.; Kaminsky, M. P.; Verhoeven, T. W. G. M.; Koers, E. J.; Baldus, M.; Weckhuysen, B. M. Platinum-Promoted Ga/Al2O3 as Highly Active, Selective, and Stable Catalyst for the Dehydrogenation of Propane. *Angew. Chemie - Int. Ed.* **2014**, *53* (35), 9251–9256. https://doi.org/10.1002/anie.201404460.

(36) Virnovskaia, A.; Rytter, E.; Olsbye, U. Kinetic and Isotopic Study of Ethane Dehydrogenation over a Semicommercial Pt,Sn/Mg(Al)O Catalyst. *Ind. Eng. Chem. Res.* **2008**, *47* (19), 7167–7177. https://doi.org/10.1021/ie800361a.

(37) Siddiqi, G.; Sun, P.; Galvita, V.; Bell, A. T. Catalyst Performance of Novel Pt/Mg(Ga)(Al)O Catalysts for Alkane Dehydrogenation. *J. Catal.* **2010**, *274* (2), 200–206.

https://doi.org/10.1016/j.jcat.2010.06.016.

(38) Galvita, V.; Siddiqi, G.; Sun, P.; Bell, A. T. Ethane Dehydrogenation on Pt/Mg(Al)O and PtSn/Mg(Al)O Catalysts. *J. Catal.* **2010**, *271* (2), 209–219. https://doi.org/10.1016/j.jcat.2010.01.016.

(39) Saerens, S.; Sabbe, M. K.; Galvita, V. V.; Redekop, E. A.; Reyniers, M. F.; Marin, G. B. The Positive Role of Hydrogen on the Dehydrogenation of Propane on Pt(111). *ACS Catal.* **2017**, *7* (11), 7495–7508. https://doi.org/10.1021/acscatal.7b01584.

(40) Valcárcel, A.; Ricart, J. M.; Clotet, A.; Illas, F.; Markovits, A.; Minot, C. Theoretical Study of Dehydrogenation and Isomerisation Reactions of Propylene on Pt(111). *J. Catal.* **2006**, *241* (1), 115–122. https://doi.org/10.1016/j.jcat.2006.04.022.

(41) Shao, C. T.; Lang, W. Z.; Yan, X.; Guo, Y. J. Catalytic Performance of Gallium Oxide Based-Catalysts for the Propane Dehydrogenation Reaction: Effects of Support and Loading Amount. *RSC Adv.* **2017**, *7* (8), 4710–4723. https://doi.org/10.1039/c6ra27204e.

(42) Seebach, D.; Hässig, R.; Gabriel, J. 13 C-NMR.-Spektroskopie von Organolithiumverbindungen Bei Tiefen Temperaturen. Strukturinformation Aus Der 13 C, 6 Li-Kopplung. *Helv. Chim. Acta* **1983**, *66* (1), 308–337. https://doi.org/10.1002/hlca.19830660128.

(43) McGarrity, J. F.; Ogle, C. A. High-Field Proton NMR Study of the Aggregation and Complexation of n-Butyllithium in Tetrahydrofuran. *J. Am. Chem. Soc.* **1985**, *107* (7), 1805–1810. https://doi.org/10.1021/ja00293a001.

(44) Sahu, R. K.; Mukherjee, D.; Tiwari, J. P.; Mishra, T.; Roy, S. K.; Pathak, L. C. Influence of Foreign Fe Ions on Wet Chemical Synthesis of Pt Nanoparticle Thin Films at Ambient Temperature : In Situ versus Direct Addition. *J. Mater. Chem.* **2009**, *19*, 6810–6815. https://doi.org/10.1039/b908080e.

(45) Ivanova, A. S.; Slavinskaya, E. M.; Gulyaev, R. V; Zaikovskii, V. I.; Stonkus, O. A.; Danilova, I. G.; Plyasova, L. M.; Polukhina, I. A.; Boronin, A. I. Metal – Support Interactions in Pt/Al2O3 and Pd/Al2O3 Catalysts for CO Oxidation. *Appl. Catal. B Environ.* **2010**, *97*, 57–71. https://doi.org/10.1016/j.apcatb.2010.03.024.

(46) Zhu, M.; Sun, G.; Xin, Q. Effect of Alloying Degree in PtSn Catalyst on the Catalytic Behavior for Ethanol. *Electrochem. Acta* **2009**, *54*, 1511–1518. https://doi.org/10.1016/j.electacta.2008.09.035.

(47) Liu, L.; Lopez-haro, M.; Lopes, C. W.; Rojas-buzo, S.; Concepcion, P.; Manzorro, R.; Simonelli, L.; Sattler, A.; Serna, P.; Calvino, J. J.; Corma, A. Structural Modulation and Direct Measurement of Subnanometric Bimetallic PtSn Clusters Confined in Zeolites. *Nat. Catal.* **2020**, *3*, 628–638. https://doi.org/10.1038/s41929-020-0472-7.

(48) Chen, S.; Chang, X.; Sun, G.; Zhang, T.; Xu, Y.; Wang, Y.; Pei, C.; Gong, J. Propane Dehydrogenation: Catalyst Development, New Chemistry, and Emerging Technologies. *Chem. Soc. Rev.* **2021**, *50* (5), 3315–3354. https://doi.org/10.1039/d0cs00814a.

(49) C.Perego; Peratello, S. Experimental Methods in Catalytic Kinetics. *Catal. Sci. Technol.* **1999**, *52*, 133–145.

Chapter 3

3

UNIVERSITAT ROVIRA I VIRGILI
INNOVATIVE NANOCATALYSTS FOR SUSTAINABLE NON-OXIDATIVE DEHYDROGENATION OF PROPANE
Laia Gil Jiménez

4

One-Pot Organometallic Approach for Pt and PtSn NPs catalysts for PDH

4.1 Introduction

The propane dehydrogenation (PDH) has been proposed as one of the most promising approaches to obtain propylene. As mentioned in Chapter 1, the most efficient for catalysts are generally based on PtSn systems supported onto Al_2O_3.[1–3] In this chapter, the application of innovative synthetic methodologies for the preparation of stable PtSn-based catalysts supported onto alumina-based supports and the study of their stability under relevant reaction conditions are described.

PtSn-catalysts.

PtSn-catalysts should display certain physicochemical properties such as small size and appropriate electronic properties of the NP to reach high activity and selectivity in the PDH process.[1–3] Although many studies have described the roles of Sn, the exact active structures under reaction conditions are still under continuing debates.[4,5] Both geometric (Sn separates large Pt aggregates into smaller clusters, thus avoiding the structure-sensitive coke formation)[6] and electronic effects (strong electron transfer between Sn and Pt promotes the desorption of propylene and coke transfer from Pt sites to the support)[7,8] were reported to contribute to the performance of these catalysts. In addition, it was recently demonstrated that the Sn species can help the redispersion of the Pt clusters during the regeneration operation.[4] Proposed structures for $PtSn/Al_2O_3$ catalysts are displayed in **Figure 4.1**, note that initially the Sn was already added to the support.[1,9] It seems that various chemical states of Sn coexist, namely Sn (0) and/or SnO_{2-x}. [1,9]

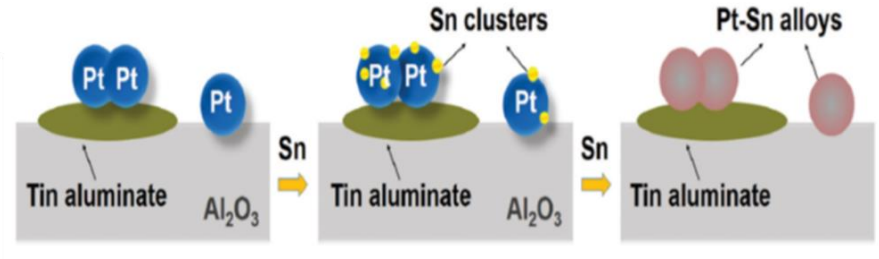

Figure 4.1. Illustration of possible models of $PtSn/Al_2O_3$ based catalysts. [1,9]

Recent examples revealed that Pt clusters modified with partially reduced SnO_x species, [4] including encapsulation or coating of the Pt-active phase by SnO_x,[5] displayed outstanding activity, selectivity and stability in propane dehydrogenation. For instance, Corma and coworkers reported subnanometric bimetallic PtSn clusters confined in zeolites (MFI) promoted with K^+ that were highly active in PDH at 600º C.[5] The structural evolution of the freshly prepared catalysts was studied under H_2 flow at high temperatures and is displayed in **Figure 4.2**. [5] They report that different PtSn structures could coexist within the catalysts.

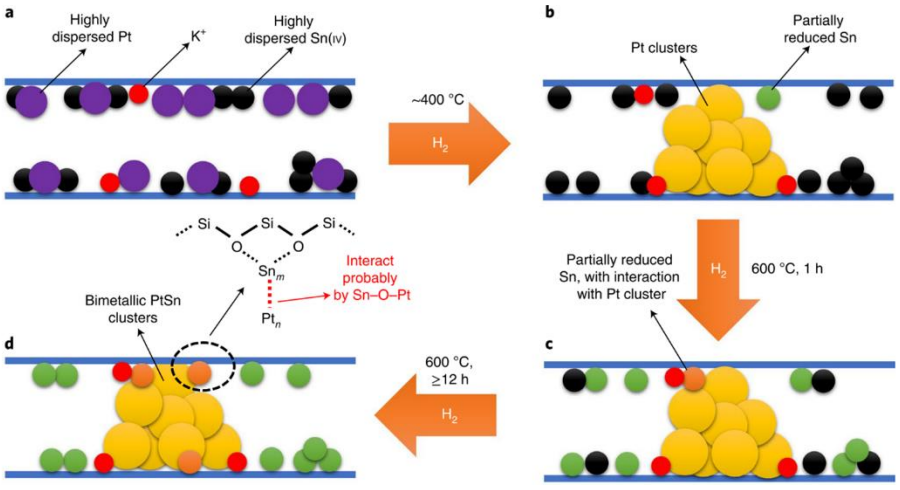

Figure 4.2. Structural proposal of freshly prepared K-PtSn@MFI during reduction with H_2. (a) Pt and Sn (IV) are dispersed in the channels of the zeolite. (b) After a reductive treatment with H_2 at 400 ºC, Pt atoms form subnanometric Pt clusters, whereas only some of the Sn (IV) species are reduced. (c) when the temperature increased to 600 ºC, the vast majority of Sn (IV) species were reduced to Sn (II), the latter ones remaining separated from the Pt clusters. (d) After long time flow of H_2, some of the reduced Sn migrate to the Pt clusters and PtSn bimetallic clusters

with reduced Sn interacted with the external surface of Pt clusters formed in the channels of the MFI zeolite.[5]

Therefore, one of the current challenges in PDH is the design and development of catalysts through innovative protocols that maximize the control of their physical-chemical properties and provide suitable interactions with the support.

Alumina is one of the most widely catalyst support for the dehydrogenation of alkanes due to its competitive price and outstanding properties such as high thermal conductivity and stability, high specific surface area and uniform pore size distribution.[1–3] Methodologies applied so far for the control of the acid-base properties of the alumina supports involved basic treatments prior to catalyst impregnation.[1–3] These treatments result in the poisoning the strong acid sites and avoid the coke deposition on catalyst surface. Such methods are used in the commercial Pt PDH catalysts: OLEFLEX® (Pt-Sn/K(Na)-Al_2O_3), LINDE-BASF-STATOIL® (Pt-Sn/MgAlO), STAR® (Pt-Sn/$ZnAl_2O_3$/CaO-Al_2O_3) and FCDh® (Pt-Ga/K-Si-Al_2O_3).[1–3] Alternatives to this approach generally involve: (a) the treatment of the catalyst with a metal compound such as Pb to block the active sites responsible for the coke formation,[10] or (b) the application of alternative synthetic procedures such as the surface organometallic approach, which permit the selective Sn-deposition onto the Pt-NP surface, thus avoiding the accumulation of Sn on the support.[11–19]

One-pot organometallic approach (OPOA).

Over the last years, our group reported the use of the one-pot organometallic approach, initially described by Chaudret,[20] as an alternative strategy for the preparation of supported metal nanoparticles.[21,22,23] This approach is based on the controlled decomposition of organometallic precursors in the presence of

the support and a stabilizing agent, usually an organic ligand such as triphenylphosphine (PPh_3) or N-heterocyclic carbenes (NHCs).

These materials displayed improved catalytic performances (activity, selectivity, and stability) due to the great control on the nanoparticle physical (i.e., high surface-to-volume ratio compared to standard heterogeneous catalysts) and chemical properties (i.e., possibility of modulation by the selection of the stabilizer or ligand to provide the transformation of the substrate into a specific product).

In this context, the preparation of supported metal nanoparticles via colloidal methods offers the possibility to fine-tune the properties of the active phase at structural and surface level.[24–30,54] Moreover, the colloidal-NPs can be utilized as models for the characterization of the active phase of the catalysts, providing information which is hardly accessible when diluted onto solid carriers. The effect of the interactions of the ligands with the NP surfaces on their physico-chemical properties has been corroborated by different techniques such as electron microscopy, [38,39] spectroscopic techniques (NMR, [40–44] IR,[45–47] XRD[48] or XPS[32,33]) and deutero-labelling experiments.[49,50] For instance, CO adsorption-FT-IR-studies conducted using Rh-NPs stabilized by these different ligands suggested differences in the CO-coordination modes probably because of the different interaction of the ligand with the Rh-NP surface (**Figure 4.3**). [24,26,51]

Furthermore, NMR-studies suggested differences in the ligand stability, sorption on the NP surface and coordination strength on the NP surface. [24,26,51]

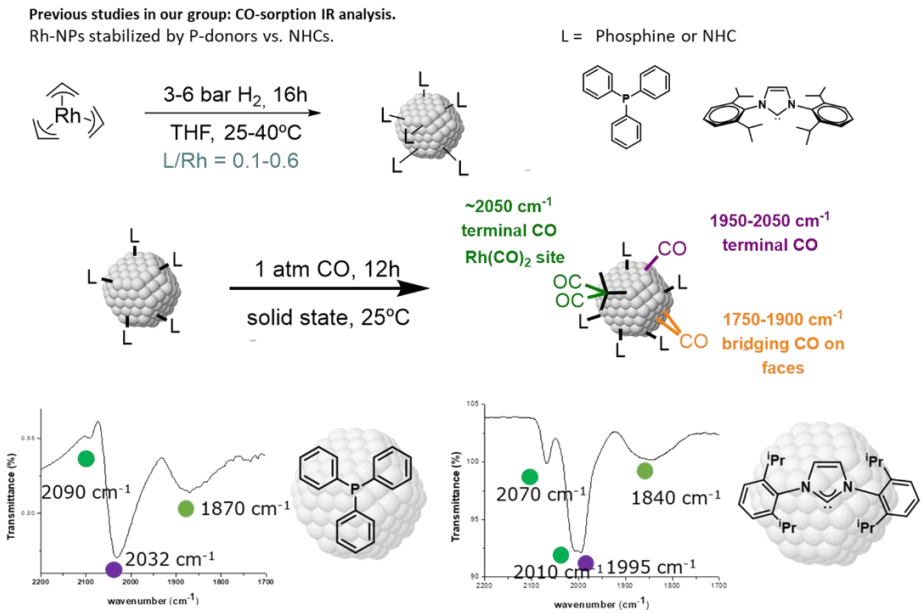

Figure 4.3. CO coordination modes in FT-IR studies of Rh-NPs with different ligand, PPh_3 and NHC.[26,51]

Metal phosphides, P-doped metal alloys, can also modify the electronic and geometric structures of NPs, having a similar behavior to bimetallic alloys.[52,53] In comparison with bimetallic alloys, P is more electronegative and offers additional flexibility towards the tuning of catalyst properties, which is of interest for catalyst design.[54]

Recently, platinum phosphides (PtP_2) NPs supported on silica catalysts were prepared via incipient wetness impregnation method, using H_3PO_4 as the phosphorus source, and exhibited a mean size of *ca.* 2-3 nm.[55] The authors reported the coexistence of Pt in both metallic or higher oxidation states, even after treatment in H_2 at 550 ^oC. The presence of other species such as platinum phosphides (PtP_2) was reported where the Pt^{2+} ions are separated by P_2^{2-}, therefore no Pt-Pt bonds were present, and the distance between two Pt atoms was 4.02 Å compared to 2.78 A Å in the Pt fcc cell. The XPS analyses of PtP_2/SiO_2 and Pt/SiO_2 after a reduction at 550 ^oC under H_2, revealed two components in the Pt 4f bands that corresponded to Pt $4f_{7/2}$ and Pt $4f_{5/2}$. In

PtP_2 catalyst, the Pt4f $_{7/2}$ had a binding energy of 73.0 eV, 1.2 eV higher than that of Pt/SiO_2 (71.8 eV), which the authors attributed to Pt^{2+} NPs, also consistent with a shifting observed in XANES to higher energies of 1.5 eV. Regarding the P, the peak P 2 p was studied and found at 135.3 eV, suggesting that the vast majority of P was present as P^{5+}. XPS and XANES displayed indirect measurements of the energy of the filled 5d orbitals, which are directly related with the catalytic performance.[56] These electronic effects minimized the bond strength of adsorbates which its consistent with its catalytic properties since PtP_2/SiO_2 and Pt/SiO_2 catalysts were tested in PDH reaction (**Figure 4.4**). The propane dehydrogenation rate was lower in the first case, but excellent propylene selectivity was obtained.[55]

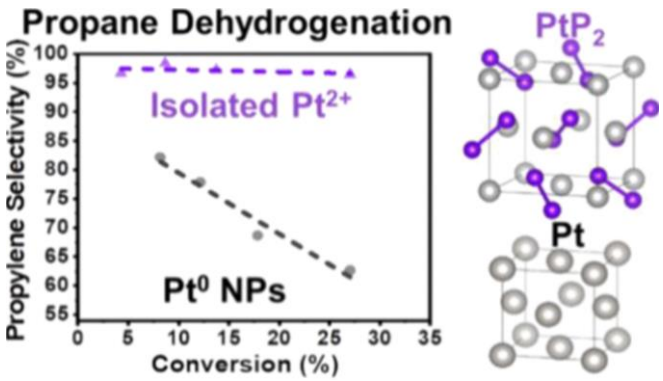

Figure 4.4. PtP_2/SiO_2 and Pt/SiO_2 catalysts tested in PDH reaction and their propane conversion and propylene selectivity.[55]

Other groups reported the study of the introduction of phosphorus (0%, 10% and 25% wt. P) in $Ni/\gamma Al_2O_3$ for the selective conversion of furfural to cyclopentanone via the incipient wetness impregnation.[57] The authors showed that phosphorus species could react with the support and the metal, creating an $AlPO_4$ phase, reducing the specific area of the catalysts. Nickel phosphide species were detected using XRD analysis (Ni_2P, Ni_3P and $Ni_{12}P_5$) and XPS analyses showed changes in the chemical states of Ni (**Figure 4.5** left). Indeed, when no P was added, the peaks at 855.6 and 862.0 eV were assigned

to Ni (δ+) reduced by H_2 and Ni (2+) ions, respectively. This result thus revealed that Ni was not completely reduced under H_2 atmosphere at 600 C^o. When 10% P was added, the Ni 2p peaks were located at 856.2 and 862.1 eV, and assigned to Ni (δ+) in the nickel phosphide and Ni (2+) ions with phosphate ions, respectively.[58] The authors mentioned that the amount of Ni (δ+) reduced species decreased from 5.7% to 1.8% when the P loadings increased from 10% to 25%, revealing that phosphorus additions hinders the Ni reduction. Moreover, the shifting at higher binding energies suggest that P and Ni form an alloy. Concerning P 2p (**Figure 4.5** right), three peaks were analyzed on the catalyst surface. When 10% P was used, the peaks at 133.2 and 133.9 eV were ascribed to reduced P (δ^{1-}) and reduced P (δ^{2-}), respectively.[59] The peak at 134.6 eV was assigned to $H_2PO_3^-$ located in the passivated layer of catalysts. By XRD, authors confirmed the presence of Ni_3P phase. When 25%P was used, peaks were observed at a higher binding energy, suggesting the formation of a new phosphide phase. using XRD analysis, the authors attributed these peaks to $Ni_{12}P$ and Ni_2P.

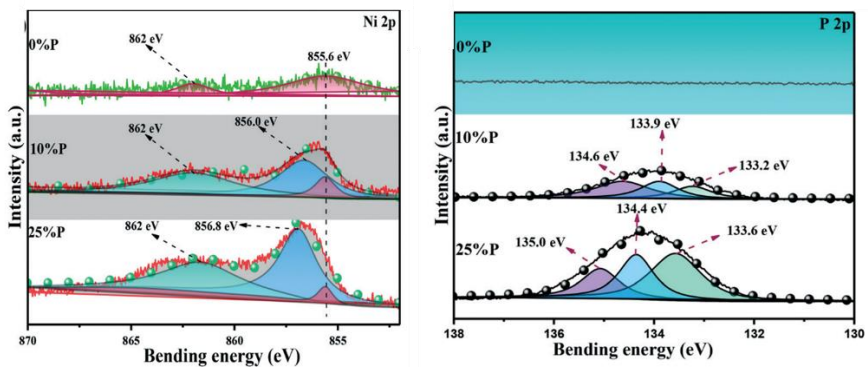

Figure 4.5. XPS deconvolutions (left) Ni 2p and (right) P 2p of Ni-xP@Al_2O_3 (x = 0, 10 or 25% wt. P).[57]

Other authors reported that the phosphorus content that modifies the change of phase, depending on the relative molar ratio (Ni:P). [60]

Corma and co-workers described the interaction of the P-based molecules (i.e., trimethylphosphine oxide (TMPO)) with the SnOx-extra-framework structures on the support in Pt-Sn PDH catalysts supported onto zeolites.[5,61,62] The interaction of these probe molecules is related with the Lewis acidity of framework and extra-framework Sn species dispersed onto the aluminosilicate supports. The authors observed by ^{31}P NMR that initially, the TMPO (Lewis base) interacted with Sn sites (Lewis acid) but after a thermal treatment by hydrogen (H_2) at 600 ^{o}C, the ^{31}P peak intensity decreased as the Sn species evolved to other species (Pt-SnO_x) which do not interact with the TMPO.

The use of dimethyl imidazolium carboxylate as NHC precursor (**Figure 4.6**) revealed particularly efficient for the preparation of small and well-defined supported monometallic (Pt, Ni, Cu, Rh and Pd) and bimetallic nanoparticles (NiCu and PdCu).[21,22,23]

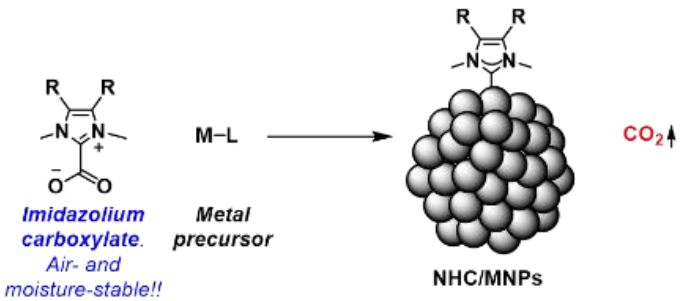

Figure 4.6. NHC NPs stabilization.[25]

A recent review collects relevant examples using the organometallic approach methodology.[63] The main advantages of using NHC relies on its ability to electro-donate density to the metal, resulting in a strong coordination. In comparison to phosphines, carbenes are not easily oxidized. [63]

For instance, the interaction of different imidazolium-amidinate ligands with Ni NP surface has been reported for selective dehydrogenation of alkynes, using the organometallic approach (**Figure 4.7**).[64] By XPS analyses the chemical state and coordination mode of the ligands was studied.

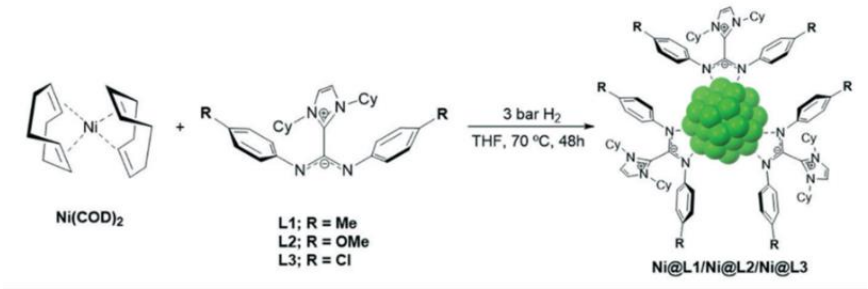

Figure 4.7. Ni NPs stabilized with various imidazolium-amidinate ligands (L1, L2 and L3).[64]

Herein, we report the application of the one-pot organometallic approach (OPOA) for the preparation of PtSn-NPs supported onto alumina for the first time. To the best of our knowledge, no examples of catalysts were reported using carbene ligands (NHC) and triphenylphosphine (PPh_3) as stabilizers for alkane dehydrogenation reactions.

In contrast to other synthetic approaches, the organometallic approach offered the opportunity to prepare the corresponding colloidal PtSn systems for their use as model samples for characterization to provide insights into the catalyst structure.

Various Pt and PtSn catalysts were synthesized following the OPOA and characterized by combination of techniques such ICP-OES, N_2-physisorption, TEM, STEM-EDS, STEM-HAADF, XRD, XPS, ^{31}P NMR, and TGA analyses. The possible effect of the ligand (samples prepared using no ligands, sub-stoichiometric amounts of PPh_3 or of 1,3-diemthylimidazolium carboxylate (NHC-CO_2) was particularly looked at. The catalysts performance was evaluated in the propane dehydrogenation (PDH) reaction and the scope of

the best performing catalyst was extended to the dehydrogenation of butane and 1-butene.

As depicted in **Scheme 4.1**¡Error! No se encuentra el origen de la referencia., this methodology offers the possibility to access well-defined PtSn bimetallic nanostructures using a one-pot approach, offering a simple alternative to previous multistep routes.

Scheme 4.1. Schematic illustration of one-pot organometallic approach to obtain supported PtSn bimetallic stabilized NPs and its advantages.

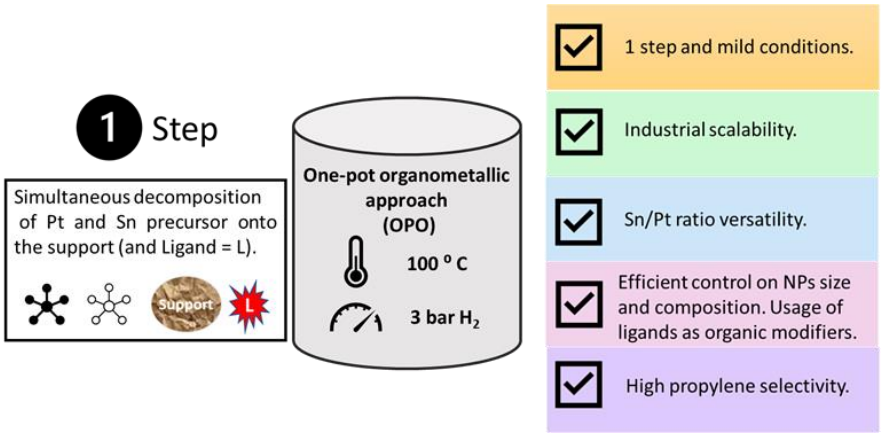

4.2 Results and Discussion

The bimetallic Pt-Sn catalysts were prepared in a Fisher Porter vessel via the organometallic approach.[20] First, a brief optimization of conditions was performed, including metal precursor, organic stabilizing agent, concentration of precursors, temperature, and time to produce small (i.e., 1-2 nm) and well-dispersed colloidal and supported NPs.

4.2.1 Synthesis and characterization

4.2.1.1 Initial optimization of synthesis parameters

Catalysts for the Propane Dehydrogenation reaction (PDH) were synthesized by the one-pot organometallic approach evaluating different reaction variables typical of colloids chemistry.

The effect of the stabilizing agent was evaluated through the preparation of 5 sets of colloidal Pt-NPs by decomposition of $Pt_2(dba)_3$ in THF under 3 bar H_2 at r.t. in the presence / absence of 0.2 equivalents of organic molecules: PVP, none, octadecyl amine (ODA), triphenylphosphine (PPh_3), and 1,3-dimethyimidazolium carboxylate (NHC-CO_2) (**Scheme 4.2**).

Scheme 4.2. Preparation of Pt ligand capped colloidal NPs using organometallic approach and various stabilizing ligands.

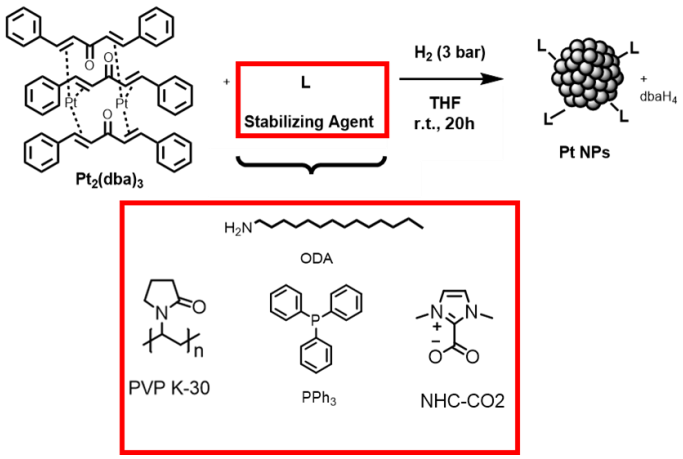

The decomposition of the Pt-precursor was quantitative obtaining in all cases small Pt-NPs. Analysis of TEM images (**Figure 4.8)**. revealed mean diameters of 1-2 nm for Pt-NPs/PVP and 2-3 nm Pt-NPs for the rest of samples. The Pt-NPs obtained using PVP were very similar to those previously reported by Phillipot *et al*.[46]

The main effect of the ligand was related with the formation of large Pt-NPs aggregates. In the presence of PVP (Pt1a), the NPs formed were well-dispersed and no aggregates were observed, while the use of NHC-CO_2 (Pt1e) and PPh_3 (Pt1d) as stabilizing agents provided some degree of agglomeration. In

contrast, when ODA (Pt1c) or no stabilizing agent (Pt1b) were tested, large amounts of agglomerates were detected.

In view of these results, the NPs stabilized by PVP seemed the most suitable. However, since PVP stabilization of Pt-NPs requires the use of larger amount of polymer (much higher than ligand amount) and that its removal from the Pt-NP surface could be complicated and result in the formation of coke (catalyst deactivation) at high temperature, subsequent studies were conducted using NHC-CO_2 and PPh_3 as stabilizing agents.

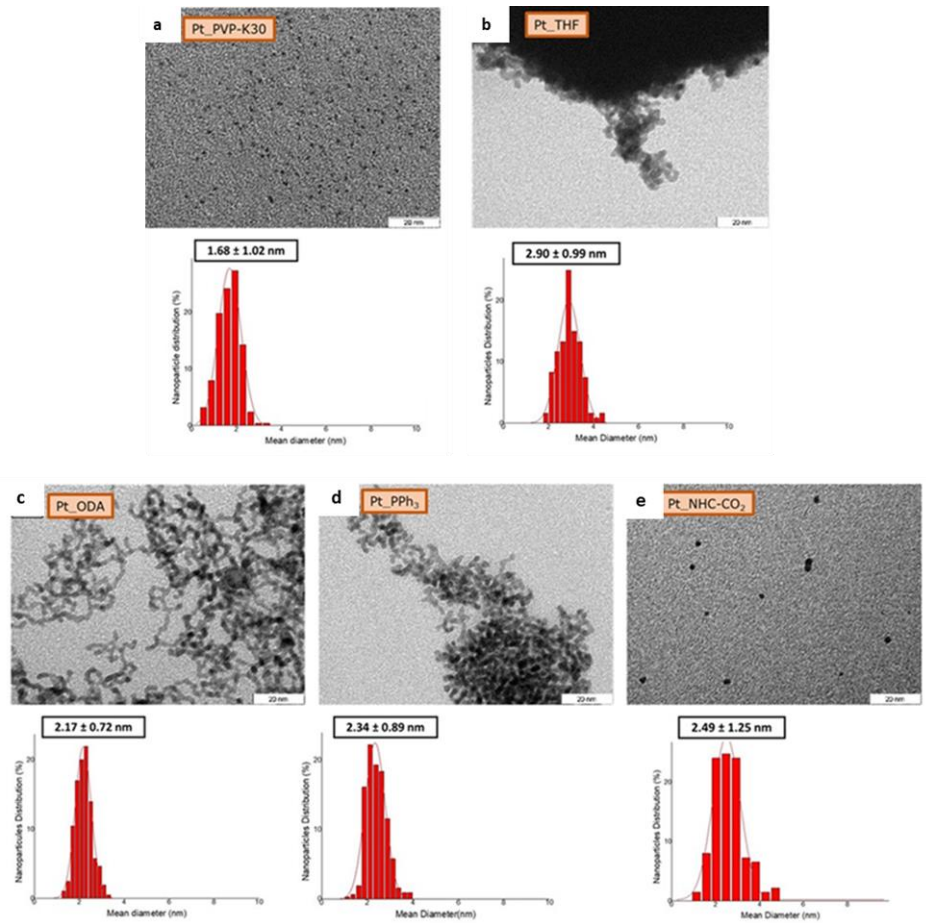

Figure 4.8. TEM Pt-NPs via organometallic approach stabilized with (a) PVP, Pt1a, (b) no stabilizer, Pt1b, (c) ODA (Pt1c), (d) PPh_3 ,Pt1d, and (f) NHC-CO_2, Pt1e.

The synthesis of supported Pt-NPs was initially studied with no extra stabilizing agents for 20h at r.t.. Two metal loadings (1 and 2 wt.% Pt) and two supports Al_2O_3 (Pt3a-b), $LiAl_2O_3$ (Pt4a-b), were initially studied using toluene as solvent. ICP-OES analyses indicated a Pt (wt%) content was: 1.0% and 0.98% for Pt(1%)@Al_2O_3-rt (Pt3a) and Pt(1%)@$LiAl_2O_3$-rt (Pt4a), and 2.0% and 1.9% for Pt(2%)@Al_2O_3-rt (Pt3b) and Pt(2%)@$LiAl_2O_3$-rt (Pt4b), respectively. The formation of small Pt-NPs onto the supports was confirmed by TEM (**Figure 4.9**), when using 1 wt.% Pt content. The NPs were smaller (1.1-1.7 nm) than with 2 wt.% Pt (1.9-2.6 nm). However, samples with 2 wt.% Pt composition were selected to facilitate the characterization of the resulting materials due to the higher metal content.

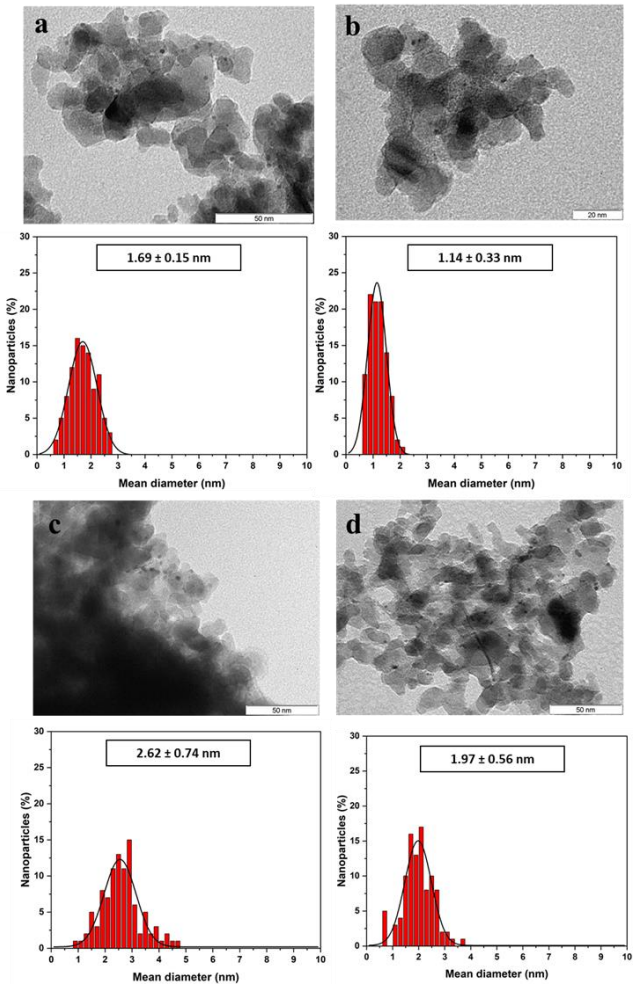

Figure 4.9. TEM Pt-NPs with 1 wt% Pt weight supported onto (a) Pt3a, Al_2O_3 (b) Pt4a, $LiAl_2O_3$ and using 2 wt% Pt supported onto (c) Pt3b, Al_2O_3 (d) Pt4b, $LiAl_2O_3$ prepared by organometallic approach at r.t.

The effect of the reaction time and temperature was also tested at 40 h and at 100 ^{o}C. Pt-NPs with 2 wt%. Pt supported onto aluminas (Al_2O_3 or $LiAl_2O_3$) were stabilized without any stabilizing agent Pt(2%)@Al_2O_3 (Pt5), Pt(2%)@$LiAl_2O_3$ (Pt6**b**) or with PPh_3 Pt(2%)-P@Al_2O_3 (Pt7), Pt(2%)- P@$LiAl_2O_3$ (Pt8). TEM images (**Figure 4.10**) revealed that the NPs synthesized in the presence of PPh_3 have a slightly smaller size (1.2-1.3 nm) than those prepared without ligand (1.6-1.8 nm).

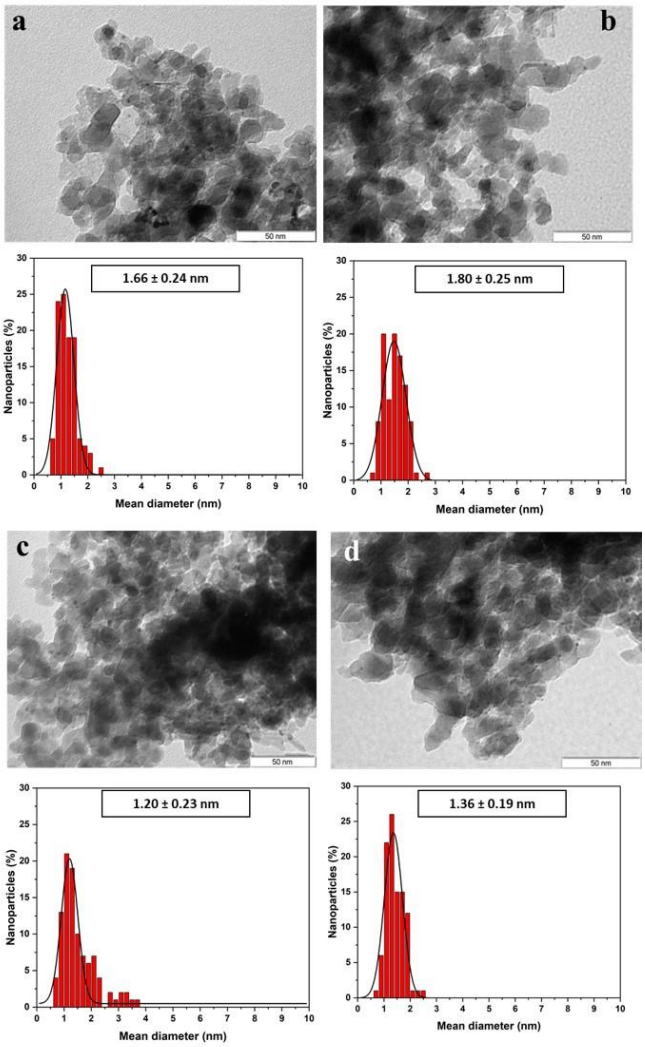

Figure 4.10. TEM Pt(2%)-NPs supported on Al_2O_3 (a, Pt5) and $LiAl_2O_3$ (b, Pt6) and stabilized with PPh_3 supported on Al_2O_3 (c, Pt7) and $LiAl_2O_3$ (d, Pt8) at 100 C for 40 h.

Monitoring of $SnBu_4$ decomposition by GC-TCD.

The in-situ decomposition of the Sn (IV) precursor was monitored using a GC-TCD (**Figure 4.11a**). The results indicated that the Sn precursor was only partially decomposed, and the decomposition rate was affected by nature of the support in the following order: Al_2O_3 > $LiAl_2O_3$ >> No support. Moreover, a synthesis temperature at 100 ^oC was needed for its decomposition. This behavior can be attributed to the presence of protons with amphoteric

character on the alumina surface, i.e., Al-OH groups. The lower reactivity of lithiated alumina compared to untreated material is thus explained since less OH groups are available. Furthermore, in the absence of Pt (**Figure 4.11a**), lower decomposition of Sn precursor was observed, indicating that Pt species are involved in the Sn precursor decomposition, in agreement with previous reports from Basset and co-workers.[13] To further study the decomposition of the precursor, the colloidal system in the presence and absence of Pt precursor was assessed (**Figure 4.11b**). We can observe that, when no Pt is added, no Sn is decomposed, and no Sn-NPs were formed. However, once Sn is added with the presence of Pt, 5% decomposition of $SnBu_4$ was observed.

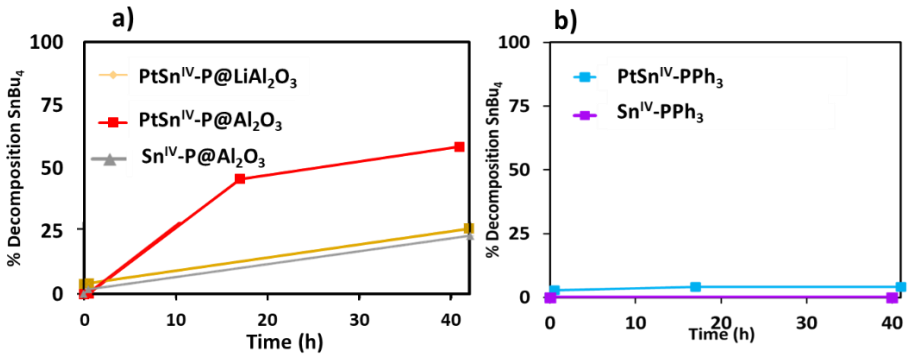

Figure 4.11. GC monitoring of $SnBu_4$ decomposition at 100° C with the presence of PPh_3 with a) supported bimetallic catalysts, b) monometallic Sn catalyst and c) colloidal NPs.

BET Area.

The surface BET areas and pore volume values were measured (**Table 4.1**). No relevant differences in area and pore volume values were observed between the catalysts, suggesting a partial filling of the support pores without blocking them. This thus indicated that the support pores remained available, and that the propane could diffuse inside the structure.

Table 4.1. BET area and total pore volume.

Sample	BET (m^2/g)	Total pore volume (cm^3/g)
Al_2O_3	116	0.69
$Pt(1)@Al_2O_3$	134	0.71
$Pt(2)@Al_2O_3$	113	0.60
$Pt(2\%)/Sn^{IV}(1)\text{-}P@Al_2O_3$	126	0.71
$LiAl_2O_3$	102	0.69
$Pt(1)@LiAl_2O_3$	115	0.66
$Pt(2)@LiAl_2O_3$	105	0.55
$Pt(2)/Sn^{IV}(1)\text{-}P@LiAl_2O_3$	122	0.69

4.2.1.2 Supported PtSn catalysts by OPOA

A nominal value of 2 Pt wt.% was initially used with a Pt/Sn molar ratio of 1. The Pt precursor Pt_2dba_3 and Sn precursor ($SnBu_4$ or $C_{12}H_{26}N_2Sn$) were decomposed at 100 ^oC under H_2 atmosphere in the presence of 0.2 equivalent of stabilizing ligand (none, PPh_3 = P, NHC-CO_2= NHC) per Pt using toluene or THF as solvent. The synthesis was performed in the presence of the support (Al_2O_3 or $LiAl_2O_3$ with 0.45 wt.% Li, (**Scheme 4.3**), and produced 6 catalysts (**Table 4.2**¡Error! No se encuentra el origen de la referencia.). Sample labels given in this table are used hereafter to reference specific catalysts. Once formed, the supported catalysts were washed thoroughly with the reaction solvent and with hexane and dried under reduced pressure.

Scheme 4.3. One-pot organometallic approach preparation for the supported bimetallic-ligand capped NPs.

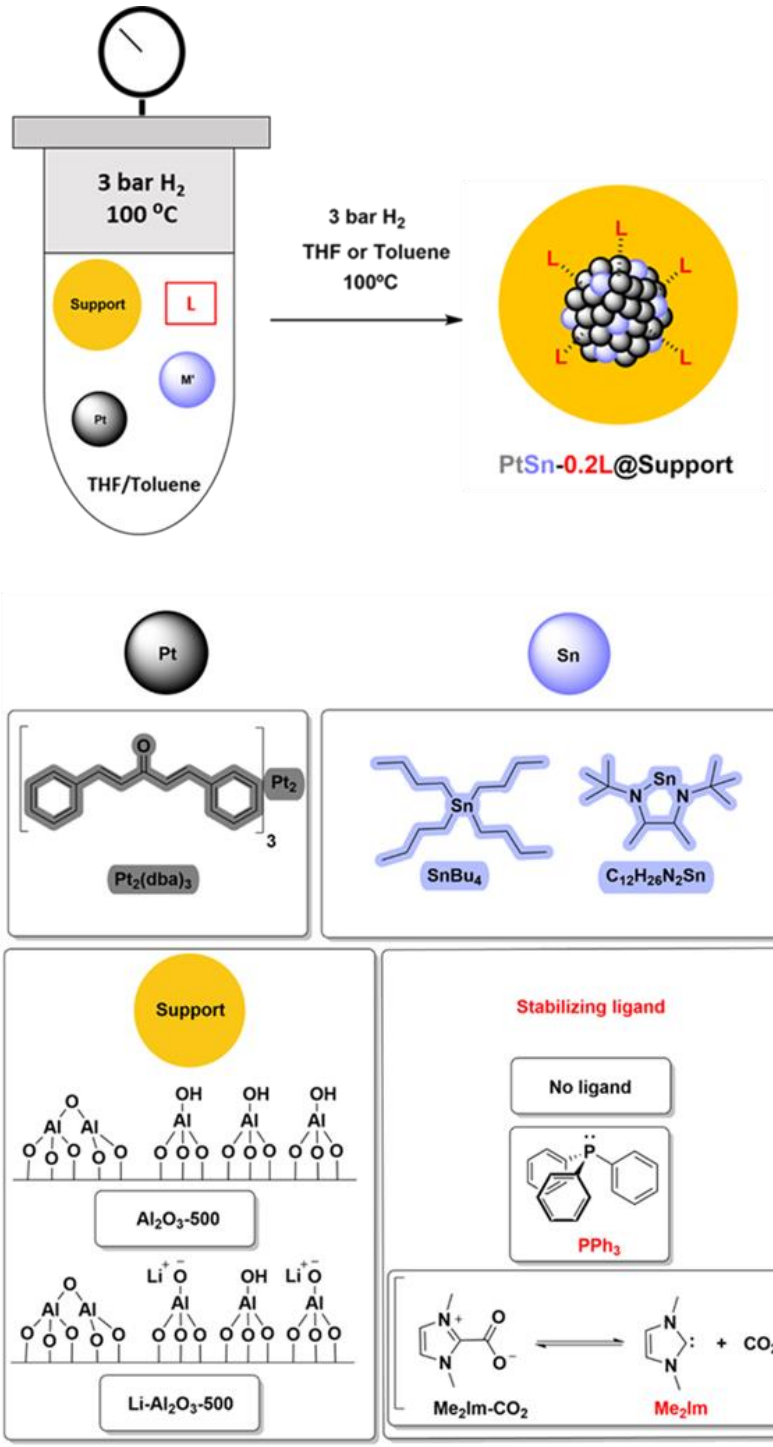

Table 4.2. Supported bimetallic catalysts prepared by one-pot organometallic approach.

Catalyst	Sn precursor	Ligand
$PtSn^{IV}$-P@Al_2O_3	$SnBu_4$	PPh_3
$PtSn^{II}$-P@Al_2O_3	$C_{12}H_{26}N_2Sn$	PPh_3
$PtSn^{IV}$-NHC@Al_2O_3	$SnBu_4$	NHC-CO_2
$PtSn^{II}$-NHC@Al_2O_3	$C_{12}H_{26}N_2Sn$	NHC-CO_2
$PtSn^{IV}$-P@$LiAl_2O_3$	$SnBu_4$	PPh_3
$PtSn^{IV}$@Al_2O_3	$SnBu_4$	none

The formation of NPs was first confirmed by STEM-HAADF analysis. Small and well dispersed NPs were obtained in all cases with a mean diameter of 1.3 – 2.0 nm. No significant differences in size were observed by variation of the support (Al_2O_3 or $LiAl_2O_3$) or of the Sn precursor used (**Figure 4.13**). STEM-EDS mappings of $PtSn^{IV}$-P@Al_2O_3 shows the Sn distribution onto both the support and the Pt-NP, while the P is mainly located at the surface of the Pt-NPs (**Figure 4.12,**a). STEM-EDX mappings of $PtSn^{IV}$@Al_2O_3 shows that more Sn was located on the Pt-NP than onto the support (**Figure 4.12,** b).

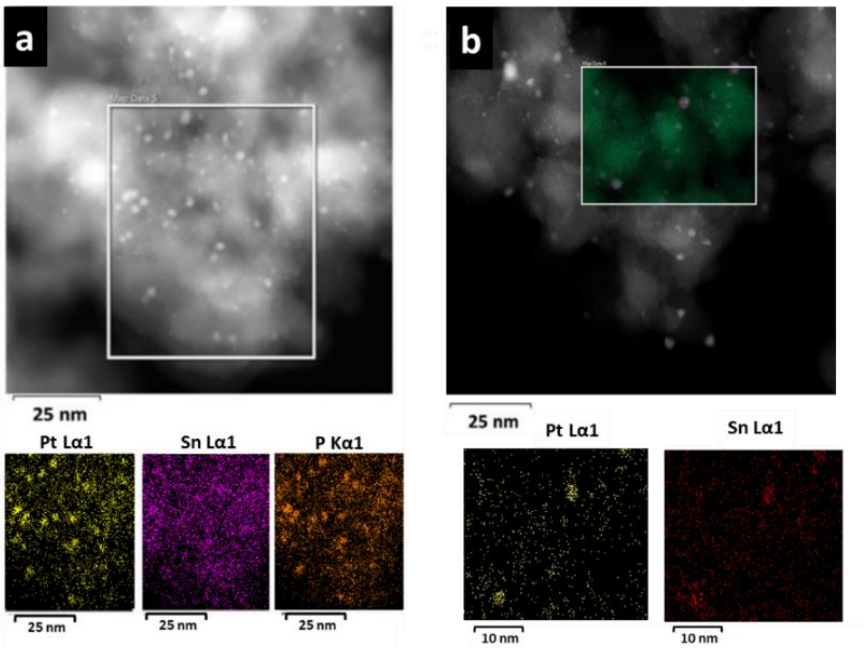

Figure 4.12. EDS-STEM of (a) $PtSn^{IV}$-P@Al_2O_3 and (b) $PtSn^{IV}$@Al_2O_3.

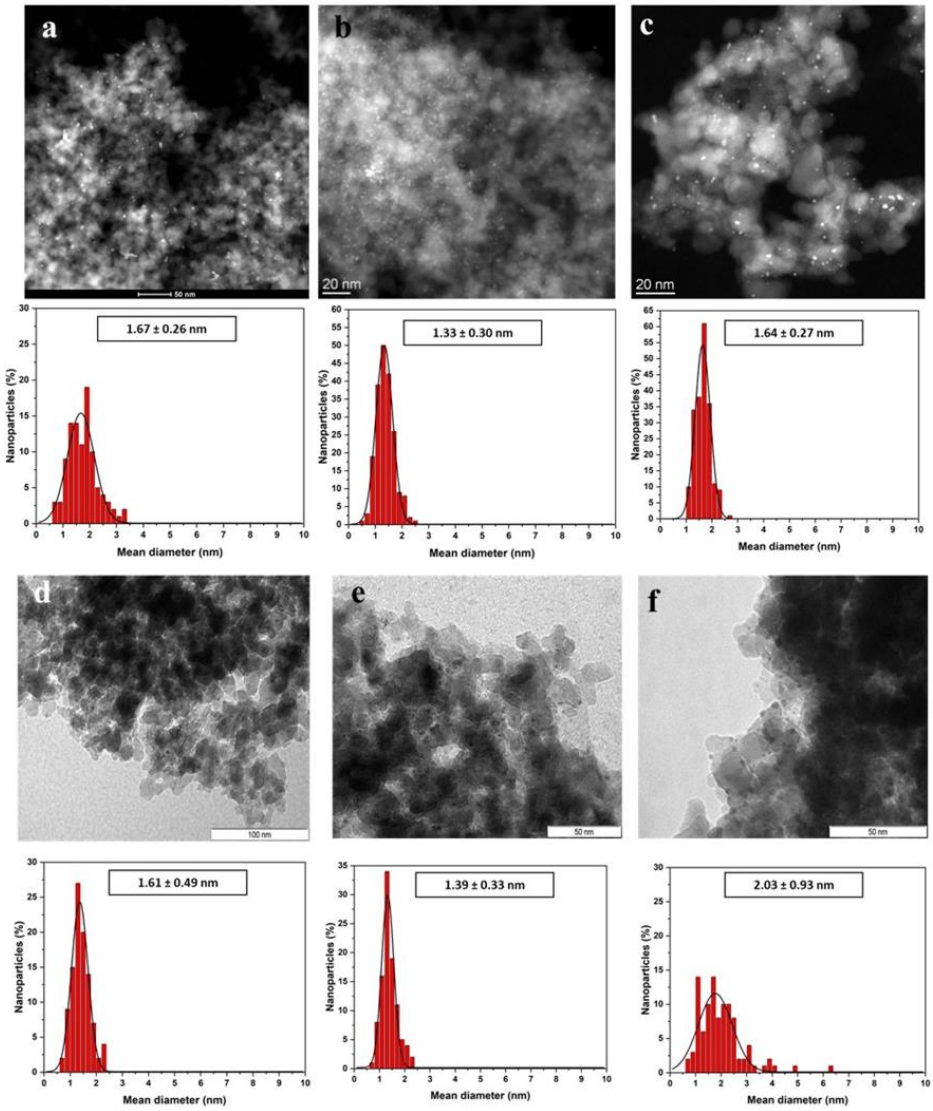

Figure 4.13. HAADF or TEM pictures and mean sizes of the supported catalysts (with 2 wt.%Pt and 1 wt.% Sn) a) $PtSn^{IV}@Al_2O_3$, b) $PtSn^{IV}$-P@Al_2O_3, c) $PtSn^{IV}$-P@$LiAl_2O_3$, d) $PtSn^{IV}$-NHC@Al_2O_3, e) $PtSn^{II}$-P@Al_2O_3 and f) $PtSn^{II}$-NHC@Al_2O_3.

X-Ray Diffraction (XRD) analysis of the synthesized materials was also performed. However, the XRD patterns observed for all catalysts exhibited main peaks at 2θ = 37°, 45.9° and 66.9° corresponding to the bare support γ-Al_2O_3 phase (JCPDS 01-080-0956) (**Figure 4.14**¡Error! No se encuentra el origen de la referencia.¡Error! No se encuentra el origen de la referencia.). This

suggested that the structure of the support remained unaltered and that the Pt NPs were small and well dispersed onto the surface of the support, in agreement with HAADF-STEM observations and previous reports.[65,66,67,68]

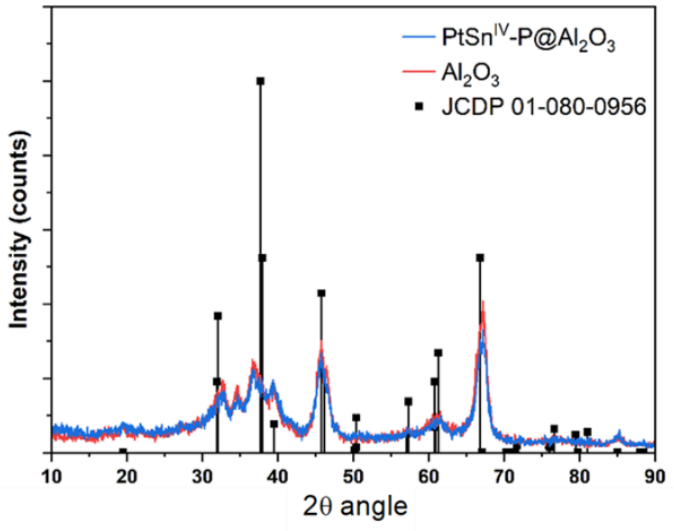

Figure 4.14. XRD diffractogram of PtSn^{IV}-P@Al_2O_3, γ-Al_2O_3. (γ-Al_2O_3-JCPDS: 01-080-0956).

The in-situ decomposition of the Sn (IV) precursor was monitored by GC analyses and as commented before, the Sn precursor was partially decomposed. The decomposition rate was affected by nature of the support in the following order: Al_2O_3 > $LiAl_2O_3$ >> No support, suggesting that the Sn precursor reacted both with the support and the Pt NPs. Once again, in the case of $LiAl_2O_3$, the decomposition was lower than with Al_2O_3 since many of the reactive hydroxyl groups had reacted with the BuLi.

Inductively coupled plasma – optical emission spectrometry (ICP-OES) results also indicated that Sn precursor decomposition was greater with Al_2O_3 than when $LiAl_2O_3$ was used as support, i.e., 1.1 wt.% Sn and 0.7 wt.% Sn, for PtSn^{IV}-P@Al_2O_3 and PtSn^{IV}-P@$LiAl_2O_3$, respectively. Therefore, the relative amounts of Pt and Sn depend on the ligand and the Sn precursor. All Pt and Sn compositions and Sn/Pt ratios (mol/mol) are listed in **Table 4.3**, Sn/Pt ratio (a).

The same Sn/Pt ratios were compared with X-ray photoelectron spectroscopy (XPS) and for all the catalysts, the ratio was higher than that obtained by ICP-OES, which suggests Sn segregation at the surface (**Table 4.3**, Sn/Pt ratio (b)).

Surface area of bare supports and Pt based catalysts was analyzed using Brunauer, Emmet and Teller (BET) method, as explained before. The difference in area and pore volume values between the bare supports and supported catalysts, indicates there is partial filling of the support pores without blocking them, implying that diffusion of propane inside the porous structure could take place.

The freshly prepared catalysts were measured by X-ray photoelectron spectroscopy (XPS) to investigate the atomic composition and oxidation state of each element. The characteristic peak Pt 4f could not be analyzed due to overlapping of Al 2p peak, therefore Pt was studied using Pt 4d band and Sn with 3d band, respectively (**Table 4.3**, XPS). Pt 4d deconvolutions of the supported catalysts are found in **Figure 4.15** and Sn 3d in **Figure 4.16.**

The Pt monometallic supported catalyst (Pt-PPh_3@Al_2O_3) revealed Pt 4 d with 99% of a Pt (0) component. In contrast, the PtSn catalysts displayed Pt 4d bands composed by combinations of two components, one attributed to the Pt (0) and another attributed to the Pt (δ+) species. The ratio between these two components was affected by the Sn/Pt molar ratio, the stabilizing agent, and the alumina support. This behavior highly suggested that the control of these three variables resulted in variation of the electron density at the Pt surface.

Table 4.3. Catalyst properties of PtSn supported catalysts synthesized by OPOA.

	M loading, wt %[a]		Sn/Pt (mol/mol)			XPS	
Catalyst	Pt	Sn	ICP	XPS	NPs size (nm)	$Pt\delta^{+}/Pt^{0}$	$Sn^{IV}/Sn^{II}/Sn^{0}$
$SnO_{2-x}P@Al_2O_3$	-	1.4	-	-	-	-	100 / 0 / 0
$PtP@Al_2O_3$	1.6	-	-	-	1.2 ± 0.3	1 / 99	-
$PtSn^{IV}@Al_2O_3$	1.6	1.4	1.4	2.0	1.7 ± 0.3	32 / 68	49 / 34 / 17
RED-$PtSn^{IV}@Al_2O_3$	1.6	1.4	1.4	2.3	1.7 ± 0.3	6 / 94	67 / 4 / 29
$PtSn^{IV}$-$P@Al_2O_3$	1.7	1.1	1.1	1.5	1.3 ± 0.3	18 / 82	22 / 38 /40
$PtSn^{IV}$-$P@LiAl_2O_3$	1.7	0.7	0.7	1.2	1.6 ± 0.3	17 / 83	1 / 76 / 23
$PtSn^{II}$-$P@Al_2O_3$	1.5	0.8	0.9	1.8	1.4 ± 0.3	27 / 73	36 / 48 / 16
$PtSn^{IV}$-NHC@Al_2O_3	1.6	0.4	0.4	1.7	1.6 ± 0.5	11 / 89	96 / 4 / 0
$PtSn^{II}$-NHC@Al_2O_3	1.6	0.9	0.9	2.6	2.0 ± 0.9	40 / 60	23 / 25 / 52

[a] Quantified by ICP-OES analysis; [b] Quantified by XPS analysis. [c] measured by TEM.

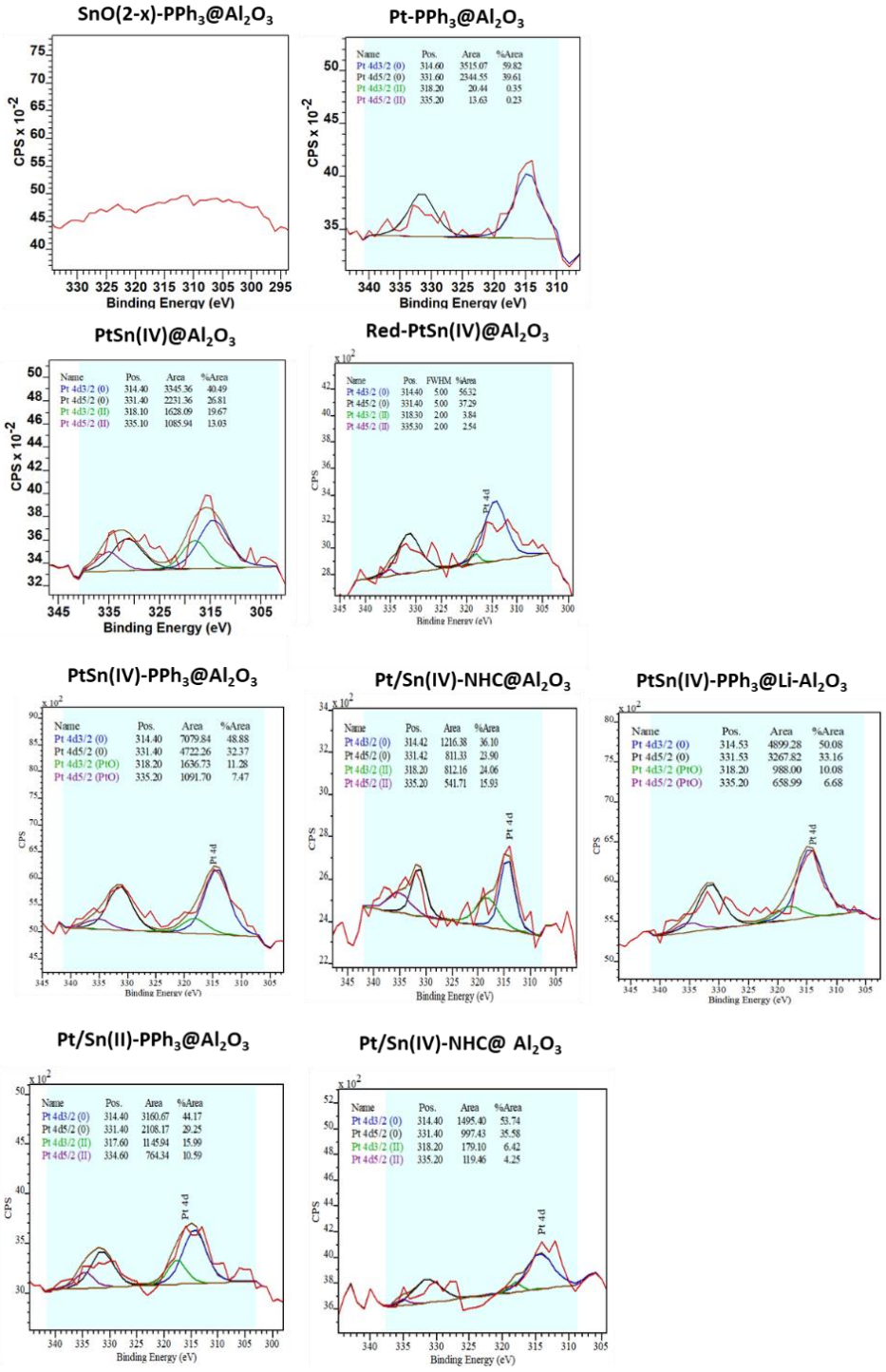

Figure 4.15. XPS Pt 4d deconvolutions.

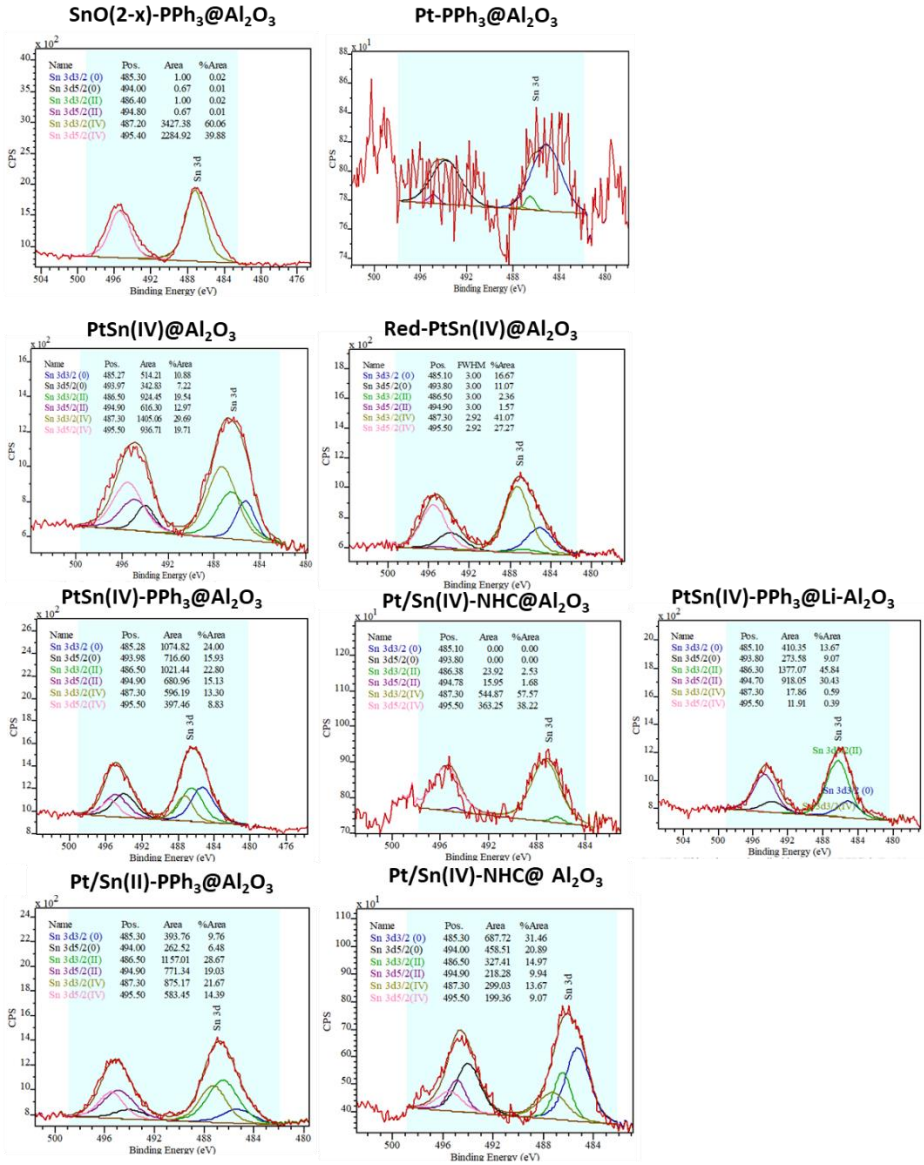

Figure 4.16. XPS Sn 3d deconvolutions.

The Sn component, Sn content and the Sn/Pt molar ratio varied depending on the ligand (PPh_3 and NHC), Sn precursor (Sn (IV) or Sn (II)) and the support (Al_2O_3 or Li-Al_2O_3). All the Sn 3d deconvolutions of the supported catalysts are displayed in the **Figure 4.16.** A blank sample was prepared by reaction of the $SnBu_4$ precursor, PPh_3 and Al_2O_3 under H_2 atmosphere and 100º C. After

washing and isolation, the monometallic Sn supported catalyst (SnO_{2-x}-P@Al_2O_3) was analyzed, revealing the presence of tin attached to the support surface probably as Sn oxide species, i.e., SnO_{2-x} or tin aluminates ($Sn_xAl_2O_4$). Previous studies revealed that in PtSn@Al_2O_3 systems, in the reduced catalyst, most of the tin is present in a valence state higher than Sn (0), which was consistent with tin being present as an eggshell of "tin aluminate" surrounding the alumina support with the Pt (0) supported on the "tin aluminate."[69]

Here, when no ligand was added and when Sn (IV) was used, the Sn-precursor preferentially reacted with the alumina support thus forming Sn oxide species (83%), i.e., SnO_{2-x} or tin aluminates ($Sn_xAl_2O_4$) ($PtSn^{IV}$@Al_2O_3). For the samples containing PPh_3, a reduction of the content of Sn oxide species, attributed to the reaction of Sn precursor with the support, was observed together with an increase in the proportion of the species detected at lower binding energies (i.e., Sn (II) and Sn (0)), corresponding to the Sn on a PtSn-NP alloy structure. In contrast, when the catalysts were prepared in the presence of NHC-ligand, no clear tendency was observed. When the Sn (IV) precursor was used, the Sn-content appeared essentially as Sn (IV), whereas when the Sn (II) precursor was used, the Sn-content and distribution of the components was similar to those recorded with PPh_3. This behavior was attributed to the possible reactivity of the stabilizing agent with the two different Sn precursors.

Comparing the results obtained using the Sn (IV) and Sn (II) precursors, the catalyst synthesized using the Sn (IV) precursor displayed lower proportion of components at higher binding energies, related with the Sn oxide species located on the support, and a higher proportion of the components at lower binding energies attributed to the Sn forming part of the PtSn-NP alloy. This tendency seems to be contradictory since a higher proportion of reduced Sn in the samples prepared using the Sn precursor in the lower oxidation state. However, this tendency could be explained by the higher reactivity of the Sn

(II) respect to the Sn (IV) precursor with the support than with the Pt-NP surface thus resulting in the formation of SnO_x.

As could be expected, the catalysts supported onto Li-Al_2O_3 displayed much lower proportion of Sn oxide species (attributed to the reaction of the Sn precursor with the support) and a greater proportion of Sn (II) and Sn (0) species, which are related with the PtSn-NP alloy structure.

Finally, a selected sample was reduced under H_2 flow at 500^o C and analyzed by XPS to study the evolution of the Pt and Sn component. The thermal treatment under hydrogen flow resulted in only slight variations of the oxidation states of Sn species on the support of the catalyst surface, being the Sn in low oxidation states (Sn (0)) incorporated in the PtSn alloy structure and the Sn in higher oxidation (Sn (δ+)).

This experiment suggested that either the reduction of Sn in higher oxidation state (Sn (δ +)) was inefficient, which could be explained by their location on the support surface as SnO_x or as tin aluminates (i.e., $SnAl_2O_4$ or $SnAlO_3$). The presence of this Sn species on the surface of the PtSn/Al_2O_3 catalyst was previously reported in the literature[4,5] and there is still a debate on the importance of the chemical states of Sn, the metallic state, oxidation state or coexistence of Sn (0) and Sn (n+) ($n = 0 \leq x \leq 4$). The positive effect of the presence of partially reduced species Sn (n+) ($n = 0 \leq x \leq 4$) interacting with the support and the PtSn-NP surface was reported.[5] Blekkan and co-workers studied the degree of reduction of Pt and Sn in PtSn/Al_2O_3 using TPR and studying the catalysts under hydrogen flows at 600 ^{o}C and 940 ^{o}C. They reported that Pt was fully reduced whereas 35 % of the Sn was reduced at 600 ^{o}C and 60% at 940 ^{o}C.[70]

The calculated Sn/Pt ratios were greater by XPS analysis than that measured by ICP-OES (**Table 4.3,** above), suggesting Sn segregation at the surface of the

catalyst, and indicating that the Pt-surface is more electron deficient. The extend of the segregation seems to be affected by the support, ligand and precursor used.

Although, the presence of phosphorus on the surface of the NP was confirmed by EDX in the catalysts synthesized in the presence of PPh_3, XPS analysis did not reveal any information on the P (P2p band) and N (N1s band) of the stabilizing ligands, probably because the P and N contents were below the detection limit.

To obtain more information about the effect of the thermal treatment under on the catalyst sample, Thermogravimetric analyses (TGA) of $PtSn^{IV}@Al_2O_3$ fresh catalyst and reduced Red-$PtSn^{IV}@Al_2O_3$ were conducted. In the fresh catalyst, a weight loss of 6% was observed at 620 ^oC, which could indicate that part of the $SnBu_4$ precursor was present on the NP surface. The presence of ligand would not explain such a weight loss since sub-stoichiometric amounts were used. After reduction of the sample at 550 ^oC under H_2, a smaller weight loss was observed (3%). This suggests that similar amounts of organic matter are present before and after reduction.

In conclusion, a series of PtSn catalyst supported onto Al_2O_3 have been prepared by the OPOA approach. These catalysts displayed small NP with good nanoparticle distribution onto the support. XPS revealed that the Sn content, Sn/Pt ratio and the extent of Sn segregation at the surface of the catalyst varied depending on the ligand, Sn precursor and alumina support.

4.2.1.3 PtSn colloidal NPs by OPOA

The corresponding colloidal ligand capped bimetallic nanoparticles with 0.2 equivalents of stabilizing ligand (or with no stabilizing agent) and with Sn (II) or Sn (IV) precursors were prepared (**Scheme 4.4**).

Scheme 4.4. PtSn-L NPs with L = none, PPh_3 or NHC-CO_2, using organometallic approach.

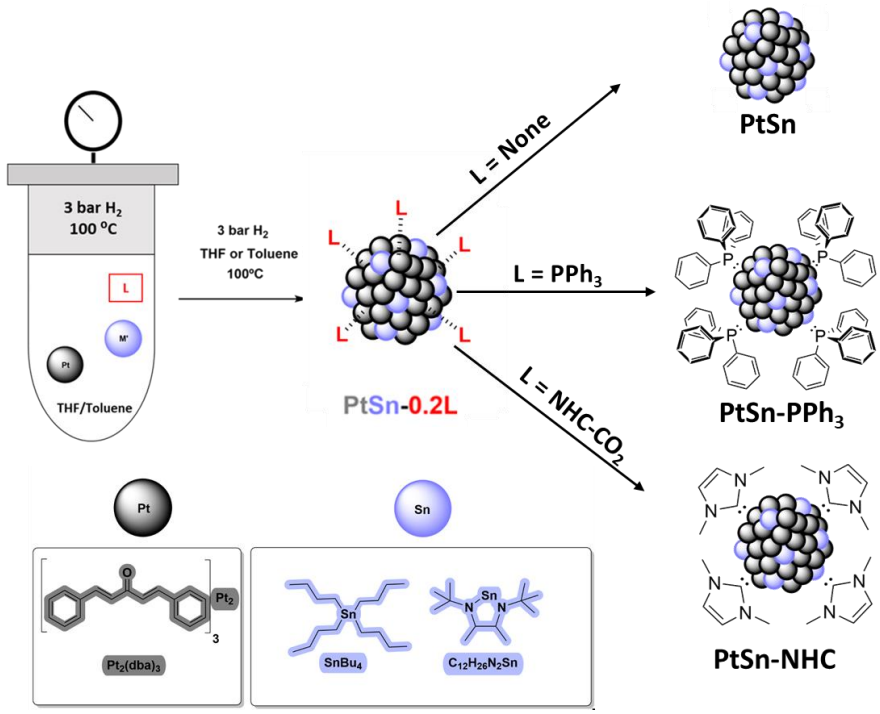

A total of 6 colloidal bimetallic NPs were synthesized **Table 4.4**.

Table 4.4. All the PtSn bimetallic colloidal NPs prepared with Pt_2dba_3.

Colloid	Sn precursor	Ligand
$PtSn^{IV}$	$SnBu_4$	None
$PtSn^{II}$	$C_{12}H_{26}N_2Sn$	None
$PtSn^{IV}$-PPh_3	$SnBu_4$	PPh_3
$PtSn^{II}$-PPh_3	$C_{12}H_{26}N_2Sn$	PPh_3
$PtSn^{IV}$-NHC	$SnBu_4$	NHC-CO_2
$PtSn^{II}$-NHC	$C_{12}H_{26}N_2Sn$	NHC-CO_2

TEM images of the PtSn NPs stabilized with Sn^{IV} with no ligand ($PtSn^{IV}$), PPh_3 ($PtSn^{IV}$-P), and NHC·CO_2 ($PtSn^{IV}$-NHC), are displayed in **Figure 4.17**. Analogously, PtSn NPs stabilized with Sn^{II} with no ligand ($PtSn^{II}$), PPh_3 ($PtSn^{II}$-P), and NHC·CO_2 ($PtSn^{II}$-NHC), are displayed in **Figure 4.18**.

When no ligand was used, aggregates were obtained. When PPh_3 was used, the size of the resulting NPs was smaller than when NHC-CO_2 was used.

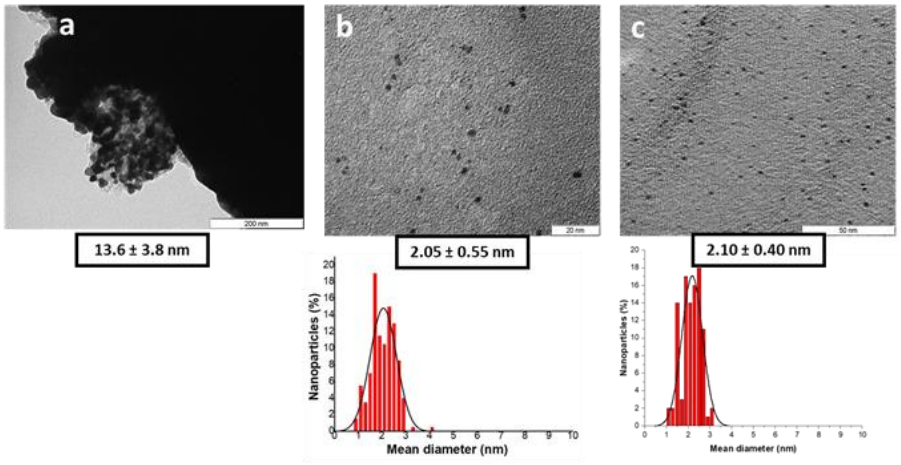

Figure 4.17. TEM images and histograms of colloidal $PtSn^{IV}$ NPs with a) no stabilizing agent a) ($PtSn^{IV}$), b) PPh_3 (($PtSn^{IV}$-P) and c) NHC·CO_2 (($PtSn^{IV}$-NHC).

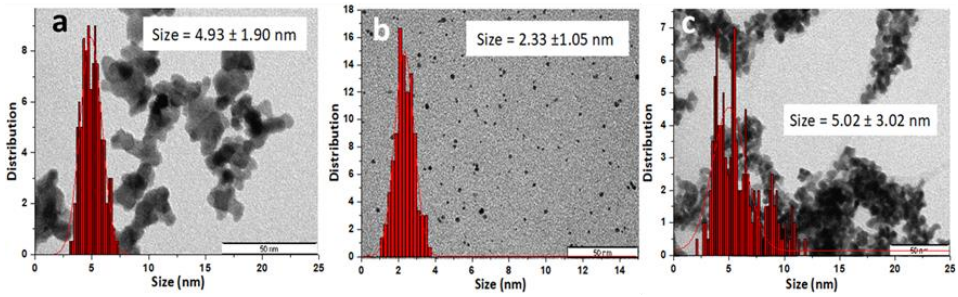

Figure 4.18. TEM images and histograms of colloidal $PtSn^{II}$ NPs with a) no stabilizing agent ($PtSn^{II}$), b) PPh_3 (($PtSn^{II}$-P) and c) NHC·CO_2 (($PtSn^{II}$-NHC).

The organic content was estimated by thermogravimetric analyses (TGA) of the Sn^{II} colloidal samples ($PtSn^{II}$, $PtSn^{II}$-PPh_3 and $PtSn^{II}$-NHC) (**Figure 4.19**). The summary of mass losses and temperature intervals is collected in **Table 4.5**.

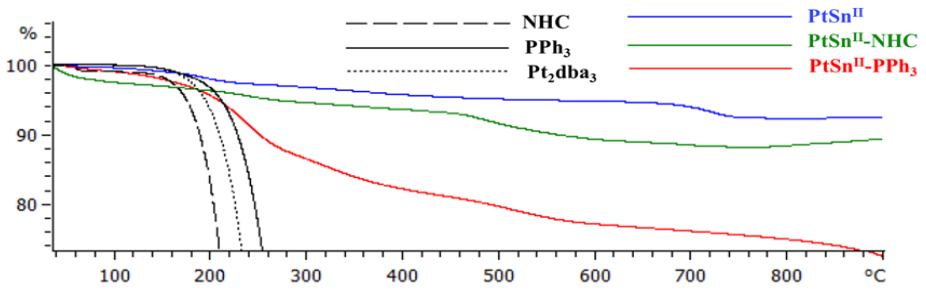

Figure 4.19. TGA profile of $PtSn^{II}$, $PtSn^{II}$-PPh_3 and $PtSn^{II}$-NHC, Pt precursor (Pt_2dba_3) and ligands (NHC and PPh_3).

Table 4.5. Percentages or organic and metal substances in $PtSn^{II}$ NPs.

Colloid	T (º C)	ΔMass (wt.%)	Metal content (wt.%)
$PtSn^{II}$	50-218 218-687 687-744	2 4 1	92
$PtSn^{II}$-NHC	50-100 100-463 465-764	3 4 5	88
$PtSn^{II}$-P	50-173 173-266 266-482 482-570 570-900	3 8 9 2 6	72

It is noteworthy that in the 3 cases, the loss of only small amounts of organic matter was detected. The NPs stabilized with PPh_3, $PtSn^{II}$-P, presented the larger weight loss, which can be related to the higher molecular weight of the ligand. The next sample with more organic matter was $PtSn^{II}$-NHC, and the NPs without stabilizer presented the lowest quantity of organic matter. The metal content in these samples were 72% for $PtSn^{II}$-P, 88% for $PtSn^{II}$-NHC, and 92% for $PtSn^{II}$.

Furthermore, the higher reactivity of the Sn (II) precursor with respect to the Sn (IV) precursor was corroborated by the ICP analysis of the samples (**Table 4.6**).

Table 4.6. Metal weight (%) calculated by ICP-OES in $PtSn^{II}$ NPs.

Colloid	Pt wt.%	Sn wt.%	Metal content (wt.%)	Pt/Sn molar ratio
$PtSn^{II}$	50	39	89	0.8
$PtSn^{IV}$	71	13	84	0.3
$PtSn^{II}$-NHC	52	39	91	0.8
$PtSn^{IV}$-NHC	61	6	67	0.2
$PtSn^{II}$-P	46	35	80	0.8
$PtSn^{IV}$-P	58	8	66	0.2

Since XRD analysis of the supported systems did not provide any information on the crystalline phase of the Pt-based NPs, the analogous colloidal NPs obtaining with the Sn (IV) precursor ($PtSn^{IV}$, $PtSn^{IV}$-PPh_3 and $PtSn^{IV}$-NHC NPs) were analyzed by XRD at room temperature and at the temperature of PDH reaction (530 ^{o}C). These analyses were performed under inert atmosphere (N_2) using a BRUKER MTC-HIGHTEMP chamber.

When the $PtSn^{IV}$ NPs colloids were analyzed at r.t., the only crystalline phase observed was Pt *fcc* (space group Fm-3m) with the main peaks at 2θ = 39.7°, 46.2°, 67.4 and 81.2° (ICDD card 01-071-3756). The crystallite size was *ca.* 3.66 nm. At 530 ^{o}C, the first diffractogram at time zero, showed Pt and Pt_3Sn alloy (space group Pm-3m) exhibiting the main peaks at 2θ = 38.3°, 44.5°, 64.8°, 77.9° and 82.1° (ICDD card 01-072-2976, ICSD 183076) with a relative amount of Pt 4.4 wt.% and Pt_3Sn 95.6 wt.%. The crystallite size was 4.49 nm for Pt phase and 14.13 nm for the alloy Pt_3Sn. After 1 h of analysis, the 6 diffractograms taken showed that the relative amounts of the two phases changed to Pt 55.6 wt.% and Pt_3Sn 44.4 wt.%. The crystallite size after 1h at 530 ^{o}C is 13.88 and 19.98 nm, respectively for the correspondent Pt and Pt_3Sn phases. In **Figure 4.20,** the main XRD diffractograms of $PtSn^{IV}$ NPs are displayed.

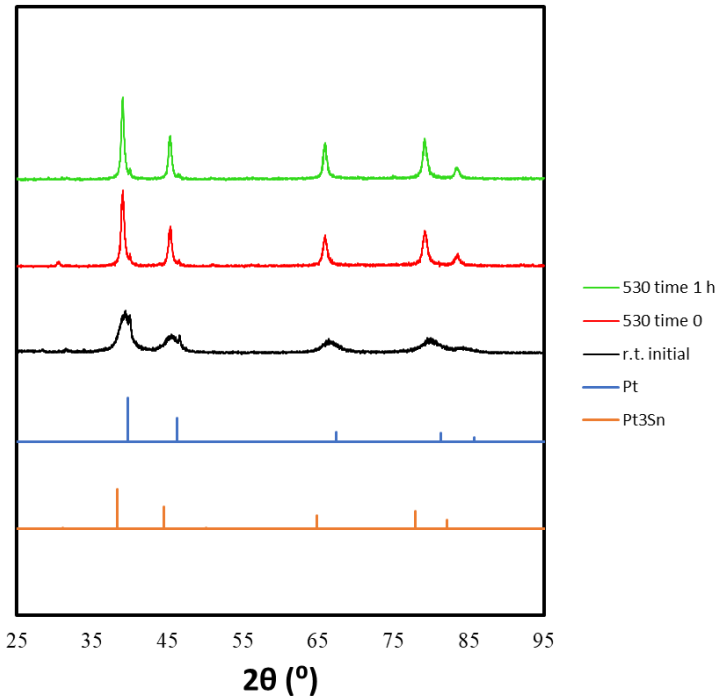

Figure 4.20. XRD diffractograms of $PtSn^{IV}$ colloidal NPs at r.t. (black), at 530 °C initial time (red) and at 530 °C after 1 h (green). Pt (blue) and Pt_3Sn (orange) crystallographic phases are displayed.

When $PtSn^{IV}$-PPh_3 was analyzed at room temperature, the apparent crystalline phase was Pt (0)-fcc (100 % wt.) with a crystallite size of 1.41 nm, which is in accordance with the TEM mean size between 1.5 – 2.6 nm. The first diffractogram at 530 ºC showed again two different crystalline phases, Pt and Pt_3Sn with a wt. % of 62.5 and 37.5 % respectively, showing a displacement toward the alloy phase in comparison with the colloid without ligand. The crystallite size was 3.94 nm for Pt and 7.60 nm for Pt_3Sn. After only 712 s, three phases were detected: Pt (72.4 wt%.), Pt_3Sn (23.1 wt%.) and Pt_5PSn (4.5 wt%.), with a crystallite size of 5.11 nm, 26.10 nm and 30.69 nm, respectively. The Pt_5PSn phase presents the main peaks at 2θ = 31.6°, 34.1°, 37.6°, 40.6°, 45.3°and 60.4° (ICDD card 01-082-6797, ICSD 647972, P4/mmm), thus, confirming that part of the P from the ligand was incorporated into the metal

structure. In **Figure 4.21,** the main XRD diffractograms of $PtSn^{IV}$-PPh_3 are showed.

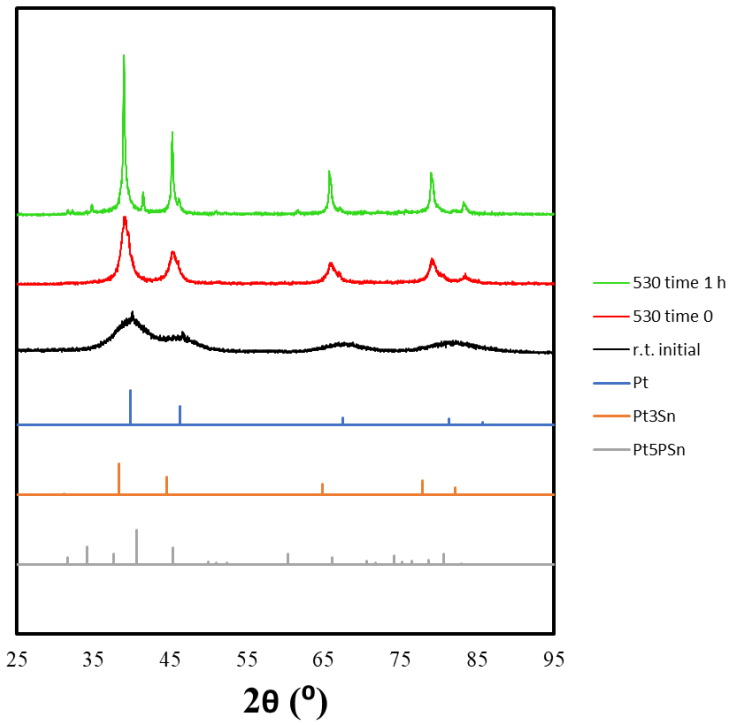

Figure 4.21. XRD diffractograms of $PtSn^{IV}$-PPh_3 colloidal NPs at r.t. (black), at 530 °C initial time (red) and at 530 °C after 1 h (green). Pt (blue), Pt_3Sn (orange) and Pt_5PSn (grey) crystallographic phases are displayed.

At the end of the experiments (after 1 h), the same three crystalline phases were detected, and the proportion showed that the Pt and Pt_3Sn are the most abundant phases: Pt (48.0 wt %.) and Pt_3Sn (43.3 wt %.) leaving around an 8.7 wt % of Pt_5PSn.

The sample with the heterocyclic carbene (NHC) was studied as well (**Figure 4.22**). For $PtSn^{IV}$-NHC, at r.t., only Pt (100 % wt.) was detected with a crystallite size of 1.5 nm, which is in accordance with the TEM mean size between 1.7 – 2.5 nm. The first diffractogram at 530 ^{o}C showed two different crystalline

phases, Pt and Pt_3Sn with a wt. % of 70.1 and 29.9 % respectively. The crystallite size was 4.15 nm for Pt and 5.54 nm for Pt_3Sn.

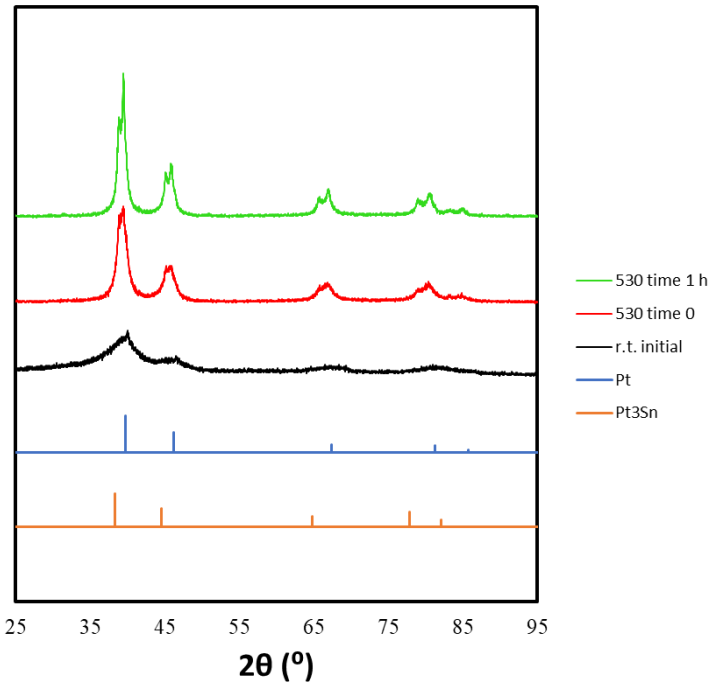

Figure 4.22. XRD diffractograms of $PtSn^{IV}$-NHC colloidal NPs at r.t. (black), at 530 °C initial time (red) and at 530 °C after 1 h (green). Pt (blue) and Pt_3Sn (orange) crystallographic phases are displayed.

In contrast with the NPs stabilized with triphenylphosphine, in all the analyses only two phases were observed. At the end of the experiments (after 1 h), the same two crystalline phases were observed in the proportion Pt (62.7wt %.) and Pt_3Sn (37.3wt %.).

Comparing the XRD values obtained after 1 h of treatment, the PtSn colloid contain more alloy Pt_3Sn (44.4%wt.) than PtSn-PPh_3 (43.3%wt.), since the latter also exhibits the Pt_5PSn phase. The PtSn-NHC colloid is the one that contains more Pt phase (62.7 %).

The main structures found in the XRD patterns of samples are Pt, Pt_3Sn and Pt_5PSn (**Figure 4.23**Figure 4.28).

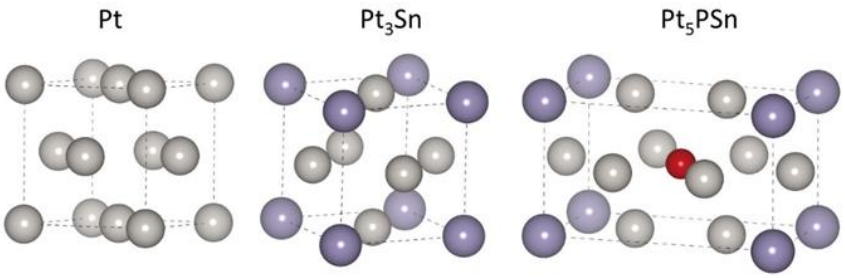

Figure 4.23. Pt, Pt_3Sn and Pt_5PSn crystalline 3D structures.

All the distribution (in weight percentage) of all the crystalline phases, their crystallite size and cell parameters are expressed in the Experimental Section of the present chapter as well as the Rietveld Refinement used.

In conclusion, these results clearly indicated that the presence or not of PPh_3 during the PtSn nanoparticle synthesis resulted in similar Sn/Pt molar ratios but with a different crystalline phase behavior, i.e., PtSn-PPh_3 colloidal nanoparticle displayed the incorporation of P in the PtSn-NP structure and much higher Pt/Pt_3Sn molar ratios than PtSn (**Figure 4.24**). This behavior could be ascribed to the PPh_3 coordination and blockage of the Pt-sites avoiding the interaction with the Sn-precursor during the nanoparticle synthesis, thus, reducing the final Pt_3Sn alloy content. However, for PtSn-NHC, this was not the case and the highest Pt/Pt_3Sn ratio was obtained. Although the formation of Pt nitrides was previously reported, the conditions of this study did not give rise to such material. Decomposition of the NHC ligand could be too fast.

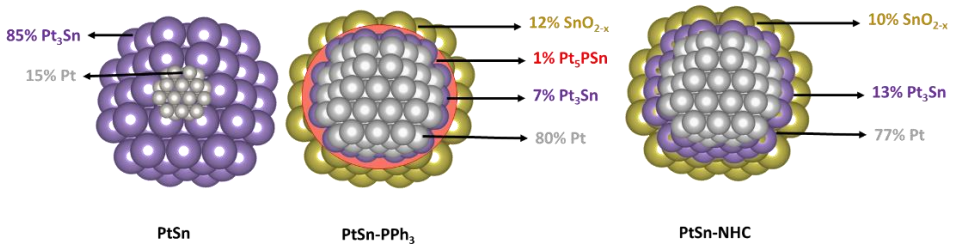

Figure 4.24. Illustration of the PtSn, PtSn-PPh_3 and PtSn-NHC nanoparticles assuming that the rest of the tin is in the form of tin oxides. All the % are expressed in mol/mol.

When colloidal NPs were analyzed by XPS, a band attributed to Pt (0) – ligand interaction was observed. When $PtSn^{IV}$ systems with different ligands ($PtSn^{IV}$-P and $PtSn^{IV}$-NHC) (**Figure 4.25,** Pt (a,d)**)** were analyzed, this new component Pt(0)-L was measured as *ca*. 40% in both P and NHC-stabilized systems, which correspond to the percentage of surface Pt atoms in nanoparticles of this size (2.1 nm) using the Van Hardeveld-Hartog (VHH) model.[77]

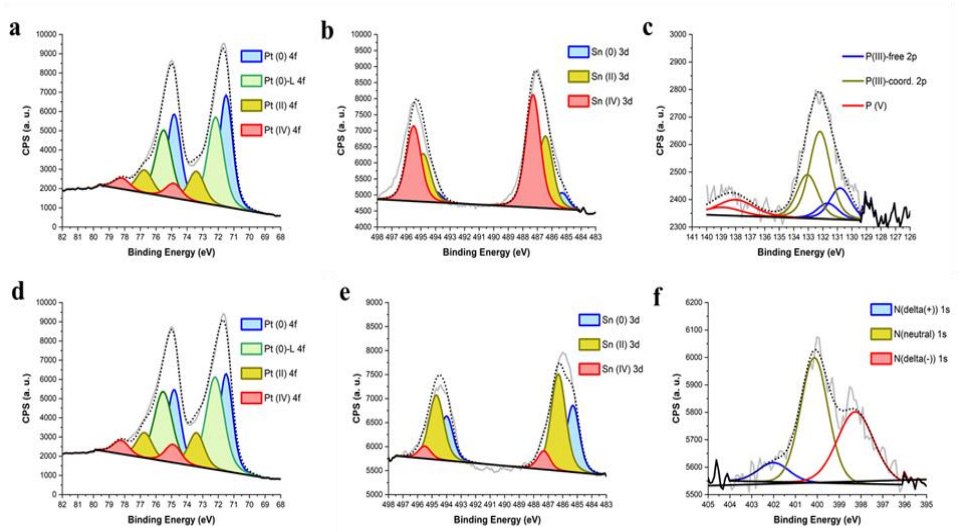

Figure 4.25. XPS of $PtSn^{IV}$-PPh_3 (a) Pt, b) Sn and c) P compositions and $PtSn^{IV}$ -NHC) (d) Pt, e) Sn and f) N compositions).

The theoretical consideration for the calculation of the number of total atoms (Nt) and surface atoms (Ns) to gain further characterization of the metal nanoparticles was calculated using the Van Hardeveld and Hartog (VHH)

model,[78] which is based on the principle that atoms at the surface of a metal can be differentiated according to the number and arrangement of their nearest neighbors. Using different algebraic equations for the population of atomic site depending of the coordination numbers were reported as a function of the cluster edge length *m*, which can be expressed as a number of atoms for several geometries.[79,80] Here, the VHH model was used to extract the approximate number of atoms in the nanoparticle, using the structure and diameter of the nanoparticles determined by TEM. For the $PtSn^{IV}$-P and $PtSn^{IV}$-NHC, both possess a mean size NPs of 2.1 nm. After applying the equations, Ns and Nt are calculated (**Table 4.7**¡Error! No se encuentra el origen de la referencia.).

Table 4.7. Ns and Nt calculations for $PtSn^{IV}$-PPh_3 and $PtSn^{IV}$-NHC using the VHH model.

	$PtSn^{IV}$-PPh_3	$PtSn^{IV}$-NHC
Mean size (nm) by TEM	2.05	2.10
Ns	172	174
Nt	341	346
Ns/Nt	0.5	0.5

Sn components were also extracted from XPS (**Figure 4.25,**b,e) measurements and revealed that Sn is mainly in +2 and +4 oxidation states when P is used, whereas 35% of Sn is in its metallic form when NHC is the stabilizer. The Sn in low oxidation states (Sn (0)) incorporated in the PtSn alloy structure and the Sn in higher oxidation (Sn (δ+)). This behavior could be ascribed to the coordination of the stabilizing agent (PPh_3 or NHC) and blockage of the Pt-sites avoiding the interaction with the Sn-precursor during the nanoparticle synthesis, thus, reducing the final Pt_3Sn alloy content.

The presence of P and NHC ligands was confirmed through the detection of bands in the P 2p (**Figure 4.25** c) and N 1s regions, in agreement with previous reports. [81,64] Furthermore, compared to the 78% of the Pt surface accessible to the covered by ligands, we have measured that only a fraction of the PPh_3 and NHC ligands is interacting with the Pt-NP surface and the rest of PPh_3 and NHC remained in a second-coordination sphere interacting with PtSn-L-NPs. All the characterization of PtSn colloids is displayed in **Table 4.8**.

Table 4.8. PtSn Colloids characterization properties.

Colloid	Sn/Pt [a] (mol/mol)	XRD Phase/ Crystallite size at r.t.	NPs size (nm) [b]	Pt (IV/II/0-L/0)	Sn (IV/II/0)
$PtSn^{IV}$	0.3	Pt 3.66 nm	14 ± 4	-	-
$PtSn^{II}$	1.2	Pt + PtSn 4.80 nm	5 ± 1	-	-
$PtSn^{IV}$-PPh_3	0.2	Pt 1.41 nm	2.1 ± 0.5	7 / 18 / 42 / 33	56 / 44 / 0
$PtSn^{II}$-PPh_3	1.3	Pt + shoulder 0.77 nm	2 ± 1	6 / 13 / 40 / 41	57 / 36 / 7
$PtSn^{IV}$-NHC	0.2	Pt 1.51 nm	2.1 ± 0.4	8 / 14 / 44 / 34	9 / 56 / 35
$PtSn^{II}$-NHC	1.3	Pt + PtSn hex. 3.14 nm	5 ± 3	-	-

[a] Quantified by ICP-OES analysis; [b] measured by TEM.

Since the XPS results indicated the presence of the PPh_3 stabilizing ligand on the colloidal samples, we have conducted liquid and solid state-NMR analyses after precipitation of the colloids. The samples were thoroughly washed with hexane and analysis of these washings and when a sample was analyzed by $^{31}P\{H\}$-NMR, no signals were detected, which suggested that the PPh_3 is present within the catalysts, presumably at the Pt surface. $^{31}P\{H\}$-NMR spectra of the colloidal samples (entries 2 and 3) and supported catalysts (entries 4 to 6) and PPh_3 as blank (entry 1) are displayed in **Figure 4.26**. Solid state-NMR analyses of the colloids were carried out but no ^{31}P NMR signals could be detected, presumably probably because of the broadening of the signals due to the proximity of these molecules to the surface of the Pt-NP.

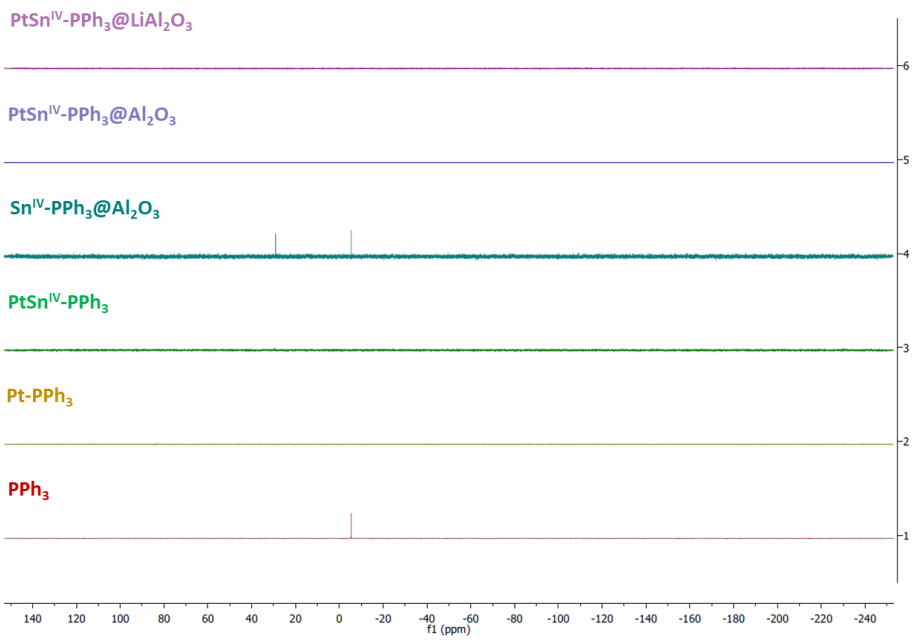

Figure 4.26. $^{31}P\{H\}$-NMR (161 MHz, CDCl3, n = 128 scans) of PPh_3 (1), Pt-PPh_3 (2), PtSn^{IV}-PPh_3 (3), Sn^{IV}-PPh_3@Al_2O_3 (4), PtSn^{IV}-PPh_3@Al_2O_3 (5) and PtSn^{IV}-PPh_3@$LiAl_2O_3$.

In conclusion, supported PtSn onto alumina's (Al_2O_3 and $Li(0.45)Al_2O_3$) and colloidal PtSn samples have been prepared by OPOA and characterized by various microscopic and spectroscopic techniques. In all cases, small and well-

dispersed bimetallic nanoparticles were obtained with mean diameters of ca. 1.3-2.0 nm. According to ICP-OES analysis and GC-MS monitoring of the synthesis, the rate of Sn decomposition was influenced by the acidity of the support and the obtained Pt/Sn ratio revealed dependent on the nature of the ligand stabilizer and of the Sn precursor. The more basic ligand (NHC) provided NPs with a lower Sn wt.% compared to the catalyst stabilized with the less basic PPh_3, or when no stabilizing ligand was used. The results revealed the formation of small and well dispersed NPs, probably composed by Pt_3Sn and Pt crystalline phases for PtSn catalysts, and with the extra Pt_5PSn phase in PtSn-PPh_3, confirming the P incorporation into the structure. The rest of the tin to attain the composition determined by ICP is present as tin oxides or tin aluminates either on the surface of the NP or on the surface of the support. The presence of stabilizing ligand (PPh_3 or NHC) on the surface of the NP has been recorded by combination of EDS and XPS experiments and highly suggested the presence or not of stabilizing ligand during the PtSn nanoparticle synthesis resulted in similar Sn/Pt molar ratios but with a different crystalline phase behavior, i.e., PtSn-PPh_3 colloidal nanoparticle displayed much higher Pt/Pt_3Sn molar ratios than PtSn catalyst. This behavior could be ascribed to the PPh_3 coordination and blockage of the Pt-sites avoiding the interaction with the Sn-precursor during the nanoparticle synthesis, thus, reducing the final Pt_3Sn alloy content.

4.2.2 Catalytic evaluation in PDH

The influences of the ligand stabilizer (PPh_3 and NHC-CO_2) and of the Sn precursor ($Sn^{(IV)}Bu_4$ and N,N'-Di-t-butyl-2,3-diamidobutanetin (II)) on the supported catalysts onto Al_2O_3 were examined in PDH at 530 °C on Al_2O_3 supported catalysts with a 2 wt.% Pt. The catalysts stabilized by PPh_3 ($PtSn^{II}$-P@Al_2O_3 and $PtSn^{IV}$-P@Al_2O_3) showed an initial propane conversion near the equilibrium (23.0% and 23.6%, respectively). After a rapid deactivation, the

conversion remained stable and reached 12.6% and 14.4%, respectively, after 15h on stream. When $PtSn^{II}$-NHC@Al_2O_3 and $PtSn^{IV}$-NHC@Al_2O_3 were tested under the same conditions, the initial propane conversions were significantly lower (15.7% and 6.2%, respectively). The catalyst $PtSn^{II}$-NHC@Al_2O_3, deactivated very rapidly, conversion dropped to 1.8% after 15 h on stream whereas $PtSn^{IV}$-NHC@Al_2O_3 exhibited much lower conversions but without apparent deactivation throughout the experiment (5.0% conversion after 15 h on stream). High selectivity to propylene (>97%) was afforded for all catalysts and was maintained during the whole time on steam (**Figure 4.27**).

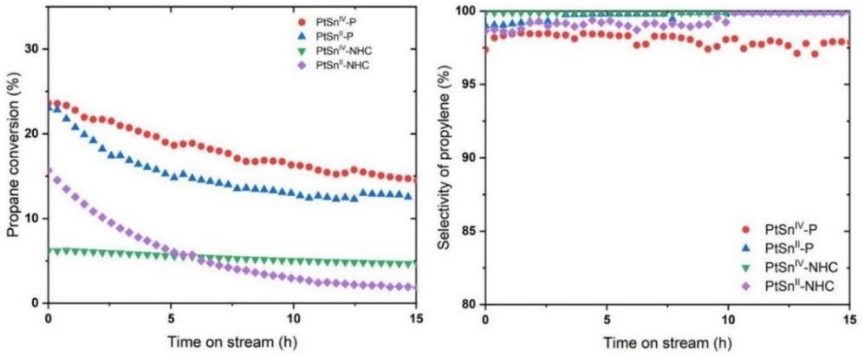

Figure 4.27. Propane conversion and propylene selectivity over $PtSn^{IV}$-P@Al_2O_3 (red), $PtSn^{II}$-P@Al_2O_3 (blue), $PtSn^{IV}$-NHC@Al_2O_3 (green) and $PtSn^{II}$-NHC@Al_2O_3 (purple). Reaction conditions: 530 °C, atmospheric pressure, $C_3H_8/H_2/Ar$ = 3/1/21 (mL/min), and GHSV = 60000 $mL \cdot gcat^{-1} \cdot h^{-1}$.

The effect of the support was studied by testing the $PtSn^{IV}$-P@$LiAl_2O_3$ catalyst (0.45 wt.% Li) (Figure 4.28). Lower initial conversion was observed (20%) and it decreased up to 9.7 % after 15 h on stream. Comparable deactivation with the $PtSn^{IV}$-P@Al_2O_3 (similar deactivation constants (K_d) between 0.04-0.05) and selectivity to propylene was measured.

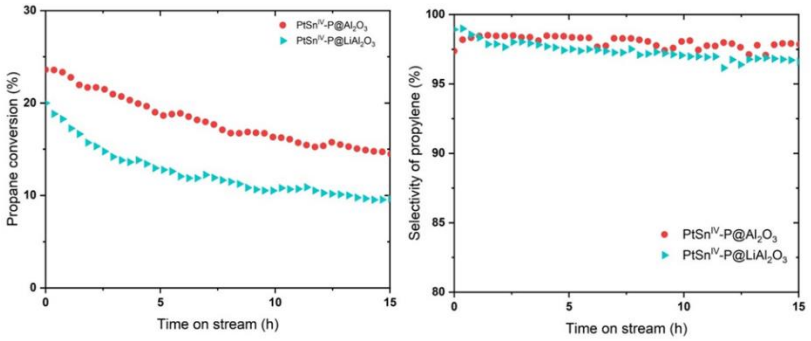

Figure 4.28. Propane conversion and propylene selectivity over PtSn^{IV}-P@Al_2O_3 (red) and PtSn^{IV}-P@$LiAl_2O_3$ (turquoise). Reaction conditions: 530 °C, atmospheric pressure, $C_3H_8/H_2/Ar$ = 3/1/21 (mL/min), and GHSV = 60000 mL·gcat^{-1}·h^{-1}.

The effect of small quantities of CO_2, given its mild oxidant nature, was examined with PtSn^{IV}-P@Al_2O_3.[82] Initially, a slightly lower conversion was achieved with the CO_2 poisoning (19.8%), however the catalyst remained more stable over time with the addition of CO_2 (19.0% at 15 h and 16.6% at 40 h) and the propylene selectivity over propylene was improved (>99%) (**Figure 4.29**). The K_d value was 0.0034, improved compared with the same catalyst without the CO_2 in the feed, 0.0405.

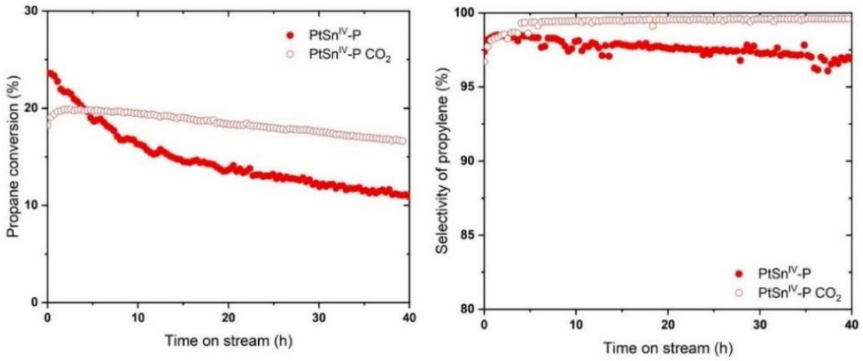

Figure 4.29. CO_2 poisoning effect on the propane conversion and propene selectivity over PtSn^{IV}-P@Al_2O_3 without CO_2 poisoning (filled red) and with CO_2 poisoning (unfilled red). Reaction conditions: 530 °C, atmospheric pressure, $C_3H_8/H_2/Ar$ = 3/1/21 (mL/min) and 200 ppm of CO_2 in the feed, and GHSV = 60000 mL·gcat^{-1}·h^{-1}.

To study the scope of alkane/alkene feedstock the $PtSn^{IV}$-P@Al_2O_3 catalyst was also evaluated in the butane and 1-butene dehydrogenation (**Figure 4.30**).

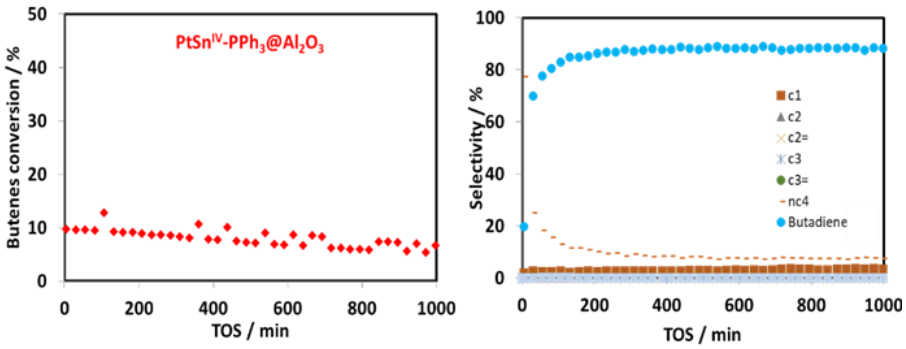

Figure 4.30. Butenes conversion and selectivity of PtSn-PPh_3@Al_2O_3. 530 ^oC, 60.000 mLtotal·gcat-1·h-1 using 3 C4:1H_2:21 Ar.

Concerning the thermodynamic equilibrium conversion using the reaction conditions: 3C_4: 1H_2:21Ar at 530 ^oC, the maximum theoretical conversion is 13.8%. The tested catalyst showed an initial conversion of 10% with a slow deactivation to 6.8% after with a high butadiene selectivity of 70% at the beginning of the catalysis and 88% after 600 min. The hydrogenation product was the main side-reaction observed with a selectivity to butane of 25% initially and 7.7% after 600 min. This test proved that also the catalysts are valid for the butane dehydrogenation reactions.

Then, $PtSn^{IV}$@Al_2O_3 catalyst was tested under the same PDH conditions, high initial conversion, and selectivity over propylene (25.6% and >97%, respectively) were observed. Moreover, the activity remained stable over time (20.6% after 15 h and 20.5 % after 24 h) (see Supporting Information for details). Those values indicated a greater propylene productivity than the ligand capped catalysts. For comparison purposes, one of the benchmark catalysts Linde-BASF-Statoil was tested under the same catalytic conditions, obtaining an initial conversion of 7.5% (4.0% after 7.5 h on stream) and a

propylene selectivity of 83%. This experiment showed that the two catalysts ($PtSn^{IV}@Al_2O_3$ and $PtSn^{IV}$-P@Al_2O_3) outperform the benchmark catalyst Linde-BASF-Statoil in terms of both activity and propylene selectivity (**Figure 4.31**).

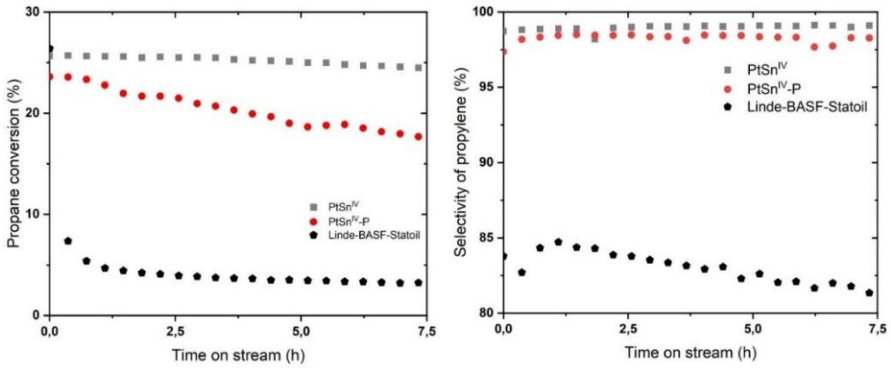

Figure 4.31. Ligand effect vs benchmarking catalyst on the propane conversion and propene selectivity over $PtSn^{IV}@Al_2O_3$ (grey), $PtSn^{IV}$-P@Al_2O_3 (red) and Linde-BASF-Statoil (black) supported onto a hydrotalcite. Reaction conditions: 530 °C, atmospheric pressure, $C_3H_8/H_2/Ar$ = 3/1/21 (mL/min), and GHSV = 60000 $mL \cdot gcat^{-1} \cdot h^{-1}$.

The mean size of the reduced NPs ($PtSn^{IV}@Al_2O_3$ and $PtSn^{IV}$-P@Al_2O_3) was measured by TEM (**Figure 4.32**).

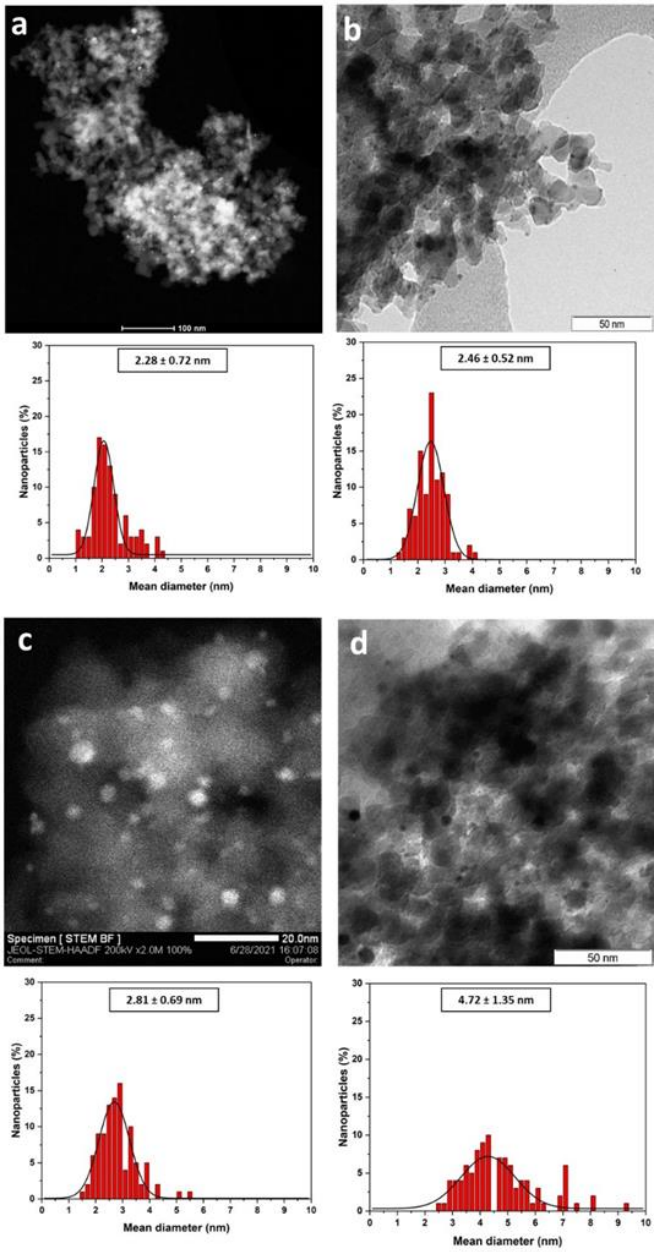

Figure 4.32. Mean size of the supported catalysts: $PtSn^{IV}@Al_2O_{3,(a)}$ reduced and (b) after 16 h of time of streaming in PDH and $PtSn^{IV}$-P@Al_2O_3, (c) reduced and (d) after 16 h of time of streaming in PDH.

$PtSn^{IV}@Al_2O_3$ and $PtSn^{IV}$-P@Al_2O_3) of the reduced systems (*ca.* 2.3 nm and *ca.* 2.8 nm, respectively) and after 16 h of TOS the catalyst containing PPh_3 ($PtSn^{IV}$-

P@Al_2O_3) grow fast (ca. 4.7 nm), fomenting the coke formation and explaining the faster deactivation over time whereas the $PtSn^{IV}$@Al_2O_3 remained almost in the same size (*ca.* 2.5 nm) (**Table 4.9**).

Table 4.9. NPs sizes of the catalyst fresh, reduced and after being tested.

	NPs size (nm)[b]		
Catalyst[b]	Fresh	Reduced	Tested after 16 h
$PtSn^{IV}$-P@Al_2O_3	1.3 ± 0.3	2.8 ± 0.7	4.7 ± 1.3
$PtSn^{IV}$@Al_2O_3	1.4 ± 0.4	2.3 ± 0.7	2.5 ± 0.5

[a] All catalysts were synthesized with a theoretical metal content of 2 wt% Pt and 2 wt.% Sn unless stated differently. [b] Obtained through TEM analyses and measuring more than 200 nanoparticles, NP sizes are quoted as the mean diameter ± the standard deviation.

The effect of Pt loading was studied by comparison of the performance of $PtSn^{IV}$-P@Al_2O_3 with that of 1Pt0.5Sn^{IV}-P@Al_2O_3, containing 1 wt.% Pt and 0.5 wt.% Sn. The catalyst containing a lower amount of Pt showed greater stability (**Figure 4.33¡Error! No se encuentra el origen de la referencia.**): It displayed lower initial activity of 22.3% but the conversion was maintained practically constant and, after 22 h on stream, it was 20.6% higher than that observed for that of 1 wt.% Pt (**Figure 4.33**, deactivation constant of 0.006). This result could be explained by the higher Pt dispersion in sample 1Pt0.5Sn^{IV}-P@Al_2O_3 resulting in lower degree of sintering. The selectivity was not affected, and in both cases a propylene selectivity of >97% was observed.

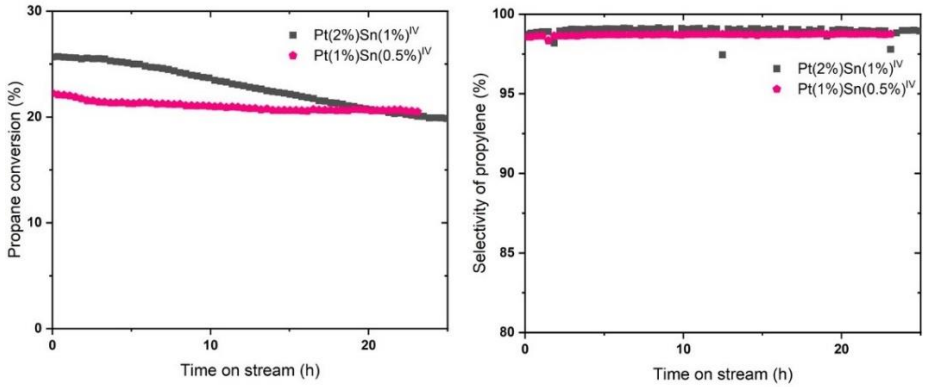

Figure 4.33. Propane conversion and propylene selectivity over $PtSn^{IV}@Al_2O_3$ with 2 wt.% Pt and 1 wt.% Sn (grey) and 1 wt.% Pt and 0.5 wt.% Sn (pink). Reaction conditions: 530 °C, atmospheric pressure, $C_3H_8/H_2/Ar$ = 3/1/21 (mL/min), and GHSV = 60000 $mL \cdot gcat^{-1} \cdot h^{-1}$.

The catalytic performance of all the PtSn systems tested for PDH at 530 °C, at atmospheric pressure under flow conditions (25 mL/min, C_3H_8, H_2, Ar = 3 / 1 / 21) and GHSV = 60000 $mL \cdot gcat^{-1} \cdot h^{-1}$, has been summarized in **Table 4.10.**

Table 4.10. PDH results for all the PtSn-based catalysts, including conversion, propylene selectivity's and K_d calculations.

Catalyst	Time (h)	Conv. (%)	Selec. (%)	K_d
$1Pt0.5Sn^{IV}@Al_2O_3$	0.0	22.3	98.5	0.0067
	15.0	20.6	98.7	
	24.0	20.5	98.7	
$PtSn^{IV}@Al_2O_3$	0.0	25.6	98.8	0.0128
	15.0	22.1	99.0	
	24.0	19.9	98.9	
	40.0	17.2	98.9	
$PtSn^{IV}$-P@Al_2O_3	0.0	23.6	98.1	0.0405
	15.0	14.4	97.8	

	24.0	13.0	97.5	
	40.0	10.9	97.0	
CO2 $PtSn^{IV}$-P@Al_2O_3	0.0	19.8	98.1	0.0034
	15.0	19.0	99.5	
	40.0	16.6	99.6	
$PtSn^{IV}$-P@$LiAl_2O_3$	0.0	20.0	98.9	0.0563
	15.0	9.7	96.7	
	24.0	9.0	96.1	
	40.0	7.7	94.1	
$PtSn^{II}$-P@Al_2O_3	0.0	23.0	99.0	0.0372
	15.0	12.6	99.9	
$PtSn^{IV}$-NHC@Al_2O_3	0.0	6.2	99.9	0.0210
	15.0	5.0	99.9	
$PtSn^{II}$-NHC@Al_2O_3	0.0	15.7	98.6	0.154
	15.0	1.8	99.9	

In conclusion, during the syntheses of these bimetallic PtSn nanoparticles, there is a surface modification of the Pt due to the stabilizing ligand (none, NHC·CO_2 or PPh_3). The ligands have an indirect effect on the final Sn amount contained in the catalysts which affects their performance in PDH. The higher Sn content is achieved by no stabilizing ligand > PPh_3 > NHC-CO_2. Since Pt content is similar in all the catalysts (containing 1.5-1.7 wt.% Pt) it is possible to represent the PDH conversion in front of the Sn/Pt ratio (M/M) (**Figure 4.34**).

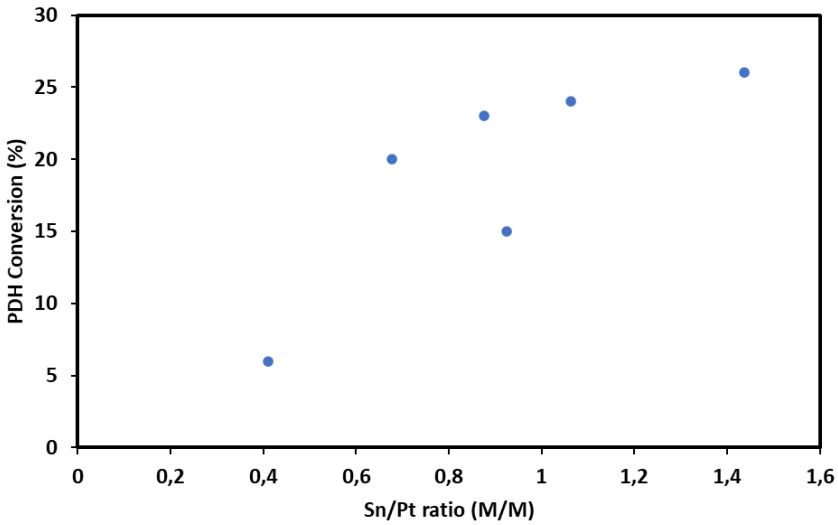

Figure 4.34. PDH conversion versus Sn/Pt ratio (M/M) content of the PtSn-L@Al_2O_3 stabilized with L =none, PPh_3 or NHC.

4.3 Conclusions

In this chapter, we have reported for the first time the preparation of the PtSn catalysts using OPOA for PDH reaction. The as-prepared catalysts were characterized by combination of microscope and spectroscopic techniques providing insights on the NP dimensions, catalyst compositions, crystalline phases, and oxidation states of the surface elements. The efficiency in the PDH of these catalysts has been evaluated at 530 ^{o}C and 1 bar revealing high initial conversions (up to 23 %), outstanding conversion stability and high propylene selectivity (99.9%). Furthermore, scope of substrate applications of the best performing catalyst has been also demonstrated by studying the dehydrogenation of butane and 1-butene to butadiene.

The effects studied during this work are the effect of the tin precursor, stabilizing agent, the effect of the support. As more detailed conclusions:

- Concerning the effect of the stabilizing agent, the PtSn/Al_2O_3-catalysts synthesized in absence of stabilizing agent provided better activity

and catalytic stability than those prepared in presence of PPh3, and this formed catalyst provided much better performance than the catalyst prepared in presence of NHC. In terms of propylene selectivity, no relevant difference was recorded, and the three catalysts provided outstanding selectivity. This behavior has been ascribed to the higher Sn/Pt loading and higher Pt_3Sn/Pt recorded for the stabilizing agent free catalyst than those recorded for the catalyst prepared in presence of stabilizing agent.

- Concerning the effect of the Pt loading, the 1Pt0.5Sn^{IV}@Al_2O_3 with 1wt.% displayed an initial conversion of 22.3% and after 24 h of time on stream, the conversion was maintained at 20.5%, whereas the PtSn(IV)@Al_2O_3 displayed higher slightly higher (25% close to the thermodynamic equilibrium conversion) initial conversion and the conversion after 24h is also around 20%. Both catalysts displayed outstanding selectivity (>99%).
- Concerning the effect of the Sn precursor, the use of Sn (IV) precursor seems to allow a more controlled deposition of the Sn onto the catalyst (deposition onto Pt-NP and onto the support) resulting in better performing catalyst. This behavior has been ascribed to the higher reactivity of the Sn (II) precursor observed with the colloidal system.
- Concerning to the support, the catalyst supported onto $LiAl_2O_3$ displayed worst results than the catalyst supported onto $Al2O_3$. This behavior has been ascribed to the lower Sn content and Sn/Pt ratios, and the presence of Sn oxide species partially reduced onto the Al_2O_3. The presence of this kind of species has been pointed out by the recent literature as one of the keys for the development of better catalyst.

- Overall, the catalyst was highly selective toward propylene throughout the experiment (>98.5% after 24h) and was stable, with a deactivation constant (k_d) of 0.0067. The OPO allows us to explore new horizons in the preparation of other catalyst for propane dehydrogenation with a very easy one-step methodology.

4.4 Experimental Details

4.4.1 General Methods.

Tris(dibenzylideneacetone)diplatinum ($Pt_2(dba)_3$) was prepared adapting the reported procedure[83] using potassium tetrachloroplatinate(II) (K_2PtCl_4, Johnson Matthey), dibenzylideneacetone (dba) and sodium acetate with metal trace levels (NaOAc), all of them from Sigma Aldrich, were purchased from commercial sources and used without further purification, unless stated differently. The tin precursors ($SnBu_4$, Sigma-Aldrich, and N,N'-Di-t-butyl-2,3-diamidobutanetin(II), Strem Chemicals), stabilizing agents (triphenylphosphine (PPh_3), from Sigma-Aldrich) were used without further purification, unless stated differently. The imidazolium carboxylate ($NHC{\cdot}CO_2$) was prepared following reported procedures.[22,84] Solvents (Toluene, tetrahydrofuran (THF) and hexane) were purchased from Scharlab and purified by MBraun Solvent Purifier Systems and degassed by freeze-pump-thaw cycles prior use. High purity gas (such as, hydrogen (H_2), nitrogen (N_2) and argon (Ar) with purity >99.999%) and hydrocarbons (propane with purity 99.9999%) were purchased from Linde. All the operations for the syntheses of ligand-capped nanoparticulated systems (either colloidal or supported) were carried out using standard Schlenk tubes, Fisher-Porter bottle techniques or in a glovebox under nitrogen atmosphere. Pyrogenic γ-Al_2O_3 from EVONIK (100 $m^2\ g^{-1}$) was pre-treated before used as reported elsewhere[85] to obtain Al_2O_3

and $LiAl_2O_3$, the supports were provided by the group of Dr. Mostafa Taoufik from the C2P2, CPE (Lyon, France).

4.4.2 Catalyst Preparation.

To prepare the bimetallic PtSn-NPs ligand capped (L), Pt-(2 wt.%)/Sn-(1 wt.%)-NPs supported onto Al_2O_3 (PtSn-L@Al_2O_3), the platinum precursor (i.e., for Pt_2dba_3, 0.274 mmol, 150 mg), tin precursor (i.e., for $SnBu_4$, 0.274 mmol, 101 mg), the selected stabilizing agent (L: none, PPh_3, NHC·CO_2) (i.e., for PPh_3, 0.054 mmol, 14.35 mg), the corresponding support (i.e., for Al_2O_3, 2.57 g) and solvent (i.e., 37.5 mL toluene) were introduced in a Fisher Porter. The mixture was pressurized with 3 bars of H_2 and stirred at 700 rpm at 100 °C during 40 h. After filtration (14-15 µm pore filter), washing with toluene and hexane and drying under vacuum, the supported $PtSn^{IV}$-P@Al_2O_3 was isolated in high yields (ca. 90-95%) and stored under inert atmosphere. Same procedure was followed to obtain $PtSn^{IV}$-NHC@Al_2O_3 (using the NHC·CO_2) or $PtSn^{IV}$- @Al_2O_3 (without adding any stabilizing agent). To obtain the $PtSn^{IV}$-P@$LiAl_2O_3$, $LiAl_2O_3$ was used as support. $PtSn^{II}$-P@Al_2O_3 and $PtSn^{II}$-NHC@Al_2O_3 were prepared using the as-described methodology with Sn (II) precursor ((N,N'-Di-t-butyl-2,3-diamidobutanetin(II)). 1Pt0.5Sn^{IV}@Al_2O_3 was prepared using a theoretical content of Pt-(1 wt.%)/Sn-(0.5 wt.%).

Herein, the syntheses of colloidal stabilized PtSn-L NPs ligand capped (L: none, PPh_3, NHC·CO_2), $PtSn^{IV}$-L is described. Pt precursor (Pt_2dba_3, 0.274 mmol,150.0 mg), the tin precursor (i.e., for $SnBu_4$, 0.274 mmol, 101.0 mg), the selected stabilizing agent (i.e. for PPh_3, 0.054 mmol, 14.35 mg), and toluene (37.5 mL) were introduced in a Fisher Porter. The mixture was pressurized at 3 bars of H_2 at 700 rpm at 100 °C during 40 h. After washing with toluene and hexane and drying under vacuum, the colloidal $PtSn^{IV}$-P were isolated in low yields (20-30%) and stored under inert atmosphere after precipitation. Same procedure

was followed for the obtention of $PtSn^{IV}$-NHC (adding 0.2 equivalents of NHC·CO_2) and $PtSn^{IV}$ (without any stabilizing agent). $PtSn^{II}$-L colloids were prepared following the same methodology described, changing the Sn (N,N'-Di-t-butyl-2,3-diamidobutanetin(II)). $PtSn^{II}$-P, $PtSn^{II}$-NHC and $PtSn^{II}$ were obtained in low yields (20-30%) and stored under inert atmosphere after precipitation.

4.4.3 Catalyst Characterization.

Inductively coupled plasma optical emission spectroscopy (ICP-OES) analyses were performed on digested samples of the materials, employing a Spectro Arcos FHS-16 spectrometer at the "Servei Cientificotècnics de la Universitat Rovira i Virgili" in Tarragona. The digestions were carried out using Ethos Easy Advanced microwave digestion system. As a general procedure, 50 mg of sample were charged in Teflon liners followed by 12 mL of a concentrated acid mixture of aqua regia (3 mL HNO3 69% and 9 mL HCl 37%). The heating program started with the increase from room temperature to 200 ºC during 30 min (approx. 6 °C/min) and followed with an isotherm at 200 °C during 1 h more. The irradiation power during all the runs was automatically controlled by the equipment to fit the temperature program. After a typical digestion, the reactors were open, and the homogeneity of the solution examined. The solutions were transferred to volumetric flasks of 50 mL and the liners washed exhaustively with Milli-Q water. Finally, the obtained solutions were analyzed by ICP-OES. Quantification of Pt and Sn is performed by comparison with the respective calibration curve constructed in the range of 0-20 ppm.

Gas Chromatography-Thermal Conductivity Detector (GC-TCD) analyses were carried out on an Agilent 7890A with a TCD detector using a column HP-Plot Q (30 m, 0.32 mm, 20 µm). All the syntheses were injected 4 times (manually). The first injection at time 0 of the reaction at r.t., afterwards, the temperature

was set to 100 °C using a silicon bath. After 30 min the second injection was done. Finally, two more injections were done at time of 20 and 40 h at 100 °C.

N2 adsorption/desorption isotherms were acquired in a Micrometrics ASAP 2020 instrument. N2 adsorption/desorption isotherms were acquired after dehydroxylation, under air-free conditions and without pretreatments.

Transmission Electron Microscopy (TEM) experiments were performed at the "Unitat de Microscopia dels Serveis Cientificotècnics de la Universitat Rovira i Virgili" in Tarragona with a JEOL model 1011 electron microscope operating at 100 kV with resolution of 3 Å. The particles size distributions were determined by a manual analysis of enlarged images. At least 200 particles on a given grid were measured to obtain a statistical size distribution and a mean diameter.

Scanning Transmission Electron Microscopy - High Angle Annular Dark Field (STEM-HAADF) images were obtained in a probe-corrected Titan Low Base (FEI) at a working voltage of 300 kV, coupled with a HAADF detector (Fischione), available in the "Advanced Microscopy Laboratory of Instituto de Nanociencia de Aragón" in Zaragoza (LMA-INMA) in Zaragoza. X-ray Energy Dispersive Spectra (EDS) were obtained with an Ultim Max (Oxford Instruments) detector. High Resolution TEM (HRTEM) imaging of the nanoparticles was performed in an image-corrected Titan (Thermofisher) operated at a working voltage of 300 kV, and equipped with a S-FEG and a spherical aberration corrector of the objective lens (CETCOR from CEOS company). TEM and HRTEM images were acquired with a bottom mounted 2Kx2K Ultrascan CCD camera from Gatan. The samples were dispersed in absolute ethanol or hexane, using ultrasonication. A drop of this solution was then deposited on a Holey carbon 300 mesh copper grid.

X-Ray Diffraction (XRD) measurements were performed at the "Unitat de Microscopia dels Serveis Cientificotècnics de la Universitat Rovira i Virgili" in

Tarragona using a a Bruker-AXS D8-Advance diffractometer with vertical theta-theta goniometer, incident- and diffracted-beam Soller slits of 2.5º, a fixed 0.5º receiving slit and an air-scattering knife on the sample surface. The angular 2θ range was between 5 and 80º. The data were collected with an angular step of 0.02º at a step/time of 0.2s, resulting in a duration of 712s. Cuk_{α} radiation was obtained from a copper X-ray tube operated at 40 kV and 40 mA. Diffracted X-rays were detected with a PSD detector LynxEye-XE-T with an opening angle of 2.94º. Sample was placed inside an MTC-HIGHTEMP chamber for *in-situ* temperature analysis. The sample was placed onto a Si(510) plate (0.5mm thick) and that onto the Pt heater. This setup was chosen to avoid both the Pt peaks of the heater and any reaction of the sample with the Pt heater. The desired temperature of the analysis was calibrated previously for this special support with a MgO (perciclase) standard. The temperature chamber, with the sample inside, was firstly evacuated with a primary bump and after a constant flow of 0.5 L/h of N_2 was maintained through the analysis. The first diffractogram was taken at room temperature and the second at the chosen temperature at a heating rate of 10^{o}/min. The temperature was maintained constant and the diffractograms were taken consecutively in such a way that the time between diffractograms was of 712s. The diffractograms were interpreted with the software DIFFRAC.EVA 5.2 from BRUKER.AXS and the database PDF-2 release 2018 from ICDD (International Center for Diffraction Data).

X-Ray Photoelectron Spectroscopy (XPS) measurements were performed at the Catalan Institute of Nanoscience and Nanotechnology (ICN2) in Cerdanyola del Vallès with a Phoibos 150 analyzer (SPEC GmbH, Berlin, Germany) in ultra-high vacuum conditions (base pressure 5E-10 mbar) with a monochromatic aluminum Kα X-Ray source (1486.74 eV). The energy resolution was measured by the FWHM of the Ag 3d5/2 peak for a sputtered

silver foil was 0.62 eV. Binding energies were calibrated relative to the C1s photoemission at 284.5. The XPS data were curve-resolved using the CasaXPS software after Shirley background subtraction. The spectra were fit with the minimum number of peaks needed to reproduce the spectral features. Gaussian (70%)–Lorentzian (30%), defined in CasaXPS as GL(30)2, profiles were used for each component.

Monodimensional (^{1}H, ^{13}C and ^{31}P) Nuclear Magnetic Ressonance (NMR) experiments were performed at the "Unitat de Microscopia dels Serveis Cientificotècnics de la Universitat Rovira i Virgili" in Tarragona on a Varian 400 MHz using deuterated chloroform (CDCl3) as a solvent. Chemical shifts (ppm) are given relative to trimethyl silane (TMS) in ^{1}H NMR (16 scans) and $CDCl_3$ in ^{13}C NMR (32-64) and frequency of deuterated solvent in ^{31}P NMR (32-64 scans).

The thermogravimetric analyses (TGA) experiments were carried out with a Mettler Toledo TGA/SDTA851 instrument. For a typical TGA experiment, 5-10 mg of sample was placed in the sample holder in the furnace and the material was heated up at a rate of 10 °C min^{-1} under N_2 flow, while the weight was recorded continuously from 30 °C to 900 °C. The weight loss of the organic part and metal were used to calculate an approximate number of ligands coordinated to the metal surface and the organic matter remaining on the surface. The ligand loss was attributed to the weight loss observed between 100 and 450 °C. For the calculation, the molecular weight of the corresponding ligands and of the metal, and the number of metal atoms at the surface from TEM data were considered.

4.4.5 XRD Measurements

Table S.1. XRD data extracted from diffractograms of $PtSn^{IV}$ NPs (Part 1).

		Crystalline phase (% wt.)		Crystallite size (nm)	
Time (s)	**T (ºC)**	**Pt**	**Pt_3Sn**	**Pt**	**Pt_3Sn**
-	30	100.0 ± 0.3	-	3.66 ± 0.09	-
0	530	4.4 ± 3.6	95.6 ± 3.6	4.49 ± 3.10	14.13 ± 0.57
712	530	58.9 ± 5.4	41.1 ± 5.8	13.24 ± 0.61	17.95 ± 1.57
1424	530	54.3 ± 5.1	45.7 ± 5.1	14.07 ± 0.69	18.32 ± 1.37
2136	530	50.1 ± 5.2	49.9 ± 5.2	13.87 ± 0.89	17.65 ± 1.30
2848	530	52.7 ± 5.1	47.3 ± 5.1	14.24 ± 0.72	19.03 ± 1.42
3560	530	55.6 ± 5.2	44.4 ± 5.2	13.88 ± 0.73	19.98 ± 1.74

Table S.2. XRD data extracted from diffractograms of $PtSn^{IV}$ NPs (Part 2).

		Cell parameters (Å)	
Time (s)	**T (ºC)**	**Pt (a)**	**Pt_3Sn (a)**
-	30	3.9883 ± 0.0011	-
0	530	3.9960 ± 0.0280	4.0201 ± 0.0007
712	530	4.0160 ± 0.0011	4.0257 ± 0.0011
1424	530	4.0154 ± 0.0012	4.0255 ± 0.0010
2136	530	4.0162 ± 0.0012	4.0241 ± 0.0010
2848	530	4.0154 ± 0.0012	4.0254 ± 0.0010
3560	530	4.0166 ± 0.0012	4.0250 ± 0.0010

Table S.3. XRD data extracted from diffractograms of $PtSn^{IV}$-PPh_3 NPs (Part 1).

		Crystalline phase (% wt.)			Crystallite size (nm)		
Time (s)	**T (ºC)**	**Pt**	**Pt_3Sn**	**Pt_5PSn**	**Pt**	**Pt_3Sn**	**Pt_5PSn**
-	30	100.0 ± 0.1	-	-	1.41 ± 0.01	-	-
0	530	62.5 ± 3.6	37.5 ± 3.6	-	3.94 ± 0.12	7.60 ± 0.46	-
712	530	72.4 ± 1.3	23.1 ± 1.3	4.5 ± 0.3	5.11 ± 0.12	26.1 ± 2.10	30.69 ± 3.46
1424	530	63.1 ± 0.8	30.5 ± 0.8	6.3 ± 0.2	4.88 ± 0.10	35.82 ± 1.82	37.41 ± 3.12
2136	530	56.6 ± 0.7	35.8 ± 0.7	7.6 ± 0.2	4.68 ± 0.11	39.17 ± 1.68	36.67 ± 2.64
2848	530	52.0 ± 0.6	39.8 ± 0.6	8.2 ± 0.3	4.34 ± 0.11	40.24 ± 1.50	35.95 ± 2.45

3560	530	48.0 ± 0.6	43.3 ± 0.6	8.7 ± 0.3	4.22 ± 0.11	41.08 ± 1.40	38.12 ± 2.50
4272	530	45.6 ± 0.6	45.5 ± 0.6	8.8 ± 0.3	3.91 ± 0.10	41.52 ± 1.30	41.35 ± 2.71
4984	530	44.9 ± 0.6	46.2 ± 0.6	8.9 ± 0.3	3.81 ± 0.10	43.93 ± 1.33	43.187 ± 2.83

Table S.4. XRD data extracted from diffractograms of $PtSn^{IV}$-PPh_3 NPs (Part 2).

		Cell parameters (Å)			
Time (s)	**T (ºC)**	**Pt (a)**	**Pt_3Sn (a)**	**Pt_5PSn (a/c)**	
-	30	3.9331 ± 0.0017	-	-	-
0	530	4.0078 ± 0.0015	4.0220 ± 0.0011	-	-
712	530	4.0141 ± 0.0007	4.0237 ± 0.005	3.9498 ± 0.0012	7.0420 ± 0.0036
1424	530	4.0133 ± 0.006	4.0237 ± 0.0003	3.9490 ± 0.0007	7.0396 ± 0.0022
2136	530	4.0129 ± 0.0007	4.0237 ± 0.0002	3.9486 ± 0.0006	7.0405 ± 0.0019
2848	530	4.0128 ± 0.0008	4.0236 ± 0.0002	3.9491 ± 0.0006	7.0383 ± 0.0018
3560	530	4.0125 ± 0.0008	4.0237 ± 0.0002	3.9490 ± 0.0005	7.0389 ± 0.0016
4272	530	4.0121 ± 0.0009	4.0238 ± 0.0002	3.9490 ± 0.0005	7.0408 ± 0.0015
4984	530	3.9543 ± 0.0009	4.0120 ± 0.0002	3.9492 ± 0.0005	7.0408 ± 0.0014

Table S.5. XRD data extracted from diffractograms of $PtSn^{IV}$-NHC NPs (Part 1).

		Crystalline phase (% wt.)		Crystallite size (nm)	
Time (s)	**T (ºC)**	**Pt**	**Pt_3Sn**	**Pt**	**Pt_3Sn**
-	30	100.0 ± 0.2	0.0	1.51 ± 0.02	-
0	530	70.1 ± 1.5	29.9 ± 1.5	4.15 ± 0.05	5.54 ± 0.19
712	530	66.6 ± 1.2	33.4 ± 1.2	4.94 ± 0.06	5.81 ± 0.16
1424	530	64.1 ± 1.0	35.9 ± 1.0	3.95 ± 0.01	6.39 ± 0.15
2136	530	64.7 ± 0.9	35.3 ± 0.9	6.18 ± 0.08	6.97 ± 0.16
2848	530	63.6 ± 0.8	36.4 ± 0.8	6.71 ± 0.08	7.67 ± 0.16
3560	530	62.7 ± 0.8	37.3 ± 0.8	7.36 ± 0.10	7.98 ± 0.17
4272	530	63.6 ± 0.7	36.4 ± 0.7	7.78 ± 0.10	8.79 ± 0.18
4984	530	62.5 ± 0.6	37.5 ± 0.6	9.69 ± 0.12	9.79 ± 0.18

Table S.6. XRD data extracted from diffractograms of $PtSn^{IV}$-NHC NPs (Part 2).

		Cell parameters (Å)	
Time (s)	**T (°C)**	**Pt (a)**	**Pt_3Sn (a)**
-	30	3.9440 ± 0.0017	-
0	530	3.9626 ± 0.0011	4.0234 ± 0.0013
712	530	3.9595 ± 0.0008	4.0192 ± 0.0011
1424	530	3.9578 ± 0.0007	4.0196 ± 0.0009
2136	530	3.9575 ± 0.0006	4.0194 ± 0.0007
2848	530	3.9571 ± 0.0005	4.0194 ± 0.0006
3560	530	3.9567 ± 0.0005	4.0191 ± 0.0006
4272	530	3.9576 ± 0.0005	4.0202 ± 0.0005
4984	530	3.9384 ± 0.0003	4.0006 ± 0.0004

The Rietveld refinement,[71] was performed with the TOPAS v6 software[72] under the so called "launch mode". The background was modelized with a 2nd order Chebyschev polynomial. The instrumental contribution to the diffraction profile was calculated with the Fundamental Parameters Approach.[73] The relative quantitative phase analysis was obtained by refining the Rietveld scale factor for each phase and applying the corresponding well-known equations.[74] The net peak width of each phase was modelled with the Double-Voigt Approach[75] by considering only the Lorentzian contribution of the crystallite size effect and discarding any contribution of the micro strain to the peak width. The averaged integral breadth was obtained from the resulting fitted Voigt function to the whole diffractogram. The Scherrer equation[76] was then applied to obtain the apparent crystallite size.

An example of the Rietveld analysis for sample PtSn-PPh_3 is showed **Figure S.1**. The Pt peaks are completely overlapped by the Pt_3Sn. However, the Pt peaks are broadener than the Pt_3Sn ones and must be included in the fitting model to ensure a good fit. The base of the Pt_3Sn peaks is much broadener than the expected and can only be explained by the presence of broad Pt peaks below.

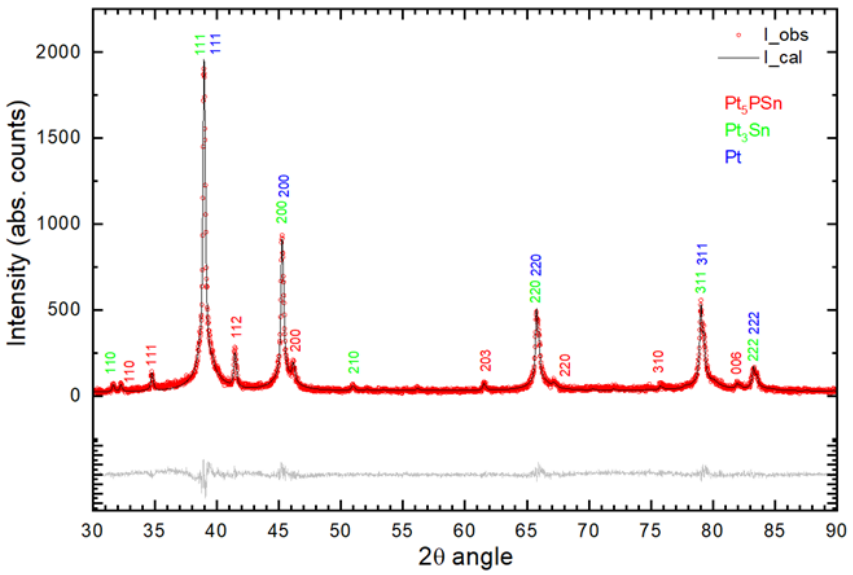

Figure S.1. Observed (red circles), calculated (black line) and difference (grey line) diffractograms for sample PtSn-PPh_3. The Miller indexes for each phase are also plotted.

4.4.5 Catalytic Activity Measurements

Propane dehydrogenation (PDH) experiments were carried under O_2 and H_2O exclusion conditions. All gases were purchased from Air Liquide and further purified in line with molecular sieves and BTS catalysts traps to assure high purity. A stainless-steel tubing was used as a continuous flow reactor (P_{total} = 1 bar, T = 530 °C) and it was packed inside an Ar filled glovebox. Typically, 25 mg of catalyst were diluted to 2.5 g with SiC. A reductive pretreatment of 16 h at 550 ^{o}C (1 °C/min) was carried out with pure hydrogen flow, prior to start the catalytic tests, the system reached room temperature and it was purged with Ar. A 3 C_3H_8: 1 H_2: 21 Ar (mL/min) gas composition was used and controlled by Brooks mass flow controllers. The Gas hourly space velocity (GSHV) was kept to 60000 mL·gcat^{-1}·h^{-1}, unless stated differently. The products were determined by an online HP 6890 GC equipped with 50 m KCl/Al_2O_3

column and FID detector. Propane conversion was calculated typically by carbon balance. Selectivity to each product was similarly obtained.

The propane conversion and propene selectivity were determined by gas chromatographic (GC-TCD) analysis of gas samples taken at regular interval. The response factor of the propane and propene were determined using argon as internal standard. The mathematical formula for the determination of the conversion and selectivity are:

$$Propane\ conversion\ (\%) = \frac{Total\ Propane_{out}}{Total\ Propane_{in}}\ x\ 100$$

$$Propylene\ selectivity\ (\%) = \frac{Total\ propylene_{out}}{Total\ propane_{in} - Total\ propane_{out}}\ x\ 100$$

The deactivation constant (k_d) was calculated at the reaction temperature (530 ^{o}C) according to the following formula:

$$\ln\left[\frac{(1-\chi_{final})}{\chi_{final}}\right] = k_d \times T + \ln\left[\frac{(1-\chi_{initial})}{\chi_{initial}}\right]$$

Where χ_{final} and $\chi_{initial}$, are the final and the initial propane conversion values and T represents the lifetime of the catalyst.

4.5 References

(1) Chen, S.; Chang, X.; Sun, G.; Zhang, T.; Xu, Y.; Wang, Y.; Pei, C.; Gong, J. Propane Dehydrogenation: Catalyst Development, New Chemistry, and Emerging Technologies. *Chem. Soc. Rev.* **2021**, *50* (5), 3315–3354. https://doi.org/10.1039/D0CS00814A.

(2) Wang, G.; Zhu, X.; Li, C. Recent Progress in Commercial and Novel Catalysts for Catalytic Dehydrogenation of Light Alkanes. *Chem. Rec.* **2020**, *20* (6), 604–616. https://doi.org/https://doi.org/10.1002/tcr.201900090.

(3) Nawaz, Z. Light Alkane Dehydrogenation to Light Olefin Technologies: A Comprehensive Review. *Rev. Chem. Eng.* **2015**, *31* (5), 413–436. https://doi.org/doi:10.1515/revce-2015-0012.

(4) Docherty, S. R.; Rochlitz, L.; Payard, P.-A.; Copéret, C. Heterogeneous Alkane

Dehydrogenation Catalysts Investigated via a Surface Organometallic Chemistry Approach. *Chem. Soc. Rev.* **2021**, *50*, 5806–5822. https://doi.org/10.1039/d0cs01424a.

(5) Liu, L.; Lopez-Haro, M.; Lopes, C. W.; Rojas-Buzo, S.; Concepcion, P.; Manzorro, R.; Simonelli, L.; Sattler, A.; Serna, P.; Calvino, J. J.; Corma, A. Structural Modulation and Direct Measurement of Subnanometric Bimetallic PtSn Clusters Confined in Zeolites. *Nat. Catal.* **2020**, *3* (8), 628–638. https://doi.org/10.1038/s41929-020-0472-7.

(6) Zhang, J.; Deng, Y.; Cai, X.; Chen, Y.; Peng, M.; Jia, Z.; Jiang, Z.; Ren, P.; Yao, S.; Xie, J.; Xiao, D.; Wen, X.; Wang, N.; Liu, H.; Ma, D. Tin-Assisted Fully Exposed Platinum Clusters Stabilized on Defect-Rich Graphene for Dehydrogenation Reaction. *ACS Catal.* **2019**, *9* (7), 5998–6005. https://doi.org/10.1021/acscatal.9b00601.

(7) Santhosh Kumar, M.; Chen, D.; Holmen, A.; Walmsley, J. C. Dehydrogenation of Propane over Pt-SBA-15 and Pt-Sn-SBA-15: Effect of Sn on the Dispersion of Pt and Catalytic Behavior. *Catal. Today* **2009**, *142* (1), 17–23. https://doi.org/https://doi.org/10.1016/j.cattod.2009.01.002.

(8) Yang, M.-L.; Zhu, Y.-A.; Zhou, X.-G.; Sui, Z.-J.; Chen, D. First-Principles Calculations of Propane Dehydrogenation over PtSn Catalysts. *ACS Catal.* **2012**, *2* (6), 1247–1258. https://doi.org/10.1021/cs300031d.

(9) Sattler, J. J. H. B.; Ruiz-Martinez, J.; Santillan-Jimenez, E.; Weckhuysen, B. M. Catalytic Dehydrogenation of Light Alkanes on Metals and Metal Oxides. *Chem. Rev.* **2014**, *114* (20), 10613–10653. https://doi.org/10.1021/cr5002436.

(10) Nakaya, Y.; Hirayama, J.; Yamazoe, S.; Shimizu, K.; Furukawa, S. Single-Atom Pt in Intermetallics as an Ultrastable and Selective Catalyst for Propane Dehydrogenation. *Nat. Commun.* **2020**, *11* (1), 2838. https://doi.org/10.1038/s41467-020-16693-9.

(11) Samantaray, M. K.; D'Elia, V.; Pump, E.; Falivene, L.; Harb, M.; Ould Chikh, S.; Cavallo, L.; Basset, J.-M. The Comparison between Single Atom Catalysis and Surface Organometallic Catalysis. *Chem. Rev. (Washington, DC, United States)* **2020**, *120* (2), 734–813. https://doi.org/10.1021/acs.chemrev.9b00238 CO - CHREAY.

(12) Al-Shareef, R.; Harb, M.; Saih, Y.; Ould-Chikh, S.; Anjum, D. H.; Candy, J.-P.; Basset, J.-M. Precise Control of Pt Particle Size for Surface Structure-Reaction Activity Relationship. *J. Phys. Chem. C* **2018**, *122* (41), 23451–23459. https://doi.org/10.1021/acs.jpcc.8b06346 CO - JPCCCK.

(13) Zhu, H.; Anjum, D. H.; Wang, Q.; Abou-Hamad, E.; Emsley, L.; Dong, H.; Laveille, P.; Li, L.; Samal, A. K.; Basset, J.-M. Sn Surface-Enriched Pt-Sn Bimetallic Nanoparticles as a Selective and Stable Catalyst for Propane Dehydrogenation. *J. Catal.* **2014**, *320*, 52–62. https://doi.org/10.1016/j.jcat.2014.09.013 CO - JCTLA5.

(14) Boualleg, M.; Basset, J.-M.; Candy, J.-P.; Caps, V.; Jumas, J.-C.; Norsic, S.; Quadrelli, E. A.; Veyre, L.; Thieuleux, C. Single-Phase Heterogeneous Pt3Sn Catalyst Synthesized by Room-Temperature Self-Assembly. *ChemCatChem* **2012**, *4* (11), 1729. https://doi.org/10.1002/cctc.201200276 CO - CHEMK3.

(15) Candy, J. P.; Humblot, F.; Didillon, B.; LePeltier, F.; Basset, J. M. Improvement in Stability and Regenerability of Silica Supported Platinum-Tin Catalysts Prepared by Surface Organometallic Chemistry. Effect of the Tin Addition Process. *Stud. Surf. Sci. Catal.* **1999**, *126*, 237–247.

(16) Bentahar, F. Z.; Bayard, F.; Candy, J. P.; Basset, J. M.; Didillon, B. Surface Organometallic Chemistry on Metals. Chemical Modification of Platinum Catalyst Surface by Reaction with Tetrabutyltin. Application to the Selective Dehydrogenation of Isobutane to Isobutene. *Spec. Publ. - R. Soc. Chem.* **1999**, *235*, 235–245.

(17) Humblot, F.; Candy, J. P.; Le Peltier, F.; Didillon, B.; Basset, J. M. Surface Organometallic Chemistry on Metals: Selective Dehydrogenation of Isobutane into Isobutene on Bimetallic Catalysts Prepared by Reaction of Tetra-n-Butyltin on Silica-Supported Platinum Catalyst. *J. Catal.* **1998**, *179* (2), 459–468. https://doi.org/10.1006/jcat.1998.2234 CO - JCTLA5.

(18) Humblot, F.; Didillon, D.; Lepeltier, F.; Candy, J. P.; Corker, J.; Clause, O.; Bayard, F.; Basset, J. M. Surface Organometallic Chemistry on Metals: Formation of a Stable ≡Sn(n-C4H9) Fragment as a Precursor of Surface Alloy Obtained by Stepwise Hydrogenolysis of Sn(n-C4H9)4 on a Platinum Particle Supported on Silica. *J. Am. Chem. Soc.* **1998**, *120* (1), 137–146. https://doi.org/10.1021/ja964405o CO - JACSAT.

(19) Humblot, F.; Candy, J. P.; LePeltier, F.; Didillon, B.; Basset, J. M. Surface Organometallic Chemistry on Metals: Formation of Surface Alloy by Stepwise Hydrogenolysis of Sn(n-C4H9)4 on Pt/SiO2. Application for the Selective Dehydrogenation of Isobutane into Isobutene. In *Book of Abstracts, 214th ACS National Meeting, Las Vegas, NV, September 7-11*; American Chemical Society, 1997; p COLL CO-64RNAO.

(20) Ely, T. O.; Amiens, C.; Chaudret, B.; Snoeck, E.; Verelst, M.; Respaud, M.; Broto, J. Synthesis of Nickel Nanoparticles . Influence of Aggregation Induced by Modification of Poly (Vinylpyrrolidone) Chain Length on Their Magnetic Properties Attracting Increasing Interest , Because They May Differ Surface or Quantum Size Effects . 1 Howeve. *Chem. Mater.* **1999**, *11* (l), 526–529.

(21) Lomelí-Rosales, D. A.; Delgado, J. A.; Díaz de los Bernardos, M.; Pérez-Rodríguez, S.; Gual, A.; Claver, C.; Godard, C. A General One-Pot Methodology for the Preparation of Mono- and Bimetallic Nanoparticles Supported on Carbon Nanotubes: Application in the Semi-Hydrogenation of Alkynes and Acetylene. *Chem. - A Eur. J.* **2019**, *25* (35). https://doi.org/10.1002/chem.201901041.

(22) De Los Bernardos, M. D.; Pérez-Rodríguez, S.; Gual, A.; Claver, C.; Godard, C. Facile Synthesis of NHC-Stabilized Ni Nanoparticles and Their Catalytic Application in the: Z -Selective Hydrogenation of Alkynes. *Chem. Commun.* **2017**, *53* (56), 7894–7897. https://doi.org/10.1039/c7cc01779k.

(23) Llop Castelbou, J.; Szeto, K. C.; Barakat, W.; Merle, N.; Godard, C.; Taoufik, M.; Claver, C. A New Approach for the Preparation of Well-Defined Rh and Pt Nanoparticles Stabilized by Phosphine-Functionalized Silica for Selective Hydrogenation Reactions. *Chem. Commun.* **2017**, *53* (22), 3261–3264. https://doi.org/10.1039/c6cc10338c.

(24) Martinez-Espinar, F.; Blondeau, P.; Nolis, P.; Chaudret, B.; Claver, C.; Castillón, S.; Godard, C. NHC-Stabilised Rh Nanoparticles: Surface Study and Application in the Catalytic Hydrogenation of Aromatic Substrates. *J. Catal.* **2017**, *354*, 113–127. https://doi.org/https://doi.org/10.1016/j.jcat.2017.08.010.

(25) Delgado, J. A.; Claver, C.; Castillón, S.; Curulla-Ferré, D.; Godard, C. Correlation between Hydrocarbon Product Distribution and Solvent Composition in the Fischer–Tropsch Synthesis Catalyzed by Colloidal Cobalt Nanoparticles. *ACS Catal.* **2015**, *5* (8), 4568–4578. https://doi.org/10.1021/cs5020332.

(26) Castelbou, J. L.; Blondeau, P.; Claver, C.; Godard, C. Surface Characterisation of Phosphine and Phosphite Stabilised Rh Nanoparticles: A Model Study. *RSC Adv.* **2015**, *5* (117), 97036–97043. https://doi.org/10.1039/C5RA21835G.

(27) Llop Castelbou, J.; Bresó-Femenia, E.; Blondeau, P.; Chaudret, B.; Castillón, S.; Claver, C.; Godard, C. Tuning the Selectivity in the Hydrogenation of Aromatic Ketones Catalyzed by Similar Ruthenium and Rhodium Nanoparticles. *ChemCatChem* **2014**, *6* (11), 3160–3168. https://doi.org/https://doi.org/10.1002/cctc.201402524.

(28) Castelbou, J. L.; Gual, A.; Mercadé, E.; Claver, C.; Godard, C. Ligand Effect in the Rh-NP Catalysed Partial Hydrogenation of Substituted Arenes. *Catal. Sci. Technol.* **2013**, *3* (10). https://doi.org/10.1039/c3cy00388d.

(29) Gual, A.; Axet, M. R.; Philippot, K.; Chaudret, B.; Denicourt-Nowicki, A.; Roucoux, A.; Castillon, S.; Claver, C. Diphosphite Ligands Derived from Carbohydrates as Stabilizers for Ruthenium Nanoparticles: Promising Catalytic Systems in Arene Hydrogenation. *Chem. Commun.* **2008**, No. 24. https://doi.org/10.1039/b802316f.

(30) Gual, A.; Godard, C.; Philippot, K.; Chaudret, B.; Denicourt-Nowicki, A.; Roucoux Alain; Castillón, S.; Claver Carmen. Carbohydrate-Derived 1,3-Diphosphite Ligands as Chiral Nanoparticle Stabilizers: Promising Catalytic Systems for Asymmetric Hydrogenation. *ChemSusChem* **2009**, *2* (8). https://doi.org/10.1002/cssc.200900079.

(31) Baquero, E. A.; Tricard, S.; Coppel, Y.; Flores, J. C.; Chaudret, B.; de Jesus, E. Water-Soluble Platinum Nanoparticles Stabilized by Sulfonated N-Heterocyclic Carbenes: Influence of the Synthetic Approach. *Dalt. Trans.* **2018**, *47* (12), 4093–4104. https://doi.org/10.1039/c8dt00240a CO - DTARAF.

(32) Martinez-Prieto, L. M.; Rakers, L.; Lopez-Vinasco, A. M.; Cano, I.; Coppel, Y.; Philippot, K.; Glorius, F.; Chaudret, B.; van Leeuwen, P. W. N. M. Soluble Platinum Nanoparticles Ligated by Long-Chain N-Heterocyclic Carbenes as Catalysts. *Chem. - A Eur. J.* **2017**, *23* (52), 12779–12786. https://doi.org/10.1002/chem.201702288 CO - CEUJED.

(33) Martinez-Prieto, L. M.; Cano, I.; Marquez, A.; Baquero, E. A.; Tricard, S.; Cusinato, L.; del Rosal, I.; Poteau, R.; Coppel, Y.; Philippot, K.; Chaudret, B.; Campora, J.; van Leeuwen, P. W. N. M. Zwitterionic Amidinates as Effective Ligands for Platinum Nanoparticle Hydrogenation Catalysts. *Chem. Sci.* **2017**, *8* (4), 2931–2941. https://doi.org/10.1039/c6sc05551f CO - CSHCCN.

(34) Baquero, E. A.; Tricard, S.; Flores, J. C.; de Jesus, E.; Chaudret, B. Highly Stable Water-Soluble Platinum Nanoparticles Stabilized by Hydrophilic N-Heterocyclic Carbenes. *Angew. Chemie, Int. Ed.* **2014**, *53* (48), 13220–13224. https://doi.org/10.1002/anie.201407758 CO - ACIEF5.

(35) Lara, P.; Suarez, A.; Colliere, V.; Philippot, K.; Chaudret, B. Platinum N-Heterocyclic Carbene Nanoparticles as New and Effective Catalysts for the Selective Hydrogenation of Nitroaromatics. *ChemCatChem* **2014**, *6* (1), 87–90. https://doi.org/10.1002/cctc.201300821 CO - CHEMK3.

(36) Lacroix, L.-M.; Gatel, C.; Arenal, R.; Garcia, C.; Lachaize, S.; Blon, T.; Warot-Fonrose, B.; Snoeck, E.; Chaudret, B.; Viau, G. Tuning Complex Shapes in Platinum Nanoparticles: From Cubic Dendrites to Fivefold Stars. *Angew. Chemie, Int. Ed.* **2012**, *51* (19), 4690. https://doi.org/10.1002/anie.201107425 CO - ACIEF5.

(37) Ramirez, E.; Erades, L.; Philippot, K.; Lecante, P.; Chaudret, B. Shape Control of Platinum Nanoparticles. *Adv. Funct. Mater.* **2007**, *17* (13), 2219–2228. https://doi.org/10.1002/adfm.200600633 CO - AFMDC6.

(38) Cano, I.; Martinez-Prieto, L. M.; Fazzini, P. F.; Coppel, Y.; Chaudret, B.; van Leeuwen, P. W. N. M. Characterization of Secondary Phosphine Oxide Ligands on the Surface of Iridium Nanoparticles. *Phys. Chem. Chem. Phys.* **2017**, *19* (32), 21655–21662. https://doi.org/10.1039/c7cp03439c CO - PPCPFQ.

(39) Axet, M. R.; Philippot, K.; Chaudret, B.; Cabie, M.; Giorgio, S.; Henry, C. R. TEM and HRTEM Evidence for the Role of Ligands in the Formation of Shape-Controlled Platinum Nanoparticles. *Small* **2011**, *7* (2), 235–241. https://doi.org/10.1002/smll.201001112 CO - SMALBC.

(40) Kinayyigit, S.; Lara, P.; Lecante, P.; Philippot, K.; Chaudret, B. Probing the Surface of Platinum Nanoparticles with 13CO by Solid-State NMR and IR Spectroscopies. *Nanoscale* **2014**, *6* (1), 539–546. https://doi.org/10.1039/c3nr03948j CO - NANOHL.

(41) Gutmann, T.; Bonnefille, E.; Breitzke, H.; Debouttiere, P.-J.; Philippot, K.; Poteau, R.; Buntkowsky, G.; Chaudret, B. Investigation of the Surface Chemistry of Phosphine-Stabilized Ruthenium Nanoparticles - an Advanced Solid-State NMR Study. *Phys. Chem. Chem. Phys.* **2013**, *15* (40), 17383–17394. https://doi.org/10.1039/c3cp52927d CO - PPCPFQ.

(42) Gonzalez-Galvez, D.; Nolis, P.; Philippot, K.; Chaudret, B.; van Leeuwen, P. W. N. M. Phosphine-Stabilized Ruthenium Nanoparticles: The Effect of the Nature of the Ligand in Catalysis. *ACS Catal.* **2012**, *2* (3), 317–321. https://doi.org/10.1021/cs200633k CO - ACCACS.

(43) Novio, F.; Philippot, K.; Chaudret, B. Location and Dynamics of CO Co-Ordination on Ru Nanoparticles: A Solid State NMR Study. *Catal. Letters* **2010**, *140* (1–2), 1–7. https://doi.org/10.1007/s10562-010-0428-7 CO - CALEER.

(44) Garcia-Anton, J.; Axet, M. R.; Jansat, S.; Philippot, K.; Chaudret, B.; Pery, T.; Buntkowsky, G.; Limbach, H.-H. Reactions of Olefins with Ruthenium Hydride Nanoparticles: NMR Characterization, Hydride Titration, and Room-Temperature C-C Bond Activation. *Angew. Chemie, Int. Ed.* **2008**, *47* (11), 2074–2078. https://doi.org/10.1002/anie.200704763 CO - ACIEF5.

(45) Gomez, S.; Erades, L.; Philippot, K.; Chaudret, B.; Colliere, V.; Balmes, O.; Bovin, J.-O. Platinum Colloids Stabilized by Bifunctional Ligands: Self-Organization and Connection to Gold. *Chem. Commun. (Cambridge, United Kingdom)* **2001**, No. 16, 1474–1475. https://doi.org/10.1039/b103781c CO - CHCOFS.

(46) Dassenoy, F.; Philippot, K.; Ould Ely, T.; Amiens, C.; Lecante, P.; Snoeck, E.; Mosset, A.; Casanove, M. J.; Chaudret, B. Platinum Nanoparticles Stabilized by CO and Octanethiol Ligands or Polymers: FT-IR, NMR, HREM and WAXS Studies. *New J. Chem.* **1998**, *22* (7), 703–711. https://doi.org/10.1039/a709245h.

(47) Bardaji, M.; Vidoni, O.; Rodriguez, A.; Amiens, C.; Chaudret, B.; Casanove, M.-J.; Lecante, P. Synthesis of Platinum Nanoparticles Stabilized by CO and Tetrahydrothiophene. Facile Conversion to Molecular Species. *New J. Chem.* **1997**, *21* (11), 1243–1249.

(48) Lara, P.; Ayvali, T.; Casanove, M.-J.; Lecante, P.; Mayoral, A.; Fazzini, P.-F.; Philippot, K.; Chaudret, B. On the Influence of Diphosphine Ligands on the Chemical Order in Small RuPt Nanoparticles: Combined Structural and Surface Reactivity Studies. *Dalt. Trans.* **2013**, *42* (2), 372–382. https://doi.org/10.1039/c2dt31646c CO - DTARAF.

(49) Rothermel, N.; Roether, T.; Ayvali, T.; Martinez-Prieto, L. M.; Philippot, K.; Limbach, H.-H.; Chaudret, B.; Gutmann, T.; Buntkowsky, G. Reactions of D2 with 1,4-Bis(Diphenylphosphino)Butane-Stabilized Metal Nanoparticles-A Combined Gas-Phase NMR, GC-MS and Solid-State NMR Study. *ChemCatChem* **2019**, *11* (5), 1465–1471. https://doi.org/10.1002/cctc.201801981 CO - CHEMK3.

(50) Breso-Femenia, E.; Godard, C.; Claver, C.; Chaudret, B.; Castillon, S. Selective Catalytic Deuteration of Phosphorus Ligands Using Ruthenium Nanoparticles: A New Approach to Gain Information on Ligand Coordination. *Chem. Commun. (Cambridge, United Kingdom)* **2015**, *51* (91), 16342–16345. https://doi.org/10.1039/c5cc06984j CO - CHCOFS.

(51) Castelbou, J. L.; Gual, A.; Mercadé, E.; Claver, C.; Godard, C. Ligand Effect in the Rh-NP Catalysed Partial Hydrogenation of Substituted Arenes. *Catal. Sci. Technol.* **2013**, *3* (10), 2828–2833. https://doi.org/10.1039/c3cy00388d.

(52) Prins, R.; Bussell, M. E. Metal Phosphides: Preparation, Characterization and Catalytic Reactivity. *Catal. Letters* **2012**, *142* (12), 1413–1436. https://doi.org/10.1007/s10562-012-0929-7.

(53) El-Refaei, S. M.; Russo, P. A.; Pinna, N. Recent Advances in Multimetal and Doped Transition-Metal Phosphides for the Hydrogen Evolution Reaction at Different PH Values. *ACS Appl. Mater. Interfaces* **2021**, *13* (19), 22077–22097. https://doi.org/10.1021/acsami.1c02129.

(54) Shi, Y.; Li, M.; Yu, Y.; Zhang, B. Recent Advances in Nanostructured Transition Metal Phosphides: Synthesis and Energy-Related Applications. *Energy Environ. Sci.* **2020**, *13* (12), 4564–4582. https://doi.org/10.1039/d0ee02577a.

(55) Kou, J.; Zhu Chen, J.; Gao, J.; Zhang, X.; Zhu, J.; Ghosh, A.; Liu, W.; Kropf, A. J.; Zemlyanov, D.; Ma, R.; Guo, X.; Datye, A. K.; Zhang, G.; Guo, L.; Miller, J. T. Structural and Catalytic Properties of Isolated Pt2+ Sites in Platinum Phosphide (PtP2). *ACS Catal.* **2021**, *11* (21), 13496–13509. https://doi.org/10.1021/acscatal.1c03970.

(56) Pryadchenko, V. V.; Srabionyan, V. V.; Avakyan, L. A.; Van Bokhoven, J. A.; Bugaev, L. A. Electronic Structure of Pt and Au Compounds Measured by X-Ray Emission and X-Ray Absorption Spectroscopies. *J. Phys. Chem. C* **2012**, *116* (49), 25790–25796. https://doi.org/10.1021/jp3073409.

(57) Gao, G.; Shao, Y.; Gao, Y.; Wei, T.; Gao, G.; Zhang, S.; Wang, Y.; Chen, Q.; Hu, X. Synergetic Effects of Hydrogenation and Acidic Sites in Phosphorus-Modified Nickel Catalysts for the Selective Conversion of Furfural to Cyclopentanone. *Catal. Sci. Technol.* **2021**, *11*, 575–593. https://doi.org/10.1039/d0cy01943g.

(58) Sehested, J.; Gelten, J. A. P.; Helveg, S. Sintering of Nickel Catalysts: Effects of Time, Atmosphere, Temperature, Nickel-Carrier Interactions, and Dopants. *Appl. Catal. A Gen.* **2006**, *309* (2), 237–246. https://doi.org/10.1016/j.apcata.2006.05.017.

(59) Yang, Y.; Ochoa-Hernández, C.; De La Peña O'Shea, V. A.; Coronado, J. M.; Serrano, D.

P. Ni2P/SBA-15 as a Hydrodeoxygenation Catalyst with Enhanced Selectivity for the Conversion of Methyl Oleate into n-Octadecane. *ACS Catal.* **2012**, *2* (4), 592–598.

(60) Landau, M. V; Herskowitz, M.; Hoffman, T.; Fuks, D.; Liverts, E.; Vingurt, D.; Froumin, N. Ultradeep Hydrodesulfurization and Adsorptive Desulfurization of Diesel Fuel on Metal-Rich Nickel Phosphides. *Ind. Eng. Chem. Res.* **2009**, *48* (11), 5239–5249.

(61) Liu, L.; Lopez-Haro, M.; Lopes, C. W.; Li, C.; Concepcion, P.; Simonelli, L.; Calvino, J. J.; Corma, A. Regioselective Generation and Reactivity Control of Subnanometric Platinum Clusters in Zeolites for High-Temperature Catalysis. *Nat. Mater.* **2019**, *18* (8), 866–873. https://doi.org/10.1038/s41563-019-0412-6.

(62) Lewis, J. D.; Ha, M.; Luo, H.; Faucher, A.; Michaelis, V. K.; Román-Leshkov, Y. Distinguishing Active Site Identity in Sn-Beta Zeolites Using 31P MAS NMR of Adsorbed Trimethylphosphine Oxide. *ACS Catal.* **2018**, *8* (4), 3076–3086. https://doi.org/10.1021/acscatal.7b03533.

(63) Cerezo-navarrete, C.; Lara, P.; M. Martínez-Preto, L. Organometallic Nanoparticles Ligated by NHCs: Synthesis, Surface Chemistry and Ligand Effects. *Catalysts* **2020**, *10* (10), 1144.

(64) López-vinasco, A. M.; Martínez-prieto, L. M.; Asensio, J. M.; Lecante, P.; Chaudret, B.; Cámpora, J.; Leeuwen, P. W. N. M. Van. Novel Nickel Nanoparticles Stabilized by Imidazolium-Amidinate Ligands for Selective Hydrogenation of Alkynes. *Catal. Sci. Technol.* **2020**, *10* (January), 293–578. https://doi.org/10.1039/c9cy02172h.

(65) Gannoun, C.; Turki, A.; Kochkar, H.; Delaigle, R.; Eloy, P. Elaboration and Characterization of Sulfated and Unsulfated V2O5/TiO2 Nanotubes Catalysts for Chlorobenzene Total Oxidation. *Appl. Catal. B Environ.* **2014**, *147*, 58–64.

(66) Gu, Y.; Liu, H.; Yang, M.; Ma, Z.; Zhao, L.; Xing, W.; Gu, Y.; Liu, H.; Yang, M.; Ma, Z.; Zhao, L. Highly Stable Phosphine Modified VOx / Al2O3 Catalyst in Propane Dehydrogenation To Cite This Version : HAL Id : Hal-02893792 Highly Stable Phosphine Modified VO x / Al 2 O 3 Catalyst in Propane Dehydrogenation. *Appl. Catal. B Environ.* **2020**, *274*, 119089.

(67) Zhang, Y.; Zhou, Y.; Qiu, A.; Wang, Y.; Xu, Y.; Wu, P. Propane Dehydrogenation on PtSn/ZSM-5 Catalyst: Effect of Tin as a Promoter. *Catal. Commun.* **2006**, *7* (11), 860–866. https://doi.org/10.1016/j.catcom.2006.03.016.

(68) Dai, Y.; Gu, J.; Tian, S.; Wu, Y.; Chen, J.; Li, F.; Du, Y.; Peng, L.; Ding, W.; Yang, Y. Gamma -Al2O3 Sheet-Stabilized Isolate Co2 + for Catalytic Propane Dehydrogenation. *J. Catal.* **2020**, *381*, 482–492. https://doi.org/10.1016/j.jcat.2019.11.026.

(69) Adkins, S. R.; Davis, B. H. The Chemical State of Tin in Platinum-Tin-Alumina Catalysts. *J. Catal.* **1984**, *89* (2), 371–379. https://doi.org/10.1016/0021-9517(84)90313-0.

(70) Holmen, A.; Blekkan, E. A. Propane Dehydrogenation over Supported Pt and Pt – Sn Catalysts : Catalyst Preparation , Characterization , and Activity Measurements. **1996**, *12* (158), 1–12.

(71) Rietveld, H. M. A Profile Refinement Method for Nuclear and Magnetic Structures. *J. Appl. Crystallogr.* **1969**, *2* (2), 65–71. https://doi.org/10.1107/s0021889869006558.

(72) Coelho, A. A. TOPAS and TOPAS-Academic: An Optimization Program Integrating Computer Algebra and Crystallographic Objects Written in C++: An. *J. Appl. Crystallogr.* **2018**, *51* (1), 210–218. https://doi.org/10.1107/S1600576718000183.

(73) Cheary, R. W.; Coelho, A. A.; Cline, J. P. Fundamental Parameters Line Profile Fitting in Laboratory Diffractometers. *J. Res. Natl. Inst. Stand. Technol.* **2004**, *109* (1), 1–25. https://doi.org/10.6028/jres.109.002.

(74) Hill, R. J.; Howard, C. J. Quantitative Phase Analysis from Neutron Powder Diffraction Data Using the Rietveld Method. *J. Appl. Crystallogr.* **1987**, *20* (6), 467–474.

(75) Balzar, D. Voigt-Function Model in Diffraction Line-Broadening Analysis. *Microstruct. Anal. from Diffr.* **1999**, 94–124.

(76) Stokes, A. R.; Wilson, A. J. C. A Method of Calculating the Integral Breadths of Debye-Scherrer Lines. *Math. Proc. Cambridge Philos. Soc.* **1942**, *38* (3), 313–322. https://doi.org/10.1017/S0305004100021988.

(77) Hardeveld, R. V. A. N.; Hartog, F. The Statistics of Surface Atoms and Surface Sites on Metal Crystals. *Surf. Sci.* **1969**, *15*, 189–230.

(78) Van Hardeveld, R.; Hartog, F. The Statistics of Surface Atoms and Surface Sites on Metal Crystals. *Surf. Sci.* **1969**, *15* (2), 189–230. https://doi.org/10.1016/0039-6028(69)90148-4.

(79) Borodzin, A.; Bonarowska, M. Relation between Crystallite Size and Dispersion On. *Langmuir* **1997**, *7463* (12), 5613–5620.

(80) Benfield, R. E. Mean Coordination Numbers and the Non-Metal-Metal Transition in Clusters. *J. Chem. Soc. Faraday Trans.* **1992**, *88* (8), 1107–1110.

(81) Clarke, C. J.; Maxwell-hogg, S.; Smith, E. F.; Hawker, R. R.; Harper, B.; Licence, P. Resolving X-Ray Photoelectron Spectra of Liquids with Difference Spectroscopy. *Phys. Chem. Chem. Phys.* **2019**, *21*, 114–123. https://doi.org/10.1039/c8cp06701e.

(82) Atanga, M. A.; Rezaei, F.; Jawad, A.; Fitch, M.; Rownaghi, A. A. Oxidative Dehydrogenation of Propane to Propylene with Carbon Dioxide. *Appl. Catal. B Environ.* **2018**, *220* (May 2017), 429–445. https://doi.org/10.1016/j.apcatb.2017.08.052.

(83) Ould Ely, T.; Pan, C.; Amiens, C.; Chaudret, B.; Dassenoy, F.; Lecante, P.; Casanove, M. J.; Mosset, A.; Respaud, M.; Broto, J. M. Nanoscale Bimetallic CoxPt1-x Particles Dispersed in Poly(Vinylpyrrolidone): Synthesis from Organometallic Precursors and Characterization. *J. Phys. Chem. B* **2000**, *104* (4), 695–702. https://doi.org/10.1021/jp9924427.

(84) Voutchkova, A. M.; Feliz, M.; Clot, E.; Eisenstein, O.; Crabtree, R. H. Imidazolium Carboxylates as Versatile and Selective N-Heterocyclic Carbene Transfer Agents: Synthesis, Mechanism, and Applications. *J. Am. Chem. Soc.* **2007**, *129* (42), 12834–12846. https://doi.org/10.1021/ja0742885.

(85) Rouge, P.; Garron, A.; Norsic, S.; Larabi, C.; Merle, N.; Delevoye, L.; Gauvin, R. M.; Szeto, K. C.; Taoufik, M. A Smarter Approach to Catalysts by Design: Combining Surface Organometallic Chemistry on Oxide and Metal Gives Selective Catalysts for Dehydrogenation of 2,3-Dimethylbutane. *Mol. Catal.* **2019**, *471* (January), 21–26.

Chapter 4

UNIVERSITAT ROVIRA I VIRGILI
INNOVATIVE NANOCATALYSTS FOR SUSTAINABLE NON-OXIDATIVE DEHYDROGENATION OF PROPANE
Laia Gil Jiménez

5

Alternative metals for PDH using SOMC-OPOA approaches

UNIVERSITAT ROVIRA I VIRGILI
INNOVATIVE NANOCATALYSTS FOR SUSTAINABLE NON-OXIDATIVE DEHYDROGENATION OF PROPANE
Laia Gil Jiménez

5

Alternative metals for PDH using SOMC-OPOA approaches

5.1 Introduction

As mentioned in Chapter 1, Pt catalysts for light alkane dehydrogenation to alkenes can be promoted with various metals, such as Ga or Sn.[1] Detailed studies on the application of the advanced synthetic methodologies for the preparation of PtSn based catalysts supported onto alumina are described in the Chapter 2 and Chapter 3. Herein, our target was to extend the scope of these synthetic methodologies to other metal compositions by replacing the metal modifier, for instance, PtGa systems, or by replacing the active metal, for instance, NiSn systems.

PtGa systems

The use of PtGa for dehydrogenation reactions was extended since, similarly to the behaviours observed with Sn, Pt-Ga alloys with various compositions were prepared by the corresponding thermal treatment (*ca.* 500^{o} C) and the selectivity toward the desired alkene was remarkably increased and attributed to geometric and electronic effects.[2] However, there are some differences between the catalytic behaviours of PtSn and PtGa systems, and one of the objectives of this chapter is to ascribe whether the catalyst preparation described in chapter 4 (OPOA) for PtSn systems could be extended for PtGa systems. Herein, a summary of the most relevant examples of PtGa systems described in the recent literature is collected.

A series of Pt catalysts (0.3wt.%) supported on gamma alumina promoted with $Ga(NO_3)_3$ (gallium loading between 0.05 and 0.66 wt.%) were prepared by impregnations and applied in the PDH reaction.[3] Comparison of the performance of mono and bimetallic catalysts showed that Ga enhanced the selectivity to propylene and decreased the catalyst deactivation and coke formation. The catalysts with Ga loading lower than 0.44wt.% resulted in less hydrogenolysis activities and prevented the blocking on Pt sites. This behavior was ascribed to the Ga modification of the metallic phase structure and a slight effect on the acidity of the support.[3]

In another study, a sequential impregnation method was applied for the preparation of the Pt/(10 wt.%)CeO_2-Al_2O_3 catalyst doped with Ga^{3+} cations. The resulting catalyst was evaluated in the PDH reaction (studied at 600º C) (**Figure 5.1**).[4] The authors observed that Ga^{3+} cations incorporated into the cubic fluorite structure of CeO_2 enhanced the lattice oxygen storage capacity and the surface oxygen mobility. As such, the reducibility of the support was enhanced, which was beneficial to eliminate the coke deposition and therefore improve the catalytic stability. DFT studies confirmed that upon addition of Ga, the desorption of propylene was improved and consequently, that the deep dehydrogenation and the coke formation were greatly supressed. The optimal Ga loading was 3 wt.%, with a Pt particle size of 1.7-2.3 nm, reaching a propane conversion of 39.4% at 600 ºC with a propylene selectivity near 99%.[4]

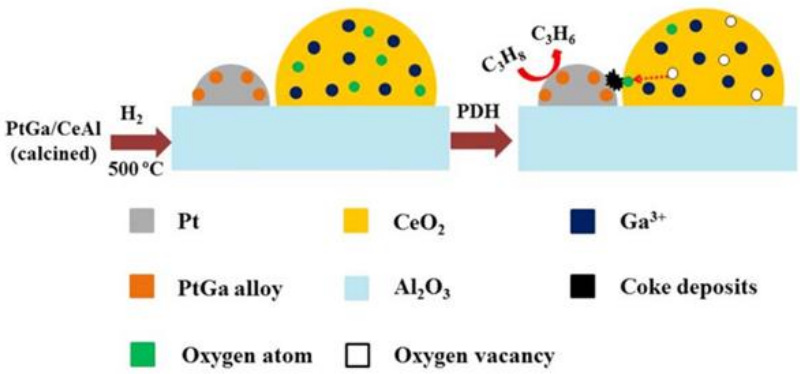

Figure 5.1. Representation of PtGa/$CeO_2Al_2O_3$ catalyst and its mechanism for PDH reaction.[4]

Bell and coworkers reported the preparation of a series of Pt/Mg(Ga)(Al)O catalysts by incipient wetness impregnation and its application in the ethane and propane dehydrogenations.[5] They observed a strong dependency of the catalytic performance on the Ga content, reaching nearly 100% selectivity using a Ga/Pt (atom/atom) ratio of 5.4 in both reactions. The authors also reported that the presence of Ga suppressed the coke formation.

The alloying of Pt with Ga was also studied using a hydrotalcite support to produce bimetallic catalysts (Pt/Mg(Al,Ga)O_x) for PDH.[6] Various Ga/Pt molar ratios (between

0 and 10) were studied with a Pt loading of 2-3 wt.%. XRD analyses were performed during a temperature programmed reduction (5% H_2) cycling with 20% O_2/N_2 at 873K and an alloy formation and segregation were revealed depending on the gas environment and Ga loading. For the highest ratio Pt/Ga, the alloy was formed at the beginning of the reduction. The presence of XRD diffraction peaks at $2\theta = 40.2^o$ and 46.5^o attributed to pure Pt and one or more PtGa alloys were observed after consecutive sequence of reduction/oxidation treatments (**Figure 5.2**). However the exact composition of the alloy was not described.[6] This study revealed a reversible alloy/segregation looping once the sample was exposed to a redox cycle (alternating 5%H_2/He and 20%O_2/N_2 at 600 ^{o}C). Therefore, stability of the catalyst was ensured during the reaction and the regeneration process.

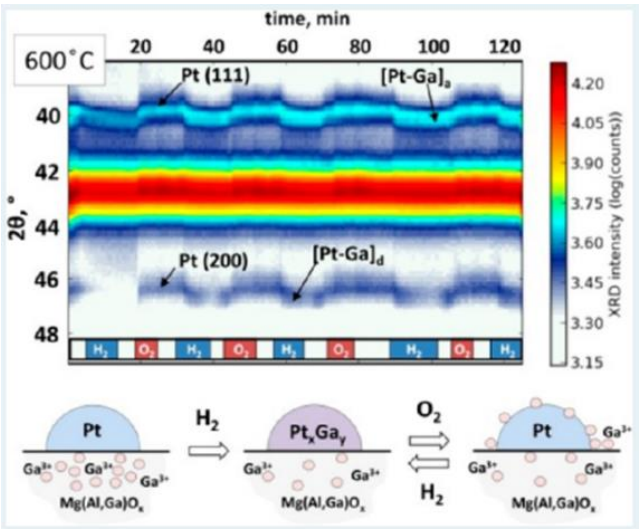

Figure 5.2. The alloying of Pt-Ga on a hydrotalcite-like support controlled by means of XRD during temperature-programmed reduction in 5% H_2/He and isothermal reduction with 5% H_2/He and oxidation cycling with 20% O_2/N_2 at 873 K.[6]

Recently, highly productive $PtGa/SiO_2$ catalysts for PDH were generated from single sites using the SOMC method.[7] $[Pt(COD)(OSi(OtBu)_3)_2]$ was grafted by SOMC/TMP approach onto silica-supported Ga^{III} single sites. The introduction of a controlled amount of Pt was performed through grafting by reaction of the -OH groups of the supports. After reductive treatment under H_2 (**Scheme 5.1 a**), highly dispersed NPs

of *ca.* 1.0 nm, were obtained even at high Pt loadings (4.37 wt.%).[7] The detailed characterization (CO adsorption IR, XPS and XAS studies) revealed that Pt-Ga alloy was formed and that a fraction of the overall Ga was located on the surface of the support. EXAFS analyses indicated that bulk Ga_2O_3 was not present. $PtGa/SiO_2$ catalyst (4.82 wt.% Pt and 1.48 wt.% Ga) showed high productivity (32%) and selectivity to propylene (99%) at 550 ^oC using 20% propane in Ar as feed. This material showed activity during 20h, according to an in situ XAS analysis, the catalyst average remained unchanged.

Scheme 5.1. (a) Synthetic procedure employed for PtGa alloyed NPs supported on Ga-doped silica using SOMC approach.[7]

To get insights into the origin of the high performance of this catalyst, DFT calculations were performed using periodic surfaces, clusters and realistic size silica supported NPs and metadynamics simulation (**Figure 5.3**).[8] Combining DFT with experimental data (XAS, TEM), the interaction between Pt and Ga was explored. At the interface of the support, interactions between metallic Pt and Ga with Si-O bonds were observed, together with additional interactions between Pt(0) with the Ga(III) Lewis acid sites . These NPs-support interactions and a possible flattening of the NPs could hinder the sintering and thus stabilize the PtGa catalyst during PDH. The authors also revealed that Pt atoms were isolated in the alloy, hindering coke formation.[8] The formation of the catalyst was further investigated. First, a fast formation of small Pt clusters/NPs at low temperature from the isolated Pt (II) sites was revealed by XANES/EXAFS techniques. Then, the Pt NPs reacted at high temperatures with isolated Ga (III) sites and alloyed PtGa particles were generated, interacting with the SiO_2. Moreover, they reported that the PtGa alloying minimized

large Pt ensembles, therefore that Pt site isolation at the surface of the NPs increased, as well with the mobility of Pt atoms in the alloyed NPs.

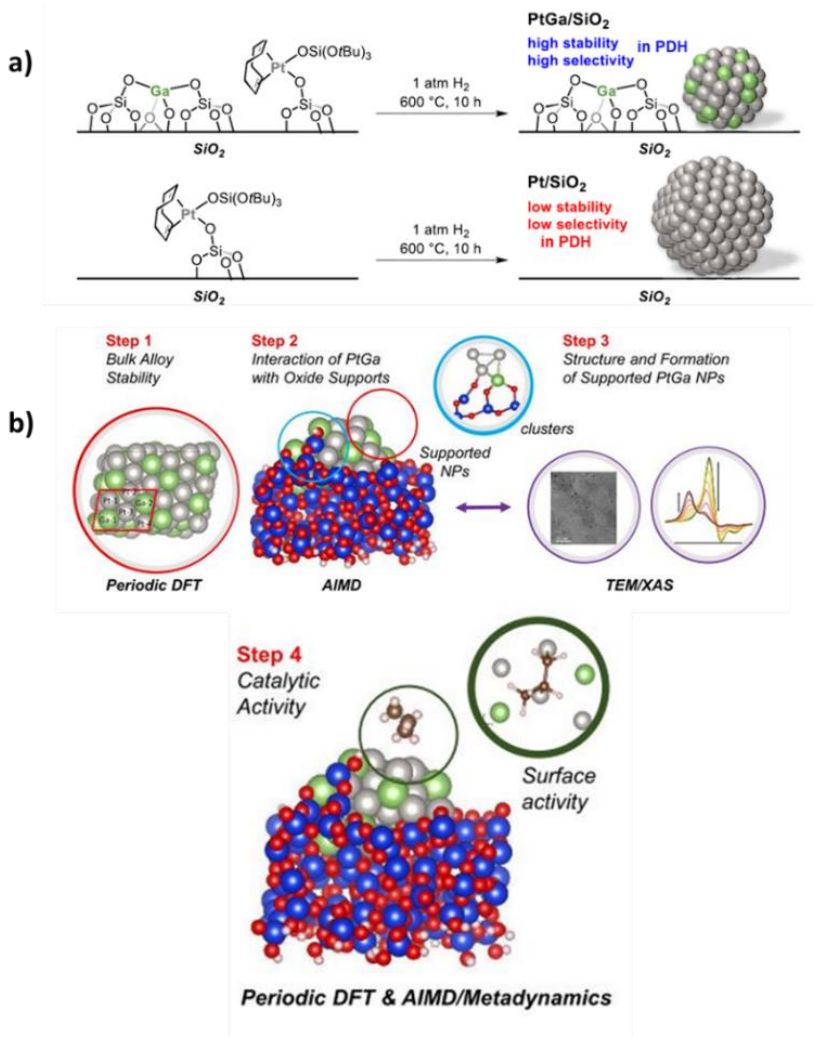

Figure 5.3. (a) State-of-the-art of SOMC/TMP of PtGa and Pt based catalyst on SiO_2 for PDH.[7] (b) Multiscale Ab Initio modelling and experimental evidence. Step 1: structure of a Pt_2Ga (311) and (111) surfaces; Step 2: interphase interaction of silica and Ga(III) single-sites with Pt(0) and Ga(0). Step 3: structure of Pt and Pt_2Ga NPs supported on SiO_2. Step 4: comparison of Pt and Pt_2Ga supported NPs in PDH.[8]

They suggested transient formation of unsaturated Pt isolated sites, highly active in the first C-H activation. Then, Pt atoms were isolated in the alloy, hindering coke formation through electronic effects. The addition of Ga to Pt diminished the affinity of Pt toward the unsaturated hydrocarbon intermediates. Moreover, a tri-

Pt-coordinated propyne intermediate (a coke formation precursor) would need partial dealloying of PtGa to provide larger Pt ensembles. Therefore, the coke formation is prevented.[8]

Other authors reported intermetallic PtGa species displaying three-fold Pt hollow ensembles and isolated Pt single atoms isolated by a Ga inert species at the surface, which were blocked by introducing Pb in the surface.[9] In **Figure 5.4**, the PDH conversion and selectivity to propylene over time are displayed and PtGa-Pb/SiO_2 (Pt/Pb = 2) (mean size of 2.4 ± 0.5 nm) catalyst exhibited 30% propane conversion with 99.6% propylene selectivity at 600^o C for 96 h. The Pb was reported to block some active Pt sites, and therefore limit the Pt specific activity as well as the Pt dispersion that was reported to decrease from 9.9% to 5.9% upon Pb deposition.[9] They reported that the single atom Pt catalysed both C-H activation but inhibited further dehydrogenation, thus explaining the minimization of side reactions and improved selectivity.

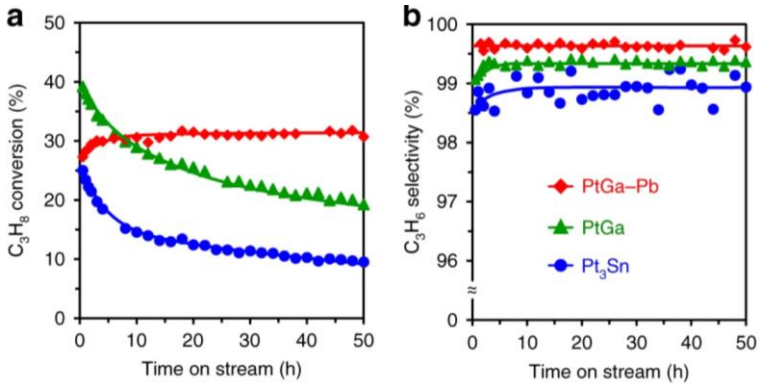

Figure 5.4. (a) Propane conversion and (b) propylene selectivity in PDH catalyzed by PtGa/SiO_2, PtGa-Pb/SiO_2 (Pt/Pb = 2) and Pt_3Sn/SiO_2.[9]

The use of Ca as a secondary modifier for this PtGa-Pb catalyst was also reported.[10] Upon addition of Ca cations, the electron density remarkably increased in the Pt1 sites in PtGa. In contrast with Pb atoms, the Ca cations were deposited around the PtGa NPs, but without covering the Pt active sites or without replacing the Pb deposited (**Scheme 5.2**). The doubly decorated catalyst PtGa-Pb-Ca/SiO_2, exhibited

a mean particle size of 2.2 ± 0.5 nm (HAADF-STEM) and EDX analysis revealed that Pt and Ga coexist in each NPs with an estimated ratio of *ca.* 1, which is similar to the structure reported without Ca. HRHAADF-STEM analysis revealed an ordered crystal structure that was attributed to PtGa intermetallic planes, in agreement with results from EXAFS curve fitting. Once Ca was added, no changes were detected in the bulk structure of intermetallic PtGa and the Pt dispersion was maintained. XANES analysis revealed a slight oxidation of Ga, and the authors suggested the existence of Ga-O-Ca interaction. The PtGa-Pb-Ca/SiO_2 catalyst exhibited an outstanding lifetime of 3067h at 600^{o}C in the presence and absence of H_2 in the feed, displaying excellent durability and stability in PDH. No sintering was detected, confirming a great thermal stability of Pt_1 in PtGa, probably because the high value ΔH_f (55.6 KJ·mol^{-1}).

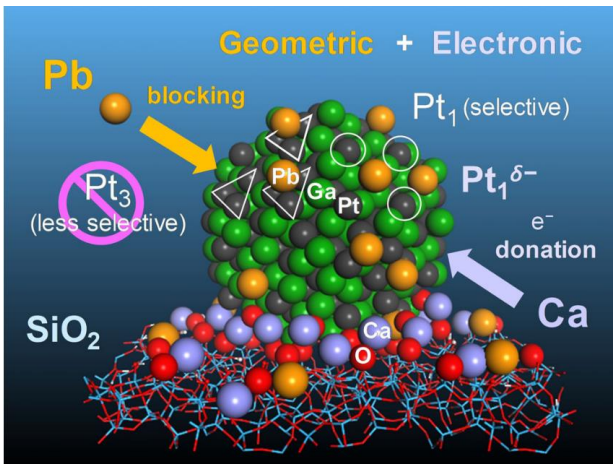

Scheme 5.2. Structure of the double decoration of the PtGa NPs supported on SiO_2 with Pb and Ca cations. Synergistic effects regarding the geometric and electronic effects are expected to enhance the propylene selectivity and the catalyst stability in PDH.[10]

Wasserscheid and co-workers reported a supported catalytically active liquid metal solutions (SCALMS) consisting of PtGa supported catalysts (2wt.% Pt) for PDH between 500 to 600^{o}C (**Scheme 5.3**).[11] They reported a new synthetic procedure by means of ultrasonication. These catalysts differ from previous PtGa compounds because they possess lower melting points and exhibit a liquid metal phase on the support, with dynamic Pt atoms at the surface during the alkane dehydrogenation

reaction. GaPt-SCALMS catalysts were synthesized on various porous supports such as SiO_2, Al_2O_3 and SiC. All the catalysts showed high activity and good selectivity to propylene. The SiC supported catalyst displayed the highest activity in PDH followed by Al_2O_3. However, the SiO_2 catalyst exhibited the highest stability and lowest cracking activity at high temperatures. HRTGA-MS analysis of all spent catalyst confirmed that most of the coke produced was originated from the support.

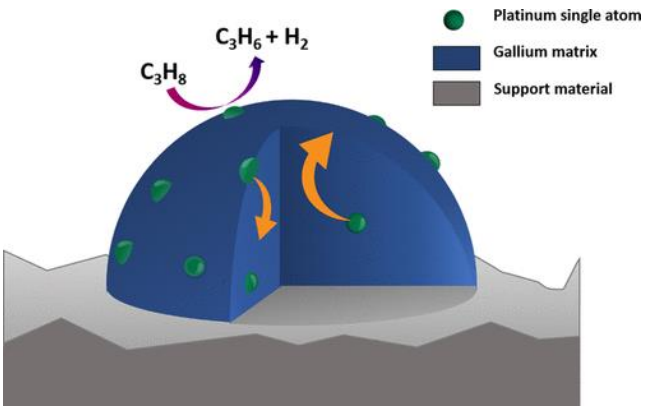

Scheme 5.3. Representation of GaPt-SCALMS catalyst for PDH. Single Pt atoms (green) in the Ga matrix (blue). The arrows indicate that at high temperatures the Pt is moving from the bulk to the surface and back.[11]

PtGa NPs confined in Silicalite-1 (MFI) for PDH reaction were also reported (**Scheme 5.4**). [12] The subsurface was studied for the first time.

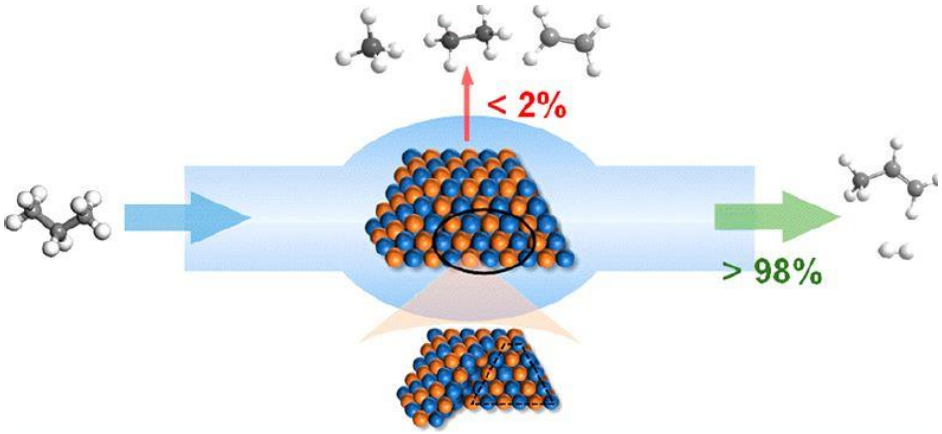

Scheme 5.4. Graphical representation of PtGa subsurface confined on MFI zeolite for high selectivity of propylene in PDH reaction. [12]

Herein, PtGa-NPs with various subsurface compositions was studied by EXAFS and EDS. A PtGa alloy subsurface increased the electron density of surface Pt active site and diminished the desorption energy of propylene, thus increasing the selectivity to propylene from 95% (when there was Pt subsurface) to 98%. The PtGa was encapsulated in MFI zeolite and displayed a strong inhibition of the sintering and coke deposition processes.

NiSn systems

Given the high cost of Pt catalysts, other alternative metals such as Ni have been developed for alkane dehydrogenation.[2] Ni alone is highly active towards C-C hydrogenolysis, and therefore, these systems generally displayed high tendency to the formation of methane and coke. To selectively activate the C-H bond of alkanes, a reported approach consists in the introduction of other elements such as S, P, Cu, Sn and Ga (**Figure 5.5**).[2,13] The geometric effect induced by the introduced elements facilitates the dispersion of Ni particles while the electronic effect was reported to minimize the desorption energy of olefins and hinder the secondary reactions.[13]

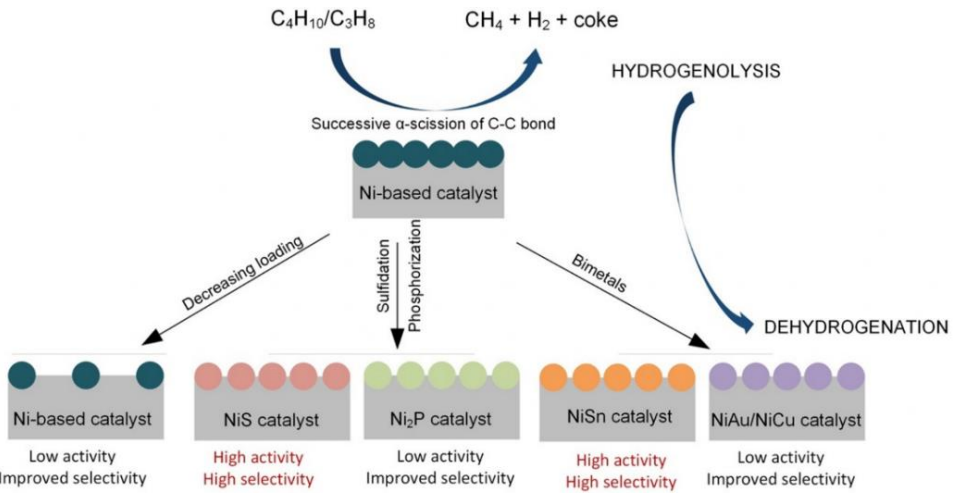

Figure 5.5. Promoting effect of different species (S, P, Sn or Au) in Ni-based catalysts for alkane dehydrogenation reactions.[13]

For instance, Ni phosphide catalysts were explored in alkane dehydrogenation.[13] Phosphorus was introduced using impregnation with ammonium dihydrogen

phosphate and Ni_2P/active carbon (AC) catalyst was prepared.[14] When tested in the dehydrogenation of isobutane, the catalytic performance of Ni_2P/AC revealed to be superior to those displayed by Ni/AC. The characterization results indicated that the improvement of the selectivity could be attributed to the partial positive charges on Ni surface in Ni_2P particles, which minimize the strength of Ni-C bond in carbonium-ion intermediates and therefore inhibit further dehydrogenation. XPS analysis of the Ni 2p binding energies revealed much higher than those reported for Ni (0) and lower than those reported for NiO, suggesting that Ni carried a partial positive charge. Regarding the P 2p band, an electron transfer from Ni to P in Ni_2P was revealed, indicating that P was charged negatively. When Cesium (Cs) was added as a modifier, an improved catalytic performance with a selectivity to isobutene of 93% at 973 K was observed. Such amelioration was attributed to an enhancement of the dispersion of Ni_2P particles due to electron transfer from Cs to Ni, thus decreasing the acid site number and strength. To explain the superior activity of Ni_2P compared to Ni and the enhancing role of Cs, a mechanism was proposed (**Scheme 5.5**).

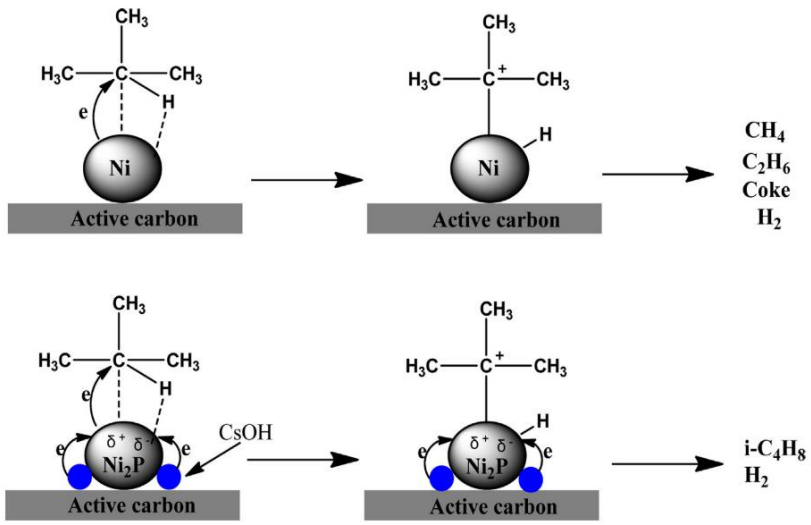

Scheme 5.5. Proposed mechanism for the isobutane dehydrogenation over Ni/AC and Cs-modified Ni_2P/AC catalysts.[14]

The strength of Ni-C bond between the Ni and the carbonium-ion intermediates and the charge type of the Ni surface will determine the path of the reaction either towards the dehydrogenation of isobutane to isobutene or towards the cracking and therefore coke or methane obtention. Regarding the Ni/AC catalyst, the C-C bond of the intermediates can be easily broken because more electrons are available at the Ni surface to attack the C-C bond, leading to side reactions.

The composition of nickel phosphide catalysts affected significatively the alkane dehydrogenation performance.[15] The P addition to Ni/SiO_2 catalyst was studied in the isobutane dehydrogenation. At Ni:P ratio of 1:1, Ni_2P is formed on the surface of the catalyst, exhibiting an optimum performance with an isobutane conversion of 22% and an isobutene selectivity of 81%. An excess of P may generate additional Bronsted acid sites, favouring the undesired cracking reactions. Nevertheless, the Ni-P based catalysts suffer from fast deactivation due to coke formation, because there is a phase transformation from Ni_2P to $Ni_{12}P_5$. For that reason, alkali promoters are generally introduced to these catalysts to increase the selectivity to olefins and prevent coke formation.[16]

Ni/SiO_2 catalysts exhibit high hydrogenolysis activity with high methane selectivity and coke formation. To overcome this issue, Sn was introduced obtaining $NiSn/SiO_2$ (Ni/Sn=1 (mol/mol)) by incipient wetness impregnation for isobutane dehydrogenation (**Scheme 5.6**).[17] XRD, TEM and XPS characterizations indicated that NiSn alloys were formed on the surface of the catalyst and that Sn introduction reduced the size of the NPs from 77 to 16 nm. XPS analysis revealed that upon Sn introduction, the Ni 2p peak shifted, suggesting that an electron transfer occurred from Sn to Ni in the NiSn alloy phase. The Ni/Sn molar ratio was determined to be 1.39, which corresponded with $Ni_{2.67}Sn$ alloy in agreement with the XRD patterns. The Sn role was interpreted as geometric and electronic because Sn helped in dispersing efficiently the Ni aggregates and diminished their size. Moreover, the ability of Ni towards the C-C scission was weakened. Sn provided electrons to Ni, increasing its electronic density, and easing the isobutene desorption from the

catalyst, which was confirmed by DFT calculations. As expected, the $NiSn/SiO_2$ selectivity to isobutene was improved significatively up to a 90% at 600 ^oC. Notably, coke was also remarkably supressed, and an outstanding catalyst stability longer than 120 h was achieved.[17]

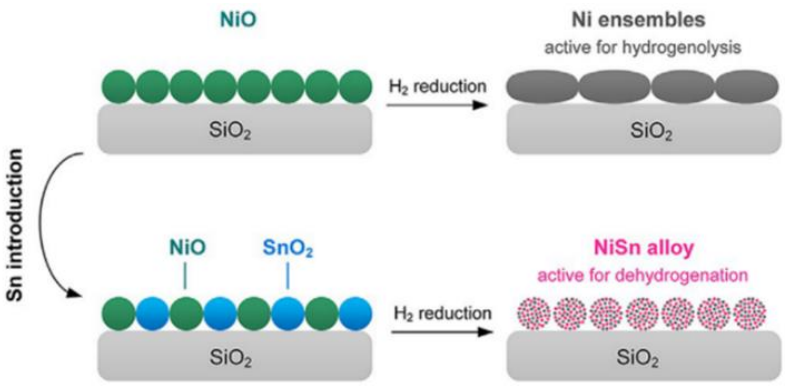

Scheme 5.6. Ni or NiSn catalyst on SiO_2 depending on the active species on the catalyst surface.[17]

Other studies regarding the nature of active tin species and its promoting effect in silica, on $Ni\text{-}SnO_x/SiO_2$ catalyst for dehydrogenation of propane were reported.[18] The nature of the active sites in PDH were studied. Tin oxide was supported on silica using incipient wetness impregnation. Authors found that dispersion played a key role in catalytic activity and stability. Using XRD, XPS, DRUV-Vis and TPR, a new polymeric species "$Si\text{-}O\text{-}Sn^{2+}$" was reported as the active species in the PDH when compared to Sn^{4+} isolated cations and Sn (0). A proposal of the mechanism was reported (**Scheme 5.7**) where the $Si\text{-}O\text{-}Sn^{2+}$ species anchored to silica were the actives sites and their stability and activity was related with the dispersion. The Ni_3Sn_2 alloy played a role of "hydrogen conductor" and not as active component, which was reported to facilitate the regeneration of active sites suppressing the reduction of the active species. Moreover, the introduction of Ni was found to remarkably improve the stability of SnO_2/SiO_2 catalyst, and they postulated that Ni_3Sn_2 alloy fomented the migration and recombination of hydrogen atoms on the

surface of the catalyst, providing a resistance to reduction. It is noteworthy that this catalyst remained active after 160 h of time on stream.

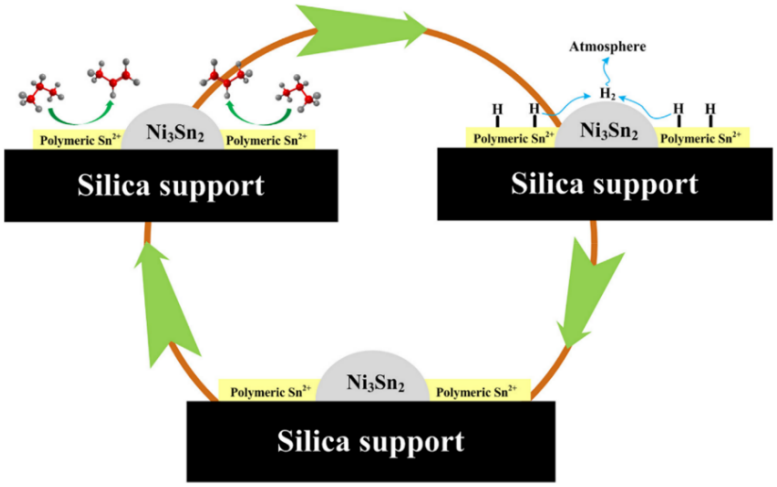

Scheme 5.7. Reaction mechanism proposed over Ni-SnO_x/SiO_2 catalyst in PDH reaction.[18]

Miller and co-workers reported the preparation of single site tetrahedral Ni (II) phosphosilicate using a two-step process consisting in (1) strong electrostatic adsorption of Ni (II) and (2) impregnation of H_3PO_4 solution and thermolysis, as highly stable and selective catalyst in PDH reaction.[19] The tetrahedral structure was verified by XANES. And more characterization by AAS, XAS and IR allowed to see the dispersed tetrahedral Ni (II) species on the surface, which was reported to provide stability in PDH at 600^o C. The presence of Ni(II)-OSi and Ni(II)-OP bonds was reported and the first bonds activated the C-H bonds of propane while the latter prevented Ni (II) from reducing in the reaction conditions.

Several non NiGa-based intermetallic compound catalysts were reported for the dehydrogenation of ethane[20] and propane.[21] A core-shell structure where Ni_3Ga alloy surrounded by a shell with different Ni and Ga compositions was reported. Ni on the surface is believed to conduct the alkane dehydrogenation, whereas the Ga present at the surface sustains the selectivity and catalyst stability. The optimal surface composition is not trivial. The propane conversion decreased, and

propylene selectivity increased when Ni/Ga molar ratio 3:1 to 1:2 (Ni/Ga molar ratio) (**Figure 5.6**).

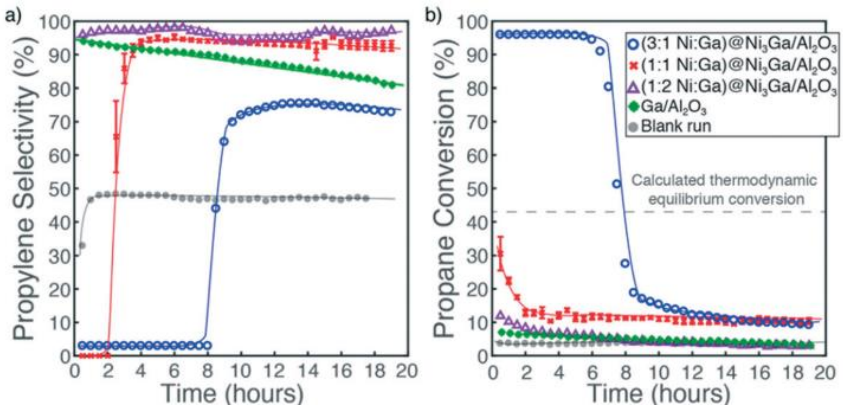

Figure 5.6. Ni_3Ga/Al_2O_3 (with various Ni:Ga loadings) and its (a) Propylene selectivity and (b) Propane conversion of PDH reaction.[21]

DFT calculations revealed that increasing the Ga amount remarkably inhibited the unselective dehydrogenation reactions leading to coke and methane formation. The catalyst with a Ni:Ga ratio (1:1) exhibited the best balance between activity and selectivity in both ethane and propane dehydrogenation reactions.[20,21] For PDH, the 1:1 Ni:Ga@Ni_3Ga/Al_2O_3 exhibited a high selectivity toward propylene (*ca.* 94%) and a moderate propane conversion of *ca.* 13% at 600 ^{o}C using Ar-diluted propane.

5.2 Results and discussion

The present section is organized according to the nature of the metals. Initially, PtGa and NiSn catalysts synthesized by OPOA will be described. Later, the efficiency of the OPOA approach for the preparation of PtSn and PtGa catalysts was evaluated in dehydrogenation processes by comparison with a new approach that combines concepts of the OPOA (i.e., stabilization of Pt-NPs by ligands) and SOMC (i.e., selective introduction of Sn on the Pt-NP surface) to synthesize. In the last part, the catalytic activity of the as-prepared catalysts will be evaluated in the PDH reaction. Selected catalysts will also be evaluated in the butadiene production from butane and 1-butene dehydrogenation.

5.2.1 Synthesis and characterization

5.2.1.1 PtGa OPOA

PtGa supported systems

The bimetallic Pt-Ga catalysts were prepared in a Fisher Porter vessel via the organometallic approach[22], as depicted in **Scheme 5.8**.

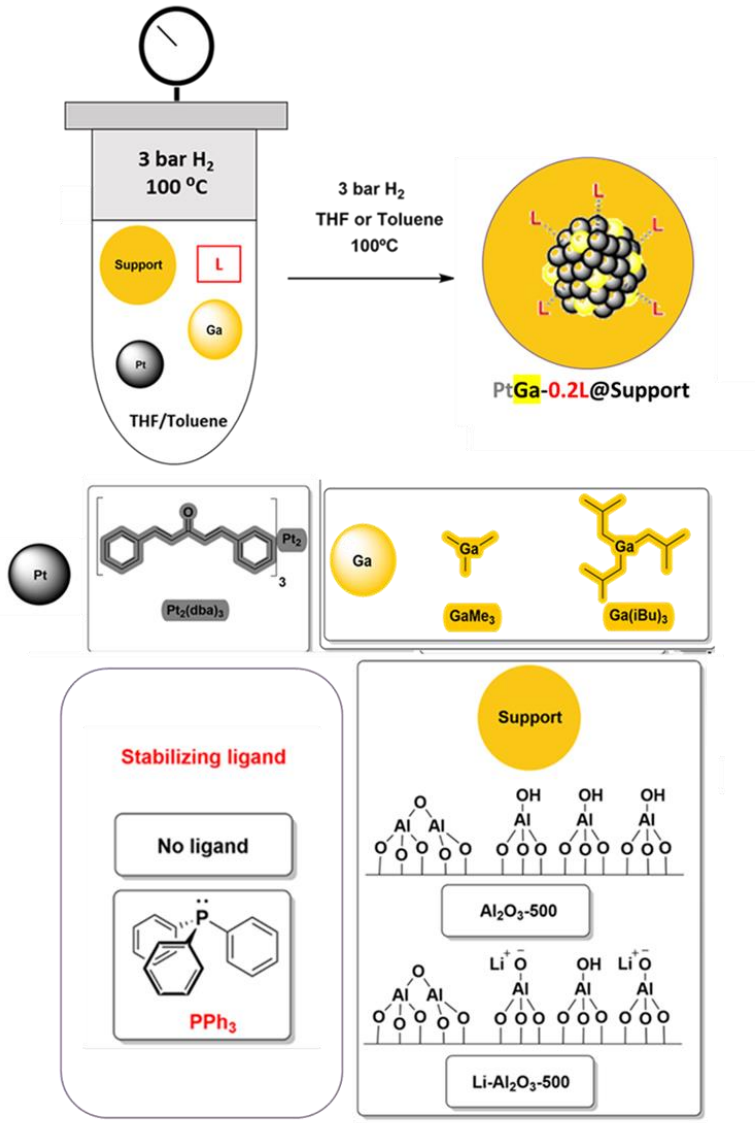

Scheme 5.8. PtGa supported NPs by one-pot organometallic approach.

A nominal value of 2 wt.% Pt was initially used with a Pt/Ga molar ratio of 1. The Pt precursor Pt_2dba_3 and Ga precursor ($GaMe_3$ or $Ga(isobutyl)_3$) were decomposed at 100 ^oC under H_2 atmosphere (3 bar) in the presence of 0.2 equivalent (0.2 mol/mol Pt) of stabilizing ligand (none, PPh_3) using toluene as solvent.

Furthermore, a PtGaSn-PPh_3/Al_2O_3 catalyst has been also prepared by simultaneous decomposition of Sn precursor ($SnBu_4$, 1 mol/mol Pt) and Ga precursor ($GaMe_3$). The synthesis was performed in the presence of the selected alumina support applied in the chapter 3 and 4 (Al_2O_3 or $Li(0.45)Al_2O_3$), and 5 catalysts were produced. Once the supported catalysts were formed, they were washed thoroughly with the reaction solvent and with hexane and dried under reduced pressure. The catalysts were produced in a 1-to-2-gram scale, and isolated as grey-powders in high yields (> 99%).

The formation of the catalysts was first confirmed by TEM and HAADF analysis (**Figure 5.7**). Small and well dispersed NPs were obtained. When $Ga(isobutyl)_3$ was used as the precursor, the NPs size was larger (2.5-4.5 nm) than when $Ga(Me)_3$ was used (1.5-3.1 nm) (**Figure 5.7 a,b**) (entries 1 and 2, **Table 5.1**¡Error! No se encuentra el origen de la referencia.). When PPh_3 was added as stabilizing agent onto Al_2O_3 or $LiAl_2O_3$, using $Ga(Me)_3$, a stabilizing ligand effect resulted in the formation of smaller NPs of 0.9-2.1 nm and 1.2-1.7 nm, respectively (**Figure 5.7c,d**) (entries 3 and 4, **Table 5.1**). The trimetallic PtGaSn catalyst supported onto Li-Al_2O_3 and using PPh_3 as a stabilizing agent (0.2 mol/ mol Pt) resulted in the formation of highly dispersed NPs of 1.3-2.3 nm (entry 5, **Table 5.1**). These particles were slightly larger than those measured for the system PtGa-PPh_3/Li-Al_2O_3 (1.88 ± 0.50 nm) **Figure 5.7 e**).

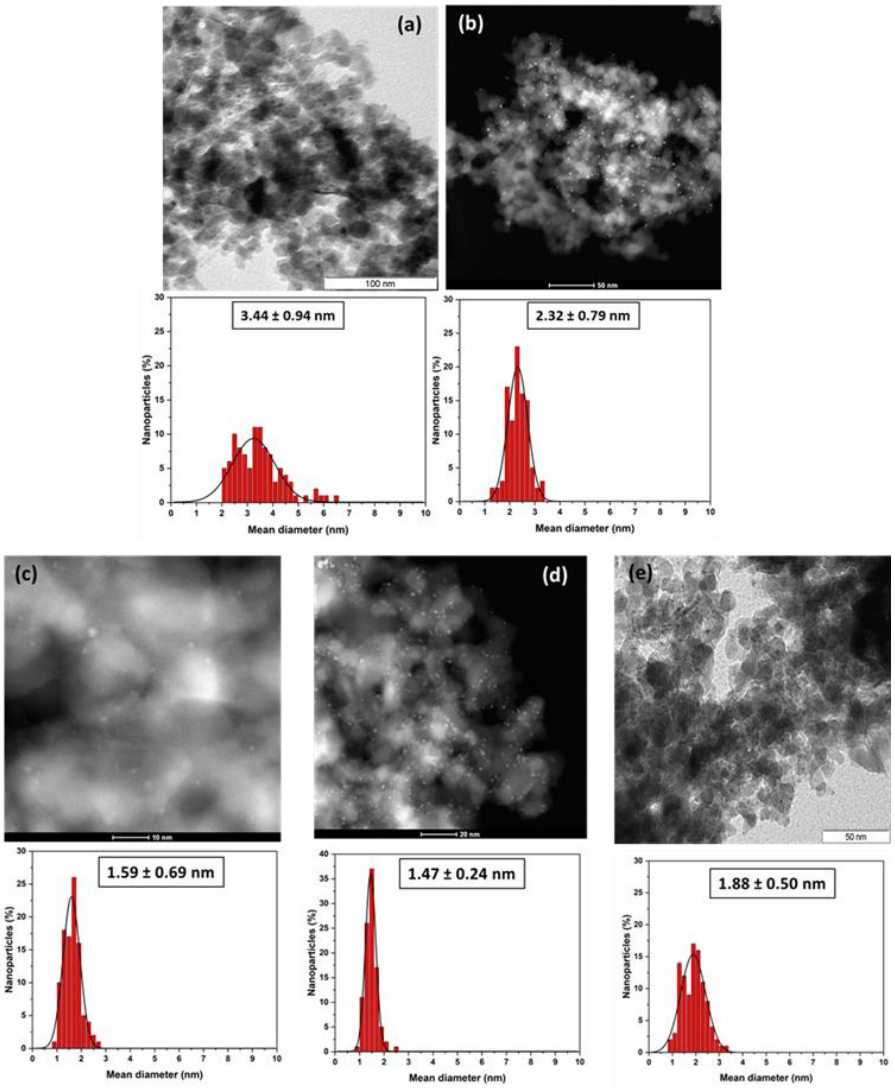

Figure 5.7. TEM or HAADF images and its size distribution histograms of (a)PtGa(isob)@Al_2O_3, (b)PtGa@Al_2O_3, (c) PtGa-PPh_3@Al_2O_3, (d) PtGa-PPh_3@Li(0.45)Al_2O_3, and (e) PtGaSn-PPh_3@Li(0.45)Al_2O_3.

STEM-EDS mappings (**Figure 5.8**) of PtGa@Al_2O_3, PtGa-PPh_3@Al_2O_3 and PtGa-PPh_3@Li(0.45)Al_2O_3 showed the Ga distribution onto both the support and the Pt-NP, while the P (once PPh_3 was added) was mainly detected at the surface of the Pt-NPs.

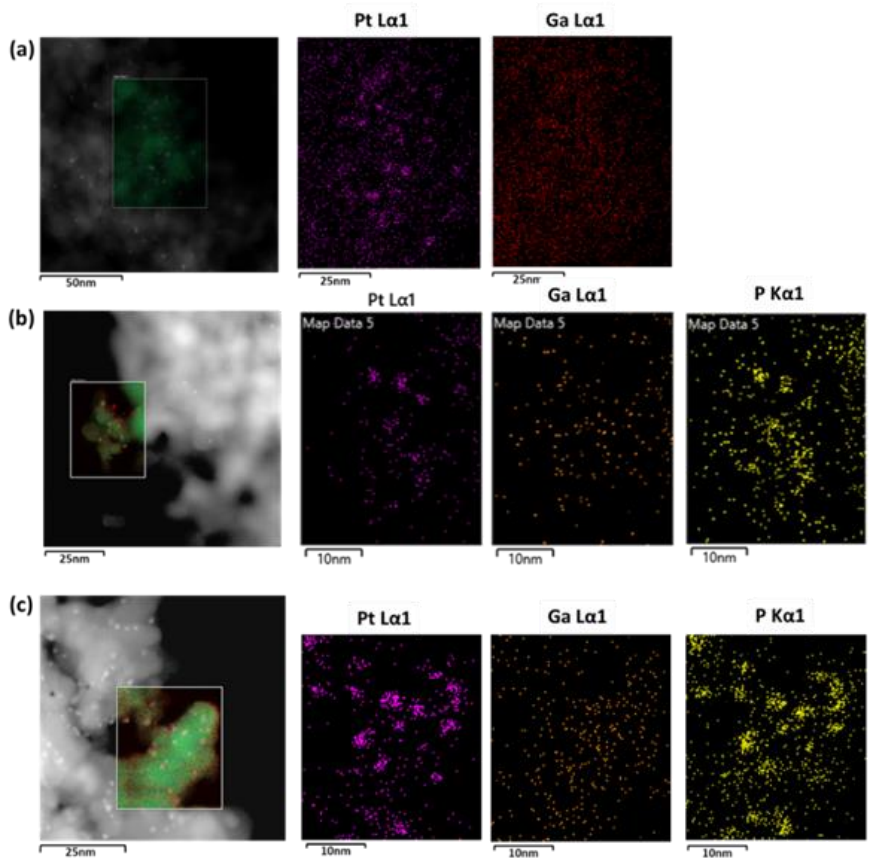

Figure 5.8. STEM-EDS mappings of (a)PtGa@Al_2O_3, (b) PtGa-PPh_3@Al_2O_3 and (c) PtGa-PPh_3@$LiAl_2O_3$.

Table 5.1. PtGa supported catalysts characterization.

Entry	Catalyst	Pt(wt.%)[a]	Ga (wt.%)[a]	Ga/Pt[a] (mol/mol)	NPs size (nm)[b]
1	**PtGa(isob)@Al_2O_3**	0.83	0.27	0.93	3.44 ± 0.94
2	**PtGa@Al_2O_3**	1.48	0.80	1.50	2.32 ± 0.79
3	**PtGa-PPh_3@Al_2O_3**	1.25	0.46	1.05	1.59 ± 0.69
4	**PtGa-PPh_3@$LiAl_2O_3$**	1.49	0.81	1.51	1.47± 0.24

5	**PtGaSn-PPh$_3$@LiAl$_2$O$_3$**	1.31	0.79 [Sn: 0.95]	1.69 [Sn/Pt: 1.20]	1.88 ± 0.50

[a] Quantified by ICP-OES analysis; [b] Obtained through TEM analyses and measuring more than 200 nanoparticles, NP sizes are quoted as the mean diameter ± the standard deviation.

ICP-OES results are summarized in **Table 5.1**. Ga/Pt (mol/mol) ratio varied from 0.9 to 1.7 depending on several factors such as the support, the presence or not of PPh_3 as stabilizing agent, and the gallium precursor. When Ga(isobutyl)$_3$ was used as a precursor, the Ga loading was very low compared with those obtained with the highly reactive Ga(Me)$_3$ (entries 1 and 2). The Ga/Pt was reduced using PPh_3 as stabilizing agent (entries 2 and 3). The effect of the PPh_3 addition observed for the PtGa systems is similar to that observed for the PtSn systems in chapter 4 and could be related with the PPh_3 tuning of the reactivity of the Pt-surface and Al_2O_3-support. Curiously, this effect of the PPh_3 was prevented by the presence of lithium in the support or by the simultaneous decomposition of $SnBu_4$ (entries 2, 3, 4 and 5, **Table 5.1**). The effect of the Li^+ on the support observed for the PtGa systems is different to that observed for the PtSn systems in Chapter 4 and could be related with the distinct reactivity of the gallium and tin precursors with the alumina-based supports.

XRD analysis of the catalysts only revealed the pattern corresponding to the support (Al_2O_3 or Li-Al_2O_3), as previously observed in Chapter 3 and Chapter 4 due to the low metal loading and overlapping of the diffraction peaks of Pt with those of alumina. No other diffraction peaks were observed, suggesting that Pt-NPs and PtGa-NPs are well dispersed onto the surface of the support. This agrees with what Basset and coworkers observed for supported catalysts onto alumina.[23] Later on, the colloidal analogues were analyzed to obtain further information about the crystalline phase and crystallite size.

Using X-Ray Photoelectron Spectroscopy (XPS), the atomic composition and oxidation state of Pt and Ga were assessed. The typical band for Pt is the 4f, with

two peaks at $Pt4f_{5/2}$ and $Pt4f_{7/2}$ described at binding energies of 74.7 eV and 71.53 eV for Pt(0), with potential additional peaks corresponding to other phases of Pt such as Pt(II) and/or Pt(IV).[24] In this Chapter, the Pt 4f band could not be used due to an overlapping with the Al 2p arising from Al_2O_3. Therefore, Pt 4d line that was weaker but not overlapped was used instead.[25] Concerning Ga, the Ga 3p bands used ($Ga3p_{3/2}$ and $Ga3d_{1/2}$).[26] The binding energies used are detailed in **Table 5.2**.

Table 5.2. Deconvolution binding energies used in CASAXPS for Pt and Ga in supported catalysts.

	$Pt4d_{3/2}$	**$Pt4d_{5/2}$**
Pt (0)	314.4-314.7 eV	331.4-331.7 eV
Pt (δ+)	317.7-318.2 eV	334.6-335.2 eV
	$Ga2p_{3/2}$	**$Ga2p_{1/2}$**
Ga (0)	1117.0 eV	1135.9 eV
Ga (δ+)	1119.0 eV	1139.9 eV

XPS analyses of $Pt@Al_2O_3$, $PtGa@Al_2O_3$, $PtGa\text{-}PPh_3@Al_2O_3$, Reduced $PtGa\text{-}PPh_3@Al_2O_3$, $PtGa\text{-}PPh_3@LiAl_2O_3$ and $Pt\text{-}PPh_3@Al_2O_3$ were performed and the results are summarized in **Table 5.3**. All the deconvolutions are showed in **Figure 5.9** and **Figure 5.10**.

Table 5.3. XPS results for PtGa supported catalysts synthesized by OPOA.

Catalyst	**ICP Ga/Pt molar**[a]	**XPS Ga/Pt molar**[b]	**XPS Pt(IV,II)/Pt(0)**	**XPS Ga(δ+) /Ga(0)**
$Pt@Al_2O_3$	-	-	1 / 99	-
$PtGa@Al_2O_3$	1.50	1.10	34 / 66	3 / 97
RED $PtGa@Al_2O_3$	1.50	1.10	0 / 100	58 / 42
$PtGa\text{-}PPh_3@Al_2O_3$	1.05	2.56	35 / 65	0 / 100
$PtGa\text{-}PPh_3@LiAl_2O_3$	1.51	2.00	39 / 61	0 / 100
$Pt\text{-}PPh_3@Al_2O_3$	-	-	1 / 99	-

[a] Quantified by ICP-OES analysis; [b] Quantified by XPS analysis.

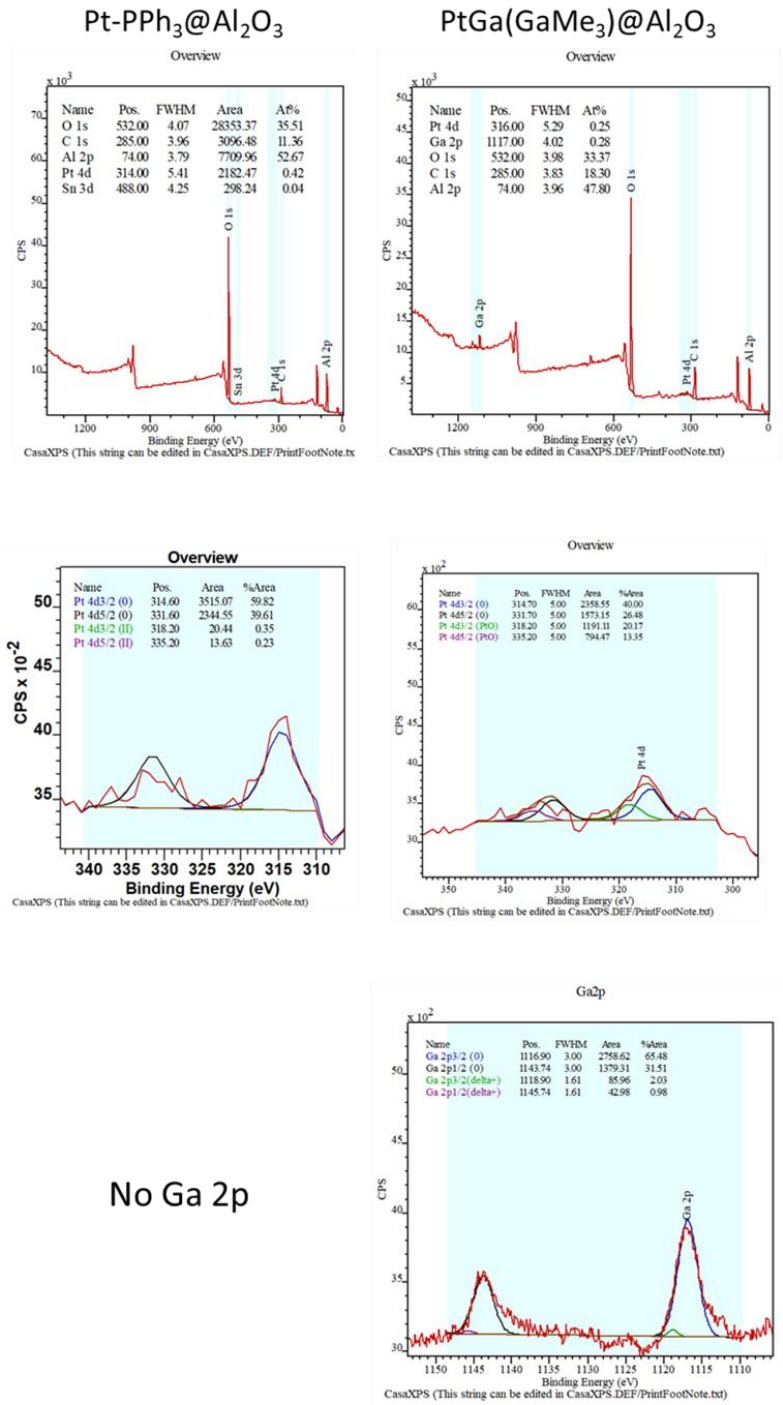

Figure 5.9. XPS deconvolution of Pt-PPh_3@Al_2O_3 and PtGa($GaMe_3$)@Al_2O_3.

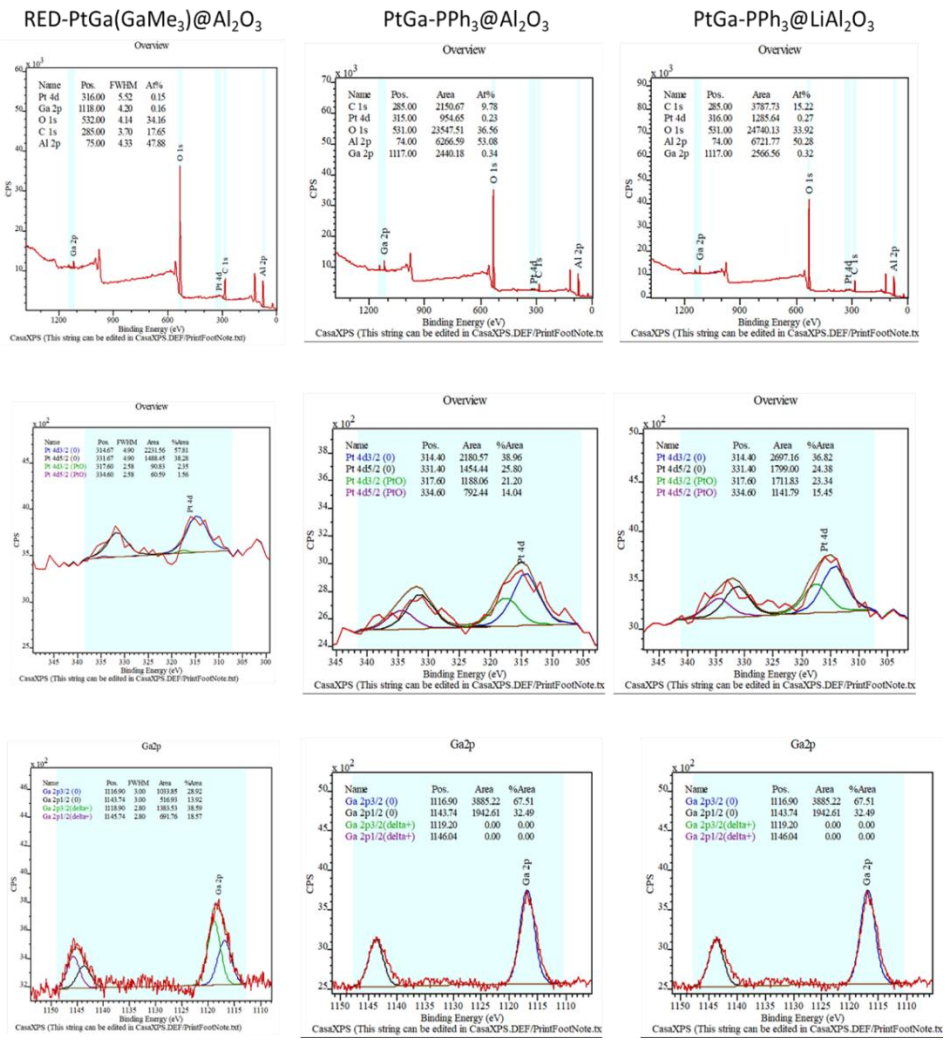

Figure 5.10. XPS deconvolution of RED-PtGa@Al_2O_3, PtGa($GaMe_3$)-PPh_3@Al_2O_3 and PtGa($GaMe_3$)-PPh_3@$LiAl_2O_3$.

Concerning the Pt composition, the monometallic Pt catalyst displayed practically only Pt-atoms in the reduced state (i.e., 99%) whereas the bimetallic PtGa catalyst displayed between 61-66% Pt (0) atoms and 34-39% Pt (IV/II) atoms. When PtGa@Al_2O_3 was reduced, all the Pt composition changed quantitatively to metallic Pt (0). The Pt-PPh_3@Al_2O_3 also showed a composition of 99% of Pt (0). This result may suggest that the Ga addition to the catalyst may result in a more electron deficient Pt-NP surface, required for reducing the alkene sorption strength and favoring its desorption.

Regarding Ga composition in the bimetallic catalyst, the Ga was mainly in the Ga (0) form (between 97-100%), with the rest of the percentage was attributed to Ga (δ+). When the catalyst was reduced, the Ga composition was unexpectedly shifted to oxidative values with a proportion of 58% and 42% for Ga (δ+) and Ga (0), respectively. This behavior can be related to the segregation of the Ga atoms onto the support (Ga (δ+) species formed by partial or full decomposition of the $Ga(alkyl)_3$ precursor and interacting with Al_2O_3 and onto the Pt-particle forming alloys (Ga (0) species present in the PtGa alloy formed by reduction of the $Ga(Alkyl)_3$ precursor. Similar observations were previously reported after thermal treatment and were described in the introduction of this chapter.[5]

However, it cannot be discarded that although all the manipulations were carried out under inert atmosphere, air exposition during sample treatment resulted in the oxidization of Ga (0) species by oxygen to Ga_2O_3. The oxidation of these gallium species agrees with the reported redox potentials for the gallium pairs (E Ga^{3+}/Ga^{2+} and E Ga^{2+}/Ga^{0} of -0.65 and –0.45 V, respectively) respect to the potentials of the oxygen (E O_2/H_2O is + 1.23 V) and proton (E H^+/H_2 is 0.00 V). Therefore, the gallium oxidation is favored in presence of moisture (oxygen and protons).

Interestingly, the Ga/Pt ratios extracted by XPS were smaller than those obtained by ICP-OES when no stabilizing agent was used, independently if the sample was fresh or reduced. However, when PPh_3 was added and independently of the support, the Ga/Pt ratio was almost twice that obtained by ICP, indicating Ga segregation on the surface. This effect was correlated with the ability of PPh_3 to coordinate to Pt-NP surfaces and its implication in the mechanism of formation of the PtGa-alloy by blocking the access of the Ga-precursors to the Pt-surfaces. Another possibility is that the decomposition of the Ga precursor is an indirect effect caused by the tuning of the support acid-basic properties by the ligand PPh_3 itself or the PPh_3 decomposition products (i.e., H_3PO_4).

XPS did not reveal any information about the P (P2p band) probably because the P content was below the detection limit. However, the presence of phosphorus on the surface of the NP was detected by EDX and the characterization of the PtGa colloid model samples described below provided more evidence on the presence of PPh_3 on the Pt-surfaces.

PtGa colloidal systems

To gain more insights into the crystalline phase of the nanoparticles and the interaction of the PPh_3 stabilizing agent with the nanoparticles, the analogous colloidal NPs (PtGa and PtGa-PPh_3) were synthesized and characterized as model samples (**Scheme 5.9**).

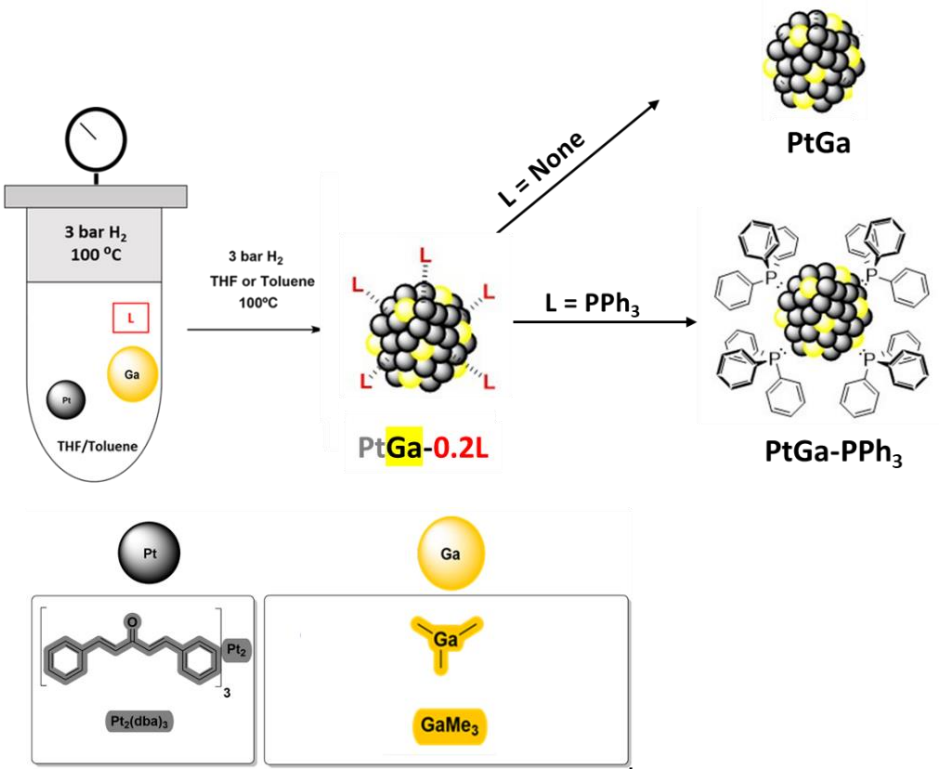

Scheme 5.9. Colloidal PtGa-L capped NPs by organometallic approach.

TEM characterization revealed (**Figure 5.11**¡Error! No se encuentra el origen de la referencia.), as expected, that when PPh_3 was added (PtGa-PPh_3) the NPs were

smaller and better dispersed (1.0-1.8 nm) than without any stabilizing agent (1.8-2.6 nm).

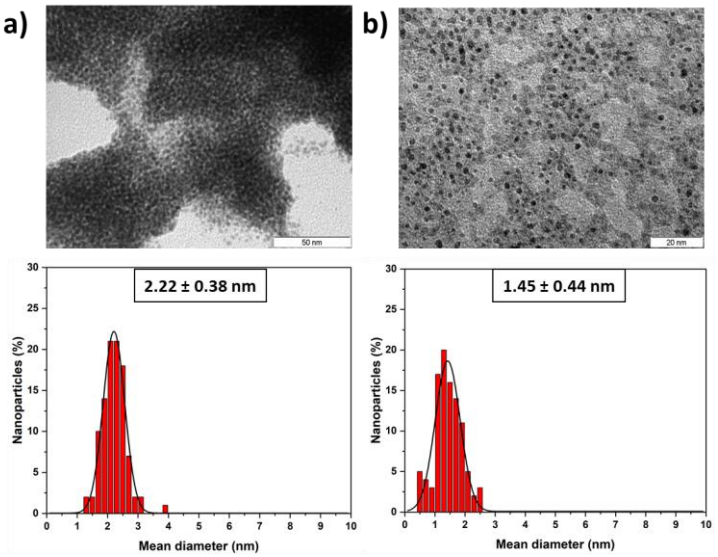

Figure 5.11. TEM images of (a) PtGa-NPs and (b) PtGa-PPh_3 and its size distribution histograms.

The Pt and Ga loadings in these systems were measured by ICP-OES and are listed in **Table 5.4**.

Table 5.4. PtGa colloid NPs characterization.

	Metal loading, wt .%[a]				XRD	
Colloid	Pt	Ga	Ga/Pt[a] (mol)	NPs size (nm)[b]	r.t.	530 1 h
PtGa	56.69	21.02	1.04	2.22 ± 0.38	Pt fcc	Pt fcc < Pt_3Ga Tetragonal
PtGa-PPh_3	47.94	19.34	1.13	1.45 ± 0.44	Pt fcc	Pt fcc > Pt_3Ga Cubic

[a] Quantified by ICP-OES analysis; [b] Obtained through TEM analyses and measuring more than 200 nanoparticles, NP sizes are quoted as the mean diameter ± the standard deviation.

These results confirmed that the Ga/Pt ratio is very similar to the theoretical ones and confirmed the full decomposition of the highly reactive $GaMe_3$ under the reaction conditions.

PtGa and PtGa-PPh_3 were analyzed by XRD at r.t. and at the temperature of catalysis (530 ^oC) under inert atmosphere (N_2) using a BRUKER MTC-HIGHTEMP chamber, to thoroughly characterize the crystalline phase and the mean crystallite sizes of the samples. Our hypothesis was that the ligand (PPh_3) interacted with the surface of the NPs, as observed in Chapter 4 with PtSn colloids. However, it is difficult to know the exact phase contribution since the NPs are very small and resulted in very broad XRD diffraction peaks.

When the PtGa NPs colloids were analyzed at r.t., the only crystalline phase was Pt *fcc* (space group Fm-3m), exhibiting the main peaks at 2θ = 39.7°, 46.2°, 67.4 and 81.2° (ICDD card 01-071-3756) and the crystallite size was *ca.* 0.96 nm. These NPs were also measured by TEM and their size was between 1.8-2.6 nm due to the aggregation of two or three crystallites. At 530 ^oC, the first diffractogram at time zero showed Pt and Pt_3Ga tetragonal alloy (space group I4/mcm) exhibiting the main peaks at 2θ = 32.3°, 40.1°, 46.4° and 68.3 (ICDD card 01-072-2976, ICDD card 00-081-5872) with a relative amount of Pt 24.6wt% and Pt_3Ga 75.4 wt%. The crystallite size was 3.00 nm for Pt phase and 3.05 nm for the alloy Pt_3Ga. After 1 h at 530 ^oC, the diffractograms showed that the relative amounts of the two phases remained practically the same. The crystallite size after 1h at 530 ^oC was 3.34 and 3.51 nm, respectively for the corresponding Pt and Pt_3Ga phases, respectively. In **Figure 5.12** the main XRD diffractograms of PtGa NPs are displayed.

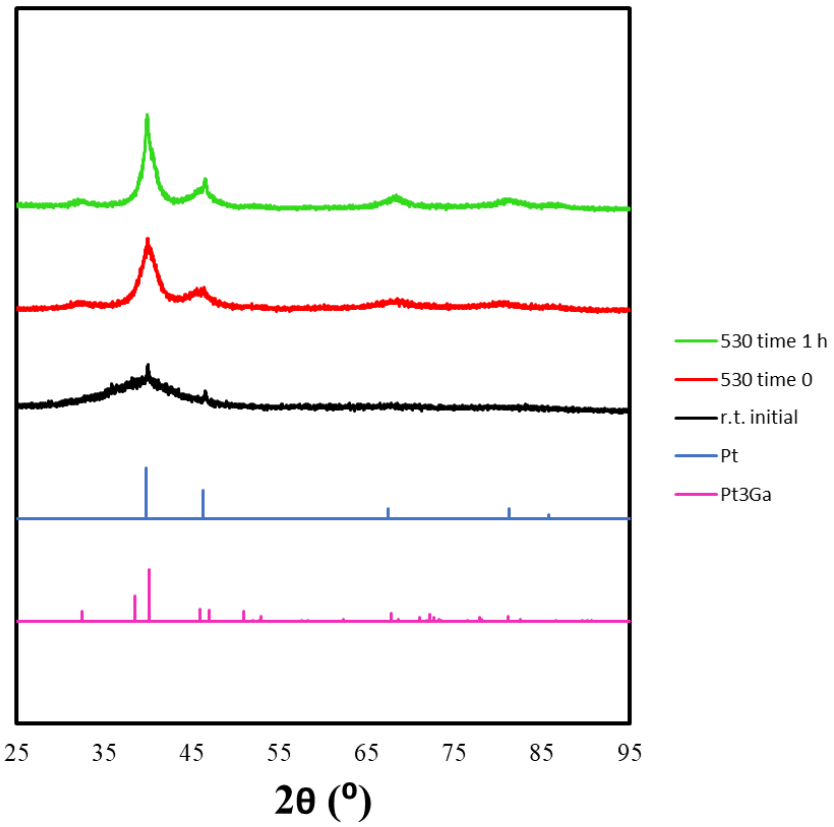

Figure 5.12. XRD diffractograms of PtGa colloidal NPs at r.t. (black), at 530 °C initial time (red) and at 530 °C after 1 h (green). Pt (blue) and Pt_3Ga (pink) crystallographic phases are displayed.

The XRD experiment was also carried out on the colloidal PtGa-PPh_3 sample. At r.t., only Pt *fcc* (100 % wt.) was detected with a crystallite size of 0.90 nm, which is in accordance with the TEM mean size previously measured between 1.0-1.8 nm (particles corresponding to aggregates of one or two crystallites). The first diffractogram at 530 ^{o}C also showed, two different crystalline phases, Pt and Pt_3Ga this time with cubic structure (space group Pm3m) with a wt. % of 75.2 and 24.8% respectively, showing a shift toward the Pt phase in comparison with the colloid without ligand. This effect has been correlated with the ability of PPh_3 to coordinate to Pt-NP surfaces. The crystallite size was 1.93 nm for Pt and 4.53 nm for Pt_3Ga. After 1 h of analysis, the diffractograms showed that the relative amounts of the two phases remained practically the same (70.2% and 28.4% of Pt and Pt_3Ga, respectively). The crystallite size after 1h at 530 ^{o}C was 2.10 and 5.60 nm,

respectively for the correspondent Pt and Pt_3Ga phases. In **Figure 5.13** the main XRD diffractograms of PtGa-PPh_3 are displayed.

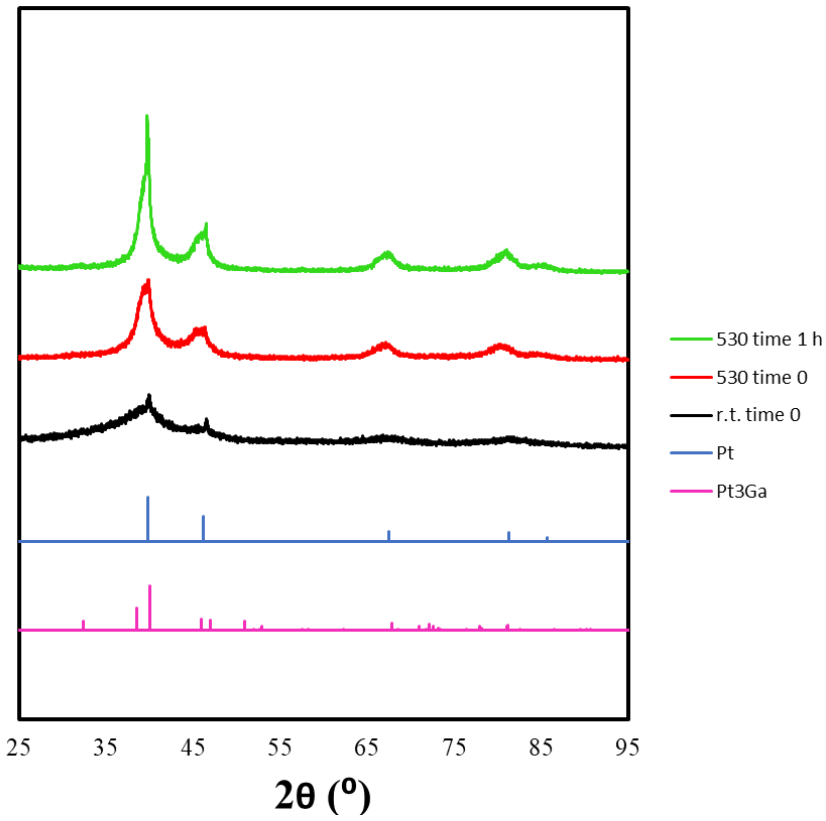

Figure 5.13. XRD diffractograms of PtGa-PPh_3 colloidal NPs at r.t. (black), at 530 °C initial time (red) and at 530 °C after 1 h (green). Pt (blue) and Pt_3Ga (pink) crystallographic phases are displayed.

The main structures observed in the XRD diffractograms were Pt and Pt_3Ga cubic and Pt_3Ga tetragonal **(Figure 5.14)**. All the distribution (in weight percentage) of all the crystalline phases and its crystallite size and cell parameters can be found in the experimental section of the present chapter (**Table S.1-Table S.4**).

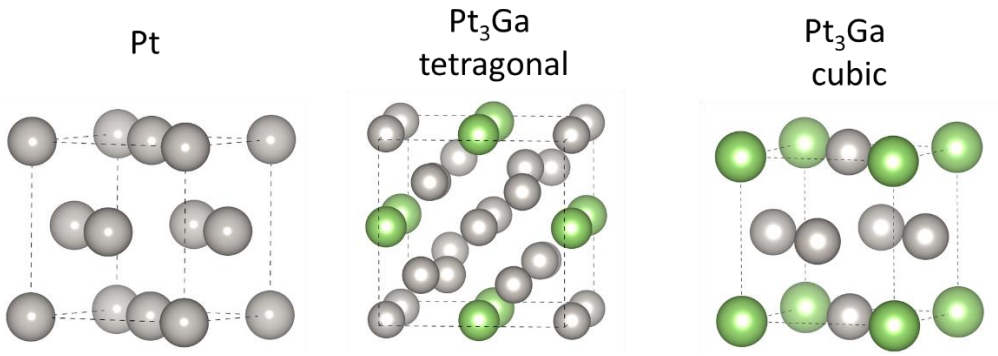

Figure 5.14. Pt, Pt_3Ga tetragonal and Pt_3Ga cubic crystalline 3D structures.

In conclusion, these results strongly indicated a tendency non-reported so far, by which the presence or not of PPh_3 during the PtGa nanoparticle synthesis resulted in similar Ga/Pt molar ratios but with a different crystalline phase behavior, i.e., PtGa-PPh_3 colloidal nanoparticle displayed much higher Pt/PtGa molar ratios than PtGa. This behavior could be ascribed to the PPh_3 coordination and blockage of the Pt-sites avoiding the interaction with the Ga-precursor during the nanoparticle synthesis, thus, reducing the final $PtGa_3$ alloy content.

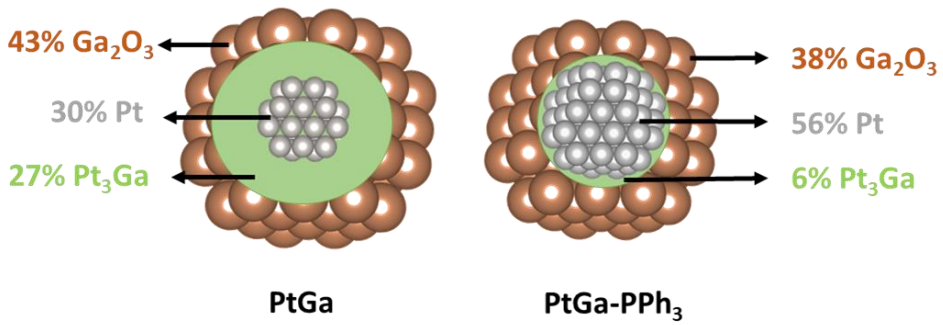

Figure 5.15. Illustration of the PtGa and PtGa-PPh_3 nanoparticles assuming that the rest of the gallium is in the form of gallium oxides.

This tendency can be extrapolated to the supported systems where the catalytic performance could be highly affected by the Pt/$PtGa_3$ molar ratios. It should be highlighted that the rest of the gallium to achieve the Ga/Pt ratio 1/1 measured by ICP-OES should be as thin-layers of gallium oxides at the surface of the particle since

no XRD-diffraction peaks corresponding to gallium phases were recorded and a proposal of the composition is displayed in **Figure 5.15**.

The freshly prepared PtGa-PPh_3 NPs were analyzed by XPS (**Figure 5.16**) to investigate the atomic composition and oxidation state of each element, using Pt 4f, Ga 2p and P2p (**Table 5.5**¡Error! No se encuentra el origen de la referencia.).

Table 5.5. XPS results of PtGa-PPh_3.

	Ga/Pt[a] (mol/mol)	Ga/Pt[b] (mol/mol)	Pt(IV)/Pt(II)/Pt(0)-L/Pt(0)	Ga(δ+)/Ga(0)	$P(III)_{coord}/P(V)/P(III)_{free}$
PtGa-PPh_3	1.13	1.26	5 / 17 / 52 / 26	44 / 56	49 / 0 / 51

[a] Quantified by ICP-OES. [b] Quantified by XPS.

Pt 4f band, could be divided in Pt(IV)/Pt(II)/Pt(0)-ligand/Pt(0), observing 5 / 17 / 52 / 26. The Pt(0)-ligand could be related with the percentage of surface Pt atoms in nanoparticles of this size (1.4 nm) using the Van Hardeveld-Hartog (VHH) model,[27] as explained in Chapter 4. Ns was 75 and Nt was 112 obtaining a Ns/Nt ratio of 0.66. Therefore, it could be estimated that *ca.* 78% of the Pt in the surface could be accessible to the PPh_3 species. Ga components revealed that Ga was in its metallic state forming PtGa alloys (56%), whereas the rest (44%) could be oxidized by accidental air exposition during sample treatment to form Ga_2O_3.

P 2p band could be divided in P(III)-coord./ P(III) free/ P(V), observing 49 / 51 / 0. The value of coordinated PPh_3 (49%) is in agreement with the value obtained for Pt(0)-ligand (52%), thus confirming the preferential interaction of PPh_3 with Pt sites than with Ga sites. Furthermore, compared to the 78% of the Pt surface accessible to the covered by PPh_3, we have measured that PPh_3 covered only 49% of the Pt surface whereas the rest of the PPh_3 remained in a second-coordination sphere interacting with PPh_3-PtGa-NPs. In that case, the Ga/Pt molar ratio obtained by XPS

was 1.26. Comparing with ICP-OES, results indicated Ga segregation on the surface of the NP which could be related with the the presence of Ga_2O_3 on the surface.

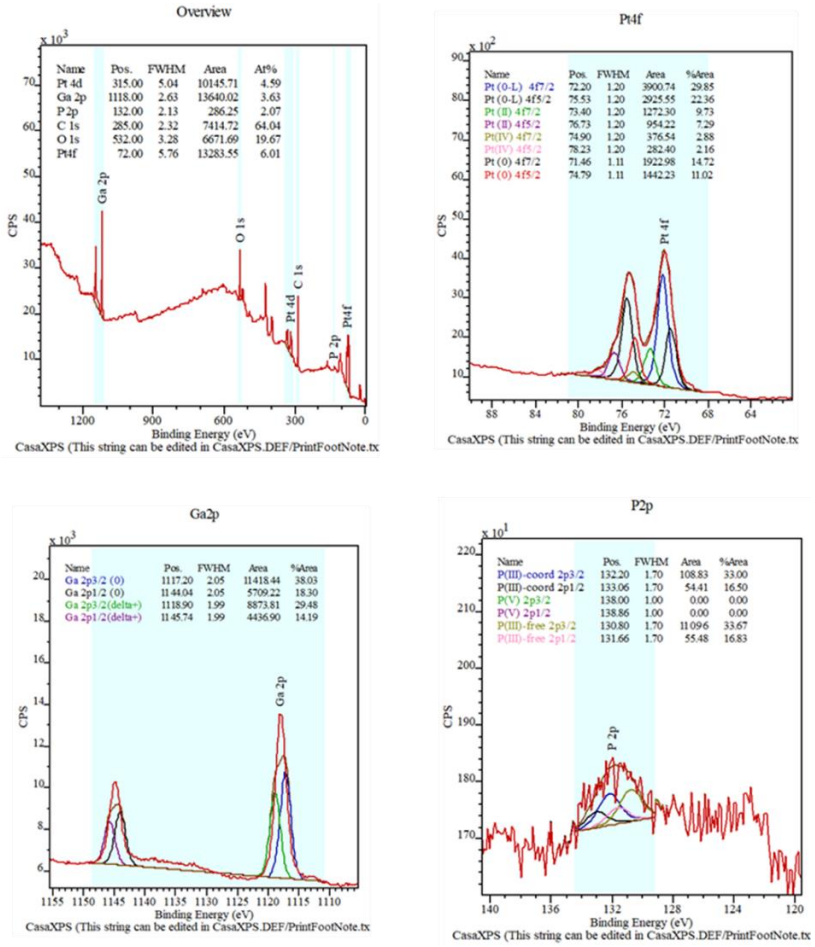

Figure 5.16. XPS deconvolutions of PtGa-PPh_3.

In conclusion, supported PtGa onto alumina (Al_2O_3 and Li-Al_2O_3) and colloidal PtGa samples were prepared by OPOA and characterized by distinct image and spectroscopic techniques. The results revealed the formation of small and well dispersed NPs probably composed by two distinct crystalline phases (Pt_3Ga/Pt) with gallium oxides either on the surface of the NP or on the surface of the support. The presence of PPh_3 ligand on the surface of the NP was evidenced by combination of EDS and XPS experiments.

5.2.1.2 NiSn OPOA

A series of Ni based catalysts were prepared using Al_2O_3 and Li-Al_2O_3 as supports and NHC and PPh_3 as stabilizing ligands. All the catalysts with nominal loadings of 2 wt.% Ni and 3.75 wt.% Sn (Ni/Sn molar ratio 1/1), were produced using $Ni(COD)_2$ and $SnBu_4$ as tin precursor under 3 bar H_2 for 40 h at 100°C (**Scheme 5.10**).

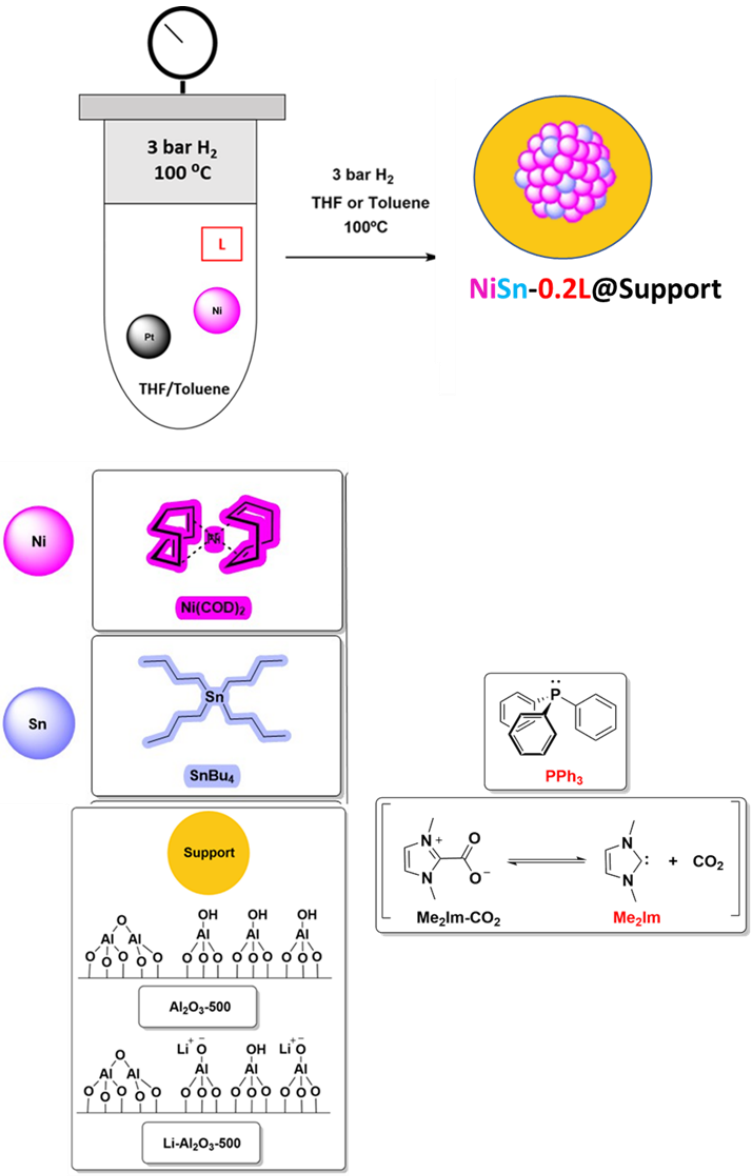

Scheme 5.10. NiSn supported NPs by one-pot organometallic approach.

The mean size of the NPs was measured by HAADF-STEM (**Figure 5.17**). A large difference in NPs sizes was observed depending on the stabilizing agent and the alumina support. The heterocyclic carbene (NHC) did not stabilize the resulting NPs since their mean size was *ca.* 7-12 nm. When PPh_3 was used as a stabilizer, large NPs were obtained only when $LiAl_2O_3$ was used as the support (9-13 nm). In contrast, small and well-dispersed NPs (1.1-1.7 nm) were obtained when Al_2O_3 was used.

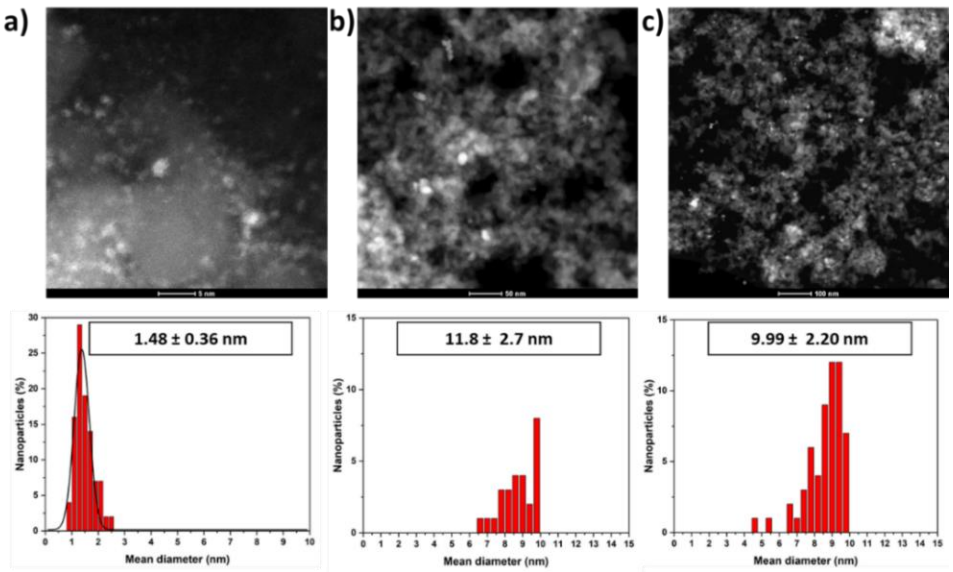

Figure 5.17. HAADF images of (a) NiSn-PPh_3@Al_2O_3, (b) NiSn-PPh_3@$LiAl_2O_3$ and (c) NiSn-NHC@Al_2O_3 and its size distribution histograms.

These three catalysts were characterized by STEM-EDS mapping (**Figure 5.18**). When PPh_3 was used, P was detected especially in the regions of the Ni-NPs but also in the support region, and Sn showed similar distribution. On the other hand, when NHC was used, the N atoms of the carbene were not detected, suggesting that NHC does not stabilize only the Ni-NPs but interacts with the support. Sn was detected on the Ni-NPs. The average weight percentage of the metals found in the surface agreed with values obtained by ICP-OES (**Table 5.6**).

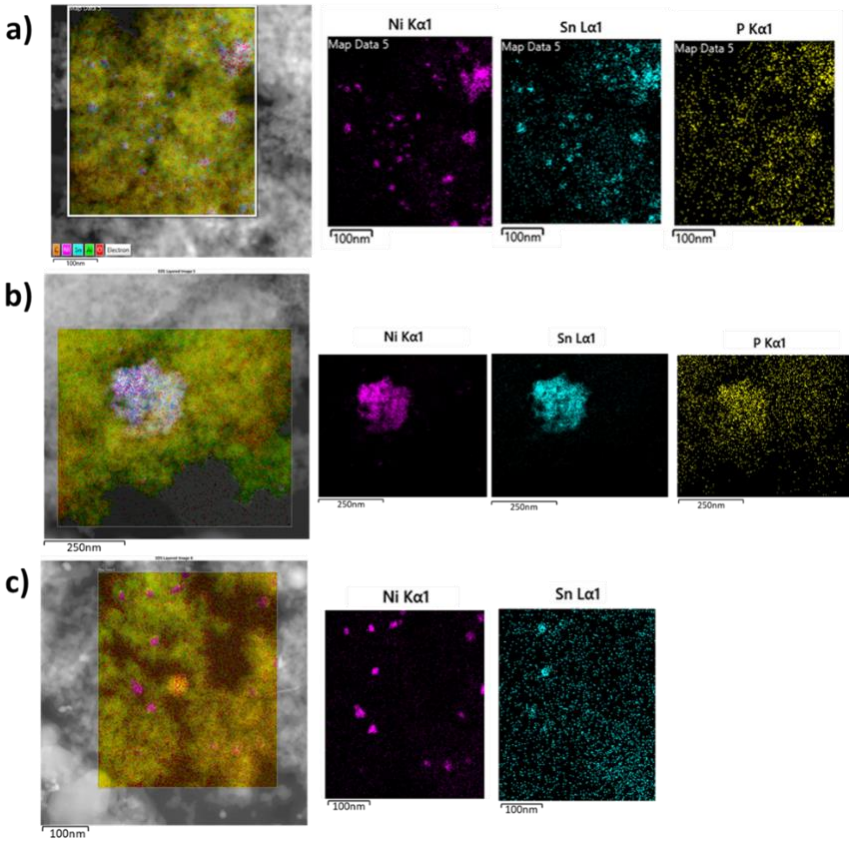

Figure 5.18. STEM-EDS mapping of (a) NiSn-PPh_3@Al_2O_3, (b) NiSn-PPh_3@$LiAl_2O_3$ and (c) NiSn-NHC@Al_2O_3 and its element distribution.

Table 5.6. EDS and ICP-OES metal loadings comparison of NiSn supported catalysts.

	EDS		ICP	
	Average Ni (wt.%)	Average Sn (wt.%)	Ni(wt.%)	Sn(wt.%)
NiSn-PPh_3@Al_2O_3	1.88	1.78	2.15	1.50
NiSn-PPh_3@$LiAl_2O_3$	1.62	1.25	1.96	1.55
NiSn-NHC@Al_2O_3	1.26	0.25	1.87	0.25

XPS analysis was performed to determine the atomic composition and oxidation state of Ni and Sn. The typical reported band for Ni is the 2p, with two peaks at Ni $2p_{5/2}$ and Ni $2p_{3/2}$ described at binding energies of 852.8 and 870.1 eV for Ni(0).[28] For Sn, the 3d bands were used ($Sn3d_{5/2}$ and $Sn3d_{3/2}$).[29] The binding energies and components used are detailed in **Table 5.7**.

Table 5.7. Deconvolution binding energies used in CASAXPS for Ni and Sn in supported catalysts.

	Ni $2p_{5/2}$	**Ni $2p_{3/2}$**
Ni (0)	852.8 eV	870.1 eV
Ni (II/IV)	853.7 eV	871.0 eV
	Sn $3d_{5/2}$	**Sn $3d_{3/2}$**
Sn (0)	485.2 eV	493.9 eV
Sn (II)	486.4 eV	494.8 eV
Sn (IV)	487.2 eV	495.2 eV

Results of XPS measurements for NiSn-PPh_3@Al_2O_3 and NiSn-PPh_3@$LiAl_2O_3$ are listed in **Table 5.8** and the deconvolutions are showed in **Figure 5.19**. The Ni composition was practically the same for both catalysts with the oxidized Ni as main species (67-70%). This indicated that oxidation could have taken place during the measurements.

Regarding Sn, when the Al_2O_3 was used, the Sn was in its most oxidized form Sn (IV) (91%) and only 9% was found in Sn (0). However, when the $LiAl_2O_3$ was used as the support, the Sn components were 55% of Sn (IV), 16 % Sn (II) and 29% Sn (0). This behavior is in agreement with those previously observed in the literature an in this thesis, i.e., the treatment with the lithium salts reduced the content of acidic protons of the alumina support, and then, the catalyst prepared using Li-Al_2O_3 displayed higher proportion of Sn interacting with the Pt forming alloys (Sn(0) species) and lower proportion of Sn interacting with the alumina support (Sn (δ+) species).

Table 5.8. XPS characterization of NiSn-PPh_3@Al_2O_3 and NiSn-PPh_3@$LiAl_2O_3$.

Catalyst	Sn/Ni (mol/mol) [a]	Sn/Ni (mol/mol) [b]	XPS Ni(II,IV)/Ni(0)	XPS Sn(IV)/Sn(II)/Sn(0)
NiSn-PPh_3@Al_2O_3	0.34	0.24	70 / 30	91 / 0 / 9
NiSn-PPh_3@$LiAl_2O_3$	0.39	0.53	67 / 33	55 / 16 / 29

[a] Quantified by ICP-OES. [b] Quantified by XPS.

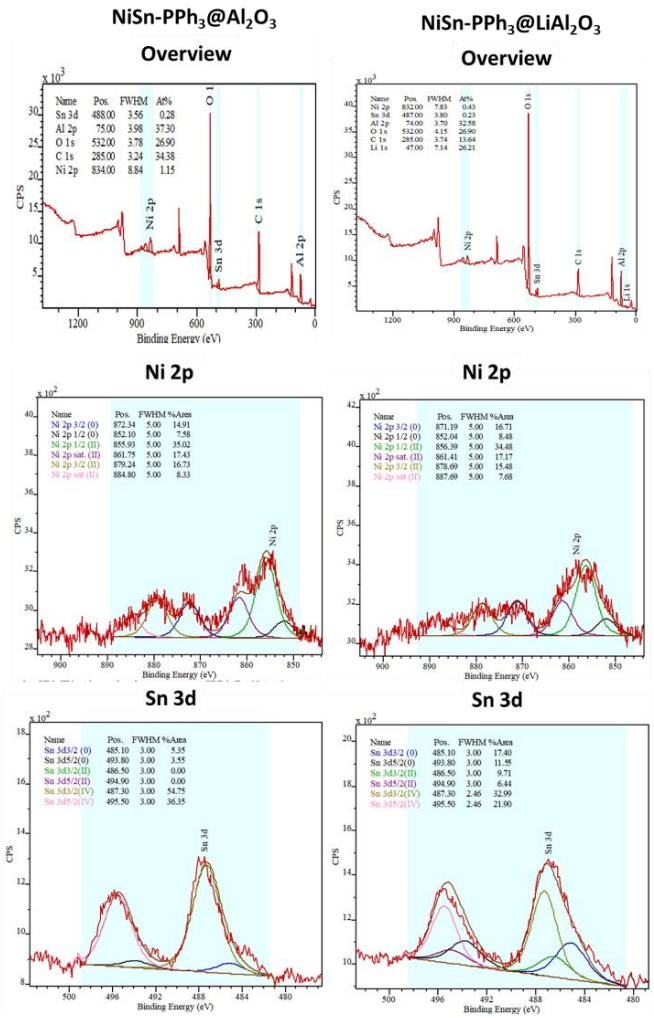

Figure 5.19. XPS deconvolutions of NiSn-PPh_3@Al_2O_3 and NiSn-PPh_3@$LiAl_2O_3$.

XPS measurements did not reveal any information about the P (P2p band) probably because the P content is below the detection limit. However, the presence of

phosphorus on the surface of the NPs was previously evidenced by EDS (as mentioned above). Attempts to prepare NiSn colloidal model samples to obtain further evidence on the whereabouts of PPh_3 on the Ni-surfaces resulted in very low yields, hampering their characterization.

In conclusion, supported NiSn onto aluminas (Al_2O_3 and Li-Al_2O_3) were prepared by OPOA and characterized by microscopic and spectroscopic techniques. The results revealed the formation of medium to large NPs probably composed by two distinct crystalline phases (NiSn/Ni). The rest of the tin to attain the composition determined by ICP is present as tin oxides either on the surface of the NP or on the surface of the support. The presence of PPh_3 ligand on the surface of the NP has been observed by EDS mapping and suggested the presence of PPh_3 during the NiSn nanoparticle synthesis controlled the NP mean diameter and Sn/Ni molar ratios. This behavior could be ascribed to the PPh_3 interaction with the Ni-sites an alumina-acid-sites which has an effect in the Sn-precursor decomposition during the nanoparticle synthesis.).

5.2.1.3 Mixed approach SOMC-OPOA

5.2.1.3.1 PtGa SOMC-OPOA

Bimetallic PtGa NPs were also prepared by a mixed approach consisting in preparing (1) supported Pt-NPs by the one-pot organometallic approach (OPOA) and (2) selective deposition of Ga(isobutyl)$_3$, onto the supported Pt-NPs, using the SOMC approach (**Scheme 5.11**).

Initially, the monometallic Pt supported NPs were synthesized with a 2 wt.% Pt (theoretical nominal value), with or without 0.2 equivalents of PPh_3 (0.2 mol PPh_3/ mol Pt). The catalysts were synthesized using Li(0.45)Al_2O_3 as the support. First, the monometallic catalysts were prepared: Pt@LiAl_2O_3 and Pt-PPh_3@LiAl_2O_3. After a reduction step with pure H_2 at 500^o C overnight to generate the Pt-hydride species on the NP surfaces, the SOMC technique was applied for the selective deposition

of Ga on the hydride covered Pt-NPs. A theoretical molar ratio of Ga/Pt (mol/mol) of 0.7 was targeted. Next, the mixture was left overnight at 80 °C with 500 mbar of H_2 for the hydrogenolysis of the grafted organometallic species and formation of PtGa catalysts: $PtGa^{SOMC}$@$LiAl_2O_3$ and $PtGa^{SOMC}$-PPh_3@$LiAl_2O_3$.

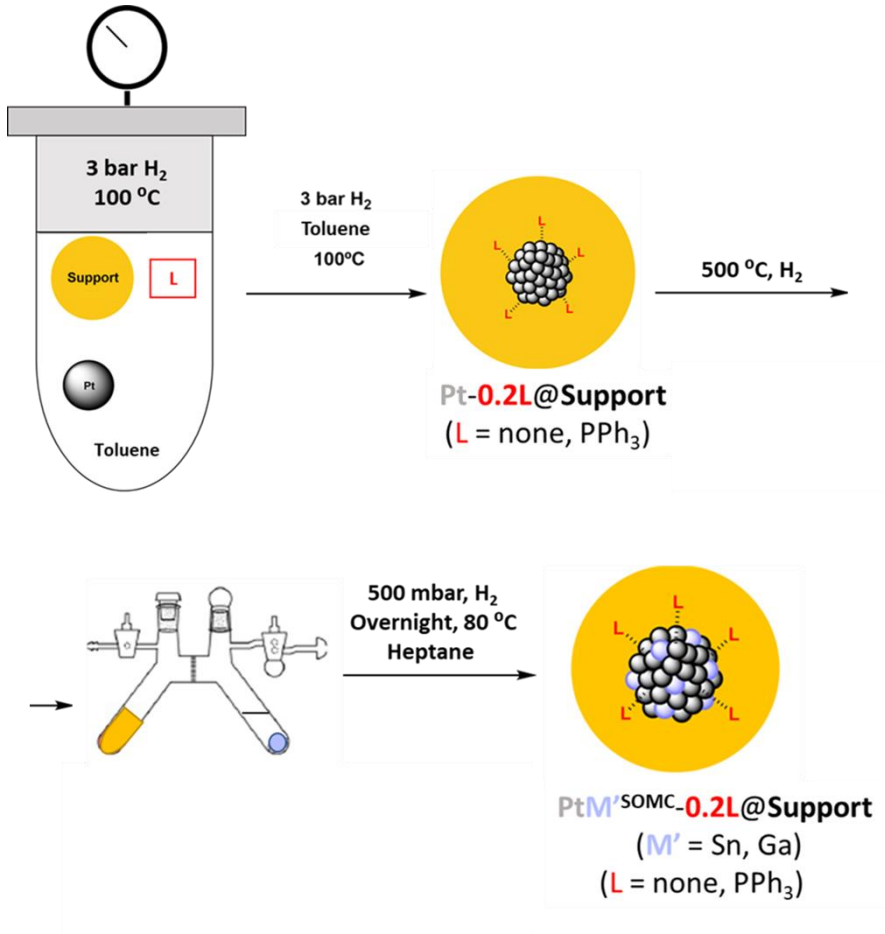

Scheme 5.11. Mixed approach using OPOA-SOMC to obtain PtM'^{SOMC}-L@Support, where M' = Sn, Ga; L = none, PPh_3 and Support = Li-Al_2O_3.

The mean size NPs were measured by TEM or HAADF (**Figure 5.20**). The presence of the PPh_3 resulted in smaller NPs (1.8-2.5 nm) than without ligand (3.0-4.7 nm). When the catalysts were reduced under pure H_2 at 550° C, both samples increased in size, although the growth was less evident for the catalysts bearing PPh_3.

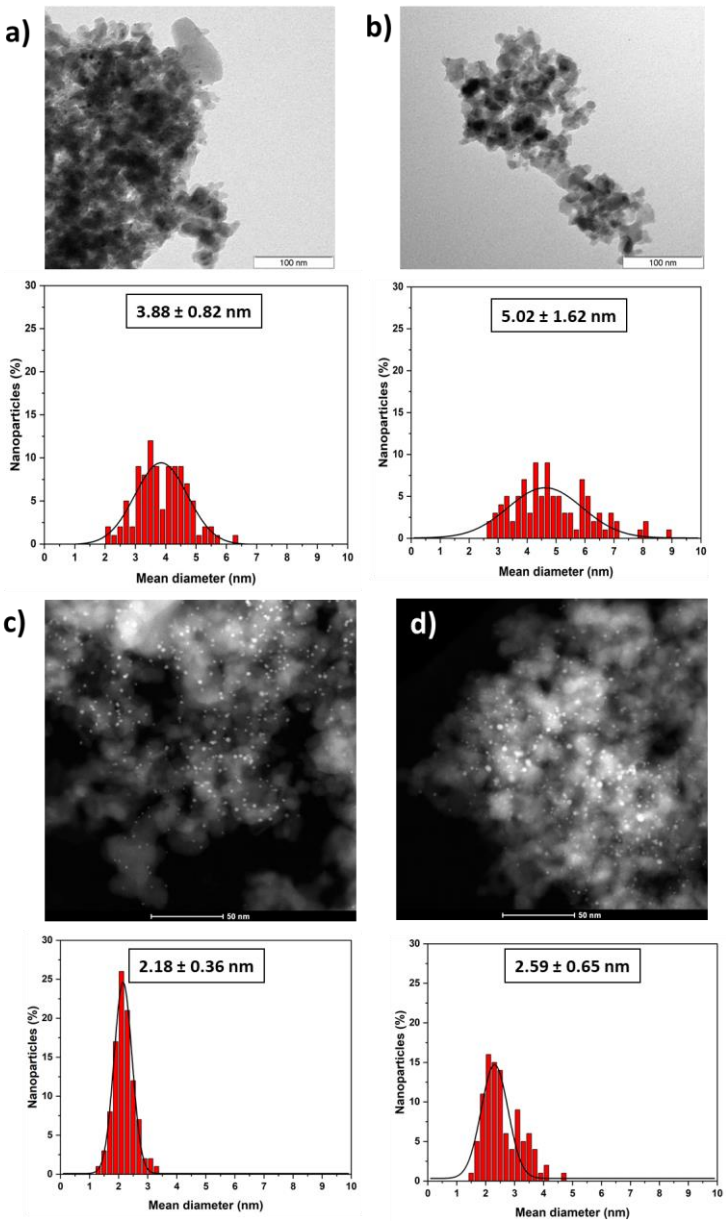

Figure 5.20. TEM images of (a) $PtGa^{SOMC}@LiAl_2O_3$ and (b) Reduced $PtGa^{SOMC}@LiAl_2O_3$ and its size distribution histograms. HAADF images of (c) $PtGa^{SOMC}$-$PPh_3@LiAl_2O_3$ and (d) Reduced $PtGa^{SOMC}$-$PPh_3@LiAl_2O_3$ and its size distribution histograms.

ICP-OES analyses revealed a lower Pt content than the theoretical value (1.3-1.4 wt.% Pt). Regarding Ga, a higher content was measured in the absence of PPh_3 (**Table 5.9**). This behavior suggests, as mentioned above, that the PPh_3 coordinated

to the Pt-surface blocks the access of the Ga atoms thus resulting in lower Pt_3Ga alloy formation.

Table 5.9. Catalyst characterization of PtGa supported catalysts synthesized by OPOA-SOMC.

Catalyst	Pt [a] (wt.%)	Ga [a] (wt.%)	Ga/Pt [a] (mol)	NPs size (nm) [b]
$PtGa^{SOMC}@Li(0.45)Al_2O_3$	1.41	2.92	5.82	3.88 ± 0.82
RED $PtGa^{SOMC}@Li(0.45)Al_2O_3$	1.41	2.92	5.82	5.02 ± 1.62
$PtGa^{SOMC}$-$PPh_3@Li(0.45)Al_2O_3$	1.30	1.09	2.33	2.18 ± 0.36
Red $PtGa^{SOMC}$-$PPh_3@Li(0.45)Al_2O_3$	1.30	1.09	2.33	2.59 ± 0.65

[a] Quantified by ICP-OES analysis; [b] Obtained through TEM analyses and measuring more than 200 nanoparticles, NP sizes are quoted as the mean diameter ± the standard deviation.

STEM-EDS mappings of $PtGa^{SOMC}$-$PPh_3@Al_2O_3$ and reduced-$PtGa^{SOMC}$-$PPh_3@Al_2O_3$ (**Figure 5.21**) showed the selective Ga distribution onto the Pt-NPs using the SOMC approach. Compared to the organometallic approach, the SOMC approach is more selective, grafting the Ga atoms onto the NP surface rather than on the alumina-based support.

XRD analysis revealed that all catalysts exhibit main diffraction peaks at 2θ = 37°, 45.9° and 66.9°, corresponding to the bare support γ-Al_2O_3 phase. This suggested that the structure of the support remains unaltered and that the PtGa NPs are small and well dispersed, in agreement with HAADF-STEM observations and previous reports.[30,31,32]

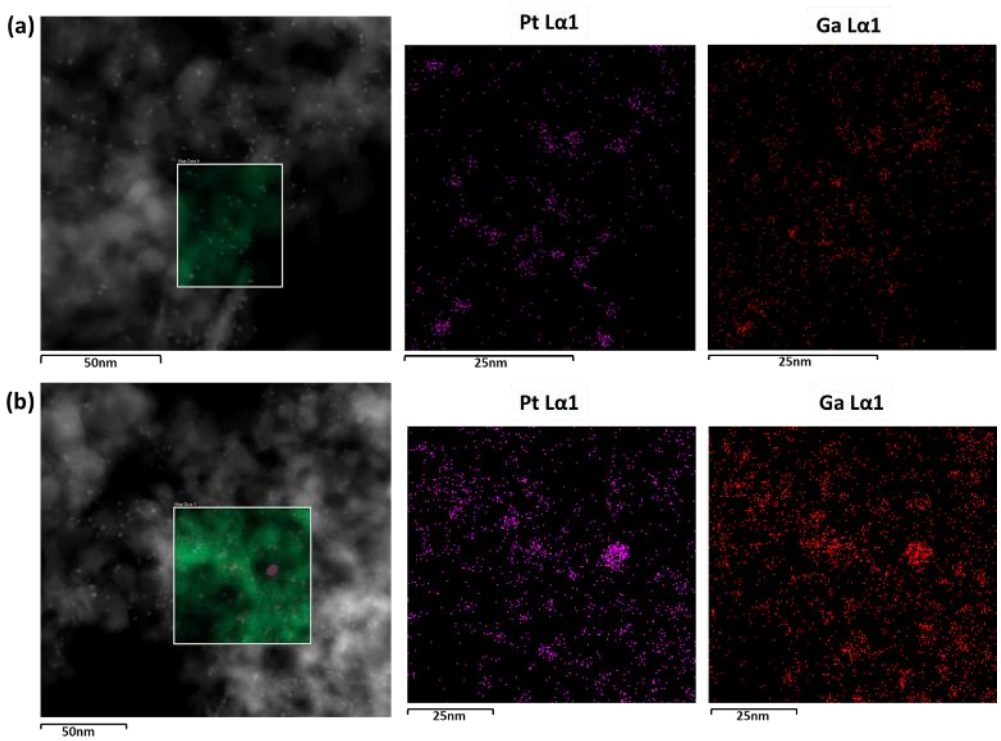

Figure 5.21. STEM-EDS mappings of (a)PtGa^{SOMC}-PPh$_3$@Al$_2$O$_3$ and (b) reduced PtGa^{SOMC}-PPh$_3$@Al$_2$O$_3$.

XPS measurements of fresh and reduced PtGa-PPh$_3$@Li(0.45)Al$_2$O$_3$ catalysts were performed and results are listed in **Table 5.10¡Error! No se encuentra el origen de la referencia.**, and the deconvolutions displayed in **¡Error! No se encuentra el origen de la referencia.**.

Table 5.10. XPS results for PtGa-PPh$_3$@LiAl$_2$O$_3$ fresh and reduced catalysts.

		XPS		
Catalyst	Ga/Pt[a] (mol)	Ga/Pt[b] (mol)	Pt(IV,II)/Pt(0)	Ga(δ+) /Ga(0)
PtGa-PPh$_3$@Li(0.45)Al$_2$O$_3$	2.33	3.4	12 / 88	0 / 100
Red PtGa-PPh$_3$@Li(0.45)Al$_2$O$_3$	2.33	7.3	17 / 83	37 / 63

[a] Quantified by ICP-OES analysis; [b] Quantified by XPS analysis.

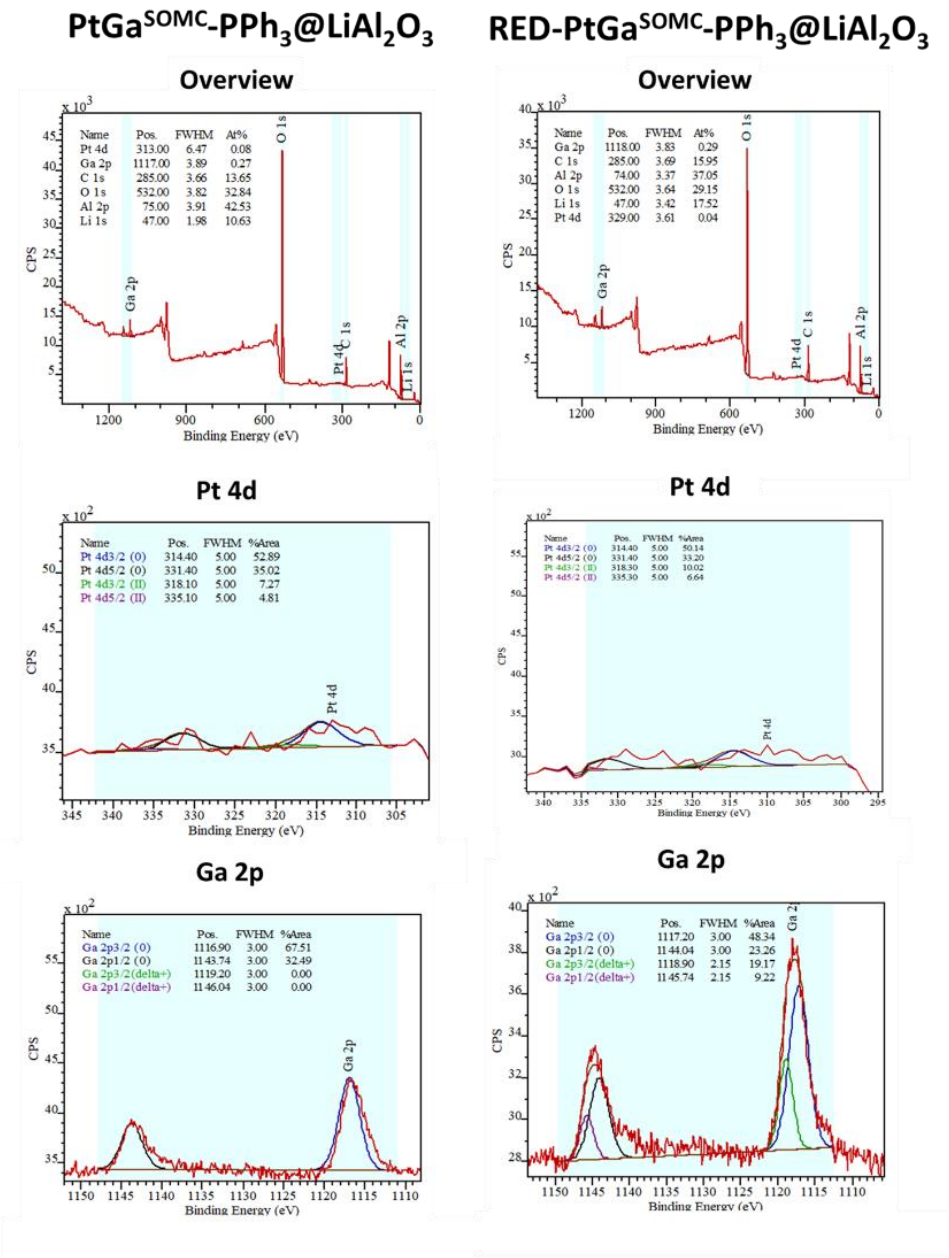

Figure 5.22. XPS values of PtGa-PPh_3@Li(0.45)Al_2O_3 fresh and reduced catalysts.

Concerning the Pt composition, the Pt (0) relative amount is almost the same in the reduced sample, thus suggesting that either these PtGa species required harsh conditions for their reduction or that the gallium incorporation in the PtGa alloy makes the Pt more electron-deficient (higher BE).

Regarding Ga composition, the behavior previously described for the PtGa catalyst prepared by OPOA was again observed, but more drastically since the thermal treatment under hydrogen flow resulted in the evolution of the fully reduced Ga species (100% Ga (0) component) to a mixture of two gallium species in a ratio (63% Ga (0) and 37 % Ga (0) for the reduced catalyst). Ga (0) was in its metallic state forming PtGa alloys (63%), whereas the rest (37%) could be oxidized by oxygen to Ga_2O_3 during sample treatment. The oxidation of these gallium species is in agreement with the reported redox potentials for the gallium pairs (E Ga^{3+}/Ga^{2+} and E Ga^{2+}/Ga^{0} of -0.65 and –0.45 V, respectively) respect to the potentials of the oxygen (E O_2/H_2O is + 1.23 V) and proton (E H^+/H_2 is 0 V), and so, the gallium oxidation is favored in presence of moisture (oxygen and protons).

No signals coming from P 2p orbitals either from PPh_3 or any other P species resulting from the thermal treatment at 500 ^oC carried out for the generation of the hydrides-Pt before the reaction with the gallium precursor by the SOMC approach.

Concerning the Ga/Pt (mol/mol) ratio calculated by XPS, it was much higher than that of ICP-OES, therefore indicating Ga segregation at the surface of the catalyst.

In conclusion, supported PtGa catalysts onto Li-Al_2O_3 were prepared by a combination of the approaches, i.e., preparation of supported Pt-NPs stabilized by PPh_3 using OPOA and selective surface modification of the Pt-NPs SOMC by Ga. These catalysts were characterized by microscopic and spectroscopic techniques. The results revealed the formation of small and well dispersed NPs probably composed by two distinct crystalline phases (Pt_3Ga/Pt) with some amounts of gallium oxides on the surface of the NP or on the surface of the support. In contrast to the other samples, the PPh_3 ligand has been removed during the thermal treatment for the preparation of the Pt-hydrides.

5.2.1.3.1 PtSn SOMC-OPOA

The PtSn supported catalysts were synthesized via the mixed OPOA-SOMC approach. The catalysts with a Pt theoretical nominal value of 2% wt. were synthesized using Al_2O_3 as the support and, with and without PPh_3 as stabilizing agent. First, the monometallic catalysts $Pt@Al_2O_3$ and $Pt\text{-}PPh_3@Al_2O_3$ were prepared via OPOA. Next, these materials were isolated and thermal treatments at 500^o C under hydrogen flow were carried out to generate the Pt-H species. Later, the SOMC approach was applied for the selective deposition of Sn using $SnBu_4$ as promoter. A theoretical ratio of Sn/Pt (mol/mol) of 0.7 was targeted. The mixture was left at 80 ^{o}C overnight with 500 mbar of H_2 for the hydrogenolysis of the grafted organometallic species and formation of PtSn catalysts: $PtSn^{SOMC}@Al_2O_3$ and $PtSn^{SOMC}\text{-}PPh_3@Al_2O_3$. A scheme of the procedure followed to prepare $PtSn^{SOMC}\text{-}PPh_3@Al_2O_3$ is showed in **Figure 5.23**.

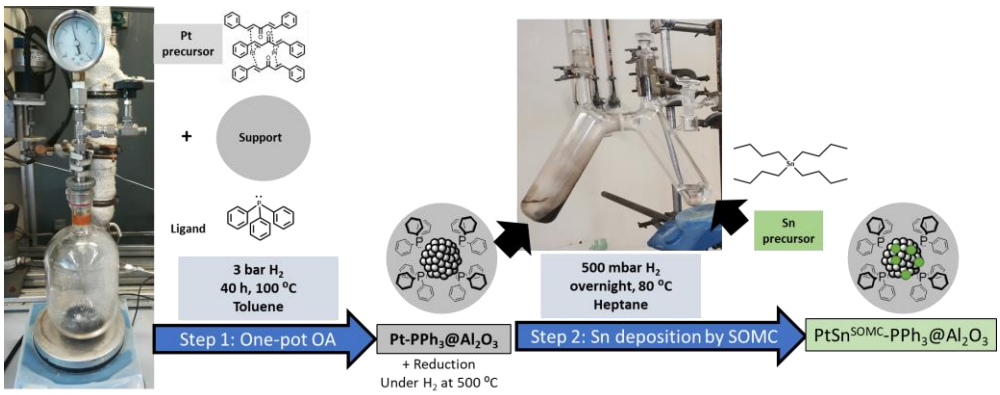

Figure 5.23. Preparation of $PtSn^{SOMC}\text{-}PPh_3@Al_2O_3$ using the OPOA-SOMC mixed approach. First, $Pt\text{-}PPh_3@Al_2O_3$ using OPOA approach were prepared. After a reduction step, the Sn was grafted using SOMC/M approach using $SnBu_4$ precursor followed by a reduction with H_2.

The mean size NPs were measured by TEM or HAADF (**Figure 5.24**). The presence of the PPh_3 resulted in smaller NPs (1.5-1.7 nm) than without ligand (2.0-3.0 nm). When the catalysts were reduced under pure H_2 at 550^o C, both samples increased in size, however the growth was less evident for the catalysts bearing PPh_3.

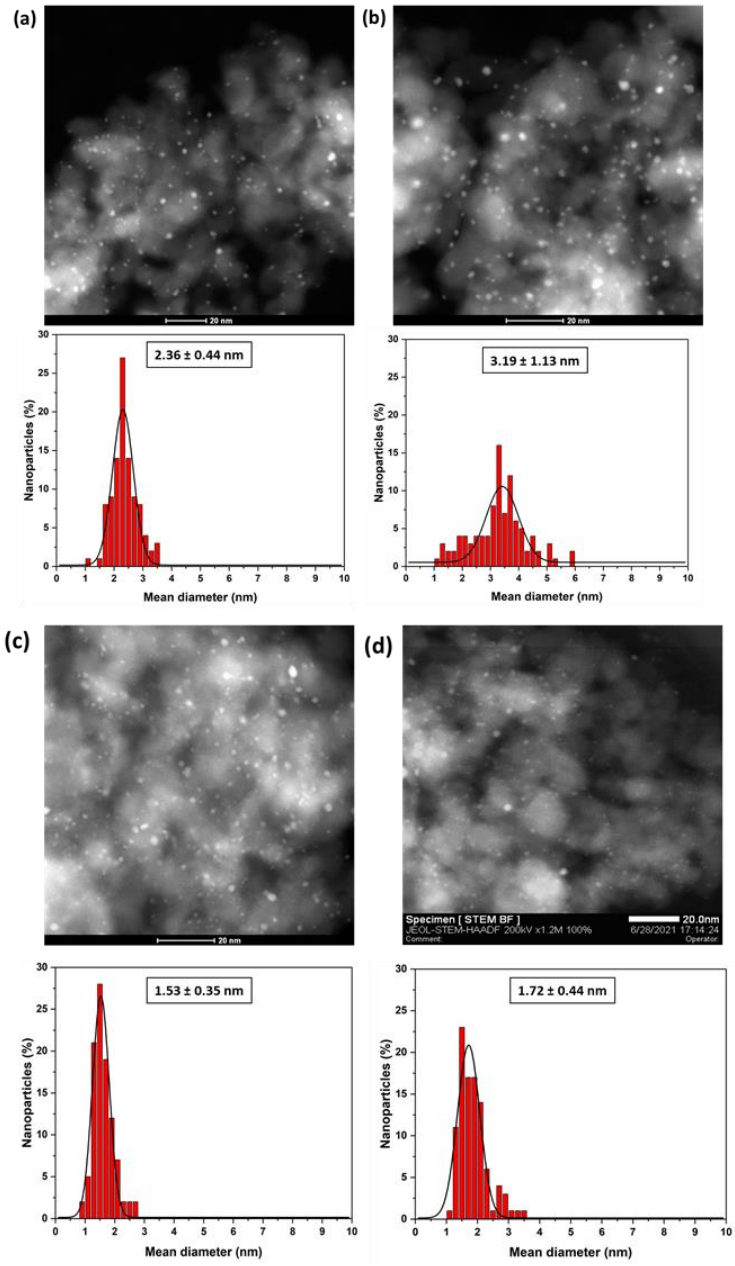

Figure 5.24. HAADF images of (a) $PtSn^{SOMC}@Al_2O_3$, (b) Red-$PtSn^{SOMC}@Al_2O_3$, (c) $PtSn^{SOMC}$-$PPh_3@Al_2O_3$ and (d) Red- $PtSn^{SOMC}$-$PPh_3@Al_2O_3$ and its size distribution histograms.

Concerning the characterization, ICP-OES analyses revealed a Pt loading of 1.3-1.4wt.% Pt. Rregarding Sn, when no PPh_3 was added, a lower Sn loading was measured in the catalyst (**Table 5.11**). Since the thermal treatment under hydrogen flow was carried out a temperature much higher than the decomposition

temperature of the PPh_3, this behavior suggests that in this case, the control on the decomposition of the tin precursor is an indirect effect of the ligand caused by the tuning of the support acid-basic properties by the ligand PPh_3 itself or the PPh_3 decomposition products (i.e., H_3PO_4).

Table 5.11. Characterization of PtSn catalysts by SOMC-OPOA approach.

Catalyst	Pt (wt. %)[a]	Sn (wt. %)[a]	Sn/Pt[a] (mol)	NPs size (nm)[b]
$PtSn@Al_2O_3$	1.29	0.55	0.70	2.36 ± 0.44
Red $PtSn@Al_2O_3$	1.29	0.55	0.70	3.19 ± 1.13
$PtSn\text{-}PPh_3@Al_2O_3$	1.21	0.79	1.07	1.53 ± 0.35
Red $PtSn\text{-}PPh_3@Al_2O_3$	1.21	0.79	1.07	1.72 ± 0.44

[a] Quantified by ICP-OES analysis; [b] Obtained through TEM analyses and measuring more than 200 nanoparticles, NP sizes are quoted as the mean diameter ± the standard deviation.

XRD analysis revealed the patterns of all catalysts exhibit main peaks at 2θ = 37°, 45.9° and 66.9° corresponding to the bare support γ-Al_2O_3 phase. This again suggested that the structure of the support remains unaltered, and that the Pt NPs are well dispersed. (JCPDS 01-080-0956).[33] No other diffraction peaks were observed, suggesting that the PtSn NPs are well dispersed onto the surface of the support and as well possessing a very small size, in agreement with HAADF-STEM observations and previous reports.[30,31,32]

STEM-EDS mappings of freshly synthesized $PtSn^{SOMC}@Al_2O_3$ and $PtSn^{SOMC}\text{-}PPh_3@Al_2O_3$ (**Figure 5.25**) showed the selective Sn distribution onto the Pt-NPs using the SOMC approach. Compared to the organometallic approach, the SOMC approach is more selective for the grafting of the Sn atoms onto the NP surface rather than on the alumina-based support. Nevertheless, although the fresh $PtSn^{SOMC}\text{-}PPh_3@Al_2O_3$ catalyst was stabilized with PPh_3, no P was detected by EDS.

However, since a reduction step is carried out before the grafting the Sn by SOMC, our hypothesis is that PPh_3 is burned and removed.

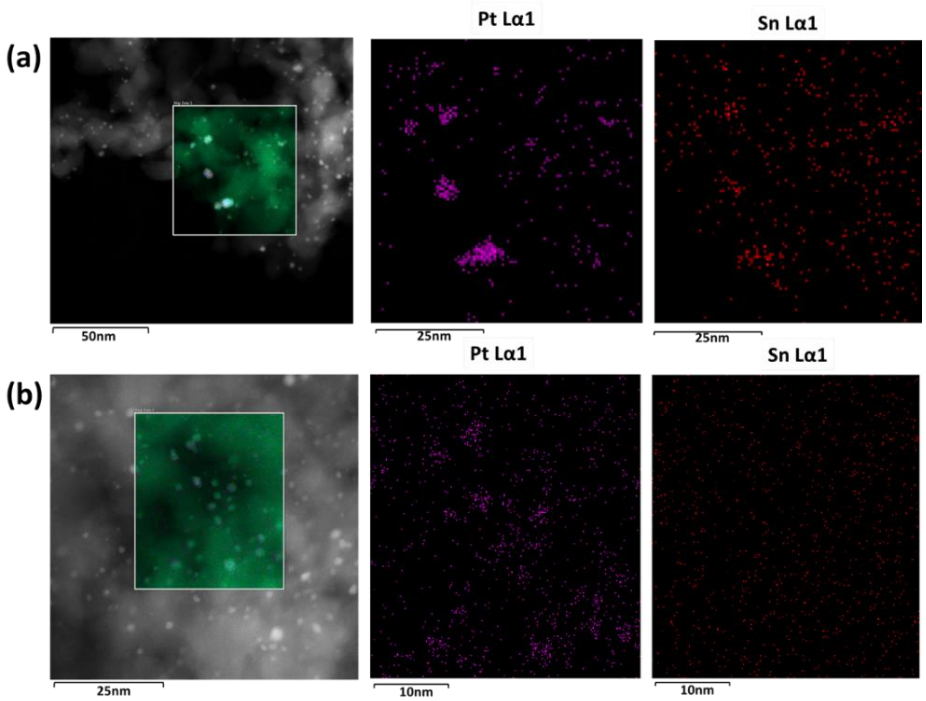

Figure 5.25. STEM EDS-mapping images of freshly synthesized catalysts(a) $PtSn^{SOMC}@Al_2O_3$ and (b) $PtSn^{SOMC}$-$PPh_3@Al_2O_3$ and its element distribution.

XRD analysis of all catalysts again revealed the patterns corresponding to the support γ-Al_2O_3 phase. This suggested that the structure of the support remained unaltered, and that the Pt NPs are well dispersed. (JCPDS 01-080-0956).[33] No other diffraction peaks were observed, suggesting that the PtSn NPs are well dispersed onto the surface of the support and as well possess a very small size, in agreement with HAADF-STEM observations and previous reports.[30,31,32]

The freshly prepared and reduced $PtSn@Al_2O_3$ catalyst was analyzed by XPS to investigate the atomic composition and oxidation state of each element (**Figure 5.26** and **Table 5.12**). The characteristic peak Pt 4f could not be analyzed due to overlapping with the Al 2p peak, and therefore Pt 4d band was used for Pt analysis and 3d band for Sn.

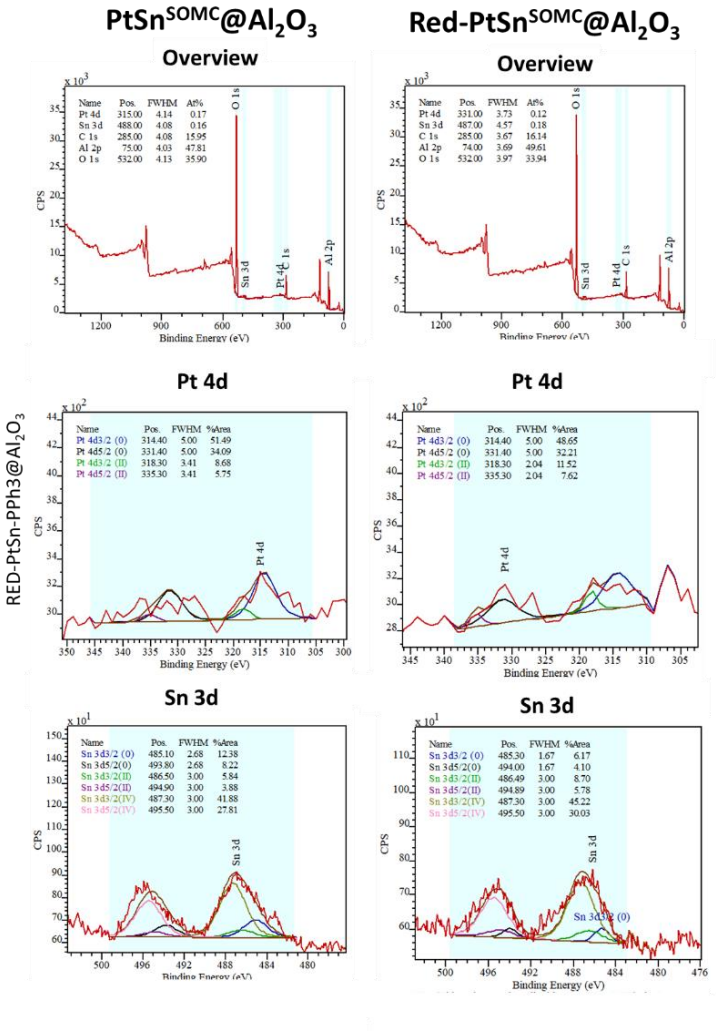

Figure 5.26. XPS deconvolutions of PtSn OPOA-SOMC catalysts.

Table 5.12. XPS results of PtSn OPOA-SOMC catalysts.

		XPS		
Catalyst	Sn/Pt [a] (mol)	Sn/Pt [b] (mol)	Pt(IV,II)/Pt(0)	Sn(IV)/Sn(II)/Sn(0)
$PtSn^{SOMC}@Al_2O_3$	1.29	1.1	14 / 86	70 / 10 / 20
Red $PtSn^{SOMC}@Al_2O_3$	1.29	1.5	19 / 81	75 / 14 / 10

[a] Quantified by ICP-OES. [b] Quantified by XPS.

Concerning the Pt composition, the Pt(0) relative amount is almost the same in the reduced sample, thus suggesting that these PtSn species required harsh conditions for its reduction or either that the tin incorporation in the PtSn alloy makes the Pt more electron-deficient (higher BE).

Regarding the Sn composition, the previously observed behavior for the PtSn catalyst prepared by OPOA was again observed and the thermal treatment under hydrogen flow resulted in only slight variation of the Sn species on the support of the catalyst surface, with Sn in low oxidation states (Sn (0)) incorporated in the PtSn alloy structure and the Sn in higher oxidation state (Sn (δ+)) on the support surface or as tin aluminates (i.e., $SnAl_2O_4$ or $SnAlO_3$).

The presence of such Sn species on the surface of the $PtSn/Al_2O_3$ catalyst has been previously reported in the literature and there is a debate on the importance of the chemical states of Sn.[34,35,36]

No signals coming from P 2p orbitals either from PPh_3 or any other P species were detected.

Additionally, another mixed approach consisting of an extra step of impregnation was performed and consisted in 3 steps: (i) preparation of the colloidal ligand capped Pt-L-NPs by the organometallic approach (OA), ii) impregnation onto the corresponding support with the freshly synthesized crude Pt-L-NPs, washing and reduction of the monometallic catalyst and finally (iii) selective deposition of the Sn promoter using the SOMC approach (**Figure 5.27**).

First, small PPh_3 capped Pt NPs (Pt-PPh_3-NPs) were synthesized via organometallic approach. The molar ratio between Pt and the ligand was the same as in the supported samples studied before, 1:0.2 (Pt/PPh_3). The colloidal NPs exhibited a mean size of 1.98 ± 0.31 nm with 62.37 wt. % of Pt and 3.57 % of P (Pt/P molar ratio 17.4) (**Figure 5.28 a**).

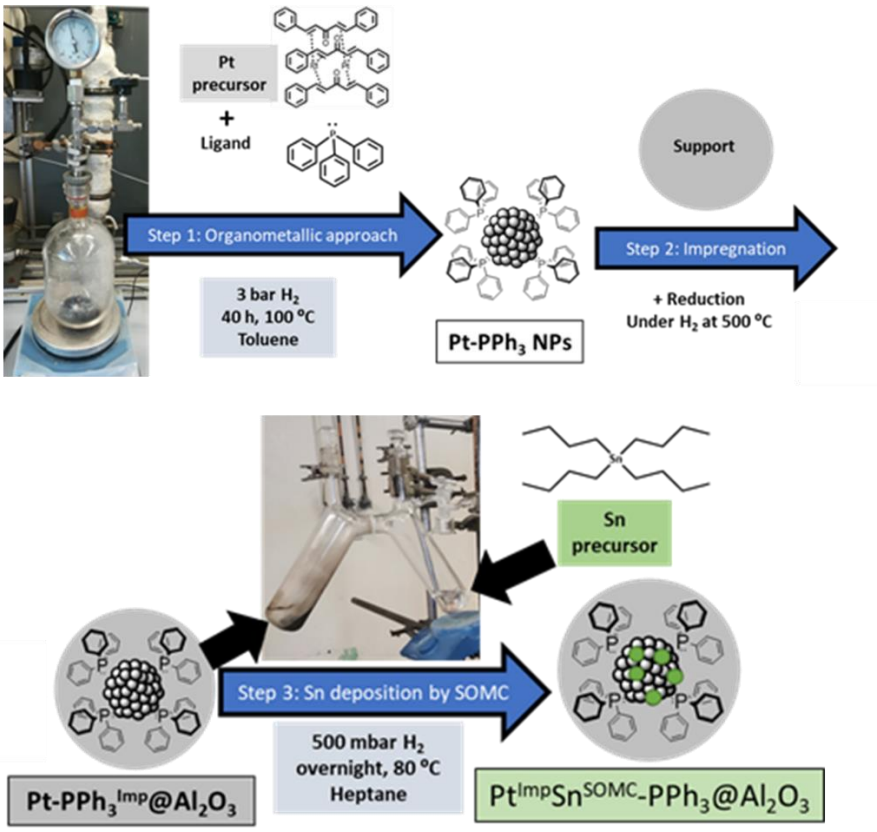

Figure 5.27. Preparation of $Pt^{imp}Sn^{SOMC}$-PPh_3@Al_2O_3 using the OPOA-Imp-SOMC mixed approach. First, Pt-PPh_3 using OPOA approach were prepared. Then, they were impregnated and reduced under H_2. Finally, the Sn was grafted using SOMC/M approach using $SnBu_4$ precursor followed by a reduction with H_2.

Consecutively, a solution of the NPs was added (to reach 2wt.% Pt) onto the desired support (Al_2O_3 or $LiAl_2O_3$) and stirred during 72h. When alumina was used as the support, most of the NPs remained unsupported. In contrast, when lithiated alumina was used, the Pt-NPs were efficiently immobilized. The Pt^{Imp}-PPh_3@$LiAl_2O_3$ catalyst was analyzed by TEM and the mean size of the particle was 1.31 ± 0.23 nm (**Figure 5.28**, c), thus smaller than the colloidal Pt on alumina (Pt^{Imp}-PPh_3@Al_2O_3**)**, that presented a mean size of 2.64 ± 0.37 nm (**Figure 5.28**, b).

The elemental analysis of the colloidal sample revealed contents of Pt 62.37 % wt and P 3.57 %, with Pt/P ratio of 17.4. When the NPs were impregnated onto alumina and lithiated alumina, the Pt contents were respectively 0.53 and 0.71 wt % (*vs.* a

nominal value of 2 wt. % Pt), and the P contents were 0.04 and 0.06 wt.%, displaying lower element contents than expected. It seems that Ostwald ripening was occurring to the NPs. Regarding the latter catalyst (Pt^{Imp}-PPh_3@$LiAl_2O_3$), a possible explanation to obtain a lower mean size than the corresponding colloidal NP could be the leaching phenomena previously reported for Pd NPs.[37] The ligands could coordinate the metallic nanoparticle and form a molecular homogeneous complex. This could explain the diminution of the mean size. Moreover, this fact was reported as well for supported PdNPs/C for catalyzed Suzuki couplings.[38] Even though the low Pt content, the Sn was deposited using SOMC and tested in the PDH reaction.

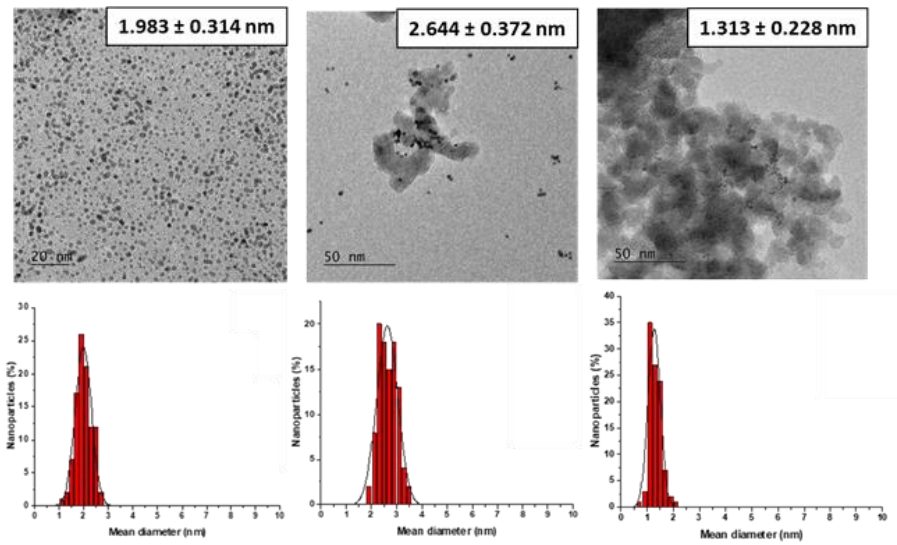

Figure 5.28. TEM images of the mixed OPOA-Imp-SOMC approach. a) Colloidal NPs (Pt-PPh_3) impregnated onto b) Al_2O_3 or c) on $LiAl_2O_3$.

In conclusion, TEM and ICP analyses suggested that impregnation processes were not effective using these alumina support (Al_2O_3 or Li-Al_2O_3) since only a small amount of Pt-NP were immobilized. This could be explained by the small pore neck mean diameters that hinder the diffusion of the Pt-NPs to the interior of the pores of the supports and the Pt-NPs were attached only on the more external layers of the alumina by weak interactions between the Pt-NP and the support. In view of

the low Pt content obtained, Sn addition by SOMC was performed and performance in PDH was evaluated.

5.2.2 Catalytic evaluation in PDH

Unless stated differently, the PDH catalytic tests were carried out inside a stainless-steel fixed bed reactor at 530 ^{o}C and 1 bar (a) of pressure, using a Gas Hourly Space Velocity (GHSV) of 15.000 mL·g^{-1}·h^{-1}, 25 mg of catalysts dispersed in SiC and the feed gases applied where 3 C_3H_8 / 1 H_2 / 21 Ar (expressed in mL/min). In the Experimental section of the present chapter, all the details and how conversion and selectivity values were obtained is detailed.

5.2.2.1 PDH of PtGa (OPOA)

(1) Effect of Ga precursor.

First, the catalysts supported on Al_2O_3 and prepared by OPOA using the Ga precursors $Ga(Me)_3$ and $Ga(isobutyl)_3$ without any stabilizing agent were tested in PDH reaction (**Figure 5.29**).

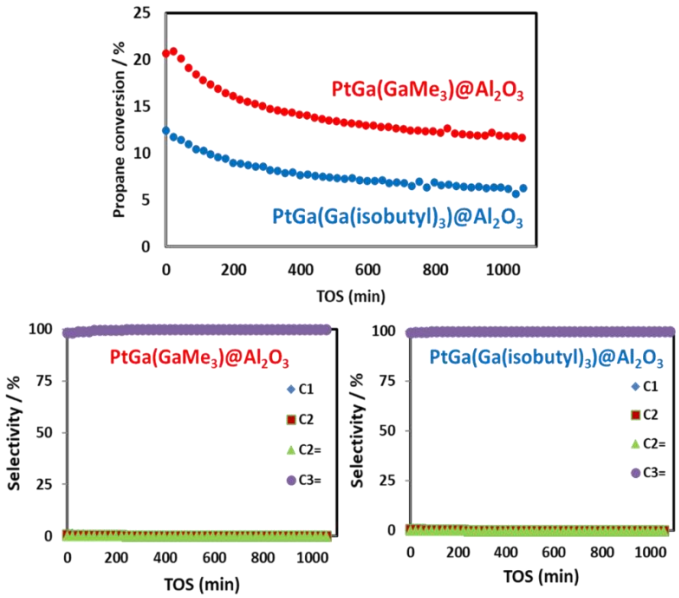

Figure 5.29. Propane conversion of PtGa@Al_2O_3 by OPOA changing the Ga precursor: $Ga(Me)_3$ (red line) or $Ga(isobutyl)_3$ (blue line) and its selectivity's in PDH reaction.

A significant difference in propane conversion was observed since when $Ga(Me)_3$ was used as the Ga precursor. The initial conversion was 20% and after 10 h (600 min) of TOS, it decreased to 13%, whereas when $Ga(isobutyl)_3$ was used, the initial propane conversion was 12.4% and after 10 h it was only 7%. On the other hand, both catalysts were highly selective toward propylene with a constant selectivity of 99.9 %. The higher activity obtained with $PtGa(Ga(Me)_3)/Al_2O_3$ could be explained by the smaller size of the particles in this catalyst and higher Ga/Pt ratio than that of the catalyst prepared using $Ga(isobutyl)_3$. The optimum Ga loading seems higher than those previously reported for related $PtGa/Al_2O_3$ systems (around $\leq$ 0.44wt.%Ga),[3] probably because the synthetic approach is different and results in distinct distribution of the catalytic active species on the support.

(2) Effect of PPh_3.

The effect of triphenylphosphine (PPh_3) was evaluated using catalysts prepared using $Ga(Me)_3$ as precursor and Al_2O_3 as a support ($PtGa/Al_2O_3$ and $PtGa\text{-}PPh_3/Al_2O_3$) in PDH reaction (**Figure 5.30**).

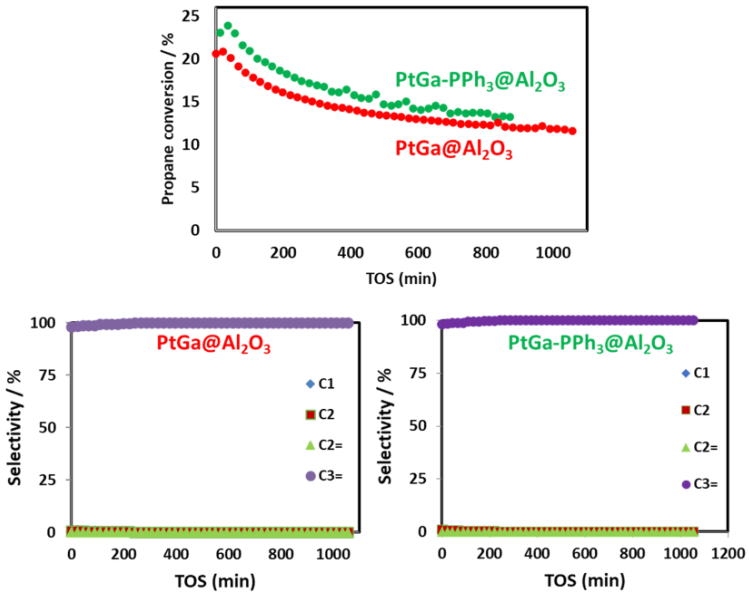

Figure 5.30. Propane conversion of $PtGa@Al_2O_3$ by OPOA effect of ligand: no ligand (red line) or PPh_3 (green line) and its selectivity's in PDH reaction.

No significant difference in propane conversion was observed (20-23%). In terms of selectivity, both catalysts provided excellent selectivity toward propylene of 99.9%. Therefore, the difference in the crystalline phases observed with different proportions of the Pt_3Ga alloy/Pt seems to result in only a very small effect on the catalytic activity, i.e., the PtGa-PPh_3@Al_2O_3 displayed higher proportion of Pt-phase and this could be the cause of the higher activity. In conclusion, PPh_3 does not have a significant effect.

(3) Effect of support.

The effect of the support was evaluated via the testing of the PtGa stabilized with PPh_3 prepared by OPOA supported on bare alumina and on lithiated alumina in the PDH reaction (PtGa-PPh_3/Al_2O_3 and PtGa-PPh_3/Li-Al_2O_3) (**Figure 5.31**).

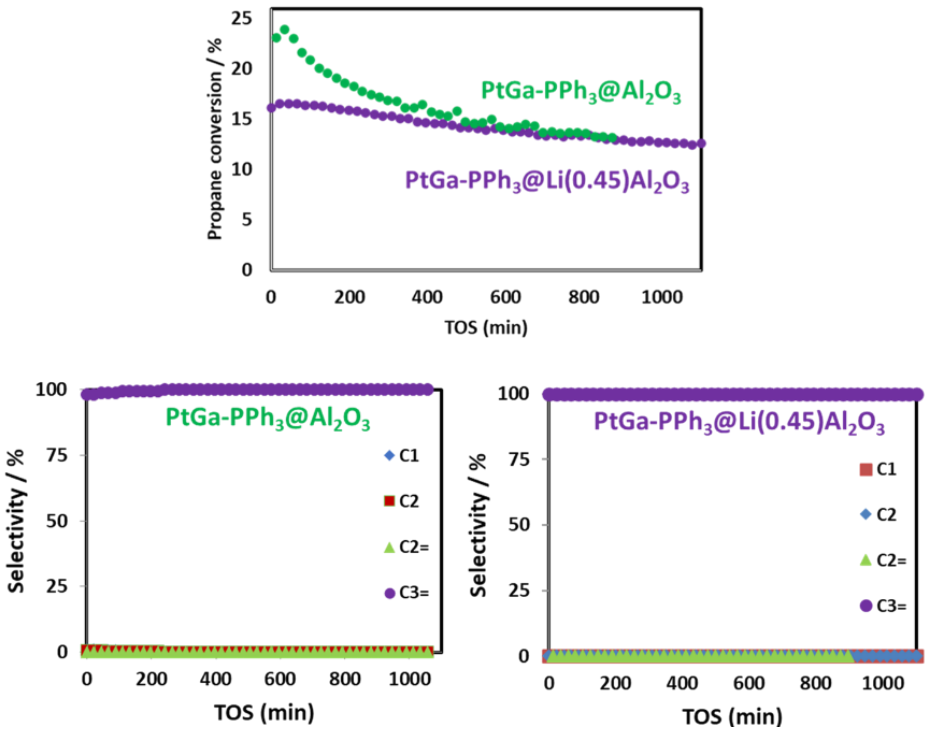

Figure 5.31. Propane conversion of PtGa-PPh_3@Support by OPOA effect of support: Al_2O_3 (green line) or $Li(0.45)Al_2O_3$ (purple line) and its selectivity's in PDH reaction.

The propane conversion is higher at initial times when the Al_2O_3 is used (23%) vs. (16.5%) $LiAl_2O_3$. However, after 10 h, both provided the same conversion (13-14 %). Moreover, both showed excellent selectivity toward propylene (99.9%). These catalysts displayed similar NP size and Pt contents, but displayed different Ga/Pt molar ratios, i.e., the catalyst with the highest initial conversion displayed the lowest Ga/Pt ratio (0.46), whereas the catalyst with less variation in the conversion displayed higher Ga/Pt ratio (0.81). This is in agreement with the literature where the Ga/Pt ratio is described a key parameter for balancing between high initial conversions and stable catalytic performances. [39]

(4) Effect of Sn as a promoter.

The effect of Sn as an additional promoter was evaluated in PDH reaction by comparison of the performance of PtGa-PPh_3/Al_2O_3 and PtGaSn-PPh_3/Al_2O_3 reaction (**Figure 5.32**).

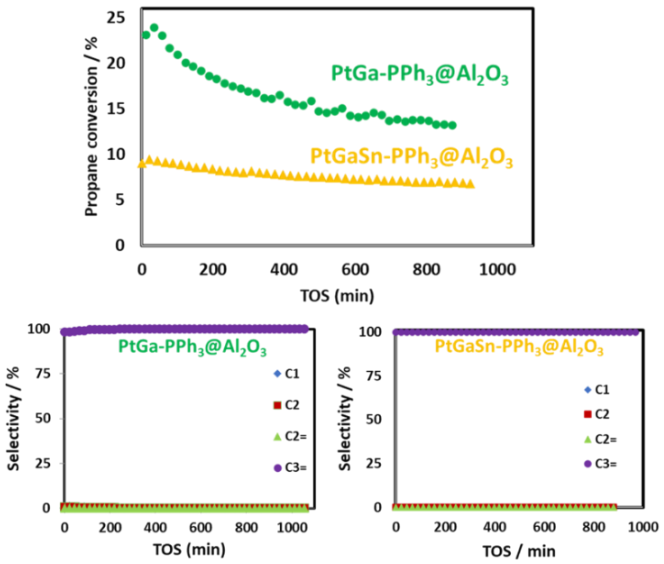

Figure 5.32. Propane conversion of PtGa-$PPh_3@Al_2O_3$ by OPOA effect of Sn as a promoter: no Sn (green line) or adding Sn (yellow line) and its selectivity's in PDH reaction.

The propane conversion was higher in the Sn free catalyst with 23% initially and 13% after 10 h of catalysis. For the Sn containing catalyst, the initial conversion was

9.3% but barely decrease after 10 h (7.3%). These results indicated that the Sn addition as a second promoter improves the catalyst stability under these conditions but lower its activity, possibly due to a full coverage of the surface of the NP. Further studies regarding the dispersion of Pt should be performed. In terms of selectivity, no difference was observed, as both exhibited excellent selectivity (99.9%) to propylene.

(5) Effect of CO_2 in the feed.

$PtSn\text{-}PPh_3/LiAl_2O_3$ was evaluated in the presence of 200 ppm CO_2 as a poison in the feed for PDH reaction (**Figure 5.33**).

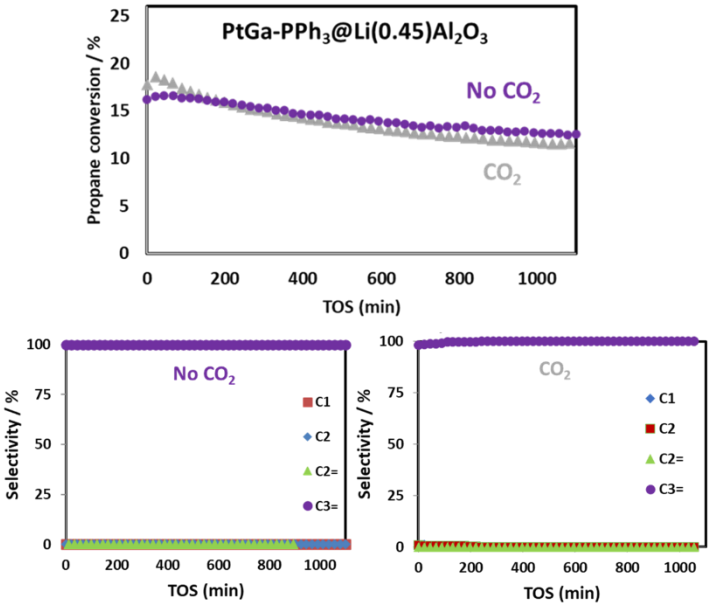

Figure 5.33. Propane conversion of $PtGa\text{-}PPh_3@Li(0.45)Al_2O_3$ by OPOA effect CO_2 as a poisoning in the feed: no CO_2 (purple line) or with CO_2 (grey line) and its selectivity's in PDH reaction.

The propane conversion (initially *ca.* 17% and 14% after 10 h of TOS) and the selectivity to propylene were barely affected by the presence of the CO_2 poison throughout the experiment. It was therefore concluded that the $PtGa\text{-}PPh_3@LiAl_2O_3$ catalyst was stable in the presence of this poison and that its performance in PDH remained unaffected when using a CO_2-containing feed.

(6) Scope of alkene feedstocks, butane and 1-butene dehydrogenation.

To extend the scope of alkane/alkene feedstock, the PtGa-PPh_3@Al_2O_3 catalyst was also evaluated in the butane and 1-butene dehydrogenation (**Figure 5.34**). Note that the equilibrium thermodynamic conversion using the reaction conditions: $3C_4$:$1H_2$:21 Ar at 530 ^oC, and that the maximum theoretical conversion is 13.8%. The tested catalyst showed an initial conversion of 10% with a slow deactivation to 5.6%. The butadiene selectivity was 77% at the beginning of the catalysis and 87% after 600 min. The hydrogenation product was the main side-reaction observed with a selectivity to butane of 16.5% initially and 7.1% after 600 min. This test proved that this catalyst is also valid for the butane dehydrogenation reactions.

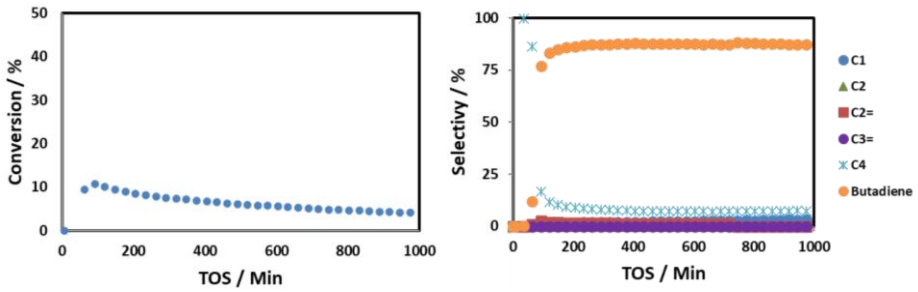

Figure 5.34. Butenes conversion and selectivity of PtGa-PPh_3@Al_2O_3. 530 ^oC, 60.000 $mL_{total}{\cdot}g_{cat}^{-1}{\cdot}h^{-1}$ using 3 C_4:$1H_2$:21 Ar.

In conclusion, the performance of all PtGa catalysts prepared via OPOA was evaluated in the PDH reaction and the results are summarized in **Table 5.13**.

Table 5.13. PtGa catalysts synthesized by the OPOA and its catalytic performance in PDH reaction.

Entry	Catalyst	C3 conv. 0 min	C3 conv. 600 min	C3= Select. 0 min.	C3= Select. 600 min.
1	PtGa(Ga(isobutyl)$_3$@Al_2O_3	12.4	7.0	99.9	99.9
2	PtGa@Al_2O_3	20.0	13.0	99.9	99.9
3	PtGa-PPh_3@Al_2O_3	23.0	14.2	94.0	99.9
4	PtGaSn-PPh_3@Al_2O_3	9.3	7.3	99.9	99.9
5	PtGa-PPh_3@Li(0.45)Al_2O_3	16.5	14.0	99.9	99.9
6	**(CO_2)** PtGa-PPh_3@Li(0.45)Al_2O_3	18.0	13.0	98.0	99.9

In general, these PtGa catalysts provided moderated-to-good conversions (up to 23%) below the thermodynamic equilibrium conversion with excellent propylene selectivity (99.9%). Regarding the Ga precursor (entries 1 and 2, **Table 5.13**), $GaMe_3$ resulted in smaller PtGa-NPs, higher Pt loading and higher Ga/Pt molar ratios in comparison with $Ga(isobutyl)_3$. No significant effect was observed when PPh_3 was added as stabilizer ((entries 2 and 3, **Table 5.13**). The effect of Sn as an additional promoter (entries 3 and 4, **Table 5.13**) showed and improved catalyst stability but lowered its activity, probably due to a full coverage of the surface of the NP and decreasing the Pt dispersion. The effect of the support provided the highest impact on the catalytic performance (entries 3 and 5, **Table 5.13**). When the alumina (Al_2O_3) was used, a higher initial conversion was obtained, whereas $LiAl_2O_3$ displayed stable conversions. Poisoning by CO_2 in the feed was studied using the latter catalysts (entries 5 and 6, **Table 5.13**) and the performance in PDH remained unaffected.

The scope of the application of these catalysts has been explored by its successful application in the dehydrogenation of butane and 1-butene.

5.2.2.2 PDH of NiSn (OPOA)

For NiSn catalysts, slightly different PDH conditions were used. 400 mg of catalysts were used and the PDH reaction was performed at 540 ^oC using a total flow of 5 mL/min composed of 1 C_3H_8 and 4 Ar (mL/min).

(1) Effect of ligand.

Two ligands were used as stabilizing ligands for the NiSn-L@Al_2O_3, where L = PPh_3 or NHC-CO_2 (**Figure 5.35**). The NiSn-NHC@Al_2O_3 catalyst displayed higher conversion than the thermodynamic equilibrium conversion because this catalyst was promoting cracking processes instead of the selective dehydrogenation of propane, and the main product produced was methane. In that case, it seems that

Ni is doing the hydrogenolysis, and that no alloyed was formed, in agreement with a big NPs size (*ca.* 11.8 nm).

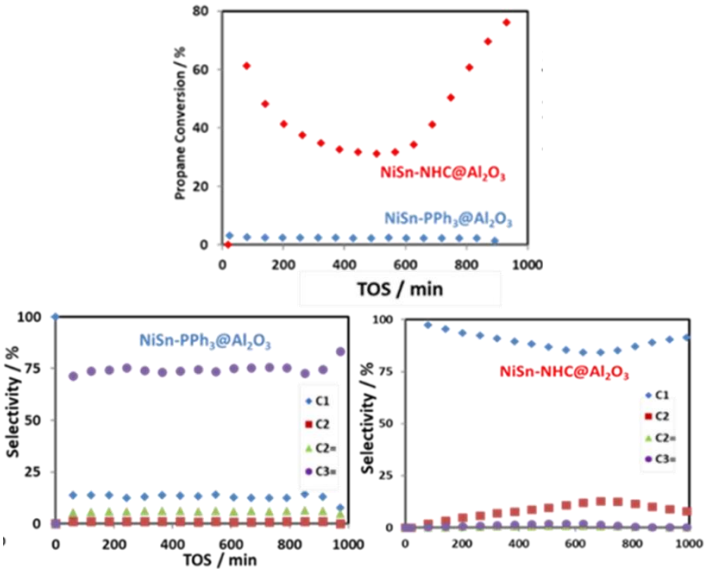

Figure 5.35. Propane conversion of NiSn-L@Al_2O_3 by OPOA effect of ligand(L): PPh_3 (blue line) or NHC (red line) and its selectivity's in PDH reaction.

When NiSn-PPh_3@Al_2O_3 was used, the propane conversion was very low but the selectivity was acceptable (*ca*. 75% to propylene). Here, the NiSn alloy could be formed as the NPs were small and dispersed (*ca.* 1.50 nm). Nevertheless, in the XRD, no information was obtained due to the low loadings of the metals.

(2) Effect of support.

The effect of the support was evaluated in PDH reaction using NiSn catalysts containing PPh_3 as stabilizing ligand and supported on bare alumina *vs.* lithiated alumina (**Figure 5.36**). When the catalyst supported on $LiAl_2O_3$ was used, a higher initial conversion was obtained (ca. 5% vs 1%). Moreover, the propane conversion increased over time and reached 8-9% after 1000 min while the activity of the Al_2O_3-supported catalyst remained unchanged. In contrast, a higher selectivity to propene was obtained with the latter catalyst (*ca.* 75%) while with the $LiAl_2O_3$ supported catalyst, methane was the main reaction product throughout the

experiment. The difference in activity between these catalysts could not be attributed to the size of the particles since the $LiAl_2O_3$ supported catalyst presented particle sizes much larger than the Al_2O_3 catalyst.

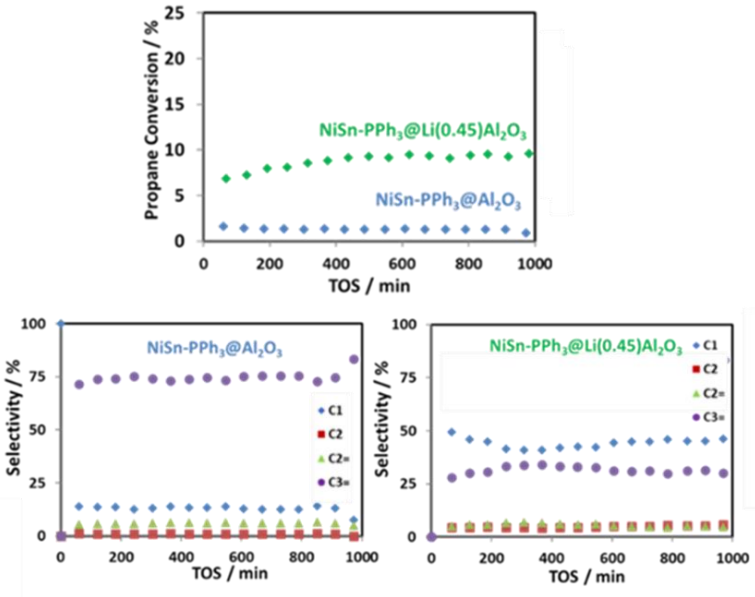

Figure 5.36. Propane conversion of NiSn-L@Al_2O_3 by OPOA effect of ligand(L): PPh_3 (blue line) or NHC (red line) and its selectivity's in PDH reaction.

In conclusion, the performance of NiSn catalysts prepared via OPOA in the propane dehydrogenation was evaluated (**Table 5.14**Table 5.13). The effect of the ligand (PPh_3 and NHC) was tested using Al_2O_3 as support (entries 1 and 2, **Table 5.14**) and NHC was fomenting the hydrogenolysis reaction, whereas PPh_3 displayed almost no conversion although the selectivity was acceptable for propylene. Then, the effect of using $LiAl_2O_3$ as a support was evaluated (entries 1 and 3, **Table 5.14**) and lead to higher conversion values. However, methane was the main reaction product.

Table 5.14. NiSn catalysts synthesized by the OPOA and its catalytic performance in PDH reaction.

Entry	Catalyst	C3 conv. 0 min	C3 conv. 600 min	C3= Select. 0 min.	C3= Select. 600 min.
1	NiSn-PPh_3@Al_2O_3	1.0	1.0	71.0	75.0
2	NiSn-NHC@Al_2O_3	0	31*	0	2
3	NiSn-PPh_3@Li(0.45)Al_2O_3	6.0	8.2	31.5	36.0

5.2.2.3 PDH of PtSn and PtGa (mixed approaches)

PtSn SOMC-OPOA.

(1) Effect of PPh_3.

The effect of the PPh_3 as ligand was also studied for PtSn using the mixed approach SOMC-OPOA in PDH reaction (**Figure 5.37**). For both catalysts, the propane conversion was the same initially (*ca*. 17%) and 9% after 10 h of TOS, independently of the PPh_3 presence. Regarding the selectivity, both presented a selectivity of 99.9% towards propylene. Since OPOA-SOMC needs a reductive step once the Pt-PPh_3/Al_2O_3 NPs are grafted, it can be assumed that the PPh_3 ligand was removed from the catalyst, explaining the similar behaviors of these materials. This behavior is contradictory to the one observed for the catalysts prepared by pure OPOA and SOMC approaches

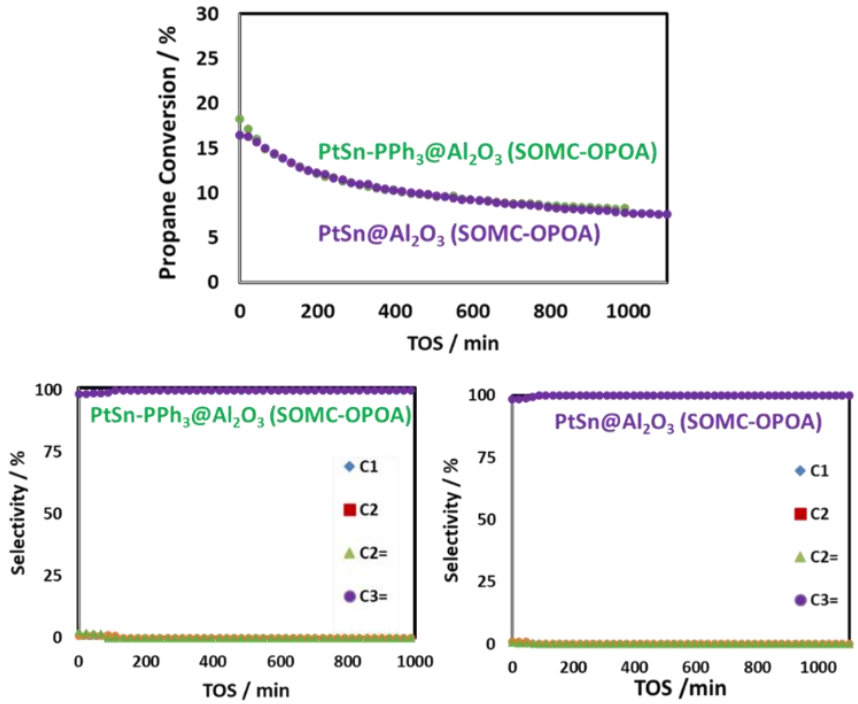

Figure 5.37. Propane conversion of PtSn@Al_2O_3 by SOMC-OPOA effect of PPh_3: presence of PPh_3 (green line) or without ligand (purple line) and its selectivity's in PDH reaction.

(2) Effect of impregnation step.

The effect of another mixed methodology including the impregnation the colloidal Pt-PPh_3 (OPOA) and then Sn deposition using SOMC was also evaluated in the PDH reaction (**Figure 5.38**). The propane conversion was much higher when SOMC-OPOA methodology was used for the catalyst preparation, starting at *ca.* 18% and 9% after 10 h of TOS. When an extra impregnation step was added, the initial conversion was 2.6% and only 1.5% after 10 h of TOS. Regarding the selectivity of the reaction, both catalysts showed excellent propylene selectivity of 99.9%. As previously discussed in the synthesis and characterization section, when the impregnation step is used, TEM analysis indicated that most NPs remained outside of the support. Therefore, the Pt loading was much lower than expected. However, the catalyst was stable under PDH conditions since the propane conversion remained constant throughout the catalytic test.

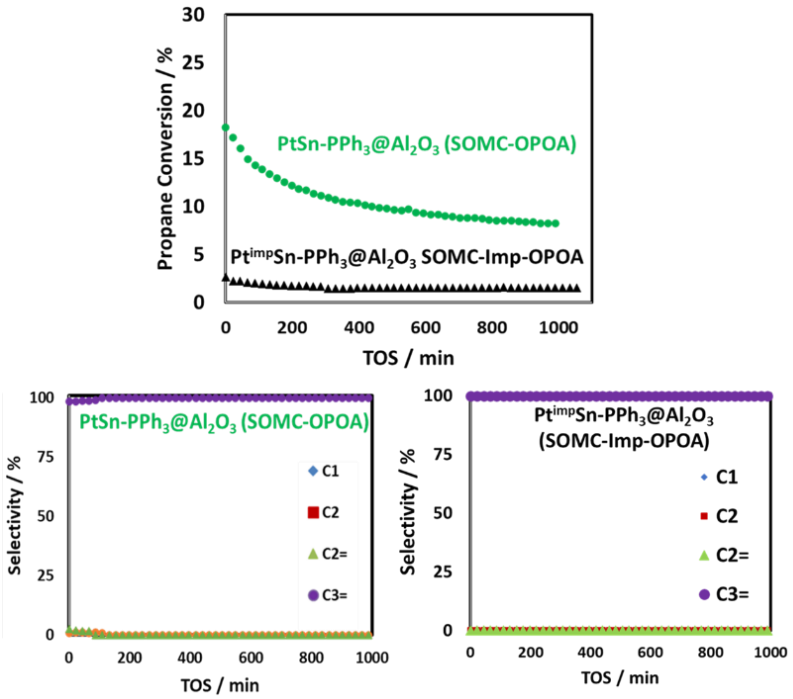

Figure 5.38. Propane conversion of $PtSn@Al_2O_3$ by SOMC-OPOA or by OPOA-Imp-SOMC: SOMC-OPOA (green line) or OPOA-Imp-SOMC (black line) and its selectivity's in PDH reaction.

In conclusion, the PtSn catalyst prepared by combination of OPOA and SOMC approaches in the PDH reaction were evaluated. Our initial idea was to combine the advantages of both methodologies, i.e., OPOA excellent control on the Pt-NP formation and SOMC outstanding control on the Sn-selective reaction with the Pt-H of the NP. However, for the PtSn catalyst supported onto alumina, the combination of approaches seems to provide much less efficient catalysts than those obtained by pure OPOA and SOMC approaches. As displayed in **Table 5.15**, the presence of PPh_3 seems not to have any effect (entries 1 and 2). Moreover, the effect of an extra impregnation step in the OPOA-SOMC methodology (OPOA-Imp-SOMC) was studied (entry 3). However, poor propane conversions were obtained (2.6%). Their selectivity was 99% to propylene.

Table 5.15. PtSn catalysts synthesized by SOMC-OPOA and SOMC-Imp-OPOA and its catalytic performance in PDH reaction.

Entry	Catalyst	C3 conv. 0 min	C3 conv. 600 min	C3= Select. 0 min.	C3= Select. 600 min.
1	$PtSn@Al_2O_3$	16.0	9.0	98.0	99.9
2	$PtSn\text{-}PPh_3@Al_2O_3$	18.0	9.0	98.0	99.9
3	$Pt^{imp}Sn\text{-}PPh_3@Al_2O_3$	2.6	1.5	99.9	99.9

PtGa SOMC-OPOA.

(1) Indirect effect of PPh_3.

The effect of the PPh_3 as ligand was also studied for PtGa catalysts using the mixed approach SOMC-OPOA in PDH reaction (**Figure 5.39**). Initially the propane conversion was a little bit higher when no ligand was used (9% *vs.* 6%). However, at TOS > 200 min, both catalysts provided the same conversion (5-6%). In contrast, both presented selectivity of 99.9% towards propylene. Once again, the reductive step required for the OPOA-SOMC methodology can explain that both catalysts have the same behavior since the PPh_3 ligand was removed/decomposed during this step. Regarding the NPs size, $PtGa/Al_2O_3$ displayed larger NPs than PtGa-

PPh_3/Al_2O_3 and the Ga/Pt molar ratios ($PtGa/Al_2O_3$ displayed higher Ga/Pt molar ratios than $PtGa\text{-}PPh_3/Al_2O_3$). This behavior is contradictory to the behavior observed so far for the catalyst prepared by pure OPOA approach, but maybe, it is only an apparent effect since the conversions achieved by the combination of approaches are much lower than those achieved by the catalyst prepared by pure OPOA approach.

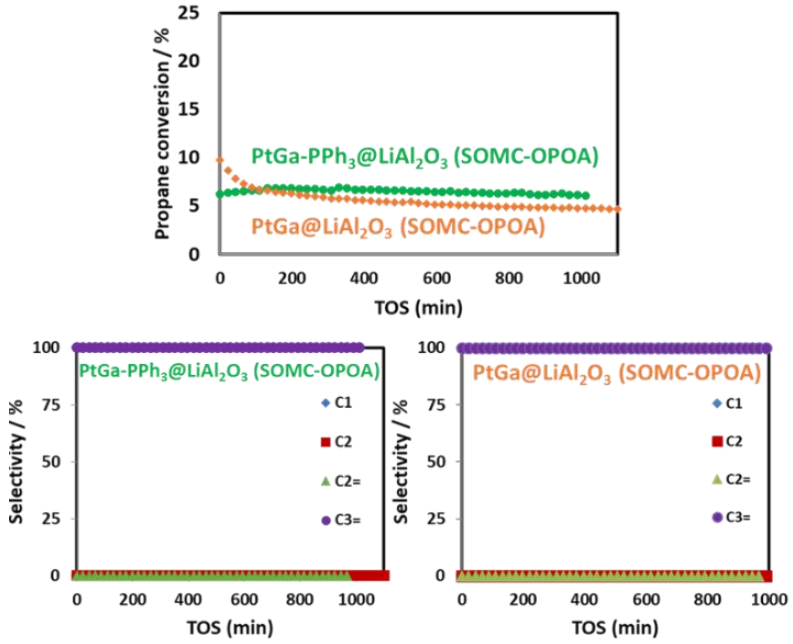

Figure 5.39. Propane conversion of $PtGa@Li(0.45)Al_2O_3$ by SOMC-OPOA effect of PPh_3 : presence of PPh_3 (green line) or without ligand (orange line) and its selectivity's in PDH reaction.

Table 5.16. PtGa catalysts synthesized by SOMC-OPOA and its catalytic performance in PDH.

Entry	Catalyst	C3 conv. 0 min	C3 conv. 600 min	C3= Select. 0 min.	C3= Select. 600 min.
1	$PtGa@Li(0.45)Al_2O_3$	9.0	5.0	99.9	99.9
2	$PtGa\text{-}PPh_3@Li(0.45)Al_2O_3$	6.0	6.0	99.9	99.9

In conclusion, the PtGa catalysts prepared by combination of OPOA and SOMC approaches in the PDH reaction were evaluated. The idea was to combine the

advantages of both methodologies, i.e., OPOA excellent control on the Pt-NP formation and SOMC outstanding control on the Sn-selective reaction with the Pt-H of the NP. However, for the PtGa catalyst supported onto alumina (**Table 5.16**), the combination of approaches seems provide much less efficient catalyst than the pure OPOA approach.

5.3 Conclusions

The one-pot organometallic approach (OPOA) was used for the first time in the preparation of PtGa and NiSn based catalysts in the propane dehydrogenation reaction. Moreover, a novel approach combining OPOA and SOMC was used to prepare PtSn and PtGa catalysts. OPOA provided an excellent control on the Pt-NP formation and SOMC and outstanding control on the Sn or Ga selective reaction with the Pt-hydrides of the NPs. The as-prepared catalysts were characterized by combination of microscopic and spectroscopic techniques providing information on the NP dimensions, catalysts compositions, crystalline phase, and oxidation state of the surface elements. The efficiency of these catalysts in the PDH reaction was evaluated.

Concerning PtGa OPOA catalysts:

- Characterization of supported and colloidal (PtGa and PtGa-PPh_3) catalysts revealed the formation of small and well-dispersed NPs probably composed by two distinct crystalline phases: Pt3Ga alloy and Pt. The rest of the Ga was proposed to be present as gallium oxide either on the surface of the NP or the support.
- The presence of the PPh_3 ligand on the NPs was observed by EDS and XPS experiments. Different Ga/Pt molar ratios were obtained. PtGa-PPh_3 nanoparticle displayed higher Ga/Pt ratios than PtGa. This behavior could be explained as: (1) the PPh_3 coordination and blockage of the Pt-sites avoiding the interaction with the Ga precursor during the NP synthesis. Thus, reducing

the final Pt_3Ga alloy; or that (2) the decomposition of the Ga precursor is controlled by the PPh_3, via a change in the support acid-basic properties.

- The effect of Ga promoter was studied in PDH. The use of $Ga(Me)_3$ as the Ga promoter provided higher conversions, with a higher Ga content in the catalyst.
- The effect of PPh_3 was studied, and XRD analyses indicated the presence of the Pt_3Ga alloy in the analogous colloids. The most promising PtGa catalyst synthesized by OPOA was PtGa-PPh_3@Al_2O_3 with an initial propane conversion of 23.0% that decreased to 14.2% after 10 h of TOS. Its selectivity to propylene started at 94% and increased to 99%.
- The effect of Sn as a second modifier was studied, however its performance in PDH was lowered probably due to the Pt surface was covered by Sn.
- No effect of CO_2 in the feed was observed during the catalytic tests.
- Additionally, the scope of possible substrates was performed studying the dehydrogenation of a mixture of butane and 1-butane. Butadiene was obtained as the major product. This experiment suggested the wide scope other dehydrogenation reactions that could be studied using these catalysts.

Regarding NiSn OPOA catalysts:

- A ligand study was performed (PPh_3 and NHC) using Al_2O_3 as the support. PPh_3 ligand revealed to have a positive role in inhibiting the hydrogenolysis, therefore suggesting that a NiSn alloy species were formed. In contrast, NHC fomented the hydrogenolysis because the main product obtained was methane, and large NPs were obtained (>10nm).
- The effect of using $LiAl_2O_3$ was evaluated, using PPh_3, and revealed higher conversion values than that of Al_2O_3. However, methane was the main product obtained. The difference in the performance is still under study.

For the OPOA-SOMC PtSn and PtGa catalysts:

- Supported PtSn and PtGa onto alumina or lithiated alumina, respectively, have been prepared by a combination of the approaches. The role of the ligand (no ligand or PPh_3) was also explored. These catalysts have been characterized by distinct image and spectroscopic techniques. The results revealed the formation of small and well dispersed NPs probably composed by two distinct crystalline phases (Pt_3Ga/Pt and Pt_3Sn/Pt) with some amounts of either gallium oxides or tin oxides on the surface of the NP or on the surface of the support.
- In contrast to the samples prepared by OPOA, the PPh_3 ligand has been removed during the thermal treatment for the preparation of the Pt-hydrides.
- PtSn and PtGa catalyst were evaluated in PDH. For both PtSn and PtGa catalysts synthesized by the combination of approaches, provided much less efficient catalysts than the pure OPOA approach.

5.4 Experimental Details

5.4.1 General Methods.

Tris(dibenzylideneacetone)diplatinum ($Pt_2(dba)_3$) was prepared adapting the reported procedure[40] using potassium tetrachloroplatinate(II) (K_2PtCl_4, Johnson Matthey), dibenzylideneacetone (dba) and sodium acetate with metal trace levels (NaOAc), all of them from Sigma Aldrich, were purchased from commercial sources and used without further purification, unless stated differently. $SnBu_4$, $GaMe_3$, Ga(isobutyl)$_3$, Ni(COD)$_2$ and PPh_3 were purchased from commercial sources and used without further purification. The imidazolium carboxylate (NHC-CO_2) was prepared following reported procedures.[41,42] Solvents (n-hexane, tetrahydrofuran and toluene) were dried under a NaK alloy and degassed by freeze-pump-thaw cycles prior use. Gases were purchased from Air liquide. All experiments were carried out under controlled atmosphere, using Schlenk and glove box techniques

for organometallic synthesis. The synthesis and handling of supported species were carried out using high-vacuum lines (ca. 1 mPa) and glove boxes. Calcination of the supports and catalyst was performed using in-house produced furnaces (C2P2, CPE) with the following general conditions, 80 mL min^{-1} oxygen flow and 250-500 ºC temperature for 16 h. The evolved gases during the grafting reaction were analyzed on a Hewlett-Packard 5890 series II gas chromatograph (GC), equipped with a flame ionization detector (FID) and an HP PLOT KCl/Al_2O_3 column (50 m × 0.32 mm). All the operations for the syntheses of ligand-capped nanoparticulated systems (either colloidal or supported) were carried out using standard Schlenk tubes, Fisher-Porter bottle techniques or in a glovebox under nitrogen atmosphere.

5.4.2 Support pre-treatment.

The corresponding preparation of Al_2O_3 and Li-Al_2O_3 was described in the experimental section of Chapter 3.

5.4.3 Catalyst Preparation.

5.4.3.1 PtGa OPOA

To prepare the bimetallic PtGa-NPs ligand capped (L), Pt-(2 wt.%)/Ga-(1 wt.%)-NPs supported onto Al_2O_3 (PtGa-L@Al_2O_3), the platinum precursor (i.e., for Pt_2dba_3, 0.274 mmol, 150 mg), gallium precursor (i.e., for $GaMe_3$, 0.274 mmol, 37.5 µL), the selected stabilizing agent (L: none, PPh_3) (i.e., for PPh_3, 0.054 mmol, 14.35 mg), the corresponding support (i.e., for Al_2O_3, 2.57 g) and solvent (i.e., 37.5 mL toluene) were introduced in a Fisher Porter. The mixture was pressurized with 3 bars of H_2 and stirred at 700 rpm at 100 °C during 40 h. After filtration (14-15 µm pore filter), washing with toluene and hexane and drying under vacuum, the supported PtGa-P@Al_2O_3 was isolated in high yields (ca. 90-95%) and stored under inert atmosphere. Same procedure was followed to obtain PtGa@Al_2O_3 (without using any stabilizing agent) To obtain the PtGa-P@$LiAl_2O_3$, $LiAl_2O_3$ was used as support. For the trimetallic catalyst, PtGaSn-P@$LiAl_2O_3$ the same preparation was used but

additionally 1 equivalent of $SnBu_4$ (0.274 mmol, 101 mg)) was introduced in the mixture of the fisher porter.

Herein, the syntheses of colloidal stabilized PtGa-L NPs ligand capped (L: none, PPh_3), PtGa-L is described. Pt precursor (Pt_2dba_3, 0.274 mmol, 150.0 mg), the gallium precursor (i.e., for $GaMe_3$, 0.274 mmol, 37.5 µL), the selected stabilizing agent (i.e. for PPh_3, 0.054 mmol, 14.35 mg), and toluene (37.5 mL) were introduced in a Fisher Porter. The mixture was pressurized at 3 bars of H_2 at 700 rpm at 100 °C during 40 h. After washing with toluene and hexane and drying under vacuum, the colloidal PtGa-P were isolated in low yields (20-30%) and stored under inert atmosphere after precipitation. Same procedure was followed for the obtention of PtGa (without any stabilizing agent).

5.4.3.2 NiSn OPOA

For the synthesis of Ni-(2 wt. %)/Sn-(1 wt. %)-NPs supported onto Al_2O_3 or $LiAl_2O_3$, $Ni(COD)_2$ (0.274 mmol, 150 mg), $SnBu_4$ (0.274 mmol, 101 mg) with 0.2 equivalents of stabilizing ligand (i.e., PPh_3 (0.054 mmol, 14.35 mg) or NHC·CO2) 2.5771 g of the corresponding support and toluene (37.5 mL) were introduced in a Fisher Porter. The mixture was pressurized with 3 bars of H_2 at 700 rpm at 100 °C during 40 h. The supported NiSn-NPs were isolated in moderate-to-high yields (80-95%) and stored under inert atmosphere after filtration (14-15 µm pore filter), washing with toluene and hexane and drying under vacuum.

5.4.3.3 PtGa and PtSn OPOA-SOMC

Step 1: Pt-L@Support following the one-pot organometallic approach (OPOA).

For the synthesis of Pt(2 wt. %)-L supported onto i.e Al_2O_3, Pt_2dba_3 (0.274 mmol, 150 mg), L (0.054 mmol), 2.5771 g of the corresponding support and toluene (37.5 mL) were introduced in a Fisher Porter. The mixture was pressurized with 3 bars of H_2 at 700 rpm at 100 °C during 40 h. The supported Pt-NPs were isolated in moderate-to-high yields (80-95%) and stored under inert atmosphere after

filtration (14-15 µm pore filter), washing with toluene and hexane and drying under vacuum. Before starting the Step 2, an overnight reduction step under H_2 550 ^oC needs to be done.

Step 2: Promoter addition (Sn or Ga) on Pt(2%)-L@Support via SOMC approach.

The second grafting is the reaction of the promoter precursor on the hydride covered Pt-NPs. Briefly, on a double Schlenk, the desired amount of i.e, $SnBu_4$ (Sn/Pt ratios 0.7) is stirred at 80 ^oC in heptane (15 mL) with the monometallic catalyst **Pt-L@Support** (max. of 1.2 g per batch) under 500 mbar of pure H_2 overnight. Then, the solid is washed 3 to 5 times to remove the unreacted Sn precursor, the gases and liquid are collected for butane analysis, the powder is then dried under vacuum (10^{-5} mbar), and, finally, it is treated under H_2 at 550 ^oC, 1 ^oC min^{-1}, 4 h for the hydrogenolysis of the grafted organometallic species and formation of the desired PtSn-NPs. Note for Ga, the Ga(isobutyl)$_3$ promoter will be used.

5.4.3.4 PtSn OPOA-Imp-SOMC

Step 1: Colloidal Pt-L-NPs following the organometallic approach (OA).

Synthesis of colloidal Pt-NPs by the organometallic approach were done following adapted literature procedure.[43] Reactions were prepared under inert atmosphere. $Pt_2(dba)_3$ (60.0 mg, 0,055 mmol) were introduced in a fisher porter vessel with the corresponding stabilizing agent, i.e., PPh_3 (6.2 mg, 0.023 mmol). Then, (15 mL) toluene anhydrous and deoxygenated were added. The reactor was pressurized with H_2 (3 bar), and the reaction was stirred at 700 rpm for 20 hours at room temperature. The solution became black due to the decomposition of the dark-purple Pt-precursor. The colloidal Pt-NPs were isolated in moderate-to-high yields (70-80%) and stored under inert atmosphere. These NPs were not precipitated or washed because step 2 needs to be done with the crude of the reaction.

Step 2: Impregnation of colloidal Pt-L-NPs onto the support:Pt(2%)-^{imp}@Support.

A determined volume of the colloidal solution (placed inside a Schlenk), depending on the metal % desired onto the support, is added onto the desired support (inside a Schlenk too) by cannula (under Ar). The mixture is stirred for 3 days. The remaining mixture is filtered under vacuum, inside the glovebox, and washed with dry degassed toluene and hexane. Finally, the material is evaporated to dryness under vacuum. Before starting the Step 3, an overnight reduction step under H_2 550 ^{o}C needs to be done.

Step 3: Promoter addition (Sn or Ga) using the SOMC approach. i.e, to obtain Pt(2%)Sn-L^{imp}@Support

The grafting is the reaction of the promoter precursor on the hydride covered Pt-NPs. Briefly, on a double Schlenk, the desired amount of i.e, $SnBu_4$ (Sn/Pt ratios 0.7) is stirred at 80 ^{o}C in heptane (15 mL) with the monometallic catalyst, Pt(2%)-L^{imp}@Support (max. of 1.2 g per batch) under 500 mbar of pure H_2 overnight. Then, the solid is washed 3 to 5 times to remove the unreacted Sn precursor, the gases and liquid are collected for butane analysis, the powder is then dried under vacuum (10^{-5} mbar), and, finally, it is treated under H_2 at 550 ^{o}C, 1 ^{o}C min^{-1}, 4 h for the hydrogenolysis of the grafted organometallic species and formation of the desired PtSn-NPs. Note for Ga, the $Ga(isobutyl)_3$ promoter will be used.

5.4.4 Catalyst Characterization.

Transmission Electron Microscopy (TEM) experiments were performed at the "Unitat de Microscopia dels Serveis Cientificotècnics de la Universitat Rovira i Virgili" in Tarragona with a JEOL model 1011 electron microscope operating at 100 kV with resolution of 3 Å. The particles size distributions were determined by a manual analysis of enlarged images. At least 200 particles on a given grid were measured to obtain a statistical size distribution and a mean diameter.

Scanning Transmission Electron Microscopy - High Angle Annular Dark Field (STEM-HAADF) images were obtained in a probe-corrected Titan Low Base (FEI) at

a working voltage of 300 kV, coupled with a HAADF detector (Fischione), available in the "Advanced Microscopy Laboratory of Instituto de Nanociencia de Aragón" in Zaragoza. X-ray Energy Dispersive Spectra (EDS) were obtained with an EDAX detector. The samples were dispersed in THF, and a small amount of solution was then deposited on a Cu-carbon grid.

N_2 adsorption/desorption isotherms were acquired in a Micrometrics ASAP 2020 instrument. N_2 adsorption/desorption isotherms were acquired after dehydroxylation, under air-free conditions and without pretreatments.

Elemental analyses were carried out by inductive plasma coupled atomic emission spectroscopy (ICP-AES) under air-free conditions by Mikroanalytisches Labor Pascher, Remagen (Germany).

Powder X-Ray Diffraction (PXRD) patterns were collected on a Bruker D8 Advance diffractometer with Bragg-Brentano geometry goniometer in Theta-Theta mode and Cu Kα1,2 X-Ray source. Diffractograms were collected in 10–70° 2θ range by ethanol dispersion over Silicon support and treated using DIFFRAC.EVA Bruker software.

H_2 chemisorption was measured manually on the high-vacuum lines using high purity H_2, an Edwards 655AB TRANS 1000 MB sensor, and an Edwards model 1575 pressure display. Around 1 g of each sample was reduced in situ at 500°C for 30 min, the surface is cleaned for 60 min under 10^{-5} mbar at 500°C, and the measurements are performed at room temperature. Total adsorption is measured stepwise, and after the sample is submitted to 60 mins the irreversible adsorption is measured as well as the total volume of the cell.

3.4.5 XRD Measurements.

The Rietveld refinement,[44] was performed with the TOPAS v6 software[45] under the so called "launch mode". The background was modelized with a 2nd order Chebyschev polynomial. The instrumental contribution to the diffraction profile

was calculated with the Fundamental Parameters Approach.[46] The relative quantitative phase analysis was obtained by refining the Rietveld scale factor for each phase and applying the corresponding well-known equations.[47] The net peak width of each phase was modelled with the Double-Voigt Approach[48] by considering only the Lorentzian contribution of the crystallite size effect and discarding any contribution of the micro strain to the peak width. The averaged integral breadth was obtained from the resulting fitted Voigt function to the whole diffractogram. The Scherrer equation[49] was then applied to obtain the apparent crystallite size.

Table S.1. XRD data extracted from diffractograms of PtGa NPs (Part 1). Pt_3Ga has a tetragonal structure.

		Crystalline phase (% wt.)		Crystallite size (nm)	
Time (s)	**T (ºC)**	**Pt**	**Pt_3Ga**	**Pt**	**Pt_3Ga**
-	30	100.0 ± 0.1	-	0.96 ± 0.07	-
0	530	24.6 ± 2	75.4 ± 2	3.00 ± 0.16	3.05 ± 0.06
712	530	25.0 ± 2	75.0 ± 2	3.05 ± 0.17	3.23 ± 0.07
1424	530	25.5 ± 2	74.5 ± 2	3.20 ± 0.18	3.42 ± 0.07
2136	530	23.4 ± 2	76.6 ± 2	3.31 ± 0.19	3.41 ± 0.07
2848	530	23.6 ± 2	76.4 ± 2	3.41 ± 0.19	3.37 ± 0.07
3560	530	24.5 ± 2	75.5 ± 2	3.34 ± 0.18	3.51 ± 0.07

Table S. 2. XRD data extracted from diffractograms of PtGa NPs (Part 1). Pt_3Ga has a tetragonal structure.

		Cell parameters (Å)		
Time (s)	**T (ºC)**	**Pt (a)**	**Pt_3Ga (a)**	**Pt_3Ga (c)**
-	30	4.1060 ± 0.0036		-
0	530	3.9824 ± 0.0037	5.4303 ± 0.0056	7.9300 ± 0.0080
712	530	3.9836 ± 0.0037	5.4334 ± 0.0043	7.9300 ± 0.0077
1424	530	3.9808 ± 0.0035	5.4340 ± 0.0041	7.9300 ± 0.0073
2136	530	3.9780 ± 0.0036	5.4377 ± 0.0042	7.9300 ± 0.0071
2848	530	3.9767 ± 0.0035	5.4397 ± 0.0040	7.9300 ± 0.0071
3560	530	3.9737 ± 0.0034	5.4388 ± 0.0037	7.9300 ± 0.0065

Table S.3. XRD data extracted from diffractograms of PtGa-PPh_3 NPs (Part 1). Pt_3Ga has a cubic structure.

		Crystalline phase (% wt.)		Crystallite size (nm)	
Time (s)	**T (°C)**	**Pt**	**Pt_3Ga**	**Pt**	**Pt_3Ga**
-	30	100.0 ± 0.1	-	0.91 ± 0.05	-
0	530	75.9 ± 0.1	24.1 ± 0.1	1.93 ± 1.3	4.53 ± 0.4
712	530	75.2 ± 2	24.8 ± 2	1.97 ± 1.4	5.13 ± 0.37
1424	530	71.9 ± 2	28.1 ± 2	1.96 ± 1.2	5.08 ± 0.33
2136	530	72.3 ± 2	27.7 ± 2	2.10 ± 1.4	5.20 ± 0.34
2848	530	72.2 ± 2	27.8 ± 2	2.15 ± 1.4	5.26 ± 0.34
3560	530	71.8 ± 2	28.2 ± 2	2.16 ± 1.4	5.12 ± 0.34

Table S.4. XRD data extracted from diffractograms of PtGa-PPh_3 NPs (Part 2). Pt_3Ga has a cubic structure.

		Cell parameters (Å)	
Time (s)	**T (°C)**	**Pt (a)**	**Pt_3Ga (a)**
-	30	4.0248 ± 0.0029	-
0	530	3.9752 ± 0.0022	3.9543 ± 0.0023
712	530	3.9749 ± 0.0020	3.9544 ± 0.0019
1424	530	3.9762 ± 0.0022	3.9544 ± 0.0017
2136	530	3.9747 ± 0.0020	3.9524 ± 0.0018
2848	530	3.9757 ± 0.0022	3.9525 ± 0.0018
3560	530	3.9760 ± 0.0021	3.9538 ± 0.0019

3.4.6 Catalyst Activity Measurements.

Propane dehydrogenation (PDH) experiments were carried under O_2 and H_2O exclusion conditions, unless stated differently. All gases were purchased from Air Liquide and further purified in line with molecular sieves and BTS catalysts traps to assure high purity. A stainless-steel tubing of a ½ inch was used as a continuous

flow reactor, containing a thermocouple that is heated by a vertical furnace (P_{total} = 1 bar, T = 530 °C) and it was packed inside an Ar filled glovebox. A 4-way valve

system alloy the inert handling and various stainless-steel fillers are used to reduce the dead volume. Typically, 25 mg of catalyst were diluted to 2.5 g with SiC. A reductive pre-treatment of 16 h at 550 ^{o}C (1 °C/min) was carried out with pure hydrogen flow, prior to start the catalytic tests, the system reached room temperature and it was purged with Ar. A 3 C_3H_8: 1 H_2: 21 Ar (mL/min) gas composition was used and controlled by Brooks mass flow controllers. The Gas hourly space velocity (GSHV) was kept to 60000 $mL \cdot gcat^{-1} \cdot h^{-1}$, unless stated differently. The products were determined by an online HP 6890 GC equipped with 50 m KCl/Al_2O_3 column and FID detector. Propane conversion was calculated typically by carbon balance. Selectivity to each product was similarly obtained.

$$Propane\ conversion\ (\%) = \frac{Total\ Propane_{out}}{Total\ Propane_{in}}\ x\ 100$$

$$Propylene\ selectivity\ (\%) = \frac{Total\ propylene_{out}}{Total\ propane_{in} - Total\ propane_{out}}\ x\ 100$$

The deactivation constant (k_d) was calculated at the reaction temperature (i.e., 530 ^{o}C) according to the following formula:

$$\ln\left[\frac{(1-\chi_{final})}{\chi_{final}}\right] = k_d \times T + \ln\left[\frac{(1-\chi_{initial})}{\chi_{initial}}\right]$$

Where χ_{final} and $\chi_{initial}$, are the final and the initial propane conversion values and T represents the lifetime of the catalyst.

5.5 References

(1) Liu, S.; Zhang, B.; Liu, G. Metal-Based Catalysts for the Non-Oxidative Dehydrogenation of Light Alkanes to Light Olefins. *React. Chem. Eng.* **2021**, 9–26. https://doi.org/10.1039/d0re00381f.

(2) Liu, S.; Zhang, B.; Liu, G. Metal-Based Catalysts for the Non-Oxidative Dehydrogenation of Light Alkanes to Light Olefins. *React. Chem. Eng.* **2020**. https://doi.org/10.1039/d0re00381f.

(3) Jablonski, E. L.; Castro, A. A.; Scelza, O. A.; Miguel, S. R. De. Effect of Ga Addition to Pt/Al2O3 on the Activity , Selectivity and Deactivation in the Propane Dehydrogenation. *Appl. Catal. A Gen.* **1999**, *183*.

(4) Wang, T.; Jiang, F.; Liu, G.; Zeng, L.; Zhao, Z.; Gong, J. Effects of Ga Doping on Pt/CeO2-Al2O3 Catalysts for Propane Dehydrogenation. *AlChE* **2016**, *62* (12). https://doi.org/10.1002/aic.

(5) Siddiqi, G.; Sun, P.; Galvita, V.; Bell, A. T. Catalyst Performance of Novel Pt/Mg(Ga)(Al)O Catalysts for Alkane Dehydrogenation. *J. Catal.* **2010**, *274* (2), 200–206. https://doi.org/10.1016/j.jcat.2010.06.016.

(6) Redekop, E. A.; Galvita, V. V.; Poelman, H.; Bliznuk, V.; Detavernier, C.; Marin, G. B. Delivering a Modifying Element to Metal Nanoparticles via Support: Pt-Ga Alloying during the Reduction of Pt/Mg(Al,Ga)Ox Catalysts and Its Effects on Propane Dehydrogenation. *ACS Catal.* **2014**, *4* (6), 1812–1824. https://doi.org/10.1021/cs500415e.

(7) Searles, K.; Chan, K. W.; Mendes Burak, J. A.; Zemlyanov, D.; Safonova, O.; Copéret, C. Highly Productive Propane Dehydrogenation Catalyst Using Silica-Supported Ga-Pt Nanoparticles Generated from Single-Sites. *J. Am. Chem. Soc.* **2018**, *140* (37), 11674–11679. https://doi.org/10.1021/jacs.8b05378.

(8) Payard, P.-A.; Rochlitz, L.; Searles, K.; Foppa, L.; Leuthold, B.; Safonova, O. V.; Comas-Vives, A.; Copéret, C. Dynamics and Site Isolation: Keys to High Propane Dehydrogenation Performance of Silica-Supported PtGa Nanoparticles. *J. Am. Chem. Soc.* **2021**, *1*, 1445–1458. https://doi.org/10.1021/jacsau.1c00212.

(9) Nakaya, Y.; Hirayama, J.; Yamazoe, S.; Shimizu, K.; Furukawa, S. Single-Atom Pt in Intermetallics as an Ultrastable and Selective Catalyst for Propane Dehydrogenation. *Nat. Commun.* **2020**, *11* (2020), 3–9. https://doi.org/10.1038/s41467-020-16693-9.

(10) Nakaya, Y.; Xing, F.; Ham, H.; Shimizu, K.; Furukawa, S. Doubly Decorated Platinum – Gallium Intermetallics as Stable Catalysts for Propane Dehydrogenation. *Angew. Chemie Int. Ed.* **2021**, *60*, 1–7. https://doi.org/10.1002/anie.202107210.

(11) Raman, N.; Wolf, M.; Heller, M.; Heene-wu, N.; Taccardi, N.; Haumann, M.; Felfer, P.; Wasserscheid, P. GaPt Supported Catalytically Active Liquid Metal Solution Catalysis for Propane Dehydrogenation − Support Influence and Coking Studies. *ACS Catal.* **2021**, *11*, 13423–13433. https://doi.org/10.1021/acscatal.1c01924.

(12) Zhang, B.; Zheng, L.; Zhai, Z.; Li, G.; Liu, G. Subsurface-Regulated PtGa Nanoparticles Con Fi Ned in Silicalite - 1 for Propane Dehydrogenation. *ACS Appl. Mater. Interfaces* **2021**, *13* (14), 16259–16266. https://doi.org/10.1021/acsami.0c22865.

(13) Wang, G.; Zhang, S.; Zhu, X.; Li, C.; Shan, H. Dehydrogenation versus Hydrogenolysis in the Reaction of Light Alkanes over Ni-Based Catalysts. *J. Ind. Eng. Chem.* **2020**, *86*, 1–12. https://doi.org/10.1016/j.jiec.2020.02.025.

(14) Xu, Y.; Sang, H.; Wang, K.; Wang, X. Catalytic Dehydrogenation of Isobutane in the Presence of Hydrogen over Cs-Modified Ni 2 P Supported on Active Carbon. *Appl. Surf. Sci.* **2014**, *316*, 163–170. https://doi.org/10.1016/j.apsusc.2014.07.119.

(15) Zhu, Q.; Zhang, H.; Zhang, S.; Wang, G.; Zhu, X.; Li, C. Dehydrogenation of Isobutane over a Ni–P/SiO2 Catalyst : Effect of P Addition. *Ind. Eng. Chem. Res.* **2019**, *58*, 7834–7843. https://doi.org/10.1021/acs.iecr.9b00032.

(16) Bocanegra, S. A.; Castro, A. A.; Guerrero-Ruíz, A.; Scelza, O. A.; de Miguel, S. R. Characteristics of the Metallic Phase of Pt/Al2O3 and Na-Doped Pt/Al2O3 Catalysts for Light Paraffins Dehydrogenation. *Chem. Eng. J.* **2006**, *118* (3), 161–166. https://doi.org/10.1016/j.cej.2006.02.004.

(17) Wang, G.; Wang, H.; Zhang, H.; Zhu, Q.; Li, C. Highly Selective and Stable NiSn/SiO2 Catalyst for Isobutane Dehydrogenation : Effects of Sn Addition. *ChemCatChem* **2016**, *8*, 3137–3145. https://doi.org/10.1002/cctc.201600685.

(18) Wang, H.; Wang, H.; Li, X.; Li, C. Nature of Active Tin Species and Promoting Effect of Nickle in Silica Supported Tin Oxide for Dehydrogenation of Propane. *Appl. Surf. Sci.* **2017**, *407*, 456–462. https://doi.org/10.1016/j.apsusc.2017.02.216.

(19) Zhang, G.; Yang, C.; Miller, J. T. Tetrahedral Nickel(II) Phosphosilicate Single Site Selective Propane Dehydrogenation Catalyst. *ChemCatChem* **2017**, *10* (5), 961–964. https://doi.org/10.1002/cctc.201701815.

(20) He, Y.; Song, Y.; Laursen, S. The Origin of the Special Surface and Catalytic Chemistry of Ga-Rich Ni3Ga in the Direct Dehydrogenation of Ethane. *ACS Catal.* **2019**, *9*, 10464–10468. https://doi.org/10.1021/acscatal.9b03402.

(21) He, Y.; Song, Y.; Cullen, D. A.; Laursen, S. Selective and Stable Non-Noble-Metal Intermetallic Compound Catalyst for the Direct Dehydrogenation of Propane to Propylene. *J. Am. Chem. Soc.* **2018**, *140*, 14010–14014. https://doi.org/10.1021/jacs.8b05060.

(22) Ely, T. O.; Amiens, C.; Chaudret, B.; Snoeck, E.; Verelst, M.; Respaud, M.; Broto, J. Synthesis of Nickel Nanoparticles . Influence of Aggregation Induced by Modification of Poly (Vinylpyrrolidone) Chain Length on Their Magnetic Properties Attracting Increasing Interest , Because They May Differ Surface or Quantum Size Effects . 1 Howeve. *Chem. Mater.* **1999**, *11* (l), 526–529.

(23) Xu, Z.; Xu, R.; Yue, Y.; Yuan, P.; Bao, X.; Abou-Hamad, E.; Basset, J. M.; Zhu, H. Bimetallic Pt-Sn Nanocluster from the Hydrogenolysis of a Well-Defined Surface Compound Consisting of [(AlO-)Pt(COD)Me] and [(AlO-)SnPh3] Fragments for Propane Dehydrogenation. *J. Catal.* **2019**, *374*, 391–400. https://doi.org/10.1016/j.jcat.2019.04.035.

(24) Sahu, R. K.; Mukherjee, D.; Tiwari, J. P.; Mishra, T.; Roy, S. K.; Pathak, L. C. Influence of Foreign Fe Ions on Wet Chemical Synthesis of Pt Nanoparticle Thin Films at Ambient Temperature : In Situ versus Direct Addition. *J. Mater. Chem.* **2009**, *19*, 6810–6815. https://doi.org/10.1039/b908080e.

(25) Ivanova, A. S.; Slavinskaya, E. M.; Gulyaev, R. V; Zaikovskii, V. I.; Stonkus, O. A.; Danilova, I. G.; Plyasova, L. M.; Polukhina, I. A.; Boronin, A. I. Metal – Support Interactions in Pt/Al2O3 and Pd/Al2O3 Catalysts for CO Oxidation. *Appl. Catal. B Environ.* **2010**, *97*, 57–71. https://doi.org/10.1016/j.apcatb.2010.03.024.

(26) Grabau, M.; Krick, S.; Rietzler, F.; Niedermaier, I.; NicolaTaccardi; Wasserscheid, P.; Maier, F.; Steinrück, H.-P.; Papp, C. Surface Enrichment of Pt in Ga2O3 Films Grown on Liquid Pt/Ga Alloys. *Surf. Sci.* **2016**, *651*, 16–21.

(27) Hardeveld, R. V. A. N.; Hartog, F. The Statistics of Surface Atoms and Surface Sites on Metal

Crystals. *Surf. Sci.* **1969**, *15*, 189–230.

(28) Ni, Y.; Mi, K.; Cheng, C.; Xia, J.; Ma, X.; Hong, J. Urchin-like Ni–P Microstructures: Facile Synthesis, Properties and Application in the Fast Removal of Heavy-Metal Ions. *Chem. Commun.* **2011**, *47* (20), 5891–5893. https://doi.org/10.1039/c1cc11640a.

(29) Fang Lu, Xiaobo Ji, Yingchang Yang, Wentao Deng, C. E. B. Room Temperature Ionic Liquid Assisted Well-Dispersed Core-Sjell Tin Nanoparticles through Catodic Corrosion. *RSC Adv.* **2013**, *3*, 18791–18793. https://doi.org/10.1039/c3ra43532f.

(30) Gannoun, C.; Turki, A.; Kochkar, H.; Delaigle, R.; Eloy, P. Elaboration and Characterization of Sulfated and Unsulfated V2O5/TiO2 Nanotubes Catalysts for Chlorobenzene Total Oxidation. *Appl. Catal. B Environ.* **2014**, *147*, 58–64. https://doi.org/10.1016/j.apcatb.2013.08.009.

(31) Gu, Y.; Liu, H.; Yang, M.; Ma, Z.; Zhao, L.; Xing, W.; Gu, Y.; Liu, H.; Yang, M.; Ma, Z.; Zhao, L. Highly Stable Phosphine Modified VOx / Al2O3 Catalyst in Propane Dehydrogenation To Cite This Version : HAL Id : Hal-02893792 Highly Stable Phosphine Modified VO x / Al 2 O 3 Catalyst in Propane Dehydrogenation. *Appl. Catal. B Environ.* **2020**, *274*, 119089.

(32) Zhang, Y.; Zhou, Y.; Qiu, A.; Wang, Y.; Xu, Y.; Wu, P. Propane Dehydrogenation on PtSn/ZSM-5 Catalyst: Effect of Tin as a Promoter. *Catal. Commun.* **2006**, *7* (11), 860–866. https://doi.org/10.1016/j.catcom.2006.03.016.

(33) Dai, Y.; Gu, J.; Tian, S.; Wu, Y.; Chen, J.; Li, F.; Du, Y.; Peng, L.; Ding, W.; Yang, Y. Gamma - Al2O3 Sheet-Stabilized Isolate Co2 + for Catalytic Propane Dehydrogenation. *J. Catal.* **2020**, *381*, 482–492. https://doi.org/10.1016/j.jcat.2019.11.026.

(34) Docherty, S. R.; Rochlitz, L.; Payard, P.-A.; Copéret, C. Heterogeneous Alkane Dehydrogenation Catalysts Investigated via a Surface Organometallic Chemistry Approach. *Chem. Soc. Rev.* **2021**, *50*, 5806–5822. https://doi.org/10.1039/d0cs01424a.

(35) Liu, L.; Lopez-haro, M.; Lopes, C. W.; Rojas-buzo, S.; Concepcion, P.; Manzorro, R.; Simonelli, L.; Sattler, A.; Serna, P.; Calvino, J. J.; Corma, A. Structural Modulation and Direct Measurement of Subnanometric Bimetallic PtSn Clusters Confined in Zeolites. *Nat. Catal.* **2020**, *3*, 628–638. https://doi.org/10.1038/s41929-020-0472-7.

(36) Holmen, A.; Blekkan, E. A. Propane Dehydrogenation over Supported Pt and Pt – Sn Catalysts : Catalyst Preparation , Characterization , and Activity Measurements. **1996**, *12* (158), 1–12.

(37) Diéguez, M.; Pàmies, O.; Mata, Y.; Teuma, E.; Gómez, M.; Ribaudo, F.; Leeuwen, P. W. N. M. v. Palladium Nanoparticles in Allylic Alkylations and Heck Reactions: The Molecular Nature of the Catalyst Studied in a Membrane Reactor. *Adv. Synth. Catal.* **2007**, *325*, 2538–2598.

(38) Jeng-Shiou; Aleksey, C.; Anthony, N. V.; P.Panarello; G.Khinast, J. Pd-Leaching and Pd-Removal in Pd/C-Catalyzed Suzuki Couplings. *Appl. Catal. A Gen.* **2007**, *325* (1), 76–86.

(39) Sattler, J. J. H. B.; Gonzalez-Jimenez, I. D.; Luo, L.; Stears, B. A.; Malek, A.; Barton, D. G.; Kilos, B. A.; Kaminsky, M. P.; Verhoeven, T. W. G. M.; Koers, E. J.; Baldus, M.; Weckhuysen, B. M. Platinum-Promoted Ga/Al2O3 as Highly Active, Selective, and Stable Catalyst for the Dehydrogenation of Propane. *Angew. Chemie - Int. Ed.* **2014**, *53* (35), 9251–9256. https://doi.org/10.1002/anie.201404460.

(40) Ould Ely, T.; Pan, C.; Amiens, C.; Chaudret, B.; Dassenoy, F.; Lecante, P.; Casanove, M. J.;

Mosset, A.; Respaud, M.; Broto, J. M. Nanoscale Bimetallic CoxPt1-x Particles Dispersed in Poly(Vinylpyrrolidone): Synthesis from Organometallic Precursors and Characterization. *J. Phys. Chem. B* **2000**, *104* (4), 695–702. https://doi.org/10.1021/jp9924427.

(41) De Los Bernardos, M. D.; Pérez-Rodríguez, S.; Gual, A.; Claver, C.; Godard, C. Facile Synthesis of NHC-Stabilized Ni Nanoparticles and Their Catalytic Application in the: Z - Selective Hydrogenation of Alkynes. *Chem. Commun.* **2017**, *53* (56), 7894–7897. https://doi.org/10.1039/c7cc01779k.

(42) Voutchkova, A. M.; Feliz, M.; Clot, E.; Eisenstein, O.; Crabtree, R. H. Imidazolium Carboxylates as Versatile and Selective N-Heterocyclic Carbene Transfer Agents: Synthesis, Mechanism, and Applications. *J. Am. Chem. Soc.* **2007**, *129* (42), 12834–12846. https://doi.org/10.1021/ja0742885.

(43) Dassenoy, F.; Philippot, K.; Ould Ely, T.; Amiens, C.; Lecante, P.; Snoeck, E.; Mosset, A.; Casanove, M. J.; Chaudret, B. Platinum Nanoparticles Stabilized by CO and Octanethiol Ligands or Polymers: FT-IR, NMR, HREM and WAXS Studies. *New J. Chem.* **1998**, *22* (7), 703–711. https://doi.org/10.1039/a709245h.

(44) Rietveld, H. M. A Profile Refinement Method for Nuclear and Magnetic Structures. *J. Appl. Crystallogr.* **1969**, *2* (2), 65–71. https://doi.org/10.1107/s0021889869006558.

(45) Coelho, A. A. TOPAS and TOPAS-Academic: An Optimization Program Integrating Computer Algebra and Crystallographic Objects Written in C++: An. *J. Appl. Crystallogr.* **2018**, *51* (1), 210–218. https://doi.org/10.1107/S1600576718000183.

(46) Cheary, R. W.; Coelho, A. A.; Cline, J. P. Fundamental Parameters Line Profile Fitting in Laboratory Diffractometers. *J. Res. Natl. Inst. Stand. Technol.* **2004**, *109* (1), 1–25. https://doi.org/10.6028/jres.109.002.

(47) Hill, R. J.; Howard, C. J. Quantitative Phase Analysis from Neutron Powder Diffraction Data Using the Rietveld Method. *J. Appl. Crystallogr.* **1987**, *20* (6), 467–474. https://doi.org/10.1107/S0021889887086199.

(48) Balzar, D. Voigt-Function Model in Diffraction Line-Broadening Analysis. *Microstruct. Anal. from Diffr.* **1999**, 94–124.

(49) Stokes, A. R.; Wilson, A. J. C. A Method of Calculating the Integral Breadths of Debye-Scherrer Lines. *Math. Proc. Cambridge Philos. Soc.* **1942**, *38* (3), 313–322. https://doi.org/10.1017/S0305004100021988.

Chapter 5

UNIVERSITAT ROVIRA I VIRGILI
INNOVATIVE NANOCATALYSTS FOR SUSTAINABLE NON-OXIDATIVE DEHYDROGENATION OF PROPANE
Laia Gil Jiménez

6

Conclusions

In this PhD manuscript, the synthesis, characterization, and performance in propane dehydrogenation reaction of various PtSn, PtGa and NiSn supported catalysts has been presented.

Pt and PtSn catalysts have been synthesized via the Surface Organometallic Chemistry (SOMC) approach, characterized, and evaluated in PDH as it was described in **Chapter 3**. The detailed conclusions that were extracted were:

- A series of Pt and PtSn-NPs supported onto $LiAl_2O_3$ prepared by SOMC/Oxide followed by SOMC/M and tested in PDH reaction. The catalysts were characterized by techniques such as TEM, HAADF-STEM, N_2-adsorption/desorption isotherms, H_2-chemisorption, DRIFT and XRD, that revealed the presence of small and well-dispersed bimetallic NPs, crucial to obtain highly active and selective catalysts for PDH.
- Moreover, an exhaustive study of the operation conditions of PDH concerning the effect of H_2, temperature and pressure, contact time, oxygen poisoning and long-time studies for stability was performed. Finally, the operation conditions were optimized to a propane/H_2 ratio of 3, feed composition of 3 C_3H_8/1 H_2/21 Ar (mL/min), 530 ^oC and 1 bar, inert preparation of the reactor inside the glovebox and, GHSV = 15.000 $mL \cdot gcat^{-1} \cdot h^{-1}$.
- The influence of Sn/Pt ratio, the loading of Li in the support and the Pt loading of the catalyst were also studied. The most promising Sn/Pt ratio was 0.7 (mol/mol), with a Li loading on the Al_2O_3 support of 0.45 wt.% Li. An initial propane conversion of 20% was obtained, still providing 18% and 14% conversion after 900 min and 3000 min of TOS. The selectivity of the optimized catalyst to propylene was always >98%, displaying an excellent performance in PDH, superior to that of the benchmark catalyst (Linde-BASF-Statoil).

Pt and PtSn catalysts were synthesized by the one-pot organometallic approach (OPOA) and applied for the first time in the PDH reaction. In **Chapter 4** The detailed conclusions that were extracted were:

- The effect of stabilizing molecules (none, PPh_3, NHC) was studied.
- Al_2O_3-based catalysts synthesized in the presence of PPh_3 or without ligand provided the best catalytic performance, whereas those supported onto $LiAl_2O_3$ and/or in the presence of NHC ligand revealed less efficient.
- The nature of the Sn precursor also influenced the catalytic performance of these materials and $SnBu_4$ was the most appropriate.
- When the P-containing catalyst was tested in the presence of CO_2, a remarkable gain in stability was observed while the selectivity to propene remained unaffected (>99%).
- Overall, the best catalyst was $1Pt0.5Sn^{IV}@Al_2O_3$ with an initial conversion of 22.3% and after 24 h of time on stream, the conversion was maintained at 20.5%. The catalyst was highly selective toward propylene throughout the experiment (>98.5% after 24h) and was stable, with a deactivation constant (k_d) of 0.0067.

- The OPO allowed us to explore new horizons in the preparation of other catalyst for propane dehydrogenation with a very easy one-step methodology.

From the study of alternative metals in PDH reaction detailed in **Chapter 5**. The one-pot organometallic approach (OPOA) was used for the first time in the preparation of PtGa and NiSn based catalysts in the propane dehydrogenation reaction.

For PtGa OPOA catalysts:

- $Ga(Me)_3$ was the Ga promoter that exhibited a better conversion, mainly due to the higher final Ga content in this catalyst. The effect of PPh_3 was

studied, and XRD analyses indicated the presence of the Pt_3Ga alloy in the analogous colloids. The most promising PtGa catalyst synthesized by OPOA was PtGa-PPh_3@Al_2O_3 with an initial propane conversion of 23.0% that decreased to 14.2% after 10 h of TOS. Its selectivity to propylene started at 94% and increased to 99%. No effect of CO_2 in the feed was observed during the catalytic tests.

Regarding NiSn OPOA catalysts:

- A ligand study was performed (PPh_3 and NHC). PPh_3 ligand revealed to have a positive role in inhibiting the hydrogenolysis, therefore suggesting that a NiSn alloy species was formed. In contrast, NHC fomented the hydrogenolysis because the main product obtained was methane, and large NPs were obtained (>10nm).

Moreover, a novel approach combining OPOA with surface organometallic chemistry (SOMC), (OPOA-SOMC) was investigated for the first time in the preparation of PtSn and PtGa supported onto alumina or lithiated alumina, respectively.

- The role of the ligand (no ligand or PPh_3) was also explored. However, since there is an aggressive reduction step, no ligand effect was observed either for PtSn and PtGa.

Chapter 6

APPENDIX

Publications

- **Patent Applications:**

It is important to highlight that part of the thesis content is protected by:

1. "**Alkane dehydrogenation nanocatalyst and process for its preparation"**. Inventors: Gil Jiménez, L.; Vicente Valverde, I.; Gual Gozalbo, A.; Godard, C.; Claver Cabrero, C. Reference: European patent application nºEP21382154.9, 24th February 2021. Patent holding body: FUNDACIÓ EURECAT.
2. **"Alkane dehydrogenation nanocatalyst and process for its preparation".** Reference: International patent application PCT number: PCT/EP2022/054574, 23rd February 2022. This international patent application PCT extended the revindications of the European patent application no.: EP21382154.9. Patent holding body: FUNDACIÓ EURECAT.

- **Publications in scientific journals**

1. **"Development of Pt-Sn propane dehydrogenation catalysts by one-pot organometallic approach"**, Laia Gil, Sara Gonzalez, Kai Szeto, Aimery De Mallman, Mostafa Taoufik, Aitor Gual, Isabel Vicente, and Cyril Godard. *Manuscript under preparation*.

2. **"Novel Pt-based catalyst for propane dehydrogenation prepared by Surface Organometallic Chemistry"** Isaias Barbosa Aragao, Laia Gil, Kai Szeto, Aimery De Mallman, Aitor Gual, Isabel Vicente, Cyril Godard and Mostafa Taoufik. *Manuscript under preparation*.

3. **"Development of Pt-Ga and Ni-Sn propane dehydrogenation catalysts by one-pot organometallic approach**", Laia Gil, Kai Szeto, Aimery De Mallman, Mostafa Taoufik, Aitor Gual, Isabel Vicente, and Cyril Godard. *Manuscript under preparation*.

Conferences and Scientific Meetings

- **Conferences:**

23-27th Jan. 2022 — *5th International Caparica Symposium on Nanoparticles, Nanomaterials and Applications.* **Shotgun presentation and Poste**r entitled "Sustainable propene production by propane dehydrogenation catalyzed by innovative nanocatalysts". L.Gil, K. C. Szeto, M.Taoufik, A. de Mallmann, I.Vicente, A.Gual and C. Godard.
Caparica (Portugal).

Awarded with the *"Excellent Shotgun Poster Prize".*

22-25th Sep. 2019 — *4th EuCheMS Conference on Green and Sustainable Chemistry.*
ICIQ, Tarragona (Spain).

- **Outreach activities related with the PhD:**

30th Mar. 2022 — **Outreach monologue about PhD** entitled "Producció de mascaretes més sostenibles: màgia o química" in the Catalan contest *"Vols saber què investigo?" organized by URV.*
Reus (Spain).

Awarded with the *"Public award: most voted monologue".*

26th Nov. 2020 — **Oral presentation** entitled "Nanocatalitzadors a la industria química" in the "*Nit Europea de la Recerca a Catalunya*".
Tarragona (Spain).

UNIVERSITAT
ROVIRA i VIRGILI